



UNIL | Université de Lausanne

Unicentre

CH-1015 Lausanne

<http://serval.unil.ch>

Year : 2023

Functions and mechanisms of m⁶A mRNA modification in *Drosophila melanogaster*

Paolantoni Chiara

Paolantoni Chiara, 2023, Functions and mechanisms of m⁶A mRNA modification in *Drosophila melanogaster*

Originally published at : Thesis, University of Lausanne

Posted at the University of Lausanne Open Archive <http://serval.unil.ch>

Document URN : urn:nbn:ch:serval-BIB_66BD093D754A8

Droits d'auteur

L'Université de Lausanne attire expressément l'attention des utilisateurs sur le fait que tous les documents publiés dans l'Archive SERVAL sont protégés par le droit d'auteur, conformément à la loi fédérale sur le droit d'auteur et les droits voisins (LDA). A ce titre, il est indispensable d'obtenir le consentement préalable de l'auteur et/ou de l'éditeur avant toute utilisation d'une oeuvre ou d'une partie d'une oeuvre ne relevant pas d'une utilisation à des fins personnelles au sens de la LDA (art. 19, al. 1 lettre a). A défaut, tout contrevenant s'expose aux sanctions prévues par cette loi. Nous déclinons toute responsabilité en la matière.

Copyright

The University of Lausanne expressly draws the attention of users to the fact that all documents published in the SERVAL Archive are protected by copyright in accordance with federal law on copyright and similar rights (LDA). Accordingly it is indispensable to obtain prior consent from the author and/or publisher before any use of a work or part of a work for purposes other than personal use within the meaning of LDA (art. 19, para. 1 letter a). Failure to do so will expose offenders to the sanctions laid down by this law. We accept no liability in this respect.



UNIL | Université de Lausanne

Faculté de biologie
et de médecine

Centre Intégréatif de Génomique

**Functions and mechanisms of m⁶A mRNA
modification in *Drosophila melanogaster***

Thèse de doctorat ès sciences de la vie (PhD)

présentée à la

Faculté de biologie et de médecine
de l'Université de Lausanne

par

Chiara PAOLANTONI

Master de l'Université "La Sapienza" de Rome

Jury

Prof. Marc Robinson-Rechavi, Président
Prof. Jean-Yves Roignant, Directeur de thèse
Prof. Brian McCabe, Expert
Prof. Mary Anne O'Connell, Experte

Lausanne
(2023)

Imprimatur

Vu le rapport présenté par le jury d'examen, composé de

Président·e	Monsieur	Prof.	Marc	Robinson-Rechavi
Directeur·trice de thèse	Monsieur	Prof.	Jean-Yves	Roignant
Expert·e-s	Monsieur	Prof.	Brian	McCabe
	Madame	Prof.	Mary Ann	O'Connell

le Conseil de Faculté autorise l'impression de la thèse de

Chiara Paolantoni

Master of Science, Università degli Studi di Roma 'La Sapienza', Italie

intitulée

**Functions and mechanisms of m⁶A mRNA
modification in *Drosophila melanogaster***

Lausanne, le 15 septembre 2023

pour le Doyen
de la Faculté de biologie et de médecine



Prof. Marc Robinson-Rechavi

Table of contents

Table of contents	I
List of figures	III
List of tables	III
List of abbreviations.....	IV
Abstract.....	VII
Résumé	VIII
1. Introduction.....	1
1.1 RNA modifications	1
1.2 Non-coding RNAs modifications	1
1.3 mRNA modifications	3
1.3.1 The 5' cap and its modifications	3
1.3.2 Guanosine modifications	4
1.3.3 Cytidine modifications	5
1.3.4 Adenosine modifications	6
1.3.5 Uridine modifications.....	6
1.3.6 Ribose modifications.....	7
1.4 m⁶A modification.....	8
1.4.1 m ⁶ A writers	9
1.4.2 Regulation of m ⁶ A deposition	13
1.4.3 m ⁶ A erasers	15
1.4.4 m ⁶ A readers.....	19
1.4.5 m ⁶ A distribution and mapping methods.....	24
1.4.6 m ⁶ A functions within the mRNA life cycle	28
1.4.7 m ⁶ A biological significance.....	35
1.4.8 m ⁶ A and cancer	38
1.5 <i>Drosophila melanogaster</i>	39
1.5.1 The fruit fly as model organism	39
1.5.2 The life cycle of <i>Drosophila melanogaster</i>	39
1.5.3 The larval neuromuscular junction	40
2. Materials and methods	42
3. Aim of the work	50
4. Preliminary remarks	51

5. Results	53
5.1 Section 1: Research article 1	53
5.2 Section 2: Research article 2	75
5.3 Section 3	104
5.3.1 Identification of m ⁶ A readers in <i>Drosophila melanogaster</i>	104
5.3.2 Dhx57 preferentially binds to m ⁶ A-modified RNA.....	105
5.3.3 mRNA targets of Dhx57 are mostly methylated	107
5.3.4 Loss of Dhx57 has no significant effect on small RNA-directed silencing pathways	110
5.3.5 Dhx57 regulates axonal growth at larval NMJs.....	111
5.4 Section 4	114
5.4.1 No obvious m ⁶ A erasers acting on mRNA in <i>Drosophila melanogaster</i>	114
5.4.2 The expression profile of Alkbh6 follows m ⁶ A levels during fly development	115
5.4.3 Expression of <i>Alkbh6</i> is upregulated in response to abiotic stress.....	117
5.4.4 <i>Alkbh6</i> mutants are more sensitive to oxidative stress and starvation.....	119
5.4.5 Loss of <i>Alkbh6</i> aggravates the effects of oxidative stress on flies	121
6. Discussion	124
6.1 Writing m⁶A in <i>Drosophila</i>	124
6.1.1 Internal architecture of the MACOM complex	125
6.1.2 Function of Hakai within the MACOM complex	126
6.1.3 Do the short and long Hakai isoforms have different functions in flies?	127
6.2 Can m⁶A be erased in <i>Drosophila</i>?	128
6.2.1 m ⁶ A on mRNA is probably not the main substrate of Alkbh6.....	129
6.2.2 What is the function of Alkbh6 in flies?	129
6.3 Reading m⁶A in the nervous system of <i>Drosophila</i>	131
6.3.1 Loss of m ⁶ A affects adult locomotion and larval NMJ morphology.....	131
6.3.2 Ythdf and Fmr1 interplay to regulate axonal growth at larval NMJs.....	132
6.3.3 Possible link between m ⁶ A and FXS	133
6.4 Dhx57 is a potential new m⁶A binding protein in <i>Drosophila</i>	134
6.4.1 What are the targets of Dhx57?.....	134
6.4.2 What is the function of Dhx57 in flies?	135
6.5 Conclusions	137
8. References	138
9. Curriculum Vitae	159

List of figures

Figure 1. Diversity of chemical RNA nucleoside modifications.	2
Figure 2. mRNA modifications.	8
Figure 3. m ⁶ A functions within the mRNA life cycle.	34
Figure 4. The <i>Drosophila melanogaster</i> life cycle at 25°C.	40
Figure 5. The <i>Drosophila melanogaster</i> larval NMJ system.	41
Figure 6. Dhx57 localizes to the cytoplasm and its expression correlates with m ⁶ A profile during fly development.	104
Figure 7. Dhx57 protein preferentially binds m ⁶ A-modified RNA in the GGACU sequence context.	106
Figure 8. Preferential binding to m ⁶ A-modified RNA is specific to Dhx57 among <i>Drosophila</i> DExH box helicases.	107
Figure 9. mRNA targets of Dhx57 are mostly methylated.	108
Figure 10. Dhx57 binding to its mRNA targets is m ⁶ A-dependent.	109
Figure 11. Loss of Dhx57 has no significant effect on small RNA-directed silencing pathways.	110
Figure 12. Dhx57 contributes to the regulation of axonal growth in the <i>Drosophila</i> larval NMJ system.	112
Figure 13. Dhx57 and Mettl3 interact genetically to control axonal growth in the <i>Drosophila</i> larval NMJ system.	113
Figure 14. No obvious mRNA m ⁶ A erasers in flies.	115
Figure 15. Alkbh6 localizes ubiquitously in the cell and its expression correlates with m ⁶ A profile during fly development.	116
Figure 16. <i>Alkbh6</i> is upregulated in response to abiotic stress.	117
Figure 17. <i>Alkbh6</i> is enriched in the nucleus and interacts with Ythdc1 upon oxidative stress and starvation.	118
Figure 18. <i>Alkbh6</i> mutant flies are more sensitive to paraquat-induced oxidative stress.	120
Figure 19. <i>Alkbh6</i> mutant flies are more sensitive to starvation.	121
Figure 20. Loss of <i>Alkbh6</i> aggravates the effects of paraquat-induced oxidative stress on flies.	123

List of tables

Table 1. Substrates and subcellular localization of proteins of the ALKBH family.	18
Table 2. Methods used for m ⁶ A mapping and quantification.	28
Table 3. Oligos used in this study.	48
Table 4. Flies generated and used in this study.	49
Table 5: Plasmids generated and used in this study.	49

List of abbreviations

1mA	N1-methyldeoxyadenosine	CNS	Central nervous system
3mC	3-methyldeoxycytidine	CPSF	Cleavage and polyadenylation specificity factors
3mT	3-methyldeoxythymidine	CRISPR-Cas9	Clustered regularly interspaced short palindromic repeats-CRISPR-associated protein 9
6mA	N6-methyldeoxyadenosine	cryo-EM	Cryogenic electron microscopy
ac⁴c	N4-cytosine acetylation	CTRL	Control
acp³U	3-(3-amino-3-carboxypropyl)uridine	D	Dihydrouridine
A	Adenosine	DART-seq	Deamination adjacent to RNA modification targets sequencing
aa	Amino acid(s)	DCP2	Decapping mRNA 2
ADAR	Adenosine deaminases acting on RNA	DNA	Deoxyribonucleic acid
ALKBH	AlkB homolog	dNTP	Deoxynucleotide triphosphate
ALYREF	Aly/REF export factor	ds	Double-stranded
AML	Acute myeloid leukemia	eIF	Eukaryotic translation initiation factor
AMPA	α -amino-3-hydroxy-5-methyl-4-isoxazole propionic acid	EJC	Exon junction complex
AMPAR	AMPA receptor	ERV	Endogenous retrovirus
ANOVA	Analysis of variance	eTAM-seq	Evolved TadA-assisted m ⁶ A seq
APA	Alternative polyadenylation	f⁵C	5-formylcytidine
BCSC	Breast cancer stem cells	f⁶A	N6-formyladenosine
BID-seq	Bisulfite-induced deletion sequencing	FDR	False discovery rate
bp	Base pair(s)	FI(2)d	Female-lethal(2)d
Btz	Barentsz	Flacc	FI(2)d-associated complex component
C	Cytidine	FTO	Fat mass and obesity-associated protein
carRNA	chromosome-associated regulatory RNA	FXS	Fragile X syndrome
CBC	Cap-binding complex	G	Guanine
CBLL1	Casitas B-lineage lymphoma-transforming sequence-like protein 1	G3BP	Ras GTPase-activating protein-binding protein
cDNA	Complementary DNA	G4	G-quadruplex
CDS	Coding sequence	GFP	Green fluorescent protein
Chr	Chromosome	GO	Gene ontology
CIMS	Crosslink-induced mutation site	gRNA	Guide RNA
CITS	Crosslink-induced truncation site	GSC	Glioblastoma stem cell
cm⁵s²U	5-carboxymethyl-2-thiouridine	GWAS	Genome-wide association study
cm⁵U	5-carboxymethyluridine	HA2	Helicase-associated domain
CMTR1/2	Cap-specific mRNA 2'-O-methyltransferase 1/2	HIF1	Hypoxia inducible factor 1
CNOT complex	CCR4-NOT complex	hm⁵C	5-hydroxymethylcytidine

hm⁵Cm	2'-O-methyl-5-hydroxymethylcytidine		1B
hm⁶A	N6-hydroxymethyladenosine	MAT2A	Methionine adenosyltransferase 2A
HNRNP	Heterogeneous nuclear ribonucleoprotein	MAZTER-seq	MazF RNase assisted cleave of RNA at unmethylated sites within ACA motifs
HRP	Horse radish peroxidase		
HYB domain	Hakai pTyr-binding domain	mcm⁵s²U	5-methoxycarbonylmethyl-2-thiouridine
I	Inosine	mcm⁵U	5-methoxycarbonylmethyl uridine
IAP	Intracisternal A particle		
IGF2BP	Insulin-like growth factor 2 mRNA-binding proteins	MEIOC	Meiosis-specific coiled-coil domain-containing
IP	Immunoprecipitation	MeRIP	m ⁶ A-methylated RNA immunoprecipitation
kb	Kilobase(s)	mES cells	Mouse embryonic stem cells
KD	Knock down	METTL	Methyltransferase Like
kDa	Kilodalton(s)	miCLIP	m ⁶ A-Methylation iCLIP
KH domain	K-homology domain	miRNA	Micro RNA
KO	Knock out	mRNA	Messenger RNA
LC-MS/MS	Liquid chromatography with tandem mass spectrometry	MSA	Muscle surface area
LINE1	Long interspersed nuclear elements	msl-2	male-specific lethal-2
LLPS	Liquid-liquid phase separation	MTase	Methyltransferase
lncRNA	Long non-coding RNA	MTD	Methyltransferase domain
m¹A	N1-methyladenosine	MZT	Maternal-to-zygotic transition
m²G	N2-methylguanosine	NAT10A	N-Acetyltransferase 10A
m₂²G	N2,N2-dimethylguanosine	ncRNA	Non-coding RNA
m³C	3-methylcytidine	NES	Nuclear export signal
m³U	3-methyluridine	Nito	Spenito
m⁵C	5-methylcytidine	NLS	Nuclear localisation signal
m⁶A	N6-methyladenosine	Nm	2'-O-ribose methylation
m⁶ACE-seq	m ⁶ A crosslinking exonuclease sequencing	NMJ	Neuromuscular junction
m⁶A-LAIC-seq	Level and isoform characterization sequencing	NRL	Nucleotide recognition lid
m⁶A-SAC-seq	m ⁶ A-selective allyl chemical labeling and sequencing	NSUN	NOP2/Sun RNA Methyltransferase
m⁶Am	N6,2'-O-dimethyladenosine	nt	Nucleotide(s)
m⁷G	N7-methylguanosine	NXF1	Nuclear RNA export factor 1
MAC	m ⁶ A-METTL complex	O⁶mG	O6-methylguanine
MACOM	m ⁶ A-METTL-associated complex	OB fold	Oligo-nucleotide binding fold
MALAT1	Metastasis-associated lung adenocarcinoma transcript 1	OED	Oxidation-elimination-dephosphorylation
MAP1B	Microtubule-associated protein	ONT	Oxford nanopore technologies
		P bodies	Processing bodies
		PABP	Poly(A) binding protein
		PCIF1	PDX1 C-terminal inhibiting factor 1

piRNA	PIWI-interacting RNA	tra	transformer
poly(A) RNA	Poly-adenylated RNA	TREX	Transcription-export complex
PQ	Paraquat	TRIBE	ADAR-editing based detection of methylated region
PRRC2A	Proline rich coiled-coil 2A	TRMT	tRNA methyltransferase
Pus	Pseudouridine synthase	TRUB	TruB pseudouridine synthase
RAM	RNMT-activating miniprotein	tRNA	Transfer RNA
RBM15	RNA Binding Motif Protein 15	TSS	Transcription start site
RBP	RNA binding protein	U	Uridine
RecA	RecombinaseA	UTR	Untranslated region
RING domain	Really interesting new gene domain	Vir	Virilizer
RLR	RIG-I-like receptor	VIRMA	Vir-like m ⁶ A methyltransferase associated
RNA	Ribonucleic acid	WDR4	WD repeat domain 4
RNAi	RNA interference	WT	Wild type
RNA PolII	RNA polymerase II	WTAP	Wilms' tumour 1-associating protein
RNP	Ribonucleoprotein complex	XIST	X-inactive specific transcript
RNMT	RNA guanine-N7 methyltransferase	YTH	YT521-B homology
ROS	Reactive oxygen species	YTHDC	YTH domain-containing protein
rRNA	Ribosomal RNA	YTHDF	YTH domain-containing family protein
RT-qPCR	Quantitative reverse transcription-PCR	ZC3H13	Zinc finger CCCH domain-containing protein 13
RUNX1T1	Runt-related transcription factor 1	αKGD	Fe(II)- and α-ketoglutarate-dependent dioxygenase
SAH	S-adenosylhomocysteine	εA	1,N6-ethenoadenine
SAM	S-Adenosyl methionine	εC	3,N4-ethenocytosine
SCARLET	Site-specific cleavage and radioactive-labelling followed by ligation-assisted extraction and thin-layer chromatography	εG	1,N2-ethenoguanine
siRNA	Small interfering RNA	Ψ	Pseudouridine
snoRNA	Small nucleolar RNA		
SNP	Single-nucleotide polymorphism		
snRNA	Small nuclear RNA		
SRSF	Serine/arginine-rich splicing factor		
ss	Single-stranded		
Sxl	Sex lethal		
T	Thymine		
TET	Ten-eleven translocation		
TGIRT	Thermostable group II intron reverse transcriptase		
THOC	THO complex subunit		
TNT-seq	Transient N6-methyladenosine transcriptome sequencing		

Abstract

In all kingdoms of life, cellular RNAs are naturally decorated with a great number of different chemical modifications that constitute the so-called epitranscriptome. Like epigenetic DNA and histone modifications, RNA modifications represent one of the important mechanisms of precise gene expression regulation in living organisms. The majority of known RNA modifications are found on abundant non-coding RNAs, such as ribosomal RNA and transfer RNA, nonetheless messenger RNA (mRNA) is also modified by a dozen different chemical marks. m⁶A (N⁶-methyladenosine) is the most abundant internal modifications on eukaryotic mRNA and is regulated by three classes of proteins: methyltransferases or “writers”, demethylases or “erasers” and m⁶A-binding proteins or “readers”. Through its effects on mRNA structure, localization, splicing, stability, and translation, m⁶A influences many biological processes, including stem cell renewal and differentiation, brain function, immunity, and cancer progression.

Over the last decade, technical progress in biochemical detection methods together with countless studies in different model organisms made m⁶A the best-characterized epitranscriptomic mark so far. Nevertheless, our understanding of m⁶A biogenesis, molecular functions as well as biological relevance is far from being complete. The main aim of this PhD thesis was to expand our knowledge of this new layer of gene expression regulation with a focus on specific aspects of the m⁶A pathway that are still poorly investigated in *Drosophila melanogaster*. Molecular biology techniques along with transcriptomic and proteomic analysis were used to characterize components of the m⁶A writer complex and to explore the function of well-known as well as potential new m⁶A readers. Gene-specific knockout and gain-of-function transgenic fly lines were generated using the CRISPR-Cas9 system to study m⁶A functions *in vivo*. Our results showed that Hakai is a conserved core component of the m⁶A methyltransferase complex and plays a key role in the stabilization of other subunits (Vir, Fl(2)d and Flacc) of the m⁶A writing machinery independently of its enzymatic activity. Characterization of the m⁶A-binding proteins revealed that Ythdf is the main m⁶A reader in the nervous system of flies and directly interacts with Fmr1 to guide its mRNA target selection. Mechanistically, we showed that the m⁶A pathway controls larval NMJ morphology primarily via the Ythdf/Fmr1-mediated translational repression of the synaptic microtubule regulator futsch. In addition, we found that the uncharacterized RNA helicase Dhx57 preferentially binds to m⁶A-modified RNA in the GGACU sequence context independently from Ythdf and that Dhx57 mutants mimic the NMJ overgrowth phenotype of most m⁶A mutants. Although the m⁶A erasers FTO and ALKBH5 are found only in vertebrate species, other members of the same family of demethylases are conserved in flies. By exploring functions and targets of the least characterized member of the ALKBH family, we showed that Alkbh6 expression increases in response to different types of abiotic stress and its loss makes flies hypersensitive to oxidative stress and starvation.

Novel findings presented in this study substantially improved our understanding of the composition of the m⁶A writer machinery as well as highlighted the importance of this modification for proper neuronal development of flies. In addition, we created an important resource of data and tools for further characterization of Dhx57 as potential new m⁶A reader and Alkbh6 as important player in the cellular response to stress.

Résumé

Dans tous les règnes du vivant, les ARN sont naturellement décorés d'un grand nombre de modifications chimiques qui constituent ce que l'on appelle l'épitranscriptome. Comme les modifications épigénétiques de l'ADN et des histones, les modifications de l'ARN représentent l'un des nombreux mécanismes de régulation de l'expression génétique dont dépendent les organismes vivants. La majorité des modifications connues de l'ARN se trouvent sur des ARN non codant abondants, tels que les ARN ribosomiaux et les ARN de transfert, mais les ARN messagers (ARNm) sont également modifiés par une douzaine de marques chimiques différentes. m⁶A (N6-méthyladénosine) est la modification interne la plus abondante sur l'ARNm eucaryote et elle est régulée par trois classes de protéines: les méthyltransférases ou "writers", les déméthylases ou "erasers" et les protéines de liaison à la m⁶A ou "readers". Par ses effets sur la structure, la localisation, l'épissage, la stabilité et la traduction de l'ARNm, m⁶A influence de nombreux processus biologiques, notamment le renouvellement et la différenciation des cellules souches, les fonctions cérébrales, l'immunité et la progression du cancer.

Au cours de la dernière décennie, les progrès techniques réalisés dans les méthodes de détection biochimique ainsi que les innombrables études dans différents organismes modèles ont fait de m⁶A la marque épitranscriptomique la mieux caractérisée à ce jour. Néanmoins, notre compréhension de la biogenèse de m⁶A, de ses fonctions moléculaires et de sa pertinence biologique est loin d'être complète. L'objectif principal de cette thèse de doctorat était d'élargir nos connaissances sur cette nouvelle dimension de régulation de l'expression génétique en se concentrant sur des aspects spécifiques de la voie m⁶A qui sont encore peu étudiés dans l'organisme modèle *Drosophila melanogaster*. Des techniques de biologie moléculaire ainsi que des analyses transcriptomiques et protéomiques ont été utilisées pour caractériser les composants du complexe de déposition de m⁶A et pour explorer la fonction de readers connus de m⁶A ainsi que de potentiels nouveaux readers de cette modification. Des lignées de mouches transgéniques de knock-out et de surexpression spécifiques de gènes ont été générées à l'aide du système CRISPR-Cas9 afin d'étudier les fonctions de m⁶A *in vivo*. Nos résultats ont montré que Hakai est un composant central conservé du complexe méthyltransférase m⁶A et qu'il joue un rôle clé dans la stabilisation d'autres sous-unités de la machinerie d'écriture m⁶A (Vir, Fl(2)d et Flacc), indépendamment de son activité enzymatique. La caractérisation des protéines liant m⁶A a révélé que Ythdf est le principal reader de m⁶A dans le système nerveux des mouches et qu'il interagit directement avec Fmr1 pour guider la sélection de l'ARNm cible. D'un point de vue mécanistique, nous avons montré que la voie m⁶A contrôle la morphologie de la jonction neuromusculaire (NMJ) larvaire principalement via la répression traductionnelle du régulateur des microtubules synaptiques futsch médiée par Ythdf/Fmr1. En outre, nous avons découvert que l'hélicase ARN non caractérisée Dhx57 se lie préférentiellement à l'ARN modifié par m⁶A dans le contexte de séquence GGACU indépendamment de Ythdf et que les mutants Dhx57 présentent un phénotype de surcroissance de la NMJ similaire à celui observé dans la plupart des mutants m⁶A. Bien que les erasers de m⁶A FTO et ALKBH5 ne soient présents que chez les vertébrés, d'autres membres de la même famille de déméthylases sont conservés chez les mouches. En explorant les fonctions et les cibles du membre le moins caractérisé de la famille ALKBH, nous avons montré que l'expression d'Alkbh6 augmente en réponse à différents types de stress abiotiques et que sa perte rend les mouches hypersensibles au stress oxydatif et jeûne.

Les nouveaux résultats présentés dans cette étude ont considérablement amélioré notre compréhension de la composition de la machinerie d'écriture de la m⁶A et ont mis en évidence l'importance de cette modification pour le bon développement neuronal des mouches. En outre, nous avons créé une ressource importante de données et d'outils pour une caractérisation plus poussée de Dhx57 en tant que nouveau reader potentiel de m⁶A et d'Alkbh6 en tant qu'acteur important de la réponse cellulaire au stress.

1. Introduction

1.1 RNA modifications

In the last decades, the notion that the RNA alphabet contains a much larger set of building blocks than the four canonical A, C, G and U nucleotides revolutionized the study of RNA biology and resulted in the birth of a novel field called epitranscriptomics. According to the MODOMICS database, more than 100 distinct types of post-transcriptional chemical modifications have been identified so far across all kingdoms of life and RNA species (Boccaletto et al., 2022). The modified ribonucleotides differ from the canonical ones both in structure and function adding a new layer of information to the sequence of RNA molecules.

The first ever RNA modification to be discovered more than half a century ago was pseudouridine (Ψ) (Cohn & Volkin, 1951). This isomer of uridine (Cohn, 1959; Yu & Allen, 1959) is overall the most frequent RNA modification and, for a short period of time, was believed to be the fifth ribonucleotide (Davis and Allen 1957). Instead, in the following years, more and more RNA modifications were added to the list for a total of 143 ribonucleoside residues known today (Boccaletto et al., 2022) (**Figure 1**). Roughly half of them involve the addition of one or more methyl groups to the ribonucleotides, making the simplest modification also the most common one. Possible targets of the methylation reaction are the four nitrogenous bases — at carbon (e.g., 5-methylcytidine (m^5C)), as well as cyclic (e.g., N1-methyladenosine (m^1A)) or exocyclic (e.g., N6-methyladenosine (m^6A)) nitrogen atoms — and the 2'OH of the ribose moiety (2'-O-methylation (Nm)). Other examples of RNA chemical modifications include deamination, carbamoylation, hydroxylation, acetylation, glycosylation, thiolation, etc. The presence of specific modifications can affect some of the biochemical properties of canonical ribonucleotides, such as charge, hydrophobicity, and base-pairing ability, giving rise to changes that in turn modulate RNA structure and processing as well as recognition by RNA binding proteins.

Most modified ribonucleotides were at first identified just within the most abundant classes of RNA, such as ribosomal RNA (rRNA) and transfer RNA (tRNA), and only later found to be present also in messenger RNA (mRNA), long non-coding RNA (lncRNA) and small RNAs. Some of these marks are essential for RNA biogenesis, folding and function, while others control dynamically the fate of specific RNA molecules in a context- or time-dependent manner.

1.2 Non-coding RNAs modifications

With approximately 17% of the total nucleotides being modified, tRNA is by far the most heavily modified species of RNA (Machnicka et al, 2014). tRNAs display a wide variety of RNA modifications, from relatively simple ones, such as m^1A , m^5C , Nm and Ψ , to very complex ones, such as 2'-O-methyl-5-hydroxymethylcytidine (hm^5Cm), 5-methoxycarbonylmethyl-2-thiouridine (mcm^5s^2U) and 3-(3-amino-3-carboxypropyl)uridine (acp^3U) (Suzuki, 2021). Modification identity, localization and prevalence is variable in different tRNAs, even within the ones that recognize alternative codons for the same amino acid residue.

1. Introduction

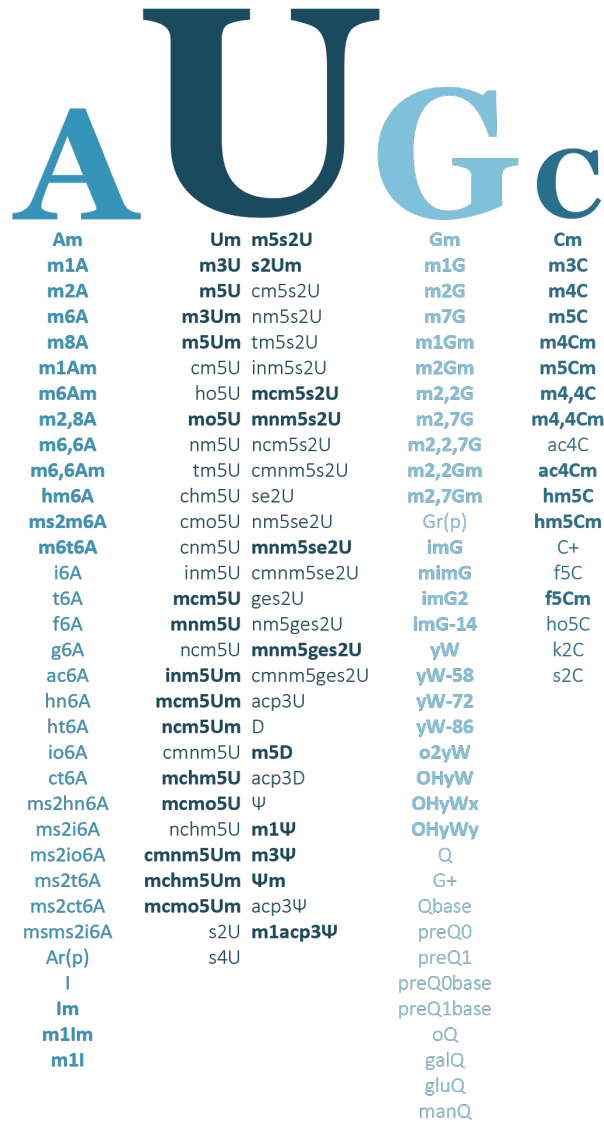


Figure 1. Diversity of chemical RNA nucleoside modifications.

RNA chemical modifications are listed below the corresponding canonical ribonucleoside. Character size of the four canonical ribonucleotides is proportional to the number of chemical modifications identified for each of them. Modifications involving methylation are highlighted in bold. Data extrapolated from the MODOMICS database (Boccaletto et al., 2022).

Two positions in the anticodon stem-loop of tRNAs represent major modification hotspots across the tree of life: modifications at the wobble position 34 ensure precise decoding either by expansion or restriction of codon-anticodon recognition, while a modified position 37 is important to avoid ribosomal frameshift and ensure translation fidelity (Suzuki, 2021). In the tRNA body, the presence of modified nucleotides was shown to mostly affect the equilibrium between flexibility and stability rather than the overall structure of tRNAs (Motorin & Helm, 2010). As a matter of fact, *in vitro* transcribed unmodified tRNA^{Phe} from *Escherichia coli* has essentially the same L-shaped tertiary structure as that of the mature fully modified tRNA^{Phe} from yeast (Byrne et al., 2010).

1. Introduction

Although the RNA component of ribosomes is also relatively highly modified (~2% of total nucleotides), the variety of modifications found in rRNA is restricted compared to tRNA. The most common modifications of eukaryotic rRNA are Nm of the sugar moiety of any nucleotide and Ψ . These modifications are synthesized in the nucleolus by enzymes that generally use RNA guides (box C/D and box H/ACA small nucleolar RNAs (snoRNAs) for Nm and Ψ , respectively) to recognize their target sites (Watkins & Bohnsack, 2012). In addition to modifications that stabilize the local folding of the rRNA scaffold, functionally important regions of the ribosome, such as the peptidyl transferase and the decoding centers, are characterized by numerous modified nucleotides that act in concert to guarantee efficient and accurate protein synthesis (Sloan et al., 2017). Interestingly, it has been recently shown that the modification profile of rRNA also contributes to ribosome heterogeneity giving rise to distinct ribosome populations able to selectively translate or fine-tune the translational efficiency of specific transcripts in response to developmental or environmental stimuli and in certain diseases (Gay et al., 2022).

RNA modifications play an important role also in the world of small RNAs. Spliceosomal small nuclear RNAs (snRNAs) are extensively modified with Ψ , Nm and the occasional m⁶A, which influence spliceosome assembly as well as the efficiency of splicing reactions. Micro RNAs (miRNAs), small interfering RNAs (siRNAs) and PIWI-interacting RNAs (piRNAs) share a common protective mechanism that uses Nm at the 3' end to prevent exonuclease degradation (Ontiveros et al., 2019).

1.3 mRNA modifications

Far from the vast range of chemical marks decorating tRNAs, only a small selection of modifications has been detected on protein coding RNAs so far (**Figure 2**). It is important to keep in mind that validating the presence of modifications on mRNA is made challenging by several difficulties, such as the low prevalence of most mRNA modifications, the almost impossibility to obtain completely pure mRNA samples as well as technical problems and biases of the available mapping methods.

1.3.1 The 5' cap and its modifications

The most distinctive, and very essential, mRNA modification is nothing else but the 5' cap (Busch 1976). The first nucleotide of almost every eukaryotic transcript is decorated with N7-methylguanosine (**m⁷G**), which is deposited by the RNMT/RAM methyltransferase complex as soon as the first tens of nucleotides are transcribed. The methylated guanosine is connected to mRNA's first nucleotide via an unusual 5' to 5' triphosphate link (m⁷GpppN), which shields the 5' end of transcripts from 5'→3' exonuclease degradation. In the nucleus, the cap is recognized by the nuclear cap-binding complex (CBC), which interacts with components of the spliceosome for efficient pre-mRNA splicing and with the nuclear export complex for directional translocation of transcripts to the cytoplasm. Always via CBC mediation, the cap is also involved in mRNA 3' end processing as well as transcription termination. In the cytoplasm, the interaction of CBC with the eukaryotic initiation factor 4G (eIF4G) is essential to recruit, among others, the RNA helicase eIF4A and the two ribosomal subunits. After a pioneer first round of translation, CBC is completely replaced by eIF4E, and mRNA circularization is driven by the interaction between eIF4G and the poly(A) binding protein (PABP): cap-dependent bulk protein synthesis can begin (Galloway &

1. Introduction

Cowling, 2019). In higher eukaryotes, the 5' end of transcripts is further modified with **Nm** of the first and second transcribed nucleotide (m⁷GpppNmNm) catalyzed by the stand-alone methyltransferases CMTR1 (Bélanger et al., 2010; Haline-Vaz et al., 2008) and CMTR2 (Werner et al., 2011), respectively. Notably, Nm at these positions is used by the innate immune system as a key signature to discriminate between self and non-self mRNAs (Abbas et al., 2017; Devarkar et al., 2016; Schuberth-Wagner et al., 2015). In the event that the cap-proximal nucleotide is Am, the adenosine can be additionally methylated at the N6 position by the methyltransferase PCIF1 (Akichika et al., 2019; Boulias et al., 2019; Sendinc et al., 2019; H. Sun et al., 2019) leading to the formation of N6,2'-O-dimethyladenosine (**m⁶Am**) in 92% of A-starting mRNAs (Akichika et al., 2019) and up to 30% of all mRNAs (C. M. Wei et al., 1975). The antibody-based miCLIP method, which can detect both m⁶A and m⁶Am, validated the presence of m⁶Am exclusively at transcription start sites (TSS) in a BCA sequence context (B = C/G/U) (Boulias et al., 2019; Linder et al., 2015; Mauer et al., 2017; Sendinc et al., 2019). The few internal m⁶Am sites derive from mRNA isoforms with alternative TSSs (Boulias et al., 2019). m⁶Am can be demethylated to Am by FTO (Mauer et al., 2017; J. Wei et al., 2018). Remarkably, the *Drosophila* Pcif1 is catalytically dead, however it retains the ability to bind the Ser5-phosphorylated CTD of Pol II, suggesting that fly Pcif1 might have evolved to function as a nuclear factor that transcriptionally regulates gene expression (Pandey et al., 2020).

Initially, m⁶Am has been reported to increase expression and stability of some of the modified mRNAs by hindering the activity of the decapping enzyme DCP2 (Mauer et al., 2017). However, following studies described different and sometimes conflicting results: on one hand m⁶Am was reported to be the most common first nucleotide of highly abundant and stable transcripts but without any direct effect on either translation or stability (Boulias et al., 2019), while on the other hand m⁶Am-containing transcripts were shown to be either better (Akichika et al., 2019) or less well translated (Sendinc et al., 2019). Further work is needed to bring order and elucidate the role of m⁶Am in mRNA function and metabolism.

1.3.2 Guanosine modifications

Recently, the existence of internal **m⁷G** in mammalian mRNA was reported by three independent groups (Chu et al., 2018; Malbec et al., 2019; L. S. Zhang et al., 2019). Transcriptome-wide mapping via m⁷G-miCLIP-seq (Malbec et al., 2019) or m⁷G-MeRIP-seq coupled with m⁷G-seq (L. S. Zhang et al., 2019), revealed that m⁷G is enriched in AG-rich contexts and is found in the 5'UTR (Malbec et al., 2019) as well as in the CDS and in the 3'UTR of transcripts (L. S. Zhang et al., 2019). The METTL1-WDR4 heterodimer complex, already known to deposit m⁷G on tRNAs, was shown to methylate a subset of these sites (L. S. Zhang et al., 2019). Interestingly, the presence of internal m⁷G correlates with high translation efficiency and the modification deposition profile is dynamically regulated in response to thermal and oxidative stress (Malbec et al., 2019). Nevertheless, mapping via m⁷G mutational profiling sequencing (m⁷G-MaP-seq), did not identify any internal m⁷G site in mRNA from *Escherichia coli* and *Saccharomyces cerevisiae* (Enroth et al., 2019), indicating that future work is required to provide more conclusive insights regarding the presence of mRNA internal m⁷G sites.

1.3.3 Cytidine modifications

Although the presence of cytidine methylation (m^5C) as well as hydroxymethylation (hm^5C) on mRNA had already been demonstrated via liquid chromatography-mass spectrometry (LS-MS) (L. Fu et al., 2015; W. Huang et al., 2016; Huber et al., 2015), accurate transcriptome-wide map of m^5C at nucleotide resolution became available only recently thanks to miCLIP (Hussain et al., 2013; Selmi et al., 2021) as well as an optimized bisulfite sequencing protocol (T. Huang et al., 2019). In human and mouse tissues, several hundred high-confidence methylation sites with variable stoichiometry (15-18% median methylation) were identified on mRNA with high density in the 5'UTR and near start codons (T. Huang et al., 2019). Approximately 60% of the sites were found to be NSUN2-dependent and enriched in the same sequence and structural context as that of m^5C sites deposited by NSUN2 on tRNA ($\underline{C}NGGG$ in the 5' end of a stem region) (T. Huang et al., 2019). A different motif ($\underline{C}TCCA$ in the loop of a stem-loop structure) was identified in NSUN2-independent sites (T. Huang et al., 2019) and only later discovered to be targeted by NSUN6 (Selmi et al., 2021). While transcripts decorated with NSUN2-deposited m^5C , especially in the CDS, are simultaneously more stable and less well translated compared to unmodified ones (Schumann et al., 2020), NSUN6-targeted motifs are enriched in 3'UTRs near translation termination sites and their presence correlates with increased transcript abundance and translation efficiency (Selmi et al., 2021). Some of the effects of m^5C might be mediated by the Y-box binding protein 1 (Ybx1), which was recently shown to preferentially recognize m^5C -modified maternal mRNAs and promote their stability during zebrafish maternal-to-zygotic transition (Y. Yang et al., 2019). Transcripts decorated with m^5C are also recognized in the nucleus by the mammalian mRNA export adaptor ALYREF, which promotes their export to the cytoplasm (X. Yang et al., 2017). Exactly as it happens to 5mC on DNA, m^5C on RNA can also be hydroxylated to hm^5C by the ten-eleven translocation (TET1-2-3) enzymes (L. Fu et al., 2014) and the modification levels varies from 0.001 to 0.004% of total cytidines in human mRNA (Huber et al., 2015). A transcriptome-wide map of hm^5C is only available in *Drosophila melanogaster*: hm^5C generated by the fly ortholog dTet is mainly localized in CDSs and its abundance on transcripts positively correlates with protein translation (Delatte et al., 2016). Interestingly, highest level both of dTet and hm^5C are observed in the fly brain and depletion of dTet (lethal at late pupal stages) leads to impaired neuronal development in larvae (Delatte et al., 2016).

Two additional cytosine modifications were recently identified on mRNA: m^3C (~0.004% of total C) deposited by the methyltransferase METTL8 (L. Xu et al., 2017) and ac^4C (~0.2% of total C) catalyzed by the acetyltransferase NAT10A and associated with enhanced transcript stability and translation efficiency (Arango et al., 2018, 2022). However, latest transcriptome-wide mapping of m^3C failed to detect METTL8-dependent modification sites in mRNA (J. Cui et al., 2021; Marchand et al., 2018) and METTL8 was shown to be instead responsible for deposition of m^3C at position 32 of mitochondrial tRNA^{Ser(UCN)} and tRNA^{Thr} (Kleiber et al., 2022; Schöller et al., 2021). Although ac^4C was shown to be present in archaeal (Sas-Chen et al., 2020) and yeast mRNA (Tardu et al., 2019), no confirmatory evidence for the presence of ac^4C in human mRNA could be found (Sas-Chen et al., 2020), suggesting that this modification is either present at ultra-low levels or completely absent in human mRNA.

1. Introduction

1.3.4 Adenosine modifications

The most common adenosine modification on mRNA is **m⁶A**. Discovery, biogenesis and functions of this RNA mark will be discussed in detail in the following chapters.

After long and bitter controversies (Wiener & Schwartz, 2021), it appears that mammalian mRNA features only scattered internal **m¹A** sites, which are methylated at low to undetectable levels (Schwartz, 2018). The only exceptionally highly methylated site, modified by TRMT10C, is located on the mitochondrial mRNA *ND5* (Safra, Sas-Chen, et al., 2017). In cytosolic mRNA, m¹A occurs in a sequence and structural context identical to that of position 58 of tRNA T-loop and is deposited by the TRMT6/TRMT61A complex (Safra, Sas-Chen, et al., 2017).

Outside the realm of methylation, adenosine can also be converted into inosine by the adenosine deaminase acting on RNA (ADAR) enzymes in a process known as **A-to-I** RNA editing (Nishikura, 2016). Since inosine is recognized by ribosomes as guanosine during translation, A-to-I changes within the CDS of mRNAs can fundamentally alter the aminoacidic sequence and consequently the function of the resulting proteins. The so-called recoding-type editing affects only a relatively small number of transcripts, mostly express in the brain. In vertebrates, one representative case is the mRNA coding for the AMPA glutamate receptor subunit *GluA2* (also known as *GluR2* or *GluR-B*), whose editing by ADAR2 leads to a Gln to Arg substitution (Q/R site) that makes the receptor channel impermeable to calcium. Notably, ~99% of the *GluA2* transcripts are edited across the mammalian brain and the prevention of calcium entry into the cell on activation of *GluA2*(R)-containing AMPARs was proposed to protect the central nervous system against excitotoxicity (Wright & Vissel, 2012). More recently, improvements in sequencing techniques and analysis methods allowed the identification of many previously unknown A-to-I editing sites across the human transcriptome. The vast majority of editing events were observed in introns and 3'UTRs harboring inverted Alu repeats forming intramolecular double-stranded RNAs. Strikingly, more than 85% of the human pre-mRNAs are subjected to editing at these regions supporting the notion that A-to-I editing plays a key role in exonization of intronic Alu repetitive elements and in the global regulation of alternative splicing (Athanasiadis et al., 2004; Nishikura, 2016).

1.3.5 Uridine modifications

Due to lack of evidence, for decades Ψ was believed not to occur naturally on mRNA. In 2014, the development of new nucleotide-resolution mapping methods (Pseudo-seq, Ψ -seq, PSI-seq) revealed that both yeast and human transcriptome contain hundreds of Ψ sites deposited by different snoRNA-dependent or -independent Ψ synthases (PUS) (Carlile et al., 2014; Lovejoy et al., 2014; Schwartz, Bernstein et al., 2014). Ψ levels of most sites are dynamically regulated in response to environmental conditions, such as cellular growth state (Carlile et al., 2014) and heat shock (Schwartz, Bernstein, et al., 2014). The prevalence of Ψ in the human transcriptome was validated and further expanded by CeU-seq, which identified thousands of Ψ sites in mRNA and ncRNA from HEK293T cells (X. Li et al., 2015) and TRUB1 (Carlile et al., 2019; Safra, Nir et al., 2017) was proposed as the predominant mRNA pseudouridylating enzyme in humans. In human cancer cells, Pseudo-seq on chromatin-associated nascent RNA showed that Ψ is deposited co-transcriptionally with an enrichment in introns flanking alternatively spliced exons and within splicing factor binding sites. Depletion of the identified pre-mRNA

1. Introduction

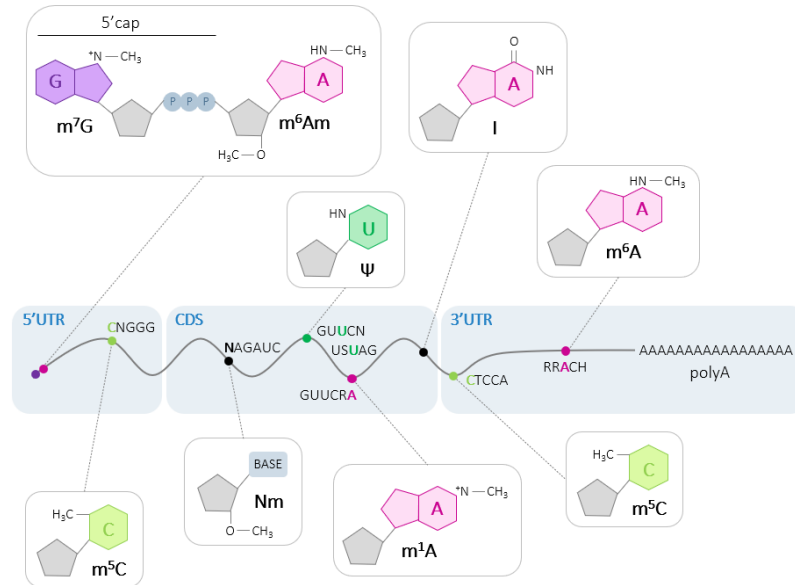
PUS enzymes (PUS1, PUS7 and RPUSD4) considerably affected alternative splicing as well as alternative polyadenylation (Martinez et al., 2022). Making use of the reactivity of bisulfite towards Ψ , two independent labs recently developed new methods that allow transcriptome-wide Ψ detection and provide stoichiometry information for abundant Ψ sites: BS-induced deletion sequencing (BID-seq) (Dai et al., 2023) and pseudouridine assessment via bisulfite/sulfite treatment (PRAISE) (M. Zhang et al., 2023). Hundreds of Ψ sites mostly located in CDSs and 3'UTRs were identified within GU Ψ CN and US Ψ AG (S=C/G) motifs (Dai et al., 2023; M. Zhang et al., 2023). Although it is clear that multiple PUS enzymes contribute to pseudouridylation of mammalian mRNAs, the majority of Ψ sites in mRNA were shown to be deposited by TRUB1, resulting in increased transcript stability and stop codon readthrough in specific cases (Dai et al., 2023).

In 2022, dihydrouridine (**D**) was discovered as a component of the mRNA epitranscriptome thanks to two newly developed mapping methods based on chemical conversion (Rho-seq (Finet et al., 2022) and D-seq (Draycott et al., 2022)). Hydrogenation of uridine to dihydrouridine by the dihydrouridine synthases (DUS) represents the second most abundant tRNA modification and is typical of the homonym tRNA D-loop (Machnicka et al., 2014). D is a structurally unique modification, whose presence has the potential to destabilize RNA helical conformation and allow greater molecular flexibility. D sites were identified on a subset of yeast and human mRNAs, prevalently within the CDS. In a couple of specific cases, D was shown to have a role in either splicing regulation (Draycott et al., 2022) or translation repression (Finet et al., 2022), however the overall functional relevance of D on mRNA is still under investigation.

1.3.6 Ribose modifications

In addition to its conspicuous presence on rRNAs, tRNAs and snRNAs as well as at the first and second cap-proximal nucleotides, **Nm** has been recently discovered at internal sites on mRNA thanks to the development of Nm-seq to map 2'-O-methylation at nucleotide resolution in low abundant RNA species (Dai et al., 2017). Unlike 2'OMe-seq (Incarnato et al., 2017) and RiboMeth-seq (Birkedal et al., 2014; Krogh et al., 2016; Marchand et al., 2016), which have a negative readout and rely on Nm ability to pause RT in the presence of limited amounts of dNTPs or to protect nucleotides from alkaline hydrolysis, respectively, Nm-seq takes advantage of repetitive rounds of oxidation-elimination-dephosphorylation (OED) to eliminate unmodified nucleotides and enrich for Nm-modified ones at the 3' end of RNA fragments (Dai et al., 2017; Hsu, Fei et al., 2019). In human mRNA, 2'-O-methylation is found on every base (highest abundance on uridine) and Nm sites concentrate mostly within the CDS directly upstream of an AGAUC consensus sequence (Dai et al., 2017). Although the enzyme catalyzing Nm deposition on mammalian transcripts is still unknown and questions were raised on the validity of the Nm-seq method (Grozhek & Jaffrey, 2018), Spb1 was identified as the predominant mRNA Nm methyltransferase in yeast and was shown to catalyze mostly Um on hundreds of transcripts (Bartoli et al., 2018). The functional consequences of the presence of Nm on mRNA are still unclear.

1. Introduction



	m ⁷ G	m ⁶ Am	m ⁵ C	Nm	ψ	m ¹ A	I	m ⁶ A
Writers	RNMT-RAM (cap) METTL1-WDR4 (AG-rich regions)	PCIF1 (BCA) B=C/G/U	NSUN2 (CNGGG, stem 5' end) NSUN6 (CTCCA, hairpin loop)	CMTR1-2 (next to cap) Spb1, yeast (NAGAUC)	TRUB1 PUS7, PUS1, RPUSD2 (GUUCN and USUAG) S=C/G	TRMT6-61A (GUUCRA, tRNA T-loop like structure) R=A/G	ADAR1-2	METTL3-14 +MACOM (RRACH) R=A/G, H=A/C/U
Erasers	-	FTO	-	-	-	ALKBH3	-	ALKBH5, FTO
Readers	-	-	ALYREF YBX1	-	-	-	-	YTHDF1-2-3 YTHDC1-2 ...
Abundance	0.45% (global) 0.02-0.05% (internal)	0.02-0.05%	0.025-0.095%	0.01-0.15%	0.2-0.6%	0.015-0.05%	1/17000 nt (rat brain)	0.4-0.7%

Figure 2. mRNA modifications.

Structure and localization of the main modifications found on mRNA are depicted above. Abundance and enzymes involved in the deposition, removal and recognition of each modification are listed in the table below.

1.4 m⁶A modification

The presence of m⁶A on RNA was discovered in the mid-1970s (Desrosiers et al., 1974; Perry & Kelley, 1974; C. M. Wei et al., 1975). Not long after this finding, m⁶A was the first methylated nucleotide to be detected at mRNA internal positions with approximately two m⁶A modifications every thousand nucleotides in mRNA from HeLa cells (C. M. Wei et al., 1976). Moreover, m⁶A residues were shown to be nonrandomly located but exclusively found within an A/GAC consensus sequence (C. M. Wei et al., 1976) as well as clustered in the 3' end of cellular (Carroll et al., 1990; Horowitz et al., 1984; Narayan & Rottman, 1988) and viral transcripts (Beemon & Keith, 1977; Kane & Beemon, 1985). During the 1990s, using an adapted *in vitro* methylation assay (Narayan & Rottman, 1988) and synthetic RNA substrates, the mRNA m⁶A methyltransferase was identified and partially purified from HeLa cells nuclei (Bokar et al., 1994; Tuck, 1992) revealing surprising complexity and a multimeric nature. The m⁶A-catalyzing enzyme resulted to be composed of two sub-complexes: MT-A (200 kDa) and MT-B (875 kDa) (Bokar et al., 1994, 1997). For a long time, the identity of the individual protein components of the complex remained

1. Introduction

unknown except for the 70 kDa protein MT-A70 (today renamed as METTL3), identified as carrier of the SAM-binding activity and part of MT-A (Bokar et al., 1994, 1997).

Before more light could be shed on the composition of the m⁶A methyltransferase complex, and more than three decades after m⁶A was first discovered on mRNA, interest in the field was reawakened by the publication of the first transcriptome-wide analysis of the mammalian m⁶A profile (Dominissini et al., 2012; Meyer et al., 2012). Two independent research groups developed antibody-based mapping methods (MeRIP-seq (Meyer et al., 2012) and m⁶A-seq (Dominissini et al., 2012)), which showed that m⁶A decorates thousands of mammalian transcripts with an evolutionary conserved enrichment near stop codons and in 3'UTRs as well as within long internal exons. Results of these studies fully recapitulated, and to a small extent expanded, the previously established m⁶A motif RRACH (R = A/G, H = A/C/U) (Dominissini et al., 2012; Meyer et al., 2012). Although this short consensus sequence is scattered throughout the transcriptome, the conserved distinctive profile of m⁶A along transcripts suggested that methylation enrichment in long exons and close to stop codons might have been of functional importance for splicing and translation regulation.

During the following decade, the number of publications about m⁶A grew exponentially year after year and the modification was shown to be involved in the regulation of many aspects of mRNA metabolism and beyond. The characterization of the m⁶A methyltransferase complex as well as the functions of the modification in molecular and biological processes will be described in the following chapters.

1.4.1 m⁶A writers

Three decades after its discovery (Bokar et al., 1994; Tuck, 1992), we currently have a solid knowledge about the protein composition of the m⁶A methyltransferase complex. As mentioned in the previous chapter, deposition of m⁶A on mRNA and lncRNA is catalyzed by a large protein entity of ~1000 kDa in size, which is composed of two multimeric sub-complexes: a smaller 200 kDa m⁶A-METTL complex or MAC (previously known as MT-A) and a larger 875 kDa m⁶A-METTL-associated complex or MACOM (previously known as MT-B) (Knuckles et al., 2018). In 2014, three independent groups used phylogenetic analysis coupled with tandem-affinity purification and identified METTL14 as partner of METTL3 and second element of the MAC complex (J. Liu et al., 2014; Ping et al., 2014; Y. Wang et al., 2014). Additionally, after that the corresponding plant (Fip37 (Zhong et al., 2008)) and yeast (Mum2 (Agarwala et al., 2012)) homologs were shown to directly interact with METTL3, Wilms' tumor 1-associating protein (WTAP) was validated as member of the complex also in mammals and zebrafish (J. Liu et al., 2014; Ping et al., 2014). Over the following years, other four proteins were demonstrated to be part of the MACOM complex together with WTAP: Vir-like m⁶A methyltransferase associated (VIRMA) (Schwartz, Mumbach et al., 2014), RNA-binding motif protein 15 (RBM15/15B) (Lence et al., 2016; Patil et al., 2016), zinc finger CCCH domain-containing protein 13 (ZC3H13) (Guo et al., 2018; Knuckles et al., 2018; Wen et al., 2018) and HAKAI (Růžička et al., 2017). The different subunits of the m⁶A methyltransferase complex are collectively known as “m⁶A writers”.

1. Introduction

– The MAC complex: a collaborative effort to write m⁶A

The MAC module of the m⁶A writer complex corresponds to the METTL3-METTL14 pseudosymmetric heterodimer. The two enzymes belong to the family of class I methyltransferases (MTases I) and form the catalytic core of the m⁶A writer complex. Similar to DNA 6mA MTases, enzymes that deposit m⁶A on RNA catalyze transfer of the methyl group of the S-adenosyl-methionine (SAM or AdoMet) donor substrate to target adenosines via a nucleophilic substitution (SN₂) reaction, which generates S-adenosyl-homocysteine (SAH or AdoHcy) as by-product. METTL3 and METTL14 share ~25% sequence identity and are both characterized by the presence of a classic MTase domain (MTD) with a Rossmann-type fold of alternating α -helices and β -sheets accommodating the [DNSH]PP[YFW] active site (Iyer et al., 2016). Nevertheless, partial crystal structures revealed that METTL3 is the sole SAM-binding, and therefore catalytically active, component of the MAC complex (Śledź & Jinek, 2016; P. Wang et al., 2016; X. Wang et al., 2016). Unlike the canonical active site of METTL3 (DPPW), METTL14 displays a degenerate catalytic motif (EPPL), which is unable to accommodate either the methyl donor substrate or the acceptor adenosine due to steric hindrance. Thus, the main function of METTL14 is not to transfer methyl groups but to provide structural support to the active conformation of METTL3. Moreover, extensive surface interactions between the MTD of METTL14 and the MTD of its partner in the MAC complex are essential to form an evolutionarily conserved electropositive groove for RNA binding (Śledź & Jinek, 2016; P. Wang et al., 2016; X. Wang et al., 2016). Two CCCH-type zinc finger motifs in the N-terminal region of METTL3 (Śledź & Jinek, 2016; P. Wang et al., 2016) and the C-terminal RGG repeats of METTL14 (Schöller et al., 2018) were also shown to be involved in target RNA recognition.

m⁶A deposition occurs co-transcriptionally and the METTL3-METTL14 heterodimer localizes in the nucleus with enrichment in nuclear speckles (Ping et al., 2014). Nuclear localization is driven by a nuclear localization signal (NLS) located in the N-terminal region of METTL3, while METTL14 is imported to the nucleus only in complex with METTL3 (Schöller et al., 2018).

Although the MAC complex is phosphorylated at several sites on both METTL3 (S2-43-48-50-219-243-350 and T348) and METTL14 (S399), their functional relevance is not entirely clear yet. METTL3's phosphorylated residues do not affect its catalytic activity, nuclear localization or binding to WTAP, and phosphorylation of METTL14 is not involved in either interaction with METTL3 or methylation activity of the MAC complex (Schöller et al., 2018). In contrast, sumoylation of four Lys residues (K177-211-212-215) in the N-terminal region of METTL3 significantly reduces its methyltransferase activity, probably impeding interaction with substrate RNAs (Y. Du et al., 2018). Just recently, phosphorylation of METTL3 (S43/S50/S525) and WTAP (S306/S341) by ERK has been shown to trigger deubiquitination of METTL3 by USP5 resulting in stabilization of the m⁶A methyltransferase complex (H. L. Sun et al., 2020). In addition, phosphorylation at S43 by ATM has been reported to activate METTL3 in response to DNA damage for efficient double strand breaks repair (C. Zhang et al., 2020).

– The MACOM complex: MAC's little helpers

The MACOM complex includes all the regulatory subunits of the m⁶A writer complex, which are not catalytically active but contribute to the correct assembly, localization, and function of the complex: WTAP, VIRMA, RBM15, ZC3H13 and HAKAI. Remarkably, back in 2013 almost all the MACOM components

1. Introduction

were found among the most strongly enriched proteins in the interactome of WTAP (Horiuchi et al., 2013), long before their involvement in m⁶A deposition was demonstrated.

WTAP is a nuclear protein known for its contribution to splicing regulation (Horiuchi et al., 2013; Little et al., 2000). In addition to the presence of a N-terminal NLS (Schöller et al., 2018), WTAP distribution in nuclear speckles is mediated by interaction with the SR-like proteins BCLAF1/THRAP3 (Horiuchi et al., 2013). As WTAP plays an essential role during development and cell cycle progression, its loss results in early embryonic lethality in plants (Vespa et al., 2004), flies (Granadino et al., 1990) and mice (Fukumami et al., 2008) as well as compromised tissue differentiation in zebrafish (Ping et al., 2014). The *Drosophila* homolog of WTAP, female-lethal-2-d (Fl(2)d), participates in the regulation of the alternative splicing of *Sex-lethal* (*Sxl*), a key controller of sex determination and dosage compensation in insects (Granadino et al., 1990). Within the m⁶A writer complex, the physical interaction between the N-terminal coiled-coil region of WTAP and the N-terminus of METTL3 allows specific localization of the METTL3-METTL14 heterodimer to nuclear speckles (Ping et al., 2014; Schöller et al., 2018) and depletion of WTAP leads to strong reduction of m⁶A levels on mRNA (Lence et al., 2016; J. Liu et al., 2014; Ping et al., 2014; Schwartz, Mumbach et al., 2014).

VIRMA, also known as KIAA1429, was identified among the most enriched factors in a proteomic screen that used METTL3 or WTAP as bait to unveil the composition of the human m⁶A methyltransferase complex (Schwartz, Mumbach et al., 2014). This result was in line with a previous study showing interaction between the fly homolog of VIRMA (Virilizer or Vir) and Fl(2)d in the context of *Sxl* splicing (Hilfiker et al., 1995; Ortega et al., 2003). Subsequently, VIRMA was proposed to have a role in guiding the writer complex for preferential installation of m⁶A near stop codons and in the 3'UTR of mRNAs (Yue et al., 2018). In this context, RNA-dependent interaction between VIRMA and the polyadenylation cleavage factors CPSF5 and CPSF6 suggested a possible role of the m⁶A methyltransferase complex in alternative polyadenylation (Yue et al., 2018). Similar to WTAP, loss of VIRMA is lethal (Hilfiker et al., 1995) and results in reduced m⁶A levels on mRNA (Lence et al., 2016; Schwartz, Mumbach et al., 2014).

RBM15 and its paralogue **RBM15B** were identified as subunits of the mammalian writer complex in the context of m⁶A deposition on the lncRNA X-inactive specific transcript (*XIST*) (Patil et al., 2016). miCLIP experiments revealed that *XIST* contains more than 70 m⁶A sites in the A-repeat domain (Linder et al., 2015) critical for X-chromosome inactivation in female placental mammals (C. J. Brown et al., 1991). RBM15 and RBM15B were shown to bind to METTL3 in a WTAP-dependent manner and to recruit the writer complex to *XIST* for adenosine methylation (Patil et al., 2016). m⁶A residues on *XIST* are recognized by YTHDC1 (see chapter 1.4.4) and are necessary for efficient *XIST*-mediated gene silencing (Patil et al., 2016). Concurrently, data produced in our lab showed that the fly homolog of RBM15, Spenito (Nito), is a component of the m⁶A methyltransferase complex in *Drosophila* and, as other m⁶A writers, is involved in *Sxl* splicing and sex determination (Lence et al., 2016). Depletion of both vertebrate RBM15/15B and fly Nito results in a substantial drop of m⁶A levels on mRNA (Lence et al., 2016; Patil et al., 2016).

ZC3H13 and its fly homolog Flacc (also known as Xio) were described in parallel as m⁶A writers in three independent studies (Guo et al., 2018; Knuckles et al., 2018; Wen et al., 2018). Mouse ZC3H13 contributes to the correct nuclear localization of the MACOM complex (Wen et al., 2018). Additionally, ZC3H13 stabilizes the interaction between WTAP and RBM15 in mouse ESC (Wen et al., 2018) as well as in flies (Knuckles et al., 2018). Like other members of the writer complex, depletion of ZC3H13/Flacc

1. Introduction

decreases global mRNA m⁶A levels (Guo et al., 2018; Knuckles et al., 2018; Wen et al., 2018) and compromises proper sex determination in *Drosophila* (Guo et al., 2018; Knuckles et al., 2018).

HAKAI, also known as Casitas B-lineage lymphoma-transforming sequence-like protein 1 (CBLL1), represents the latest addition to the m⁶A writer complex. Although the E3 ubiquitin ligase HAKAI had been previously identified as part of a protein complex including WTAP, VIRMA and ZC3H13 in mammalian cells (Horiuchi et al., 2013; Wan et al., 2015), its role in m⁶A writing was described for the first time in *Arabidopsis thaliana* (Růžička et al., 2017). *HAKAI* mutant plants show mild developmental defects and reduced m⁶A levels (Růžička et al., 2017). A few years later, work from our lab (Bawankar et al., 2021) and others (Y. Wang et al., 2021) validated HAKAI as a member of the m⁶A machinery in flies and further characterized its molecular function within the m⁶A pathway (see chapter 5.1).

While the structure of the MAC complex was extensively characterized (Śledź & Jinek, 2016; P. Wang et al., 2016; X. Wang et al., 2016), the exact composition and stoichiometry of the MACOM complex has still not been completely elucidated. In 2022, structure of the core of human MACOM (WTAP, VIRMA and ZC3H13), in complex or not with MAC, was resolved for the first time via cryo-electron microscopy (cryo-EM) (Su et al., 2022). Although RBM15/15B and HAKAI failed to be included in the assembly, the partial cryo-EM structure of MACOM provides interesting insights: I) WTAP dimerizes through coiled-coil interactions and each monomer is formed by four tandem helices and three linkers, II) VIRMA consists of twenty ARM-like domains and strongly interacts with WTAP, also in the absence of ZC3H13, forming the MACOM core, III) binding of the C-term domain of ZC3H13 to VIRMA induces conformational changes in the structure of the complex, IV) the MAC-MACOM coupling happens mainly through interaction between METTL3 and WTAP. Additionally, MACOM subunits were confirmed to be critical for efficient RNA substrate binding and enzymatic activity of the m⁶A writer complex and their absence, especially ZC3H13, dramatically reduced both parameters (Su et al., 2022). Further studies are still needed to uncover the complete and definitive structure of the MAC-MACOM complex, which in turn would help to obtain a comprehensive picture of the functional organization of the m⁶A-depositing machinery.

– Additional m⁶A writers

In addition to the MAC-MACOM complex, which catalyzes m⁶A deposition on most sites on mRNA as well as on lncRNA and miRNA, other individual m⁶A methyltransferases, acting on different RNA species, have been characterized over the years.

Although the presence of a single m⁶A site (A43) on the U6 snRNA had been known since the 1980s (Epstein et al., 1980; Harada et al., 1980), **METTL16** was only recently identified and characterized as the methyltransferase responsible for its deposition (Aoyama et al., 2020; Pendleton et al., 2017; Warda et al., 2017). Along with m⁶A, U6 is decorated with one m²G, three Ψ and eight Nm sites (Epstein et al., 1980; Harada et al., 1980). U6 modified nucleotides are highly evolutionary conserved and reside around functionally important regions, which interact with the pre-mRNA or with other snRNAs (Gu et al., 1996). Unlike the METTL3-METTL14 heterodimer, METTL16 uses a combination of sequence and structure to recognize its RNA targets, which are accommodated in a large positively charged groove (Pendleton et al., 2017; Ruzskowska et al., 2018). Notably, METTL16 can homodimerize, but dimer formation is not always necessary for its catalytic activity (Pendleton et al., 2017; Ruzskowska et al., 2018). Among the small number of METTL16-dependent m⁶A sites on mRNA, one is found within the 3'UTR hairpins of human *MAT2A* in a sequence context (UACAGAGAA) identical to that of the methylation site on U6 (Pendleton et

1. Introduction

al., 2017; Shima et al., 2017; Warda et al., 2017). *MAT2A* mRNA encodes for the enzyme responsible for SAM synthesis and its expression is regulated by SAM levels themselves. High intracellular levels of SAM induce *MAT2A* methylation by METTL16, generating a transcript isoform with one unspliced intron, which is recognized by YTHDC1 and degraded in the nucleus. Conversely, in SAM-limiting conditions, shortage of methyl donor leads to prolonged METTL16 occupancy at *MAT2A* 3'UTR, which promotes the splicing of the otherwise retained intron with consequent translation of *MAT2A* and rise of the intracellular SAM levels (Doxtader et al., 2018; Pendleton et al., 2017; Shima et al., 2017). Even though the metastasis-associated lung adenocarcinoma transcript 1 (*MALAT1*) lncRNA was the first RNA target of METTL16 to be identified (Brown et al., 2016) and one m⁶A residue (A8290) was mapped in the vicinity of the METTL16-binding site on *MALAT1* (Y. Z. Chang et al., 2021; D. Jin et al., 2019; Linder et al., 2015), the methylated adenosine at this location is found within a RRACH consensus sequence and its deposition appears to be METTL3-dependent (Y. Z. Chang et al., 2021; D. Jin et al., 2019; Linder et al., 2015). Interestingly, the presence of m⁶A on one hairpin of *MALAT1* (A2515) represents one example of the so-called “m⁶A switch” (N. Liu et al., 2017), a structural remodeling mechanism consisting in m⁶A-induced destabilization of RNA secondary structures, which in turn alters the accessibility of RNA-binding proteins (RBPs) in a positive or negative way (see chapter 1.4.4).

METTL5 (Ignatova et al., 2020; Leismann et al., 2020; Rong et al., 2020; van Tran et al., 2019) and **ZCCHC4** (H. Ma et al., 2019; Pinto et al., 2020; Ren et al., 2019) were recently identified as highly specific enzymes responsible for m⁶A installation at two functionally important sites on eukaryotic rRNA, A1832 on 18S and A4220 on 28S, respectively. METTL5 forms an obliged heterodimer with the methyltransferase coactivator TRMT112, which is dispensable for catalytic activity but is needed to give stability to its partner (van Tran et al., 2019). Unlike other methyltransferases, structural data revealed that ZCCHC4 exists in an autoinhibitory conformation. Binding with the 28S rRNA was proposed to displace ZCCHC4's regulatory loop from the catalytic site changing its conformation from inactive to active (Ren et al., 2019). Although they catalyze only a single base methylation each, loss of METTL5 (Sepich-Poore et al., 2022) or ZCCHC4 (H. Ma et al., 2019; Pinto et al., 2020) has a significant impact on global translation and gene expression. Notably, in agreement with the link between frameshift variants of human *METTL5* and intellectual disability (Richard et al., 2019), flies lacking *Mettl5* display impaired orientation and walking behavior (Leismann et al., 2020).

1.4.2 Regulation of m⁶A deposition

Despite the major role played by m⁶A in post-transcriptional gene regulation, the factors responsible for spatial regulation of its deposition across the transcriptome are still poorly understood.

Over the years, several potential mechanisms, which involve subunits of the MACOM complex, transcription factors or chromatin marks as “pilots” of METTL3 target selectivity, have been proposed to explain the 3'UTR-biased distribution of m⁶A.

Among the MACOM components, VIRMA was suggested to drive m⁶A deposition in the 3'UTR of transcripts in virtue of its interaction with some of the mRNA cleavage and polyadenylation factors (Yue et al., 2018).

Looking at the distribution of chromatin marks, Huang and colleagues reported that histone H3 trimethylation at Lys36 (H3K36me3), a mark associated with active transcription, is characterized by an

1. Introduction

enrichment in the CDS and 3'UTR that matches to that of the m⁶A transcriptomic profile. Genetic manipulation of the H3K36me3 methyltransferase (SETD2) or demethylase (KDM4A) results in substantial changes in m⁶A levels at the corresponding RNA sites. Mechanistically, H3K36me3 was shown to be directly recognized by METTL14, which mediates the binding between the m⁶A writer complex and actively transcribing RNA polymerase II (Pol II) to drive local m⁶A co-transcriptional installation (H. Huang et al., 2019).

Regulation of m⁶A deposition via transcription factor-mediated recruitment of the m⁶A writer complex to specific chromatin locations has also been described. The chromatin-associated zinc finger protein 217 (ZFP217) and the SMAD2-3 proteins were both shown to influence the m⁶A landscape by binding to METTL3, but with opposite outcomes on ESCs fate. During embryonal development, ZFP217 restricts m⁶A deposition on key pluripotency-related genes (e.g., *Nanog*, *Sox2*, *Klf4*) by sequestering METTL3 and consequently stabilizing their expression (Aguilo et al., 2015), while SMAD2-3 promote binding of the m⁶A writer complex to those same transcripts to target them for degradation and initiate cellular differentiation (Bertero et al., 2018). Another recent study revealed that the nuclear RNA-binding protein TARBP2 is able to recruit the m⁶A writer complex to its RNA targets to promote intron retention and degradation by the nuclear exosome (Fish et al., 2019). In acute myeloid leukemia (AML) cells, METTL3 was shown to be recruited at transcriptional start sites by interaction with the CAATT-box binding protein CEBPZ, leading to CDS m⁶A deposition and consequent enhanced translation of mRNAs that are essential to maintain cancer growth (Barbieri et al., 2017). Furthermore, springing from the high degree of overlap between m⁶A distribution and miRNAs target sites, miRNA-bound Dicer was proposed to regulate m⁶A deposition via modulation of METTL3 binding to mRNAs (T. Chen et al., 2015).

A correlation between m⁶A deposition and transcription rate was described by Slobodin and colleagues, who reported that slow transcription by Pol II results in higher m⁶A levels on mRNAs. Specifically, low rate of transcription elongation was shown to enhance Pol II interaction with METTL3 and in turn co-transcriptional m⁶A deposition within CDSs, resulting in reduced translation efficiency of the methylated transcripts (Slobodin et al., 2017).

Very recently, three independent labs put forward a new model describing the binding of exon junction complexes (EJCs) to spliced transcripts as one of the major factors shaping m⁶A distribution on mRNA. EJCs components, likely in conjunction with other RBPs, are proposed to block METTL3-mediated m⁶A deposition in proximity to exon-exon junctions and within short exons, giving rise to the uneven m⁶A profile characterized by enrichment in 3'UTRs and long internal exons (He et al., 2023; Uzonyi et al., 2023; X. Yang et al., 2022). According to this theory, m⁶A distribution recapitulates nuclear splicing and in turn controls cytoplasmic stability of mRNAs. Notably, the vast majority of budding yeast mRNAs are intronless but still display m⁶A enrichment at 3'UTRs, suggesting that other factors might be in play to control m⁶A distribution (Schwartz et al., 2013). In addition, this model of local steric blockage of METTL3 by EJCs does not account for m⁶A scarcity at 5'UTRs.

Overall, despite all the proposed models, future work is still needed to fully comprehend the mechanisms underlying the unique m⁶A profile.

1.4.3 m⁶A erasers

Going hand in hand with the term m⁶A writers, “m⁶A erasers” refers to RNA-demethylating enzymes that are able to convert m⁶A back to A. Although the identification of two different enzymes demethylating m⁶A on mRNA was an important discovery in the field, recent studies partially revised the notion of m⁶A as a modification that can be formed and removed in a dynamic way.

– FTO

The fat mass and obesity-associated (**FTO**) protein was the first enzyme to be tested for m⁶A demethylation activity (Jia et al., 2011) based on its preference for single-stranded nucleic acid substrates (Z. Han et al., 2010) and its belonging to the AlkB homolog (ALKBH) family of Fe(II)- and α -KG-dependent dioxygenases (Gerken et al., 2007). In mammals, the ALKBH family includes the nine homologues of the *Escherichia coli* AlkB protein: ALKBH1-8 and FTO. ALKBH5 and FTO appeared late in evolution and are found only in vertebrate species, while the other seven members of the family are conserved across all metazoans. Bacterial AlkB is well-known for its role in the repair of DNA alkylation damage (e.g., 1mA, 3mC) via oxidative demethylation. Over the time, AlkB homologues were shown to catalyze demethylation on an expanding range of substrates, including DNA, RNA and proteins (Fedeles et al., 2015) (**Table 1**).

FTO was initially reported to target 3mT in ssDNA as well as m³U on ssRNA (Gerken et al., 2007; Jia et al., 2008) and the study by Jia and colleagues showed for the first time that FTO proficiently demethylates m⁶A on both ssDNA and ssRNA *in vitro* and that m⁶A levels on mRNA are affected by FTO depletion/overexpression in mammalian cells (Jia et al., 2011; Meyer et al., 2012). More in details, FTO was shown to oxidize m⁶A to A via N6-hydroxymethyladenosine (hm⁶A) and N6-formyladenosine (f⁶A) intermediates, which are relatively stable and detectable on mammalian mRNA (Y. Fu et al., 2013). In addition, MeRIP-seq data from *FTO* KO mouse brains revealed an increase in the number of m⁶A sites, albeit limited to a subset of transcripts involved in neuronal signaling, compared to CTRL brains (Hess et al., 2013). Strikingly, the extra m⁶A peaks identified in *FTO* mutant mice were later shown to be enriched at the 5' end of transcripts and to reflect m⁶Am rather than m⁶A (Mauer et al., 2017). Indeed, *in vitro* and *in vivo* conversion of m⁶Am to Am by FTO on capped RNA is obtained with significantly higher efficiency — and with less FTO *in vitro* — than m⁶A demethylation (Mauer et al., 2017). Furthermore, while FTO does not display strict dependence on the presence of the m⁶A consensus motif for substrate selectivity (S. Zou et al., 2016), it shows a strong preference for m⁶Am within the mRNA 5' cap structural context (Mauer et al., 2017). Thus, the relatively mild effect of changes in FTO expression on mRNA m⁶A and m⁶Am levels, together with the strict nuclear localization of FTO in most cells and tissues (Hess et al., 2013; Jia et al., 2011), prompted the search for alternative FTO RNA targets within the nucleus. miCLIP analysis in *FTO* KO mice revealed increased methylation at the first nucleotide of snRNAs as well as extensive splicing defects, suggesting that m⁶Am on snRNAs might be among the main targets of FTO demethylation activity (Mauer et al., 2019). Despite FTO being a predominantly nuclear protein, it was reported to localize in both nucleus and cytoplasm of some mammalian cell lines (e.g., HEK293T, 3T3-L1) and to preferentially demethylate m⁶A on nuclear mRNAs as well as both m⁶A and m⁶Am on cytoplasmic transcripts in these cells (J. Wei et al., 2018). Additionally, m⁶A on the U6 snRNA and m¹A on tRNAs were

1. Introduction

reported as other substrates of FTO, demethylation of the latter leading to increased protein translation efficiency (J. Wei et al., 2018).

Accumulating evidence demonstrated that dysregulation of FTO expression contributes to tumorigenesis and poor prognosis in several types of cancer. In most of the cases, aberrantly high expression of FTO promotes cancer proliferation, metastasis and drug resistance (Y. Li et al., 2022). As the name implies, FTO is also involved in genetic predisposition to obesity. Different genome-wide association studies (GWAS) identified several *FTO* variants common in the general population that are associated with high body mass index and risk of obesity (Azzam et al., 2022). Although they were initially shown to correlate with increased *FTO* transcript levels (Berulava & Horsthemke, 2010), *FTO* obesity-associated SNPs are mainly located within the first intron of *FTO*, which harbors enhancer elements regulating the expression of neighboring genes (i.e., *IRX3* and *RPGRIP1L*), suggesting a possibly indirect role of FTO in obesity pathology (Smemo et al., 2014; Stratigopoulos et al., 2014). Nevertheless, several mechanisms linking m⁶A demethylation by FTO to the etiology of obesity were proposed over the years (Azzam et al., 2022). Most recently, it has been reported that adipose tissue-specific deletion of *FTO* in mice results in reduced m⁶A on the hypoxia inducible factor 1 subunit alpha (*Hif1a*) mRNA, which leads to YTHDC2-dependent increase of *Hif1a* translation. High levels of HIF1A promote white-to-beige adipocytes transition and thermogenesis, which act in combination as anti-obesity mechanisms (R. Wu et al., 2021). Nevertheless, the majority of data available so far come from studies focusing on *FTO* depletion/overexpression in mouse and human adipocytes and the consequences of human *FTO* variants in adipogenesis and obesity will need to be more accurately elucidated in the future.

– ALKBH5

Shortly after FTO demethylation activity towards m⁶A was first reported, systematic screening of the rest of the members of the ALKBH family identified **ALKBH5** as another demethylase targeting m⁶A on mRNA (Zheng et al., 2013). ALKBH5 exhibits no m⁶Am demethylation activity (Mauer et al., 2017), while it can demethylate m⁶A on ssDNA/ssRNA *in vitro* and its depletion leads to a slight increase of mRNA m⁶A levels as well as accelerated mRNA export in HeLa cells (Zheng et al., 2013). In addition to the double-stranded β -helix (DSBH) fold common to all ALKBH proteins, ALKBH5 presents a unique rigid loop in its nucleic acid binding region that sterically hinders dsDNA/dsRNA accommodation (Aik et al., 2014; Feng et al., 2014; C. Xu, Liu, et al., 2014). In mouse, highest expression of ALKBH5 is in testis and its loss results in altered testis size and morphology as well as widespread spermatocytes apoptosis with consequent defects in spermatogenic maturation (Zheng et al., 2013). Recently, it has been proposed that aberrant spermatogenesis in *ALKBH5* KO male mice may be explained by involvement of ALKBH5-dependent m⁶A removal in the regulation of the gradual shortening of mRNA 3'UTRs that is critical for spermatids meiotic progression (Tang et al., 2018). Like FTO, several studies highlighted that ALKBH5 is frequently dysregulated in multiple types of cancers. Depending on cancer type, altered expression of ALKBH5 influences tumorigenesis in a positive or negative fashion (Qu et al., 2022). One example is ALKBH5 overexpression in breast cancer stem cells (BCSC), which results in a less m⁶A-modified and more stable *Nanog* mRNA, that in turn promotes BCSC proliferation under hypoxic conditions (C. Zhang et al., 2016).

Mirroring the rapid and recurrent changes in DNA methylation and histone modifications at the base of the epigenetic regulation of transcription, discovery of the existence of m⁶A demethylases (Jia et al.,

1. Introduction

2011; Zheng et al., 2013) gave rise to the exciting idea of reversible m⁶A methylation as new layer of dynamic regulation of gene expression. However, not so many studies have corroborated this theory at the molecular level so far. As a matter of fact, FTO has been found to physiologically act on m⁶Am rather than m⁶A (Mauer et al., 2017) and only a limited amount of m⁶A sites have been validated as direct targets of ALKBH5 demethylation activity. Furthermore, it has been shown that, throughout the life cycle of mRNA, m⁶A levels are generally quite stable, rather than dynamically regulated, and that m⁶A distribution in HeLa cells cytoplasmic mRNAs is almost indistinguishable from that of the corresponding chromatin-associated nascent pre-mRNAs and nuclear mRNAs (Ke et al., 2017). These observations suggest that cytoplasmic m⁶A demethylation might be a fairly rare event that is circumscribed to specific tissues and conditions and underline the need for further investigation to elucidate the relevance of demethylation in the global regulation of m⁶A distribution on mRNA.

– Substrates of the other ALKBH proteins

Despite being the closest homolog to bacterial AlkB, only after discovery of its predominantly mitochondrial localization, mammalian **ALKBH1** was validated as a functional demethylase that repairs 3mC on ssDNA/ssRNA (Westbye et al., 2008). However, the cellular localization of ALKBH1 has been a matter of debate. In 2012, Ougland and colleagues reported a strict nuclear localization for ALKBH1 and showed that its loss alters the methylation status of histone H2A leading to delayed neuronal differentiation in mESCs (Ougland et al., 2012). A later study could not validate this finding, but rather proposed ALKBH1 as a DNA 6mA demethylase. More specifically, ALKBH1 was shown to tightly regulate the levels of 6mA in order to promote transcription of LINE1 transposons but at the same time prevent genomic instability during embryonic stem cell differentiation (T. P. Wu et al., 2016). In addition, crystal structure of mouse ALKBH1 revealed its unique preference for 6mA-modified bubbled or locally unpaired DNA (M. Zhang et al., 2020). More recently, ALKBH1 was shown to recognize m⁵C at position 34 on mitochondrial tRNA^{Met} and cytoplasmic tRNA^{Leu} and oxidize it to either f⁵C only or hm⁵Cm and f⁵C, respectively (Haag et al., 2016; Kawarada et al., 2017). Since oxidation of m⁵C to f⁵C at position 34 allows mitochondrial tRNA^{Met} to recognize AUA as well as AUG (both coding for Met), ALKBH1-dependent f⁵C is an essential modification for proper mitochondrial protein synthesis. Along the same line, ALKBH1 catalyzes demethylation of m¹A at tRNA position 58 in order to reduce translation initiation in response to glucose deprivation (F. Liu et al., 2016). The latest identified substrate of ALKBH1 demethylating activity is m³C on mRNA of mammalian cells (C.-J. Ma et al., 2019).

Very similarly to bacterial AlkB, mammalian **ALKBH2** and **ALKBH3** protect cells from alkylation damage by catalyzing oxidation of 1mA and 3mC on DNA (Aas et al., 2003; Duncan et al., 2002; Ringvoll et al., 2006). While ALKBH2 prefers dsDNA, ALKBH3 acts more efficiently on ssDNA and repairs alkylation damage on RNA as well (Aas et al., 2003). In addition, human ALKBH2 is active towards 1,N⁶-ethenoadenine (εA), 3,N⁴-ethenocytosine (εC) and 1,N²-ethenoguanine (1,N²-εG) lesions caused by lipid oxidation on dsDNA (Ringvoll et al., 2008; Zdzalik et al., 2015). ALKBH3 repairs only εC on ssDNA (Zdzalik et al., 2015) and demethylates also m⁶A specifically on tRNAs (Ueda et al., 2017).

ALKBH4 catalyzes demethylation of a monomethylated site in the actin protein (K84me1), which regulates interactions within the actomyosin complex for proper cytokinesis and cell migration (M.-M. Li et al., 2013), and METTL4-deposited 6mA on dsDNA (Kweon et al., 2019).

1. Introduction

Already known for playing a role in alkylation- and oxidation-induced programmed necrosis (D. Fu et al., 2013), **ALKBH7** was recently reported to exhibit demethylation activity towards N₂,N₂-dimethylguanosine (m₂²G) at position 26 of the tRNA^{Ile} and m¹A at position 58 of the tRNA^{Leu(UUA/G)} in mitochondrial nascent polycistronic RNA (L.-S. Zhang et al., 2021).

Unique among ALKBH proteins, **ALKBH8** possesses a C-terminal SAM-dependent methyltransferase domain in addition to the canonical AlkB-like domain. ALKBH8 was shown to form a heterodimer with TRM112 and catalyze the methyl esterification of cm⁵U and cm⁵s²U to mcm⁵U and mcm⁵s²U, respectively, at the wobble position of certain tRNAs (Cavallin et al., 2022; Y. Fu et al., 2010; Songe-Møller et al., 2010). Furthermore, mcm⁵U on tRNA^{Gly(UCC)} acts as precursor for hydroxylation to (S)-mchm⁵U by the AlkB-like domain of ALKBH8 (Y. Fu et al., 2010; van den Born et al., 2011). Although strictly localized to the cytoplasm, HITS-CLIP analysis recently revealed interaction of ALKBH8 with nuclear RNA targets (e.g., C/D box snoRNAs), whose functional significance will have to be addressed in the future (Cavallin et al., 2022).

ALKBH6 is the only member of the family whose targets have not been identified yet (see chapter 5.4).

ALKBH protein	Substrates	Subcellular localization
ALKBH1	<ul style="list-style-type: none"> • 3mC/m³C on mitochondrial ssDNA/ssRNA • Histone H2A • 6mA on bulged DNA • m⁵C on mitochondrial tRNA^{Met} and cytoplasmic tRNA^{Leu} • m¹A on tRNA • m³C on mRNA 	<ul style="list-style-type: none"> • Nucleus and cytoplasm • Mitochondria
ALKBH2	<ul style="list-style-type: none"> • 1mA and 3mC on dsDNA • εA, εC and 1,N²-εG on dsDNA 	<ul style="list-style-type: none"> • Nucleus (enrichment in the nucleolus)
ALKBH3	<ul style="list-style-type: none"> • 1mA/m¹A and 3mC/m³C on ssDNA/RNA • εC on ssDNA • m⁶A on tRNA 	<ul style="list-style-type: none"> • Nucleus and cytoplasm
ALKBH4	<ul style="list-style-type: none"> • Actin (K84me1) • 6mA on dsDNA 	<ul style="list-style-type: none"> • Nucleus and cytoplasm
ALKBH5	<ul style="list-style-type: none"> • m⁶A on mRNA 	<ul style="list-style-type: none"> • Nuclear speckles
ALKBH6	<ul style="list-style-type: none"> • NA 	<ul style="list-style-type: none"> • Nucleus and cytoplasm
ALKBH7	<ul style="list-style-type: none"> • tRNA^{Ile} m₂²G26 and tRNA^{Leu(UUA/G)} m¹A58 on mitochondrial nascent polycistronic RNA 	<ul style="list-style-type: none"> • Nucleus and cytoplasm • Mitochondria
ALKBH8	<ul style="list-style-type: none"> • cm⁵U to mcm⁵U and cm⁵s²U to mcm⁵s²U (MT domain) at the wobble position of specific tRNAs • mcm⁵U to (S)-mchm⁵U (AlkB-like domain) at the wobble position of tRNA^{Gly(UCC)} 	<ul style="list-style-type: none"> • Cytoplasm
FTO	<ul style="list-style-type: none"> • 3mT on ssDNA • m³U on ssRNA • m⁶A on mRNA • Cap m⁶Am on mRNA and snRNA • m¹A on tRNA 	<ul style="list-style-type: none"> • Nuclear speckles • Nucleus and cytoplasm

Table 1. Substrates and subcellular localization of proteins of the ALKBH family.

1.4.4 m⁶A readers

The presence of m⁶A affects the fate of RNA via two main mechanisms: it can be specifically recognized and directly bound by the so-called “m⁶A readers” or it can alter the secondary structure of RNA in a way that favors/hinders the access to canonical RBPs (m⁶A switch).

– YTH-domain containing proteins

In vitro pull-down of m⁶A-modified RNA probes coupled with quantitative protein mass spectrometry contributed to the identification of most m⁶A-binding proteins. The first to be discovered as well as the most studied m⁶A readers are proteins containing the YT521-B homology (YTH) domain (Dominissini et al., 2012). Originally identified as a novel RNA-binding domain in the human splicing factor YT521-B and its eukaryotic homologues (Stoilov et al., 2002), the YTH domain was then crystallized and shown to possess an aromatic cage of two to three Trp residues able to specifically bind m⁶A-modified RNAs (F. Li et al., 2014; Luo & Tong, 2014; C. Ma et al., 2019; Theler et al., 2014; C. Xu et al., 2015; C. Xu, Wang, et al., 2014; Zhu et al., 2014). Mutations of the aromatic cage residues dramatically reduce m⁶A recognition without affecting the overall RNA binding ability of the YTH domain (Zhu et al., 2014).

The mammalian genome encodes for five YTH m⁶A readers: two YTH domain containing (YTHDC1-2) proteins and three YTH domain family (YTHDF1-2-3) proteins. YTHDF1, YTHDF2 and YTHDF3 are three paralogs with very similar aminoacidic sequence and a C-terminal YTH domain. Notwithstanding the same name, YTHDC1 and YTHDC2 are not paralogs and are related to the other YTH proteins only for harboring the homonymous domain (Patil et al., 2018). While YTHDF proteins display a strict cytoplasmic localization (A. Li et al., 2017; Shi et al., 2017; X. Wang et al., 2014, 2015; Zhou et al., 2015), localization of YTHDC1 is exclusively nuclear (Hartmann et al., 1999) and YTHDC2 is found in both nucleus and cytoplasm (Wojtas et al., 2017). The YTH domain is highly evolutionary conserved (Stoilov et al., 2002) and members of the YTH family are found across the whole eukaryotic phylogenetic tree. *Arabidopsis thaliana* has thirteen genes encoding for YTH proteins (AtYTH01-13) (D. Li et al., 2014), while budding yeast only has one (Mrb1 or Pho92) (Schwartz et al., 2013). *Drosophila melanogaster* has one homolog of YTHDC1 (Ythdc1) and one of the YTHDF family (Ythdf), while *C. elegans* does not have any. Notably, the fission yeast Mmi1 protein has the canonical aromatic pocket within its YTH domain, but it does not bind to m⁶A-containing RNAs (C. Wang et al., 2016).

• YTHDF proteins

Despite sharing ~70% amino acid identity and almost the exact same YTH domain (Patil et al., 2018), the three YTHDF paralogs have been initially reported to mediate distinct effects upon binding to m⁶A-modified mRNAs. While YTHDF1 was shown to promote translation of its methylated targets by interacting with ribosomes and translation initiation factors (X. Wang et al., 2015), binding of YTHDF2 would target m⁶A-modified mRNA to cytoplasmic decay sites for degradation by the CCR4-NOT deadenylase complex (H. Du et al., 2016; X. Wang et al., 2014). Playing both sides, YTHDF3 was shown to enhance translation together with YTHDF1 as well as to stimulate YTHDF2-mediated decay of the methylated targets that it shares with its paralogs (A. Li et al., 2017; Shi et al., 2017).

More recently, reanalysis of available CLIP datasets revealed that YTHDF1, YTHDF2, and YTHDF3 display comparable binding preference for the different variants of the m⁶A motif and recognize

1. Introduction

essentially the same set of m⁶A sites throughout the transcriptome (Zaccara & Jaffrey, 2020). Furthermore, the YTHDF paralogs were shown to share the same subcellular localization within RNPs or stress granules, a common pool of high-confidence protein interactors — including subunits of the CCR4-NOT complex, protein involved in RNA degradation and stress granules components — as well as the same destabilizing effect on bound m⁶A targets (Zaccara & Jaffrey, 2020). In support of a model of binding and functional redundancy for the YTHDF proteins, another independent study observed dosage-dependent functional compensation between YTHDF1, YTHDF2 and YTHDF3 in mESCs (Lasman et al., 2020). While single KO of each of the *YTHDF* genes is viable and lacks any obvious phenotype, triple KO mESCs display increased stability of m⁶A-modified transcripts as well as impaired differentiation capacity, resembling the phenotype observed upon KO of *METTL3* (Batista et al., 2014; Bertero et al., 2018; Geula et al., 2015). In mice, YTHDF2 was shown to be the only YTHDF protein absolutely required for proper gametogenesis (Ivanova et al., 2017; Lasman et al., 2020). Unlike YTHDF1 and YTHDF3, YTHDF2 is found in both nucleus and cytoplasm in oocytes as well as in both spermatogonia and spermatocytes in testes, and the embryonic lethality of *YTHDF2* KO cannot be compensated by its paralogs (Lasman et al., 2020).

Equally shared by the three paralogs, YTHDF proteins possess the ability to undergo liquid-liquid phase separation (LLPS) *in vitro* and *in vivo* via interactions between their low-complexity prion-like domains (Gao et al., 2019; Ries et al., 2019). LLPS is enhanced by the presence of polymethylated m⁶A-modified RNAs, whose binding act as platform that locally concentrates YTHDF proteins into liquid droplets. Upon different types of stress (e.g., heat shock, oxidative), YTHDF proteins relocalize to cytosolic stress granules and their loss results in reduced granules formation and poor mRNA recruitment to stress granules (Anders et al., 2018; Y. Fu & Zhuang, 2020; Ries et al., 2019). Unlike previously reported in mouse embryonic fibroblasts and HeLa cells (Zhou et al., 2015), heat shock-induced increase in expression and relocalization to the nucleus of YTHDF2 was not observed by Ries and colleagues in mESCs (Ries et al., 2019).

- **YTHDC1**

YTHDC1 harbors four NLS and it is the only YTH protein that localizes to the nucleus in non-stress conditions. In addition, Glu-rich and Glu/Arg-rich regions mediate specific localization of YTHDC1 to subnuclear dots adjacent to nuclear speckles called “YT bodies” (Hartmann et al., 1999; Nayler et al., 2000). More recently, it has been shown that m⁶A-bound YTHDC1 proteins undergo LLPS forming nuclear YTHDC1-m⁶A condensates (nYACs), where methylated mRNAs are protected from exosome-dependent degradation (Cheng et al., 2021).

In one way or another, nearly all mRNA processing events occurring within the nucleus have been linked to m⁶A and YTHDC1. In agreement with its previously reported interaction with components of the spliceosome (Hartmann et al., 1999; Imai et al., 1998), YTHDC1 was shown to participate in splicing regulation through modulation of the localization to nuclear speckles of the Ser/Arg-rich splicing factor 3 and 10 (SRSF3 and SRSF10) (W. Xiao et al., 2016). Briefly, YTHDC1 recruits SRSF3 and in parallel blocks the access of SRSF10 to its pre-mRNA targets, promoting exon inclusion over skipping (W. Xiao et al., 2016). Depletion of either YTHDC1, SRSF3 or *METTL3* results in a common pool of 160 exons undergoing skipping, suggesting that YTHDC1 regulates splicing in an m⁶A-dependent manner (W. Xiao et al., 2016). In addition to splicing defects, loss of YTHDC1 in mouse oocytes causes extensive alternative

1. Introduction

polyadenylation (APA) and oocyte maturation arrest (Kasowitz et al., 2018). In line with a previously suggested role of m⁶A in the regulation of proximal alternative polyA choice (Ke et al., 2015), YTHDC1 was shown to interact with pre-mRNA 3' end processing factors (i.e., CPSF6, SRSF3 and SRSF7) to influence 3'UTR length via APA (Kasowitz et al., 2018).

In complex with SRSF3, which acts both as splicing factor and nuclear export adaptor protein, YTHDC1 was shown to promote nuclear export of m⁶A-modified transcripts by facilitating their incorporation into RNPs including hypo-phosphorylated SRSF3 and the nuclear export factor 1 (NXF1) (Roundtree et al., 2017). Consistently, another study showed that the transcription-export (TREX) complex, recruited to methylated mRNAs by the m⁶A writer complex, interacts with YTHDC1 for efficient nuclear export (Lesbirel et al., 2018).

In agreement with its localization, iCLIP experiments revealed that YTHDC1 exhibits prominent binding to nuclear ncRNAs, such as *NEAT1*, *MALAT1* and *XIST*. Despite the molecular mechanism being not completely clear yet, binding of YTHDC1 to many of the m⁶A residues spread along *XIST* lncRNA was shown to be necessary for efficient gene silencing of the X chromosome (Patil et al., 2016).

- **YTHDC2**

While the YTHDF proteins and YTHDC1 are overall disordered proteins with low-complexity except for the YTH domain, YTHDC2 possesses several RNA-binding domains, including a N-terminal Arg/His-rich domain, a central RNA helicase domain interrupted by two protein-protein interaction Ankyrin repeats, and a C-terminal oligo-nucleotide binding (OB) fold. On account of its RNA helicase domain, YTHDC2 is considered a member of the DExH box helicase family and displays ATP-dependent 3'→5' RNA unwinding activity (Jain et al., 2018; Wojtas et al., 2017).

In sharp contrast to the other YTH proteins, YTHDC2 binds predominantly to intergenic regions and introns and its binding profile correlates very weakly with the known m⁶A distribution on RNA (Patil et al., 2016). In line with this, the binding affinity of YTHDC2 to m⁶A-modified RNA is significantly lower than that of its fellow members of the YTH family (Wojtas et al., 2017; C. Xu et al., 2015).

Unlike the other ubiquitously expressed YTH proteins, YTHDC2 is highly enriched in testis. *YTHDC2* mutant germ cells fail to properly transition to the meiotic RNA expression program leading to arrested differentiation and apoptosis in both testes and ovaries with consequent mice infertility (Bailey et al., 2017; Hsu et al., 2017; Jain et al., 2018; R. Liu et al., 2021; Wojtas et al., 2017). In mouse testis, YTHDC2 binds to U-rich regions in the 3'UTR of its mRNA targets and it was proposed to destabilize mitotic transcripts during meiotic entry in complex with the meiosis specific with coiled-coil domain (MEIOC) protein (L. Li et al., 2022; Wojtas et al., 2017) and the exoribonuclease XRN1 (Hsu et al., 2017; L. Li et al., 2022; Wojtas et al., 2017). Notably, the helicase activity of YTHDC2, which is normally limited by the presence of Ankyrin repeats in between the two RecA modules of the helicase domain, is enhanced by interaction of XRN1 with the repeats themselves (L. Li et al., 2022). Recently, catalytically dead mutations in the helicase domain, but not in the YTH domain, of YTHDC2 were shown to phenocopy genetic null mutants, suggesting that the helicase activity of YTHDC2 is necessary for proper mouse gametogenesis independently from its m⁶A-binding ability (L. Li et al., 2022; R. Liu et al., 2021; Saito et al., 2022).

1. Introduction

– Other m⁶A-binding proteins

In addition to reproducible enrichment of the YTH proteins, pull-down experiments using m⁶A-modified/unmodified probes and mass spectrometry recovered additional proteins that preferentially bind to an m⁶A-modified RNA sequence, such as the Fragile X messenger ribonucleoprotein 1 (FMR1) (Edupuganti et al., 2017; Worpenberg et al., 2021) and the insulin-like growth factor 2 mRNA-binding proteins (IGF2BPs) (H. Huang et al., 2018).

FMR1 (together with its human paralogs FXR1 and FXR2) was identified as a sequence-context-dependent m⁶A reader in mouse, fly and human cells (Arguello et al., 2017; Edupuganti et al., 2017; Worpenberg et al., 2021). FMR1 possesses four RNA binding domains, three KH and one RGG domain, which are all required for preferential m⁶A binding (Edupuganti et al., 2017). FMR1 is well-known for its role as negative translational regulator and mutations in the human *FMR1* gene lead to the Fragile X syndrome (FXS), which is the most prevalent form of inherited intellectual disability and the prime monogenic cause of autism (Rousseau et al., 2011). Despite that some of FMR1 consensus sequences identified by CLIP experiments (ACU[GU], UGGA, GAC) (Anderson et al., 2016; Ascano et al., 2012; Hsu, Shi, et al., 2019) highly resemble the canonical m⁶A motif, the transcriptome-wide binding profile of FMR1 (Ascano et al., 2012) does not overlap as perfectly as that of the YTH proteins with the m⁶A distribution on mRNA, suggesting that FMR1 preferentially binds m⁶A-modified RNA, but m⁶A is not indispensable for its binding to RNA. Notably, FMR1 is found among the interactors of all three YTHDF paralogs (Youn et al., 2018) and it was shown to interact with YTHDF2 in an RNA-independent way (F. Zhang et al., 2018), suggesting that FMR1 may indirectly bind to m⁶A via interaction with YTHDF proteins. Mechanistically, on one hand, FMR1 was reported to support the stability of its m⁶A-modified long mRNA targets in competition with YTHDF2, whose binding accelerates mRNA decay upon depletion of FMR1 in mouse neuronal cells (F. Zhang et al., 2018). On the other hand, we showed that the *Drosophila* homolog of FMR1 inhibits the translation of transcripts involved in the regulation of axonal growth in collaboration with Ythdf (see chapter 5.2). Although its N-terminus contains a functional NLS, FMR1 mainly localizes within cytoplasmic RNP particles thanks to a nuclear export signal (NES) encoded by the first amino acids of exon 14 (Eberhart et al., 1996; Fridell et al., 1996; Sittler et al., 1996). Nevertheless, in agreement with previous findings (Kim et al., 2009), FMR1 was reported to bind m⁶A-modified mRNAs in the nucleus and promote their export to the cytoplasm in cooperation with Exportin-1 (also known as CRM1) (Edens et al., 2019; Hsu, Shi, et al., 2019). In mouse cortex, *FMR1* KO results in aberrant transcript nuclear retention of, among others, components of the Notch and Hedgehog signaling pathways leading to delayed neural differentiation (Edens et al., 2019). In addition, FMR1 as well as YTHDC1 were described to bind to and facilitate the export of m⁶A-modified Hepatitis B viral transcripts (Geon-Woo et al., 2021).

IGF2BPs (1, 2 and 3) possess six RNA-binding domains, two RRM and four KH domains, and are known to repress translation of the *IGF2* mRNA in a dose-dependent manner via binding to its 5'UTR during late mammalian development (Jacob et al., 1999). Huang and colleagues showed that the consensus sequence of IGF2BPs (UGGAC) includes the canonical m⁶A motif and ~80% of their RNA targets contains at least one m⁶A site. IGF2BPs binding promotes stability and storage of m⁶A-modified targets, whose recognition depends on KH3-4 domains. The stabilizing effect is probably mediated by recruitment of RNA stabilizers (e.g., HuR, MATR3, PABPC1) to cytoplasmic granules in both normal and stress conditions (Huang et al., 2018). In a similar way to FMR1, all three IGF2BPs are found within the interaction network of YTHDF proteins (Youn et al., 2018), hinting to an indirect binding to m⁶A.

1. Introduction

PRRC2A (Pro rich coiled-coil 2A) was recently identified as novel m⁶A reader that regulates specification and myelination of oligodendrocyte. Specifically, m⁶A-dependent stabilization of *Olig2* mRNA by PRRC2A is essential for oligodendrocyte progenitor cells proliferation and differentiation (R. Wu et al., 2019).

Remarkably, eukaryotic initiation factor 3 (**eIF3**) can be included in the list of readers since it directly binds to m⁶A sites in the 5'UTR of transcripts to promote cap-independent translation in response to different types of cellular stress (Meyer et al., 2015).

– m⁶A switch

According to the fact that the methylamino group of m⁶A must adopt a rotated high-energy conformation in order to base pair with U, the presence of m⁶A destabilizes RNA duplexes while it strongly favors a locally unpaired single-stranded RNA structure (Roost et al., 2015; Spitale et al., 2015). The prevalence of m⁶A within single-stranded motifs could also derive from structural selectivity of the m⁶A writer complex for unpaired adenines, however this possibility is excluded by the fact that *METTL3* KO in mESCs results in increased base-pairing at METTL3-dependent m⁶A sites (Spitale et al., 2015). Many examples of how the impact of m⁶A on RNA local structure controls the accessibility to RNA binding motifs were reported over the years. The term “m⁶A switch” was coined by Liu and colleagues to describe the mechanism by which m⁶A-dependent conformational changes enhance the binding of heterogeneous nuclear ribonucleoprotein C (**HNRNPC**) to target mRNAs and lncRNAs. For instance, m⁶A at position 2577 of the *MALAT1* hairpin destabilizes base pairing with the first uridine of the opposing U₅-tract making it more accessible to HNRNPC binding. Global m⁶A reduction via METTL3-14 depletion prevents HNRNPC binding at many m⁶A switch sites leading to widespread alteration in expression level and splicing pattern of its RNA targets (N. Liu et al., 2015). RNA structure remodeling by m⁶A marks also regulates the binding of **HNRNPG** (N. Liu et al., 2017) as well as **HNRNPA2B1** (Alarcón et al., 2015; B. Wu et al., 2018) to their respective targets in the nucleus. In addition to perturbation of mRNA targets stability and splicing, loss of either HNRNPA2B1 or absence of m⁶A switch at its binding sites results in reduced production of a large subset of the m⁶A-dependent miRNAs (Alarcón et al., 2015).

– m⁶A “anti-readers”

At the opposite end of the spectrum to m⁶A readers, some RBPs are consistently and strongly repelled by the presence of m⁶A on RNA. For example, the stress granules assembly factors **G3BP1** and **G3BP2** — together with their interactors USP10, CAPRIN1 and RBM42 — preferentially bind to GGACU motifs when the adenosine is unmethylated (Arguello et al., 2017; Edupuganti et al., 2017). Loss of m⁶A results in G3BPs-mediated stabilization of their target RNAs and G3BPs binding was proposed to affect the fate of specific transcripts by competing with the m⁶A writing machinery in the nucleus and/or by promoting stabilization and storage in granules upon stress (Edupuganti et al., 2017). In mESCs, m⁶A modification was reported to block binding of **HuR** (also known as ELAVL1) to the 3'UTR of mRNAs coding for developmental regulators (e.g., *IGFBP3*) leading to their miRNA-dependent degradation and maintenance of the state of pluripotency (Y. Wang et al., 2014).

1.4.5 m⁶A distribution and mapping methods

Accurate mapping of m⁶A sites throughout the transcriptome is of high importance to functionally characterize and fully understand the biology of this RNA mark.

The first m⁶A mapping method was developed in parallel by two independent labs in 2012. Since m⁶A is inert to most chemicals and does not affect RT, both **MeRIP-seq** (Meyer et al., 2012) and **m⁶A-seq** (Dominissini et al., 2012) took advantage of anti-m⁶A antibodies to specifically immunoprecipitate methylated fragments out of randomly fragmented RNA samples, followed by identification via high-throughput sequencing. After alignment of the sequencing reads to the reference genome, the presence of distinct “peaks” in the read frequency was used to predict approximative location of m⁶A sites within a 100-200 nt range. Roughly 13,000 high-confidence m⁶A peaks from ~6,000 genes were identified revealing enrichment of m⁶A within long internal exons, near stop codons and in the 3'UTR of mRNAs (Dominissini et al., 2012; Meyer et al., 2012). During the following years, this unique m⁶A metagene profile was validated countless times and, except for *Drosophila melanogaster* that is characterized by m⁶A predominantly located in 5'UTRs (Kan et al., 2017, 2021; Worpenberg et al., 2021), it appears to be conserved across evolution. Additionally, the first transcriptome-wide mapping of m⁶A confirmed the previously identified consensus sequence (C. M. Wei et al., 1976) and, since only a small fraction of RRACH motifs appears to be methylated *in vivo*, it highlighted once again that additional factors are probably needed to guide m⁶A deposition at specific sites. In 2021, the **m⁶A-seq2** protocol was published, with the main difference that the m⁶A-IP is performed on barcoded pooled RNA samples, reducing technical variability, amount of input material and costs (Dierks et al., 2021).

Taking inspiration from the CLIP method used to map binding sites of RBPs on a transcriptome-wide scale (König et al., 2010; Ule et al., 2003), Linder and colleagues developed the miCLIP technique (Linder et al., 2015). **miCLIP** is based on the fact that UV crosslinking of m⁶A antibodies to RNA results in specific signature mutations/truncations in retro-transcribed cDNA allowing to obtain a single-nucleotide resolution map of m⁶A. In contrast to MeRIP- or m⁶A-seq, miCLIP can identify individual methylated adenosines within m⁶A clusters and m⁶A modification of rarely methylated RRACH variants (Linder et al., 2015). Technically very similar to miCLIP, **m⁶A-CLIP** revealed that m⁶A is highly enriched in the first 150-400 nt of the last exon of transcripts, regardless of whether it includes the end of the CDS, the beginning of the 3'UTR or both, and without specific preference for m⁶A deposition at or near stop codons (Ke et al., 2015). Inspired by PAR-CLIP (Hafner et al., 2010), **PA-m⁶A-seq** includes incorporation of photoactivatable ribonucleosides (4-thiouridine or 4SU) into RNA to enhance crosslinking efficiency. At sites of UV crosslinking, 4SU-induced T-to-C mutations are used to map m⁶A at high-resolution within a ~25-30 nt window (K. Chen et al., 2015). To reduce the high false positive rate of antibody-based m⁶A mapping methods, the optimized **miCLIP2** protocol combines the use of *METTL3* KO cells for calibration with a machine learning-based analysis to obtain significantly more accurate m⁶A detection (Körtel et al., 2021).

In addition to unspecific binding and cross-reactivity with m⁶Am, a major limitation of antibody-based m⁶A mapping techniques is the lack of a quantitative output. **SCARLET** (site-specific cleavage and radioactive-labeling followed by ligation-assisted extraction and thin-layer chromatography) (N. Liu et al., 2013) and **SELECT** (single-base elongation- and ligation-based PCR amplification method) (Y. Xiao et al., 2018) enable quantitative m⁶A measurement on individual RNAs, but they are not suitable for transcriptome-wide application. To overcome this issue, Molinie and colleagues developed **m⁶A-LAIC-seq**

1. Introduction

(m⁶A level and isoform characterization seq). The use of known ratios of m⁶A-modified/unmodified spike-in RNAs together with sequencing of both antibody-bound and unbound fractions, makes m⁶A-LAIC-seq able to quantify the proportion of methylated to unmethylated copies of individual transcript on a transcriptome-wide scale. Using this approach, authors observed that the m⁶A level of the majority of genes is below 50% in human embryonic stem cells. Furthermore, lack of fragmentation before IP allows for sequencing of intact full-length transcripts and analysis of m⁶A-dependent differential splicing isoform usage. As drawbacks, the method still depends on the use of efficient m⁶A antibodies and it does not provide mapping and stoichiometric information at nucleotide-resolution (Molinie et al., 2016).

Because of the challenging nature of reliable detection of m⁶A within introns, **TNT-seq** (transient N⁶-methyladenosine transcriptome seq) was established to investigate the direct role of m⁶A on alternative splicing dynamics (Louloupi et al., 2018). In TNT-seq, the addition of a bromouridine-labelling and -IP step before m⁶A enrichment enables mapping of m⁶A on nascent transcripts. Using this method, Louloui and colleagues showed that m⁶A deposition near splice junctions enhances fast constitutive splicing, while m⁶A within introns correlates with slower alternative splicing events (Louloupi et al., 2018).

Another technique that is antibody-based but provides quantitative information is **m⁶ACE-seq** (m⁶A crosslinking exonuclease seq), which relies on the fact that m⁶A-modified RNA fragments that are photo-crosslinked to anti-m⁶A antibodies are protected from subsequent 5'→3' exoribonuclease cleavage (Koh et al., 2019).

During the last few years, the pressing need for antibody-free mapping methods gave rise to a myriad of new techniques that do not rely on immunoprecipitation to detect m⁶A. For instance, **MAZTER-seq** takes advantage of the m⁶A-sensitive MazF RNase to quantitatively profile m⁶A at nucleotide-resolution (Garcia-Campos et al., 2019). MAZTER-seq does not require large amounts of starting material and can be used as orthogonal method for validation and quantitative evaluation of m⁶A sites identified using antibodies, however its detection power is limited to a single sequence context. In fact, as MazF cleaves RNA exclusively upstream of ACA motifs that are not m⁶A-modified at the first adenosine, MAZTER-seq can detect only a small percentage (16-25%) of all m⁶A sites (Garcia-Campos et al., 2019). Nevertheless, a positive correlation was observed between the degree of m⁶A stoichiometry obtained from MAZTER-seq analysis and the number of times the m⁶A site was identified in different miCLIP experiments. This suggests that individual miCLIP datasets might include different subsets of total m⁶A sites depending on the efficiency of crosslinking and antibody (Garcia-Campos et al., 2019). Another method that also uses the m⁶A-sensitive MazF endoribonuclease to map the modification within ACA motifs is **m⁶A-REF-seq** (Zhang et al., 2019).

Unlike MAZTER-/m⁶A-REF-seq, **DART-seq** (deamination adjacent to RNA modification targets seq) is a low-input antibody-independent method that allows stoichiometric detection of m⁶A in any sequence context (Meyer, 2019). In DART-seq, fusion of the cytosine deaminase APOBEC1 to the m⁶A-binding YTH domain of YTHDF2 is used to mark the location of m⁶A sites (always followed by a C) with adjacent C-to-U editing events, which can be easily detected by RT signature using classic RNA-seq. After removal of all naturally occurring C-to-U mutations as well as editing sites detected in cells expressing APOBEC1 alone or a mutant version of the APOBEC1-YTH fusion protein that does not bind to m⁶A, DART-seq produced a list of ~100,000 high-confidence m⁶A sites in a bit less than 10,000 genes. Since the C-to-U editing rate positively correlates with methylation levels, DART-seq can estimate m⁶A abundance at individual sites, and it confirmed that m⁶A is mostly a low-stoichiometry modification (Meyer, 2019). Limitations of DART-

1. Introduction

seq are its reliance on cell transfection (application of *in vitro* DART-seq is currently limited) and the potential bias coming from the binding preference of the YTH domain of YTHDF2. DART-seq was the first method to be applied to map m⁶A transcriptome-wide at single-cell resolution (**scDART-seq**) and it described high heterogeneity in both presence and stoichiometry of m⁶A sites across individual cells of a population (Tegowski et al., 2022). Another approach that does not require high amounts of starting material is adaptation of the **TRIBE** method (McMahon et al., 2016; W. Xu et al., 2018) to identify m⁶A sites by fusing the catalytic domain of the A-to-I editing enzyme ADAR to m⁶A writer and reader proteins (Worpenberg et al., 2019). In addition to the bias coming from ADAR preference to edit adenosines surrounded by a double-stranded region, TRIBE does not provide single-nucleotide resolution.

Developed in the lab of Jia, **m⁶A-SEAL** is an antibody-free chemical labelling method that combines oxidation of m⁶A to hm⁶A by FTO with DTT treatment to convert unstable hm⁶A to the more stable N⁶-dithiolsitolmethyladenosine (dm⁶A). The free thiol group on dm⁶A is then tagged with biotin for streptavidin pull-down and high-throughput sequencing allowing for transcriptome-wide m⁶A mapping with a ~200 nt resolution. m⁶A sites identified via m⁶A-SEAL overlap by 40-50% with those detected via miCLIP or DART-seq. Notably, the metagene profile of non-overlapping sites deviates considerably from that of common m⁶A sites and m⁶A-SEAL-unique sites, suggesting possible unspecific detection (Y. Wang et al., 2020).

m⁶A-label-seq (Shu et al., 2020) maps m⁶A transcriptome-wide at single-nucleotide resolution without the use of antibodies. m⁶A-label-seq relies on metabolic labelling via substitution of the methyl group (CH₃) of SAM, and consequently of m⁶A, with an allyl group (C₃H₅), which can be detected based on iodination-induced misincorporations in retro-transcribed cDNA. While m⁶A-modified mRNAs detected by m⁶A-label-seq overlap with a moderate to very good level to those identified via other mapping methods (e.g., ~80% overlap with m⁶A sites identified by DART-seq), the overlap at the level of individual m⁶A sites is very low (1-9%). Furthermore, m⁶A-label-seq requires feeding the cells with a methionine analog, which was shown to trigger cellular stress response mechanisms, possibly affecting m⁶A levels and distribution (Shu et al., 2020).

In **m⁶A-SAC-seq** (m⁶A-selective allyl chemical labeling and sequencing) (Hu et al., 2022), chemically modified allylic-SAM is used as cofactor for the bacterial enzyme MjDim1 to convert m⁶A into a⁶m⁶A, which then undergoes cyclization upon iodine treatment and generates mutations during cDNA synthesis. m⁶A abundance is extrapolated via spike-in RNAs-based normalization. Although m⁶A-SAC-seq is limited by its bias for GAC over AAC sequences, it detects m⁶A at ~75% of modified RRACH motifs with stoichiometric information. Remarkably, most of the m⁶A sites identified by m⁶A-SAC-seq display considerably different methylation levels across different mammalian cell lines (Hu et al., 2022).

By analogy with bisulfite sequencing used to map m⁵C, **GLORI-seq** (C. Liu et al., 2022) employs a combination of glyoxal and nitrous acid to achieve efficient adenosine-specific deamination to inosine. Upon A-to-I conversion, deamination-resistant m⁶A sites can be easily discriminated from canonical adenosines, which once converted to inosines are read as guanosines during RT. In HEK293T cells, more than 176,000 m⁶A sites were identified by GLORI-seq. Reported median m⁶A stoichiometry was ~40% and only 38% of the m⁶A sites displayed >50% methylation level. Interestingly, approximately one third of the detected sites lied within m⁶A clusters, which appeared to be generally highly methylated and involved in gene expression regulation (C. Liu et al., 2022).

1. Introduction

Global adenosine-specific deamination is also the strategy applied by **eTAM-seq** (evolved TadA-assisted m⁶A seq) (Y.-L. Xiao et al., 2023). eTAM-seq uses enzymatic A-to-I conversion mediated by the hyperactive tRNA adenosine deaminase TadA and produces a transcriptome-wide quantitative m⁶A profile (Y.-L. Xiao et al., 2023).

To summarize, mapping of m⁶A, and of most RNA modifications in general, relies on indirect strategies, which can be categorized in antibody-based methods, using antibodies that recognize distinct modifications with high specificity, and chemical-based methods, employing chemicals that selectively react with specific modifications leading to signature truncations or mutations during RT (**Table 2**).

Radically different from all other available technologies, the **Oxford Nanopore Technologies** (ONT) platform (Garalde et al., 2018) offers a method for direct RNA sequencing without prior conversion to cDNA and amplification. In the ONT approach, individual intact RNA molecules are driven by an electric potential into membrane-embedded nanopores and are made to travel through the pores at constant rate thanks to the action of engineered motor proteins. Distinctive shifts in current intensity produced by the passage of five nucleotides at a time through the narrowest section of the pore are recorded by high sensitivity detectors and used to computationally identify the nucleotides in transit by base-calling algorithms built around recurrent neural networks (Garalde et al., 2018). Currently, two main strategies have been developed to identify RNA modifications starting from nanopore direct RNA sequencing data. The first strategy takes advantage of the systematic and reproducible “errors” in base-calling that are caused by the presence of RNA modifications and is used by algorithms such as *EpiNano* (H. Liu et al., 2019) and *DiffErr* (Parker et al., 2020). The second strategy uses instead the changes in raw current intensity as direct readout of the presence of RNA modifications and is implemented in tools such as *Mines* (Lorenz et al., 2020), *xPore* (Pratanwanich et al., 2021) and *nanom⁶A* (Gao et al., 2021). Available strategies can be also classified in *de novo* detection methods, which requires training of the base-calling algorithm with synthetic modified and unmodified sequences, and comparative methods, which distinguish the presence of modifications by comparison with a reference unmodified sample. Algorithms such as *EpiNano* (H. Liu et al., 2019), *Nanocompore* (Leger et al., 2021) and *m6Anet* (Hendra et al., 2022) can predict m⁶A RNA modifications with ~90% accuracy for all RRACH motifs.

Although simultaneous detection by ONT of all modifications present on individual native RNA molecules is not yet a reality, rapid technological progress bodes well that research on the interplay among different marks on specific transcripts will be possible in the near future.

1. Introduction

	m⁶A mapping method	Transcriptome wide	Nucleotide resolution	Quantification output
Antibody-dependent	MeRIP-seq m⁶A-seq/m⁶A-seq2	✓	✗ ~200 nt	Enrichment
	PA-m⁶A-seq	✓	✗ ~30 nt	Enrichment
	miCLIP/miCLIP2 m⁶A-CLIP	✓	✓	Enrichment
	m⁶A-LAIC-seq	✓	✗ ~200 nt	Relative quantification of individual transcripts based on methylated/unmethylated RNA spike-ins
	m⁶ACE-seq	✓	✓	Relative quantification of individual m ⁶ A sites based on methylated/unmethylated RNA spike-ins
	TNT-seq	✓	✗ ~200 nt	Enrichment
Antibody-free	SCARLET	✗	✓	Absolute quantification of individual m ⁶ A sites
	SELECT	✗	✓	Absolute quantification of individual m ⁶ A sites
	MAZTER-seq m⁶A-REF-seq	✓ m ⁶ ACA only	✓	Relative quantification based on MazF cleavage efficiency
	m⁶A-TRIBE	✓	✗ ~500 nt	Relative quantification based on A-to-I editing rate
	DART-seq/scDART-seq	✓	✓	Relative quantification based on C-to-U editing rate
	m⁶A-SEAL	✓	✗ ~200 nt	Enrichment
	m⁶A-label-seq	✓	✓	No quantification
	m⁶A-SAC-seq	✓ Gm ⁶ AC bias	✓	Relative quantification based on RT mutation rate
	GLORI-seq	✓	✓	Absolute quantification
	eTAM seq	✓	✓	Absolute quantification
	Nanopore sequencing	✓	✓	Absolute quantification

Table 2. Methods used for m⁶A mapping and quantification.

1.4.6 m⁶A functions within the mRNA life cycle

During the last decade, m⁶A was shown to play a role in almost every aspect of mRNA processing including splicing, nuclear export, translation and decay (**Figure 3**). Most of m⁶A functions are mediated by m⁶A reader proteins, which directly bind to the modification or are influenced by its presence in their RNA-binding ability.

– m⁶A and transcription

Act I of the mRNA life cycle is transcription, the process of creating an RNA copy from a DNA template by RNA polymerase enzymes.

1. Introduction

First hints of a link between m⁶A deposition and transcription regulation come from studies showing that m⁶A affects histone modification levels by reducing the stability of mRNAs coding for histone-modifiers (Y. Wang et al., 2018) and that METTL3 localizes to the TSS of active genes on chromatin (Barbieri et al., 2017). Subsequently, co-transcriptional deposition of m⁶A on chromosome-associated regulatory RNAs (carRNAs) was reported to result in YTHDC1-mediated destabilization leading to reduced chromatin accessibility and downstream gene transcription (J. Liu et al., 2020). Conversely, work by Li and colleagues described how m⁶A-bound YTHDC1 promotes co-transcriptional removal of the repressive histone H3 dimethylation at Lys9 (H3K9me2) via recruitment of the KDM3B demethylase resulting in enhanced gene expression (Y. Li et al., 2020). Another study reported that methylation of long and stable eRNAs stimulates enhancer and gene transcription. The authors showed that m⁶A deposition on eRNAs transcribed from highly active enhancers recruits YTHDC1, whose intrinsically disordered regions promote phase separation and formation of BRD4-containing active transcriptional condensates (J. H. Lee et al., 2021). Additionally, in *Drosophila* cells, the recruitment of the m⁶A writer complex as well as Ythdc1 to promoters of highly expressed genes was shown to induce release of Pol II promoter-proximal pausing and transition to transcription elongation in an m⁶A-dependent manner (Akhtar et al., 2021). In agreement with these observations, METTL3-dependent m⁶A deposition on nascent pre-mRNAs, promoter upstream transcripts and eRNAs prevents premature RNA cleavage and paused Pol II destabilization by the Integrator complex (W. Xu et al., 2022). The interplay between the m⁶A machinery and the chromatin modifying enzymes suggests that epitranscriptomic and epigenetic modifications cooperate to increase adaptability and accuracy of gene expression control.

Interestingly, while YTHDF2 was shown to localize to mitotic chromatin to prevent potential DNA damage caused by accumulation of m⁶A-marked R-loops (Abakir et al., 2020), METTL3-dependent m⁶A deposition promotes the formation of co-transcriptional R-loops around transcription end sites, which are necessary to avoid readthrough activity of Pol II and efficient transcription termination (X. Yang et al., 2019).

– m⁶A and splicing

First indications of a possible role of m⁶A in the regulation of splicing come from early studies that observed impaired splicing of the m⁶A-modified bovine *prolactin* pre-mRNA (Carroll et al., 1990) and avian retrovirus RNA (Stoltzfus & Dane, 1982) upon SAM-dependent methylation inhibition. However, contradictory results in regard of splicing were extrapolated from the first transcriptome-wide maps of m⁶A, showing either non-significant enrichment of m⁶A peaks at exon-exon junctions (Meyer et al., 2012) or higher methylation density in multi-isoform genes compared to single-isoform ones (Dominissini et al., 2012).

In the following years, efforts were made to define the reader proteins mediating the possible role of m⁶A in splicing regulation. In virtue of YTHDC1 unique nuclear localization, its binding to m⁶A-modified transcripts was studied in relation to the nuclear steps of RNA metabolism, such as splicing and export. Notably, YTHDC1 was reported to antagonize SRSF10, a splicing factor that promotes exon skipping, while recruiting SRSF3 to its target RNAs, resulting in m⁶A-dependent exon inclusion (W. Xiao et al., 2016). Furthermore, depletion of the m⁶A indirect readers HNRNPC (N. Liu et al., 2015) and HNRNPA2B1 (Alarcón et al., 2015) results in genome-wide changes in alternative splicing patterns analogous to those observed upon METTL3 depletion, supporting a model in which m⁶A-dependent RNA switches influence

1. Introduction

the binding of pre-mRNA processing factors and regulate a subset of alternative splicing events. Mechanistic insights into m⁶A-regulated splicing were also provided by work on m⁶A eraser proteins. FTO depletion was reported to lead to increased m⁶A levels and SRSF2 recruitment at exonic splicing sites, promoting exon inclusion for thousands of genes (X. Zhao et al., 2014). Among those, *FTO* KD promoted m⁶A-dependent inclusion of exon 6 of Runt-related transcription factor 1 (RUNX1T1) leading to reduced levels of RUNX1T1 short isoform and impaired adipocyte differentiation in mouse cells (X. Zhao et al., 2014). Conversely, work from Bartosovic and colleagues reported an opposite trend of increased exon skipping upon FTO depletion in HEK293T cells (Bartosovic et al., 2017). In addition, tight regulation of m⁶A levels via demethylation by ALKBH5 was shown to be necessary for correct splicing and production of transcripts with long 3'UTRs in the nucleus of mouse spermatocytes. During the progression of spermatogenesis, transcripts with long 3'UTRs are instead marked by m⁶A and consequently degraded to allow spermatocytes to develop into elongating spermatids (Tang et al., 2018).

Since addressing the role of m⁶A in splicing regulation at the mature RNA level proved to be challenging because both splicing and m⁶A deposition occur co-transcriptionally, TNT-seq was developed to specifically detect m⁶A on nascent RNA transcripts (Louloupi et al., 2018). Analysis of splicing dynamics by TNT-seq revealed that m⁶A deposition at exonic splicing sites positively correlates with fast processed introns, while the presence of m⁶A sites within introns is associated with slowly processed ones (Louloupi et al., 2018). Moreover, authors showed a link between intronic m⁶A and alternative splicing events, while m⁶A at exonic splicing sites was shown to be associated with constitutive splicing (Louloupi et al., 2018). In line with these observations, comparison of alternatively spliced isoforms between m⁶A-modified and unmodified mRNAs by m⁶A-LAIC-seq in hESCs revealed reduced exon skipping in the m⁶A-positive fraction (Molinie et al., 2016).

In addition, both miCLIP2 and m⁶A-SAC-seq experiments detected accumulation of m⁶A at 5' splice sites of retained introns, whose loss results in increased splicing efficiency at these sites (Hu et al., 2022; Körte et al., 2021).

In *Drosophila*, m⁶A was shown to regulate alternative splicing of *Sex lethal (Sxl)* for efficient female sex determination. *Sxl* is the master determinant of fly female identity, whose downstream regulatory cascades control somatic sex determination, dosage compensation and germline development. A ratio of X chromosomes to autosomes that is equal to one allows expression of *Sxl* in females (2X:2A), while the transcript is degraded in males (1X:2A). The underlying mechanism relies on sex-specific splicing of *Sxl*: the male isoform includes the internal exon L3 that introduces a premature stop codon and targets the transcript for degradation, while this exon is skipped in females. *Sxl* is an RNA-binding protein that positively regulates its own expression as well as splicing-dependent expression of *transformer (tra)*, which is at the top of the somatic sex determination signaling cascade leading to female-specific development. In addition, *Sxl* suppresses translation of *male-specific lethal-2 (msl-2)*, which controls hyperactivation of the single X chromosome of males for dosage compensation. miCLIP data revealed m⁶A enrichment within the two introns flanking the male-specific *Sxl* exon exclusively at the developmental stage when the *Sxl* autoregulatory switch is activated in females (Kan et al., 2017). While splicing is not affected in male flies, loss of either *Mettl3*, *Mettl14* or *Ythdc1* in females results in aberrant expression of *Sxl* male-specific isoform and significant reduction of the female-specific one as well as enhanced female lethality in *Sxl* sensitized backgrounds (Hausmann et al., 2016; Kan et al., 2017; Lence et al., 2016).

1. Introduction

Despite the strong evidence supporting m⁶A involvement in the regulation of *Drosophila Sxl* sex-specific splicing (Hausmann et al., 2016; Kan et al., 2017; Lence et al., 2016) and the fact that m⁶A promotes exon inclusion (Hu et al., 2022; Körtel et al., 2021; Molinie et al., 2016; W. Xiao et al., 2016; X. Zhao et al., 2014) or exclusion (Bartosovic et al., 2017) in subsets of mammalian transcripts, the role of m⁶A in global regulation of splicing is still under debate. Some studies reported the presence of m⁶A near splice sites on both the exonic and intronic side (N. Liu et al., 2015; Louloui et al., 2018; G. Wei et al., 2021), while others did not find such enrichment (Ke et al., 2017; Meyer et al., 2012). Furthermore, the number of exons that are alternatively spliced upon depletion of METTL3 is consistently small (Dominissini et al., 2012; Geula et al., 2015; Ke et al., 2017; G. Wei et al., 2021; W. Xiao et al., 2016). As a matter of fact, the effect of m⁶A deposition/removal on splicing appears to be transcript-specific and dependent on specific downstream effectors. Additionally, alteration of the expression levels of splicing regulators whose mRNA is methylated might also indirectly contribute to the impact of m⁶A on splicing.

– m⁶A and alternative polyadenylation

m⁶A spatial bias toward the 3'UTR of transcripts suggested a possible connection with regulation of APA in mRNAs with multiple polyA sites. Notably, high density of m⁶A sites was detected in the last exon of transcripts, especially if long and coding for the 3'UTR, and the presence of m⁶A nearby the proximal polyA site was shown to inhibit proximal polyadenylation in the majority of transcripts with two APA sites (Ke et al., 2015). In contrast to what reported by Ke and colleagues, APA analysis based on m⁶A-LAIC-seq data revealed that m⁶A sites in the 3'UTR promote proximal rather than distal polyadenylation (Molinie et al., 2016). Mechanistically, Yue and colleagues proposed that VIRMA recruits the core components of the writer complex for preferential m⁶A deposition within 3'UTRs. RNA-dependent interaction of VIRMA with the polyadenylation cleavage factors CPSF5 and CPSF6 was shown to regulate APA, although mostly enhancing the selection of proximal polyadenylation sites (Yue et al., 2018). YTHDC1 was also shown to interact with CPSF6, and its loss causes extensive differential usage of APA sites and arrested maturation in mouse oocytes (Kasowitz et al., 2018).

– m⁶A and nuclear export

In higher eukaryotes, the export of most mRNAs to the cytoplasm relies on the cap- and splicing-dependent recruitment of the TREX complex within the nucleus. The TREX complex contains the multi-subunit THO complex (THOC1-2-3-5-6-7), the DExD-box RNA helicase UAP56 and RNA export adapters such as ALYREF (THOC4). Direct interaction with the cap binding complex as well as with components of the spliceosome facilitates recruitment of the TREX complex to the 5' end of spliced mRNAs. Next, ALYREF and THOC5 promote loading of the NXF1-NXT1 heterodimer onto the transcript, which mediates binding to the nucleopore element Nup62 and export of spliced mRNAs in the 5'→3' direction (Khan et al., 2022).

Consistent with early observations of significantly delayed export of mature mRNAs upon inhibition of SAM-dependent methylation (Camper et al., 1984), depletion of the m⁶A demethylase ALKBH5 in HeLa cells results in accelerated mRNA export that can be rescued only by overexpression of catalytically active ALKBH5 (Zheng et al., 2013). The nuclear m⁶A reader YTHDC1 was identified as the main mediator of the translocation of methylated transcripts from nucleus to cytoplasm. Specifically, TREX was shown to stimulate the recruitment of YTHDC1 (Lesbirel et al., 2018), which by interacting with SRSF3 and SRSF7,

1. Introduction

promotes the binding of NXF1 to facilitate export of selected m⁶A-modified transcripts (Roundtree et al., 2017). In addition to the cap binding complex and elements of the spliceosome, the m⁶A writer complex also appears to drive association of TREX with mRNA for nuclear export. Since ALYREF binding to transcripts is mainly mediated by interaction with EJCs (Gromadzka et al., 2016), it has been hypothesized that high m⁶A enrichment within long exons might help TREX recruitment in regions depleted of EJCs (Lesbirel et al., 2018). Interestingly, the delayed nuclear export of clock genes such as *Bmal1* and *Per2* that results from METTL3 depletion was shown to contribute to a phenotype of circadian period elongation (Fustin et al., 2013).

Recently, different studies reported the involvement of FMR1 in m⁶A-dependent mRNA nuclear export. FMR1 was shown to preferentially bind m⁶A-modified transcripts to facilitate their translocation to the cytoplasm via interaction with the export protein CRM1 (Edens et al., 2019; Hsu, Shi, et al., 2019). In the cortex of *FMR1* KO mice, nuclear retention of m⁶A-modified FMR1 targets involved in neurogenesis (*Ptch1*, *Dll1*, *Dlg5*, *Fat4*, *Gpr161*, and *Spop*) leads to extended maintenance of proliferating neural progenitors into postnatal stages and delayed neuronal differentiation (Edens et al., 2019). Although their role in Alzheimer's disease or other APP-related disorders has not been determined yet, transcripts coding for the APP-processing enzymes *Adam9* and *Psen1* are found among the methylated targets of FMR1 and their enrichment in cytoplasm vs nucleus is abolished in *FMR1* KO mice (Westmark et al., 2020). However, despite the *App* mRNA itself being methylated and FMRP repressing its translation, this effect seems not related to the m⁶A-dependent localization of *App* (Westmark et al., 2020).

– m⁶A and translation

In regard to the steps of the mRNA life cycle that take place within the cytoplasm, the most credited theory at first was that m⁶A could either promote translation or enhance mRNA decay according to which YTHDF paralogs it was bound to. Unlike YTHDF2, both YTHDF1 and YTHDF3 were shown to stimulate cap-dependent translation of their methylated mRNA targets, via recruitment of the translation initiation factor eIF3 for YTHDF1 (X. Wang et al., 2015) or via support to YTHDF1 function for YTHDF3 (A. Li et al., 2017; Shi et al., 2017). To explain how YTHDF1 binding to the 3' end of mRNAs, where m⁶A is enriched, could affect the recruitment of eIF3 to the 5'UTR near start codons, it was proposed that YTHDF1 may come nearby translation initiation sites thanks to the mRNA closed-loop connecting polyA-bound PABP with cap-bound eIF4F during translation (X. Wang et al., 2015). Furthermore, association between m⁶A-bound YTHDF3 and eIF4G2 was reported to drive translation initiation of circular RNAs in human cells (Y. Yang et al., 2017). However, recent studies combining reanalysis of published data with new experiments substantially challenged the notion that m⁶A recognition by YTHDFs proteins plays a role in translation initiation. None of the three YTHDF paralogs was found to be associated with actively translated mRNAs within polysome fractions and depletion of any of them did not have a significant impact on mRNA translation (Lasman et al., 2020; Zaccara & Jaffrey, 2020), suggesting that changes in translation efficiency of methylated mRNAs observed upon METTL3 depletion (Hu et al., 2022) are not directly mediated by binding of YTHDF proteins to m⁶A, but rather by indirect effects such as alteration of ribosomal transcript expression levels. Nevertheless, in mouse hippocampal neurons, YTHDF1 was shown to promote translation of some of its m⁶A-modified targets in response to neuronal stimuli facilitating in this way memory formation and learning (Shi et al., 2018).

1. Introduction

The impact of m⁶A on translation elongation was also investigated in a couple of studies. Despite causing codon-specific ribosome pausing and less active translation (Choi et al., 2016), the presence of m⁶A sites within the CDS was shown to promote global translation efficiency of mRNAs with stable secondary structures at the methylated sites (Mao et al., 2019). In agreement with previous observations that 5'UTR unwinding by YTHDC2 promotes translation initiation of metastasis-related transcripts in human cancer cells (Tanabe et al., 2016), m⁶A in the CDS was shown to be recognized by YTHDC2, whose helicase activity was critical to resolve local secondary structures and promote translation of structured mRNAs (Mao et al., 2019). Notably, YTHDC2 was reported to directly interact with 18S rRNA in close proximity to the mRNA tunnel of the 40S small ribosomal subunit, suggesting that YTHDC1 may regulate the association of its m⁶A-modified targets with ribosomes for translation (Kretschmer et al., 2018).

A mechanism by which m⁶A promotes mRNA translation in a cap-independent way was also described (Coots et al., 2017; Meyer et al., 2015; Zhou et al., 2015). More specifically, m⁶A sites in 5'UTRs are directly bound by eIF3, which in turn recruits the 40S small ribosomal subunit to initiate translation in the absence of the eIF4F complex. Several cellular stresses were reported to increase methylation levels in the 5'UTR of selected transcripts (e.g., *Hsp70*), enabling adaptive cap-independent translation initiation in response to stress conditions (Coots et al., 2017; Meyer et al., 2015; Zhou et al., 2015). Interestingly, m⁶A was recently shown to mark the 5'UTRs of previously undescribed uncapped and polyadenylated transcripts (5'UPTs) consisting of the terminal part of mRNAs cleaved off upon APA (Malka et al., 2022). 5'UPTs appear to be translated in a CAP-independent way, suggesting that the presence of m⁶A at their 5' end could enhance the recruitment of ribosomes for non-canonical protein production (Malka et al., 2022).

Acting as a reader rather than a writer of m⁶A, METTL3 itself was shown to enhance translation of a subset of m⁶A-modified transcripts independently of its methyltransferase activity (Choe et al., 2018; S. Lin et al., 2016). METTL3 bound in proximity to stop codons was shown to promote translation thanks to interaction with the eIF3h subunit of the eIF3 complex and resulting mRNA circularization (Choe et al., 2018).

– m⁶A and mRNA stability

Over the years, growing evidence highlighted that RNA modifications, especially m⁶A, play a key role in the regulation of mRNA stability. The inverse correlation between m⁶A and transcript stability became first evident in studies that reported increased mRNA half-life upon depletion of m⁶A writer proteins (i.e., METTL3, METTL14 and WTAP) in both human and mouse cells (Batista et al., 2014; J. Liu et al., 2014; Schwartz, Mumbach, et al., 2014; Y. Wang et al., 2014). Notably, m⁶A destabilizing effect is directly proportional to the number and stoichiometry of methylation sites on the mRNA (C. Liu et al., 2022; Molinie et al., 2016; Y.-L. Xiao et al., 2023).

Different papers described YTHDF2 as the main m⁶A reader protein mediating mRNA decay, either targeting transcripts to processing bodies (P bodies) and stress granules (Ries et al., 2019; X. Wang et al., 2014) or directly recruiting the CCR4-NOT deadenylase complex for degradation (H. Du et al., 2016). However, recent studies suggested a new model for the integrated function of YTHDF proteins in the regulation of methylated transcripts. Rather than each mediating distinct effects on different groups of RNA targets, all three YTHDF paralogs were shown to bind essentially to the same m⁶A-modified transcripts and to act redundantly in the regulation of mRNA decay (Lasman et al., 2020; Zaccara &

1. Introduction

Jaffrey, 2020). Accordingly, all three YTHDF proteins interact with similar protein partners, including, among the strongest interactors, subunits of the CCR4-NOT deadenylase complex (H. Du et al., 2016; Youn et al., 2018), the 5'→3' exoribonuclease XRN1 (Youn et al., 2018), and components of stress granules (Markmiller et al., 2018; Youn et al., 2018). Even though mild or no effect on mRNA stability were observed upon depletion of single paralogs, loss of all three YTHDF proteins results in significant stabilization of m⁶A-modified mRNAs, suggesting dosage-dependent functional compensation (Lasman et al., 2020; Zaccara & Jaffrey, 2020). In addition to deadenylation followed by decapping and 5'→3' exoribonucleolytic cleavage, interaction between YTHDF2 and RNase P/MRP (bridged by HRSP12) was reported to contribute to endoribonucleolytic m⁶A-mediated decay of mRNAs and circRNAs (Park et al., 2019). Despite the fact that the interaction between YTHDC2 and XRN1 suggested its involvement in regulating the stability of m⁶A-containing transcripts (Hsu et al., 2017; L. Li et al., 2022; Wojtas et al., 2017), it appears that the m⁶A-binding ability of YTHDC2 is dispensable for its function in mRNA decay (L. Li et al., 2022; R. Liu et al., 2021; Saito et al., 2022).

Opposite to the degradation-prone function of the YTHDF paralogs, binding by other reader proteins, such as IGF2BPs (H. Huang et al., 2018), FMR1 (F. Zhang et al., 2018) and PRRC2A (R. Wu et al., 2019), increases the half-life of mRNAs in an m⁶A-dependent way. Interestingly, the fact that the presence of m⁶A repels binding of the mRNA stabilizer proteins G3BPs and HuR results in a positive regulation of the stability of unmethylated mRNAs (Arguello et al., 2017; Edupuganti et al., 2017; Y. Wang et al., 2014), suggesting that the increase in mRNA stability observed upon METTL3 depletion may be partially due to binding of G3BPs/HuR to these unmethylated mRNAs.

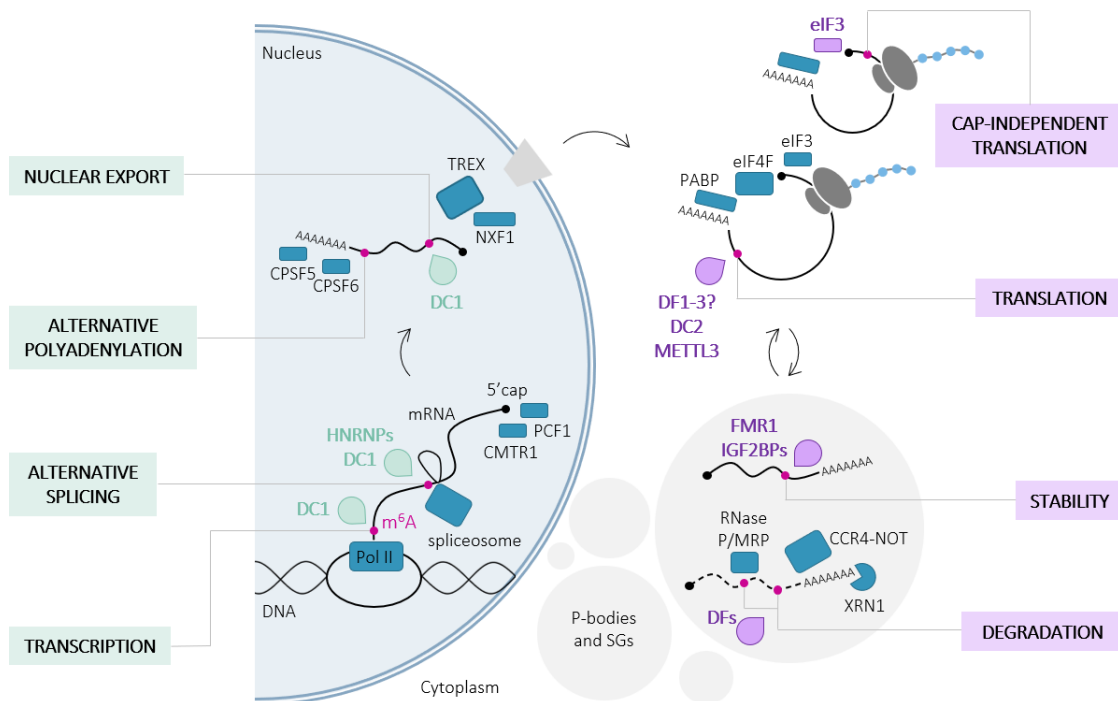


Figure 3. m⁶A functions within the mRNA life cycle.

Schematic representation of known m⁶A readers involved in different RNA processing steps. m⁶A readers in the nucleus and cytoplasm are shown in turquoise and purple, respectively.

1.4.7 m⁶A biological significance

Numerous studies have demonstrated that m⁶A and its regulators have an effect on both the physiological and pathological sides of many biological functions, and alterations in deposition, removal or recognition of m⁶A have been linked to various human diseases, including different types of cancer (J. Liu et al., 2019). Some examples of m⁶A biological significance are described in this chapter.

– Chromatin status and genome integrity

The first example of how m⁶A can have an impact on chromatin status comes from the reported function of m⁶A in *XIST*-mediated X chromosome gene silencing. In mammalian females, transcriptional inactivation of one of the two X chromosomes is required to achieve comparable expression of X chromosome-associated genes between male and females. The lncRNA *XIST*, which is expressed exclusively by the inactive X chromosome, interacts with chromatin at specific foci and generates local protein gradients that propagates silencing across the whole X chromosome (Brockdorff et al., 2020; Markaki et al., 2021). Work from Patil and colleagues revealed that *XIST* is highly methylated and recognition of its m⁶A sites by YTHDC1 is required for efficient gene silencing (Patil et al., 2016).

Several recent studies highlighted that m⁶A deposition on carRNAs is associated to silencing of endogenous retroviruses (ERVs) for maintenance of genome integrity in mESCs (Chelmicki et al., 2021; J. Liu et al., 2020, 2021; W. Xu et al., 2021). ERVs, such as intracisternal A particles (IAPs), long interspersed nuclear element 1 (LINE1) and ERVK, are mobile genetic elements scattered all over mammalian genomes that are derived from ancient retroviral infections in germ cells. Mechanisms of defense against expression and mobilization of ERVs are critical to avoid dysregulation of neighboring gene loci and ensure stability of the host genome. METTL3-dependent m⁶A deposition on ERV-derived mRNAs, predominantly IAPs, was shown to contribute to retrotransposon repression, either via YTHDC1-mediated recruitment of the methyltransferase SETDB1, which catalyzes histone H3 trimethylation at Lys9 (H3K9me3) and induces the formation of heterochromatin at ERV loci (J. Liu et al., 2021; W. Xu et al., 2021), or via YTHDF-mediated RNA decay (Chelmicki et al., 2021). Even though different publications reported m⁶A as an abundant modification of LINE1 transcripts, contrasting models were proposed regarding its function. On one hand, methylated LINE1 transcripts displayed increased ability to stabilize heterochromatin via formation of RNA-DNA hybrids (Duda et al., 2021) or recruitment of enzymes depositing repressive histone marks (J. Wei et al., 2022), while, on the other hand, the presence of m⁶A was shown to exert a positive effect on expression and retrotransposition of young LINE1s (Xiong et al., 2021). Divergency between reported models could be linked to different experimental approaches, however it is also possible that these different mechanisms cooperate for efficient regulation of retrotransposons in mESCs.

– Stress response

Upon cellular stress, increased m⁶A levels are observed in the 5'UTR of selected transcripts as a result of relocalization of YTHDF2 to the nucleus, which prevents FTO-mediated demethylation at these sites (Zhou et al., 2015). m⁶A within 5'UTRs is directly recognized by eIF3 and enables selective cap-independent translation in stress conditions, such as heat shock, which are characterized by almost complete suppression of canonical cap-dependent translation (Meyer et al., 2015; Zhou et al., 2015). In

1. Introduction

agreement with these observations, acute temperature stress was shown to induce relocalization of METTL3 together with the microprocessor complex subunit DGCR8 to heat-shock transcripts, which are co-transcriptionally marked for degradation, allowing for timely cell recovery (Knuckles et al., 2017). Binding of m⁶A by the YTHDF proteins is also critical for the formation of stress granules (Y. Fu & Zhuang, 2020).

Another example of m⁶A function during stress is the rapid and transient METTL3-mediated methylation of mRNAs at DNA damage sites upon UV irradiation. A model in which these m⁶A sites on nascent transcripts promote rapid recruitment of the DNA polymerase Pol κ to damage sites for efficient repair of DNA lesions was initially proposed (Xiang et al., 2017). Interestingly, later studies suggested that UV-induced m⁶A deposition at DNA damage sites collaborates to damage resolution either promoting accumulation of RNA-DNA hybrids for homologous recombination-mediated repair of double strand breaks (C. Zhang et al., 2020) or enhancing RNaseH1-mediated R-loop resolution (Kang et al., 2021).

In addition, m⁶A levels in the 3'UTR of mRNAs are significantly upregulated in response to reactive oxygen species (ROS)-induced stress and play an important role in protecting cells from DNA damage and apoptosis. Mechanistically, ROS trigger sumoylation of ALKBH5 via the ERK/JNK signaling pathway, resulting in reduced m⁶A demethylation by ALKBH5 and consequential rapid expression of genes involved in different biological processes including DNA damage repair (F. Yu et al., 2021).

– Maternal-to-zygotic transition

m⁶A was shown to contribute to the decay of maternal and stage-specific transcripts during maternal-to-zygotic transition (MZT) in flies (G. Zhang et al., 2022), zebrafish (Kontur et al., 2020; B. S. Zhao et al., 2017) and mouse (X. Sui et al., 2020; Y. Wu et al., 2022). While the role of m⁶A-bound YTHDF readers in maternal RNA decay was described in both zebrafish and mouse, it appears that murine YTHDF2 contributes to MZT regulation in an m⁶A-independent way (Y. Wu et al., 2022). In flies, FMR1 binding to m⁶A-modified maternal transcripts promotes cytoplasmic granule condensation, which recruits unmodified transcripts contributing to maternal RNA decay of both methylated and unmethylated mRNAs (G. Zhang et al., 2022).

– Stem cell differentiation

m⁶A is essential for mammalian development and it has been shown to be among the factors maintaining the equilibrium between ESC self-renewal and differentiation. On one hand, m⁶A methylation is required to maintain pluripotency and self-renewal capability of mESCs (Aguilo et al., 2015; Y. Wang et al., 2014; Wen et al., 2018). Mechanistically, the chromatin-associated zinc finger protein 217 (ZFP217) was shown to sequester METTL3 to avoid m⁶A-mediated destabilization of pluripotency-associated factors to safeguard ESC identity (Aguilo et al., 2015). On the other hand, METTL3-mediated m⁶A deposition promotes the transition from pluripotent to differentiation-primed state via timely reduction of the stability of key pluripotency-promoting transcripts (e.g., *Nanog*) and *METTL3* KO results in impaired cellular differentiation in mouse as well as human ESCs (Batista et al., 2014; Bertero et al., 2018; Geula et al., 2015) and early embryonic lethality in mouse embryos (Geula et al., 2015). Similar defects in embryonic development were also observed upon depletion of *METTL14* (Meng et al., 2019).

1. Introduction

In addition, the activity of m⁶A writers and readers is required for efficient hematopoietic stem cell (Jiang et al., 2021) and adipocytes (Kobayashi et al., 2018; X. Zhao et al., 2014) differentiation as well as for gametogenesis and neurogenesis.

- **Gametogenesis**

In germ cells, loss of METTL3 results in compromised spermiogenesis (Z. Lin et al., 2017; K. Xu et al., 2017) as well as oogenesis (Mu et al., 2021; X. S. Sui et al., 2020). Consistently with its high expression in testis, also ALKBH5 was shown to contribute to spermatogenesis progression (Zheng et al., 2013). From the point of view of the m⁶A reader proteins, loss of YTHDC1 causes extensive alternative splicing and polyadenylation defects in oocytes as well as loss of spermatogonia in testis (Kasowitz et al., 2018). Notably, although YTHDC2 is required for meiotic progression in mouse germ cells (Bailey et al., 2017; Hsu et al., 2017; Jain et al., 2018; R. Liu et al., 2021; Wojtas et al., 2017), its m⁶A-binding activity is dispensable for this function (L. Li et al., 2022; R. Liu et al., 2021; Saito et al., 2022). In addition to regulation of transcript dosage for proper oocyte maturation (Ivanova et al., 2017), YTHDF2 was shown to be required for the timely turnover of phase-specific mRNAs during spermatogenesis progression (Qi et al., 2022).

- **Neurogenesis**

Multiple lines of evidence indicate that m⁶A plays a central role in controlling both development and function of the nervous system. m⁶A levels are particularly high in the mouse brain (Meyer et al., 2012) as well as in the head of flies (Lence et al., 2016) and gradually increase along with the progression of neurogenesis. Depletion of m⁶A pathway components results in delayed or impaired neuronal development in several organisms. For instance, m⁶A depletion by loss of either METTL3 or METTL14 results in prolonged cell cycle and delayed differentiation of mouse cortical neural progenitors due to increased stability of neurogenesis-related transcripts that are normally m⁶A-tagged for degradation (Yoon et al., 2017). Similar developmental defects are also observed in mice depleted of YTHDF2 suggesting that the cytoplasmic reader participates to m⁶A function in cortical neurogenesis (M. Li et al., 2018). YTHDF2 was also shown to inhibit expression of neural-specific factors for maintenance of pluripotency until neuronal differentiation induction in human induced pluripotent stem cells (iPSCs) (Heck et al., 2020).

Notably, m⁶A levels are generally higher in mouse cerebellum than cortex (M. Chang et al., 2017) and contribute to regulate stability and splicing of mRNAs related to cerebellar development and apoptosis (C.-X. Wang et al., 2018). Tight regulation of m⁶A levels is essential also for postnatal development of the mouse cerebellum and depletion of either METTL3 or ALKBH5 at the P7 stage, which is characterized by the highest m⁶A levels, causes defective cerebellar development (C. Ma et al., 2018). In addition, FTO-mediated m⁶A demethylation stimulates local translation of the growth-associated protein 43 (GAP-43), which in turn promotes axonal elongation (J. Yu et al., 2018). Upon axon injury, the m⁶A machinery is required to promote local protein synthesis and axon regeneration in both central and peripheral adult mammalian nervous system (Y. L. Weng et al., 2018).

1. Introduction

– Learning and memory formation

In line with its high abundance in the synaptic transcriptome of adult mouse forebrains (Merkurjev et al., 2018), m⁶A was shown to contribute to the regulation of local dendritic translation at the base of the synaptic plasticity required for formation and maintenance of memory. In response to behavioral experience, fear conditioning or acute stress, increased m⁶A levels in different regions of the brain, such as prefrontal cortex and hippocampus, are critical for efficient memory formation in mice (Walters et al., 2017; Widagdo et al., 2016). Consistently, loss of FTO in hippocampal (Walters et al., 2017) or prefrontal cortex (Widagdo et al., 2016) neurons is sufficient to enhance fear-memory formation, while depletion of METTL3 (Engel et al., 2018; Z. Zhang et al., 2018) or YTHDF1 (Merkurjev et al., 2018; Shi et al., 2018) in hippocampus causes synaptic dysfunctions and reduces long-term memory consolidation. Mechanistically, reduced m⁶A levels were proposed to cause insufficient translation of immediate-early genes, such as *Arc* and *c-Fos*, whose rapid activation in response to neuronal activity is necessary for efficient learning (Z. Zhang et al., 2018). Furthermore, *FTO* deletion in dopaminergic neurons causes reduced protein expression of components of the dopamine-mediated inhibitory signaling, resulting in enhanced sensitivity to the locomotor- and reward-stimulatory effect of cocaine (Hess et al., 2013).

1.4.8 m⁶A and cancer

In addition to m⁶A being critical for normal reproductive and central nervous system development and function, aberrant m⁶A levels on different substrates have been associated with the pathogenesis of various types of human cancers. m⁶A methylation has been reported to either promote or suppress tumor progression depending on the nature of the affected cancer-related pathways, the direction of the change in m⁶A levels and the regulatory effect mediated by the modification on target RNAs.

m⁶A can act as tumor promoter by stimulating the expression of several tumor-specific oncogenes. For instance, abnormally high levels of METTL3 and METTL14 result in hypermodification of some oncogenic transcripts (e.g., *MYC*, *MYB*, *BCL2*, *SP1*), whose overabundant translation products impair normal hematopoietic cell differentiation and promote acute myeloid leukemia (AML) development (Barbieri et al., 2017; Vu et al., 2017; H. Weng et al., 2018). Similarly, in breast cancer cells, excessive METTL3-deposited m⁶A enhances the expression of the *HBXIP* oncogene, which in turn leads to upregulation of METTL3 via suppression of the let-7g miRNA, generating a positive feedback loop that promotes malignant cancer progression (Cai et al., 2018). While in some tumors the increased translation of oncogenic transcripts (e.g., *CDCP1* in bladder cancer (F. Yang et al., 2019), *Snail* in liver cancer (X. Lin et al., 2019)) is mediated by m⁶A-bound YTHDF readers, in lung adenocarcinoma METTL3 itself acts as m⁶A reader promoting circularization and translation of a large subset of oncogenic mRNAs, including *BRD4*, *EGFR* and *TAZ*, via binding to the subunit h of the eIF3 complex (Choe et al., 2018; S. Lin et al., 2016).

Inversely, m⁶A can also negatively regulate tumor progression by inhibiting the expression of oncogenes and/or promoting the expression of tumor suppressor genes. In glioblastoma stem cells (GSCs), high levels of ALKBH5 result in increased demethylation of the oncogene transcript *FOXM1*, whose consequently enhanced expression leads to GSC proliferation and tumorigenesis (S. Zhang et al., 2017). In line with this, overexpression of METTL3 or inhibition of FTO can significantly suppress GSC growth and cancer development (Q. Cui et al., 2017). In addition, hypoxia-induced overexpression of ALKBH5 results in increased demethylation and stabilization of *Nanog* promoting breast cancer stem cells

1. Introduction

enrichment and tumorigenesis (C. Zhang et al., 2016). Similar to ALKBH5, high levels of FTO enhance tumor progression in lung squamous cell carcinoma (J. Liu, Ren, et al., 2018) and AML (Z. Li et al., 2017) by regulating expression of *MZF1* and *ASB2/RARA*, respectively. Notably, in approximately 70% of endometrial cancers, m⁶A levels are downregulated compared to healthy tissue due to mutations in the *METTL14* gene and reduced expression of METTL3. Low m⁶A mRNA methylation has been shown to affect multiple regulators of the AKT pathway leading to increased AKT signaling, which contributes to tumorigenesis in the endometrium (J. Liu, Eckert, et al., 2018). In hepatocellular carcinoma, METTL14 downregulation was reported to negatively regulate processing of pri-miR126 in an m⁶A-dependent way, disrupting the tumor suppressor function of miR126 and thereby accelerating tumor progression and metastasis (J. Ma et al., 2017).

To summarize, the interaction between m⁶A pathway and tumor metabolism is very complex and not completely clear yet. Current knowledge indicates that m⁶A modification has a dual role in cancer promotion and suppression with m⁶A regulators playing opposite roles in different cancer types or even in the same one. Nevertheless, the widespread involvement of the m⁶A pathway in tumor initiation and progression provides the opportunity to develop new approaches for early diagnosis and treatment of several types of cancer.

1.5 *Drosophila melanogaster*

1.5.1 The fruit fly as model organism

The fruit fly *Drosophila melanogaster* is one of the most powerful model organisms used in genetics and molecular research. Flies offer many practical advantages: they are easy and cheap to maintain in a laboratory, produce large numbers of offspring and have a much shorter life cycle than vertebrates. In addition, at the beginning of this century, the euchromatic portion of the fly genome (~120 Mb) was completely sequenced using a shotgun sequencing approach (Adams et al., 2000). The genome of *Drosophila melanogaster* codes for a bit less than 14,000 genes with relatively low redundancy compared to higher organisms, making flies ideal models for genetic analysis.

Fruit flies have four pairs of chromosomes, one pair of sexual chromosomes (X/X for females and X/Y for males) and three pairs of autosomes (Chr II, Chr III and Chr IV). While recombination is completely absent in males, recombination in females is controlled using balancer chromosomes. Balancer chromosomes are chromosomes whose sequence was inverted and rearranged so many times that they lost the ability to pair and recombine with their homolog during meiosis. Balancers are extensively used in crosses as well as stock maintenance and their presence can be easily and unequivocally recognized thanks to dominant marker mutations affecting, among others, wing shape, eye color and shape, bristle length and number. In addition, except for the X-chromosome, markers are often recessive lethal so that only flies heterozygous for the balancer can survive and balancers do not take over fly stocks.

1.5.2 The life cycle of *Drosophila melanogaster*

The life cycle of fruit flies takes approximately ten days at 25°C (**Figure 4**). Stocks can also be maintained at 18°C to slow down generation time.

1. Introduction

The development of *Drosophila melanogaster* consists of four distinct stages: egg, larva, pupa, and adult. After egg fertilization, embryogenesis (17 stages) is completed in ~21h. During the next two days, the hatched larvae (first instar) mature into second and then third instar larvae. After two more days of feeding (72-120 h), third instar larvae leave the food source and go through metamorphosis during the immobile stages of pupation (four days). Finally, adult flies emerge from the pupal case and their average life span is 40-50 days.

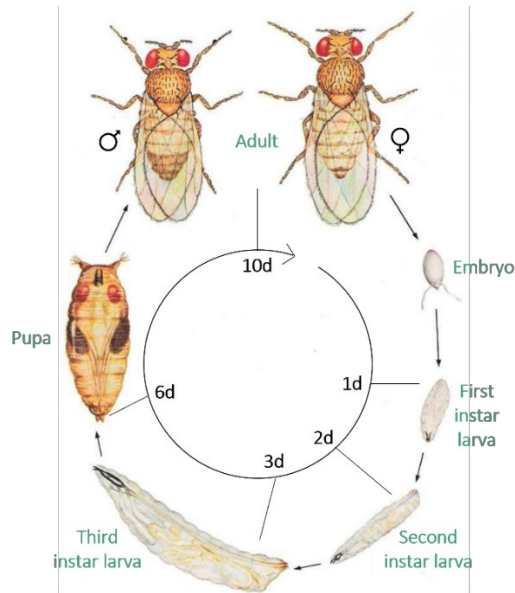


Figure 4. The *Drosophila melanogaster* life cycle at 25°C.

1.5.3 The larval neuromuscular junction

The neuromuscular junction (NMJ) is the chemical synapse at the region of contact between a motor neuron and a muscle fiber.

The larval NMJ system of *Drosophila melanogaster* is simple and stereotypic, the NMJ presynaptic terminal is large and easy to visualize, so it is widely used as a model to study neuronal development and synaptic function (Broadie & Bate, 1995; Menon et al., 2013). Larval NMJ synapses are excitatory and use ionotropic GluRs that are homologous to mammalian AMPA-type GluRs. Except for the first one (A1), each hemisegment (A2-A7) of third instar larvae displays an identical pattern of thirty muscles innervated by three peripheral motor nerves, the segmental (SN), the intersegmental (ISN) and the transverse (TN) nerve. Larval NMJs are organized in branches composed of chains of synaptic boutons. There are three types of synaptic boutons (types I, II and III), which differ in size and shape, release different neurotransmitters, and are associated with postsynaptic glutamate receptors with different subunit compositions. While type II and type III boutons are modulatory and use other neurotransmitters, type I boutons use glutamate and are further divided into Ib (big) and Is (small). Most NMJs consist of 20-50 boutons, however NMJs on muscles 6/7 can have twice as many boutons as they innervate two muscles. Most studies examine NMJs on muscles 6/7 because they contain only type I boutons and use only glutamate as neurotransmitter.

1. Introduction

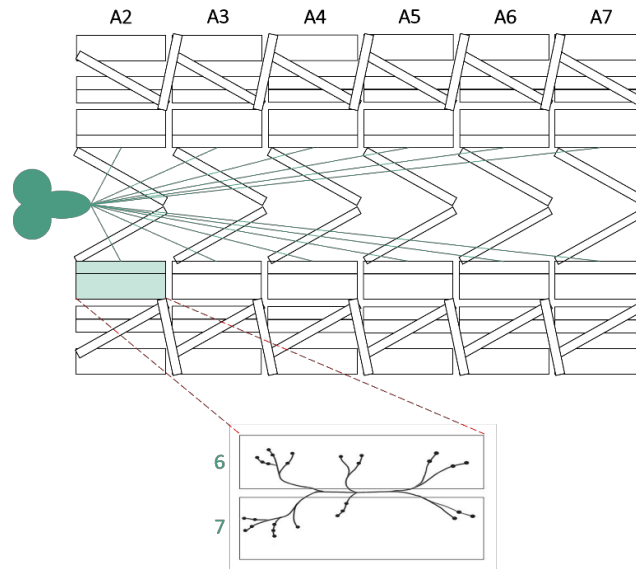


Figure 5. The *Drosophila melanogaster* larval NMJ system.

Schematic illustration of the third instar larvae dissected to expose the repeated body wall musculature and the brain with motor nerves innervating the muscles of each hemisegment (A2-A7). Zoom of the NMJ on muscles 6/7.

2. Materials and methods

Drosophila melanogaster stocks and genetics

Drosophila melanogaster fly stocks used in this study are listed in **Table 4**. Stocks were maintained at 25°C under a 12h light: 12h dark cycle on standard medium containing cornmeal, corn syrup, yeast, and agar. The control genotype for all experiments was *CantonS* unless otherwise stated. Mutant alleles for *Dhx57* and *Alkbh6* were generated using the CRISPR-Cas9 system following the previously described procedure (Kondo & Ueda, 2013) and were injected at FlyORF (University of Zurich). Two independent guide RNAs (gRNAs) per gene were designed using the gRNA design tool: www.crisprflydesign.org (see **Table 3**). Oligonucleotides were annealed and cloned into pBFv-U6.2 vector (National Institute of Genetics, Japan). Vectors were injected into embryos of *TBX-0002* flies. All flies were crossed with *TBX-0008* flies to identify positive recombinant flies by eye colour marker. Males were further crossed with *CAS-0001* females. Males carrying nos-Cas9 and U6-gRNA transgenes were screened for the expected deletion using oligos in **Table 3** and further crossed with the proper balancer line. *Dhx57^{fs}* allele produced a deletion of 2327 bp (1652-3978 bp in the genome region chrX:10894747..10899302, reverse complemented). *Alkbh6^{Δ11}* allele produced a deletion of 463 bp (260-722 bp in the genome region chr2L:10488694..10490461). UAS-FlagMyc-cDNA flies were generated by injection of UAS-FlagMyc-cDNA vectors at FlyORF. Cleaning of the genetic background of mutant fly lines (i.e., replacement of all chromosomes except for the region of mutation by recombination) was carried out via five sequential rounds of crosses with *CantonS* flies and selection.

Fly survival assay upon stress

For oxidative stress, twenty flies of specified genotype, aged 5-7 days and gender-separated, were fed daily on filter paper saturated with 5 mM of paraquat (methyl viologen dichloride hydrate, Sigma) in 5% sucrose or with 5% sucrose only. For starvation, twenty flies of specified genotype, aged 5-7 days and gender-separated, were starved with (wet starvation) or without (dry starvation) water. Stress exposure was performed with five biological replicates of twenty males/females per condition for each genotype tested. Mortality was monitored three times a day until all flies were dead. Statistically significant differences between survival curves were determined by pairwise log-rank test with a *post hoc* Bonferroni-Holm correction.

Cloning

The plasmids used in this study are listed in **Table 5**. The plasmids used for immunohistochemistry and co-immunoprecipitation assays in S2R+ cells were constructed by cloning the corresponding cDNA in the pPAC vector with N-terminal Myc-tag (Astigarraga et al., 2010) and the Gateway-based vectors with N-terminal FlagMyc-tag (pPFMW) as well as C-terminal HA-tag (pPWH) (*Drosophila* Genomics Resource Center, DGRC).

Cell culture, RNAi and transfection

Drosophila melanogaster S2R+ are embryonic-derived cells (FBtc0000150), while BG3 cells are derived from the central nervous system of third instar larvae (FBtc0000068). Cells were obtained from the DGRC

2. Materials and methods

and cultured in Schneider's *Drosophila* medium (Bioconcept) supplemented with 10% FBS (Sigma) and 1% Penicillin-Streptomycin (Sigma). The culture medium for BG3 cells was supplemented with 10 µg/ml insulin. Mycoplasma contamination was not detected. For RNAi experiments, dsRNAs were prepared using the T7 megascript Kit (NEB). 2/20 million S2R+ cells were seeded in serum-free medium in 6-well plates/10cm-dishes and treated with 15/75 µg of dsRNAs. After 6 h of cell starvation, serum-supplemented medium was added to the cells. dsRNA treatment was repeated after 48 and 96 h and cells were collected 24 h after the last treatment. dsRNA against bacterial β-galactosidase gene (*lacZ*) was used as a control for all RNAi experiments. Effectene (Qiagen) was used for plasmid transfection according to the manufacturer's protocol.

S2R+ cells exposure to stress

S2R+ cells were exposed to different types of stress. For heat or cold shock, cells were kept at 37°C or 4°C, respectively, for 2 h, followed or not by 1 h recovery at RT, or for 24 h. For oxidative stress, cells were treated with either 2 mM H₂O₂ or 50 mM PQ in serum-free medium. Cells were exposed to H₂O₂ for 30 min, followed or not by 6/12 h recovery in serum-supplemented medium, and to PQ for 4 h, followed or not by 1 h recovery in serum-supplemented medium. For starvation, cells were starved in serum-free medium for 6/24 h. For salt stress, cells were exposed to 150 mM NaCl for 2 h, followed or not by 1 h recovery in serum-supplemented medium. After stress exposure, RNA was extracted from the cells using Trizol reagent (Invitrogen) and transcript levels were quantified by RT-qPCR.

S2R+ cells immunostaining

For staining of S2R+ cells, cells were transferred to the poly-lysine pre-treated 8-well chambers (Ibidi) at the density of 2x10⁵ cells/well. After 30 min, cells were washed with PBS, fixed with 4% paraformaldehyde in PBS for 10 min and permeabilized with PBST (PBS + 0.2% Triton X-100) for 15 min. Cells were incubated with mouse anti-Myc 9B11 1:1000 (Cell Signaling, #2276) or mouse anti-HA F-7 1:1000 (Santa Cruz, sc-7392) in PBST supplemented with 10% of donkey serum at 4°C ON. Cells were washed 3x for 15 min in PBST and then incubated with secondary antibodies and 1x DAPI solution in PBST supplemented with 10% of donkey serum for 2 h at RT. After 3x 15 min washes in PBST, cells were imaged with Zeiss LSM 710 confocal microscope using the 63x objective.

NMJ immunostaining and analysis

For NMJ staining, third instar larvae were dissected in cold PBS and fixed with 4% paraformaldehyde in PBS for 45 min. Larvae were then washed in PBST (PBS + 0.5% Triton X-100) six times for 30 min and incubated overnight at 4°C with mouse anti-synaptotagmin, 1:200 (3H2 2D7, Developmental Studies Hybridoma Bank, DSHB). After 6x 30-min washes with PBST, secondary antibody anti-mouse conjugated to Alexa Fluor 488 and TRITC-conjugated anti-HRP (Jackson ImmunoResearch) were used at a concentration of 1:1000 and incubated at RT for 2 h. Larvae were washed again 6x with PBST and mounted in Vectashield (Vector Laboratories). Images from muscles 6-7 (hemisegments A2-A3) were acquired with a Zeiss LSM 710 confocal microscope. Serial optical sections at 1024 × 1024 pixels with 0.4 µm thickness were obtained with the ×40 objective. Bouton number was quantified using Imaris 9

2. Materials and methods

software. ImageJ software was used to measure the muscle area as well as NMJ axon length and branching. Statistical tests were performed in GraphPad (Prism 8).

RNA isolation, mRNA purification and RT-qPCR

Total RNA from S2R+ cells or flies was isolated using Trizol reagent (Invitrogen) and DNA was removed with DNase I treatment (NEB). mRNA was isolated by two rounds of purification with Dynabeads Oligo (dT)25 (NEB). cDNA for RT-qPCR was prepared using M-MLV Reverse Transcriptase (Promega) and transcript levels were quantified using GoTaq qPCR master mix (Promega) and oligos indicated in **Table 3**.

Western blot

For western blot analysis, proteins were separated on 10% SDS-PAGE gel and transferred on nitrocellulose membrane (Amersham). After blocking with 5% milk in PBST (PBS + 0.05% Tween) for 1 h at RT, the membrane was incubated with primary antibody in blocking solution ON at 4°C. Primary antibodies used were: mouse anti-Myc 9B11 1:2000 (Cell Signaling, #2276); mouse anti-HA F-7 1:2000 (Santa Cruz, sc-7392); mouse anti-tubulin 1:2000 (Biolegend, #903401); mouse anti-Flag M2 1:2000 (Sigma, F1804); rabbit anti-GFP 1:5000 (Torrey Pines Biolab, TP401); guinea pig anti-Mettl3 1:500 (Lence et al., 2016). The membrane was washed 3x in PBST for 10 min and incubated 1 h at RT with secondary antibody in blocking solution (1:10000). Protein bands were detected using SuperSignal West Pico Chemiluminescent Substrate (Thermo Fisher).

RNA probe pull-down

S2R+ cells were transfected with Myc-tagged constructs. 48 h after transfection cells were collected, washed with PBS and pelleted by centrifugation at 400 g for 10 min. The cell pellet was resuspended in 1 ml of lysis buffer (10 mM Tris-HCl at pH 7.4, 150 mM NaCl, 2 mM EDTA, 0.5% NP-40, 0.5 mM DTT, protease inhibitors) and rotated head over tail for 30 min at 4°C. Protein lysates were centrifuged at 18000 g for 10 min at 4°C to remove cell debris and protein concentration was determined using Bradford reagent (Bio-Rad). For individual pull-down, 1.5 mg of protein lysate were incubated with either 3 µg of biotinylated (m⁶A-modified or not) RNA probe (Dharmacon), or without probe as control, coupled to 20 µl Dynabeads MyOne Streptavidin C1 (Thermo Fisher) in 900 µl of lysis buffer at 4°C for 2 h rotating head over tail. After 3x 15 min washes with lysis buffer, bound proteins were eluted by incubation in 1x NuPage LDS supplemented with 100 mM DTT for 10 min at 70°C. Immunoprecipitated proteins as well as input samples were analyzed by western blot using mouse anti-Myc antibody or subjected to quantitative proteomic analysis as described previously (Bluhm et al., 2016). Raw files were processed with MaxQuant (version 1.5.2.8) and searched against the Uniprot database of annotated *Drosophila* proteins.

RNA immunoprecipitation (RIP)

Twenty flies were homogenised in 1 ml of lysis buffer (50 mM Tris-HCl at pH 7.4, 150 mM NaCl, 0.05% NP-40, protease inhibitors) and rotated head over tail for 30 min at 4°C. Protein lysates were centrifuged at 18000 g for 10 min at 4°C to remove cell debris and protein concentration was determined using Bradford reagent (Bio-Rad). For individual RIP, 2 mg of protein lysate were incubated with 20 µl of Pierce anti-Myc magnetic beads (Thermo Fisher) in 900 µl of lysis buffer and rotated head over tail for 2 h at 4°C.

2. Materials and methods

Beads were washed 3x for 10 min with lysis buffer. One fourth of immunoprecipitated protein-RNA complexes were eluted by incubation in 1x NuPage LDS supplemented with 100 mM DTT for 10 min at 70°C and analyzed by western blot using mouse anti-Myc antibody. RNA was isolated from the rest of the beads using Trizol reagent (Invitrogen). Expression levels of the transcripts were analyzed by RT-qPCR and enrichment was calculated normalizing transcript levels in the RIP fractions to the corresponding input and to the negative control.

Interactome

S2R+ cells were transfected with either Alkbh6-HA or GFP-HA. 48 h after transfection cells were either exposed to 50 mM PQ for 4 h or starved for 6 h in serum-free medium. After exposure to stress, cells were collected, washed with PBS and pelleted by centrifugation at 400 g for 10min. The cell pellet was resuspended in 1 ml of lysis buffer (50 mM Tris-HCl at pH 7.4, 150 mM NaCl, 0.05% NP-40, protease inhibitors) and rotated head over tail for 30 min at 4°C. Protein lysates were centrifuged at 18000 g for 10 min at 4°C to remove cell debris and protein concentration was determined using Bradford reagent (Bio-Rad). For individual IP, 2 mg of protein lysate were incubated with 2 µg of mouse anti-HA F-7 (Santa Cruz, sc-7392) conjugated with 20 µl of Protein G Dynabeads (Thermo Fisher) in 900 µl of lysis buffer and rotated head over tail for 2 h at 4°C. After 3x 10 min washes with lysis buffer, bound proteins were eluted by incubation in 1x NuPage LDS supplemented with 100 mM DTT for 10 min at 70°C. One fourth of immunoprecipitated proteins as well as input samples were analyzed by western blot using mouse anti-HA antibody, while the rest was subjected to quantitative proteomic analysis as described previously (Bluhm et al., 2016). Raw files were processed with MaxQuant (version 1.5.2.8) and searched against the Uniprot database of annotated *Drosophila* proteins.

automiG and automiW

Experiments with the automiG self-silencing reporter were performed as described in (Carré et al., 2013). After three rounds of RNAi, S2R+ cells were transfected with the automiG reporter and protein expression was analyzed via western blot using rabbit anti-GFP (Torrey Pines Biolab, TP401) and mouse anti-tubulin (Biolegend, #903401) antibodies. Experiments with the automiW self-silencing reporter were performed as described in (Besnard-Guérin et al., 2015). The RNAi fly lines used are listed in table x. Eye images of the same aged flies were acquired with a DM6000 B (Leica) microscope combined with a DFC350 FX camera using the 20x objective.

TRIBE libraries and computational analysis

TRIBE was performed as previously described (Worpenberg et al., 2019). S2R+ cells were transfected with FlagMyc-Dhx57 fused to the catalytic domain of Adar (cdAdar) or with cdAdar alone under the control of a metal-inducible promoter. 48 h after protein expression induction, cells were washed with PBS and harvested. One fourth of the cells were resuspended in 500 µl of lysis buffer (50 mM Tris-HCl at pH 7.4, 150 mM NaCl, 0.5% NP-40, protease inhibitors) and rotated head over tail for 30 min at 4°C. Protein lysates were centrifuged at 18000 g for 10 min at 4°C to remove cell debris and protein concentration was determined using Bradford reagent (Bio-Rad). Protein expression was analyzed by western blot using mouse anti-Flag antibody (Sigma, F1804). For the identification of editing events, the rest of cells were

2. Materials and methods

used for total RNA isolation using Trizol reagent (Invitrogen) and mRNA was isolated by two rounds of purification with Dynabeads Oligo (dT)25 (NEB). Purified mRNA was used for Illumina Next-generation sequencing library preparation using NEBNext Ultra II RNA Library Prep Kit for Illumina according to the manufacturer's protocol. From the TRIBE data analysis, the score is defined as a log-likelihood ratio of two conditions and, therefore, describes how different conditions are (the higher the score, the more different the A-I editing). The arbitrary SumScore cutoff used in this study is 30 to exclude low confidence targets and background from our analysis.

TGIRT libraries and computational analysis

Age-matched adult WT and *Alkbh6^{Δ11}* female flies were fed with either 5% sucrose (control) or 5mM PQ in 5% sucrose for 24h. The experiment was performed with 3 biological replicates of 15 flies per feeding. Total RNA from flies was isolated using Trizol reagent (Invitrogen) and 3 µg were treated with DNase I (NEB). RNA was directly ribodepleted with the riboPOOL kit (siTOOLS) that was completed with oligos hybridizing to 5S and 2S rRNAs following the manufacturer's protocol. The quality of RNA and ribodepletion was assessed on an Agilent 2100 Bioanalyzer. The purified ribodepleted RNA samples were fragmented for 3 min at 94°C in Magnesium RNA Fragmentation Module (NEB) and 3' ends were dephosphorylated with T4 polynucleotide kinase (Lucigen). Between 50 and 75 ng were retrotranscribed in cDNA with 1.7 µL of template-switching TGIRT enzyme. The remaining library was prepared as in (Boivin et al., 2018). After 12-13 cycles of PCR and a 1.4x cleanup with Ampure XP beads (Bekman-Coulter), the profile of TGIRT libraries were evaluated once more by Bioanalyzer (\pm 250bp average). Finally, the libraries were sequence on an Illumina Next-seq 500 platform (2x150) yielding between 9.5 and 19.9 million paired-end reads. Adapters and low-quality reads were trimmed from fastq files with cutadapt (version 3.4). rRNA sequences were filtered out with bowtie2 (-p 20 -L 15 -k 20 --fr --end-to-end) losing up to 4% of reads. The remaining reads were mapped with STAR as described in (Boivin et al., 2020) (version 2.7.8a). Finally, the reads were counted with CoCo (cc -c both -p -s 1). CPM (count per million) and TPM (transcript per million) were taken from the CoCo output. Analysis of differentially expressed genes was done with DeSeq2 and plots were drawn in R using basic functions and ggplot2 as well as on PowerPoint.

LC-MS/MS analysis of m⁶A levels

mRNA samples from flies were prepared following the above-mentioned procedures. 300 ng of purified mRNA was digested using 0.3 U Nuclease P1 from *Penicillium citrinum* (Sigma-Aldrich, Steinheim, Germany) and 0.1 U Snake venom phosphodiesterase from *Crotalus adamanteus* (Worthington, Lakewood, USA). RNA and enzymes were incubated in 25 mM ammonium acetate, pH 5, supplemented with 20 µM zinc chloride for 2 h at 37°C. Remaining phosphates were removed by 1 U FastAP (Thermo Scientific, St Leon-Roth, Germany) in a 1 h incubation at 37°C in the manufacturer supplied buffer. The resulting nucleoside mix was then spiked with 13C stable isotope labelled nucleoside mix from *Escherichia coli* RNA as an internal standard (SIL-IS) to a final concentration of 6 ng/µl for the sample RNA and 10 ng/µl for the SIL-IS. For analysis, 10 µl of the before mentioned mixture were injected into the LC-MS/MS machine. All mRNA samples were analysed in biological triplicates. LC separation was performed on an Agilent 1200 series instrument, using 5 mM ammonium acetate buffer as solvent A and acetonitrile as

2. Materials and methods

buffer B. Each run started with 100% buffer A, which was decreased to 92% within 10 min. Solvent A was further reduced to 60% within another 10 min. Until minute 23 of the run, solvent A was increased to 100% again and kept at 100% for 7 min to re-equilibrate the column (Synergi Fusion, 4 μ M particle size, 80 Å pore size, 250 \times 2.0 mm, Phenomenex, Aschaffenburg, Germany). The ultraviolet signal at 254 nm was recorded via a DAD detector to monitor the main nucleosides. MS/MS was then conducted on the coupled Agilent 6460 Triple Quadrupole (QQQ) mass spectrometer equipped with an Agilent JetStream ESI source which was set to the following parameters: gas temperature, 350°C; gas flow, 8 l/min; nebulizer pressure, 50 psi; sheath gas temperature, 350°C; sheath gas flow, 12 l/min; and capillary voltage, 3000 V. To analyse the mass transitions of the unlabelled m^6A and all ^{13}C m^6A simultaneously, we used the dynamic multiple reaction monitoring mode.

2. Materials and methods

Primers used for qPCR		Primers used for cloning	
Name	Sequence 5'→3'	Name	Sequence 5'→3'
Rpl15 qF	AGGATGCACCTTATGGCAAGC	Dhx57 half EcoRV F	atcATGGACGAATCCTCGAGAAAG
Rpl15 qR	GCGCAATCCAATACGAGTTC	Dhx57 NotI R	aaagcggccgcTCAGCTGTTTTACTAATCAA
Dhx57 qF	CTACTGCTGCTCTACCGTCG	Dhx36 EcoRV F	aaagatcATGCAGCGCGATAGGGAC
Dhx57 qR	GCAGATGGTCGATGCGAAAC	Dhx36 NotI R	aaagcggccgcTTATATGTCATCGATTCATCGGAT
Ago2 qF	CCACAGTCGCAACTACCCAT	Dhx34 EcoRV F	aaagatcATGTCTCGGATAAAGAAGAAGG
Ago2 qR	TTGCTCCATCCTTGCGGTTT	Dhx34 AgeI R	aaaaccggtTACTGTATTTCGACACTGC
Dicer2 qF	GCTTTTATGTGGGTGAACAGGG	Dhx9 half EcoRV F	atcATGGATATAAAAATCTTTTTGTACC
Dicer2 qR	GGCTGTGCCAACAAGAACTT	Dhx9 AgeI R	aaaaccggtTAAAAAGTTACCCAGCG
α-spectrin qF	CGACCCGCCCTATGTAACATA	Dhx57 frag1 NotI R	aaagcggccgcTCAATTCGGTGATTGATGATGCT
α-spectrin qR	CACGCAGTAGTCAGCCATGT	Dhx57 frag2 half EcoRV F	atcCCATCGCACTACGCACGTGG
β-spectrin qF	TGTGACACGAAAGCAGCAGT	Dhx57 frag2 NotI R	aaagcggccgcTCAAGCGCAGTACTTAGTGTCTG
β-spectrin qR	CAAGATCGGTTGGAGGCCCTT	Dhx57 frag3 half EcoRV F	atcAAGCTTAAAAAGCAGGAGCA
stj qF	GGAGCTGTTTATCTGGGC	Dhx57 NotI F TRIBE	aaagcggccgcATGGACGAATCCTCGAGAAAG
stj qR	GCCATCGAATCGACAATAGAAGC	Dhx57 NotI R TRIBE	aaagcggccgcGCTGTTTTACTAATCAAGTG
TBCE qF	AGGAACCCGCATCAAAATTGG	Primers used for CRISPR/Cas9	
TBCE qR	TCCCATTTCTATCCAGCCAG	Name	Sequence 5'→3'
Alkbh6 qF	GGGCTTTGAAGTGCAGAAAGTG	Dhx57 gRNA8 F	cttcGACTTACGTTGACGATTGCC
Alkbh6 qR	GCAATCATTCCGTTGGGATG	Dhx57 gRNA8 R	aaacGGCAATCGTCAACGTAAGTC
Alkbh6 5'UTR qF	CAATCGTTCAAAAGGACAAA	Dhx57 gRNA1 F	cttcGGCCGCTTCTCGTCTTCC
Alkbh6 5'UTR qR	TGCATCAGCTGTTGGAAAA	Dhx57 gRNA1 R	aaacGGAAGACGAGGAACGGCGCC
Alkbh8 qF	GGAGGACGCTTTGGTTTA	Dhx57 screen F	CGAGCTCGATTATATGCTGG
Alkbh8 qR	CTGCTCAGTGGTACGCTCCT	Dhx57 screen R	ACGGATCGCAATCTTCTCC
Ythdf qF	CCGAGAAAGTGCACAAGGAT	Alkbh6 gRNA1 F	cttcGATAAGGTAGCCCTAGTCA
Ythdf qR	AAACCTTGGCTCTGCTGAAG	Alkbh6 gRNA1 R	aaacTGACTAGGCCTACACTTATC
Ythdc1 qF	GGCTCGAGTTATGCGAGAAA	Alkbh6 gRNA2 F	cttcGGTCTTGGGCACATTACGGA
Ythdc1 qR	GGTGGTCTGATTTGATCCT	Alkbh6 gRNA2 R	aaacTCCGTAATGTGCCAAGACC
Mettl3 qF	AAGGAACCTGTTGAGGCTGA	CG6144 screen F	AGCTGATGCAGAATTCAAAGCC
Mettl3 qR	CACCTGTGTGGAGACAATGG	CG6144 screen R	ATGCCAAGAACATCGAATGGC
Primers used for dsRNA synthesis			
Name	Sequence 5'→3'		
LacZ T7 F	taatacagactcactatagggCAGGCTTTCTTTCACAGATG		
LacZ T7 R	taatacagactcactatagggCTGATGTTGAACTGGAAGTC		
Ythdf T7F	ttaatacagactcactataggggagaACCGATCACGGCAATAAGAG		
Ythdf T7R	ttaatacagactcactataggggagaGCACGCCGATTTAATTTGT		
Ythdc1 T7F	ttaatacagactcactataggggagaCGAATCGAATGGTGAGACT		
Ythdc1 T7R	ttaatacagactcactataggggagaCCGTGTGCTCGGAATAGGT		
Alkbh6 T7F	ttaatacagactcactataggggagaGGATTTACCGGGCTTTGAAGTGC		
Alkbh6 T7R	ttaatacagactcactataggggagaAGGTGGAATCTGAGGATACAGCTC		
Ago2 T7F	ttaatacagactcactataggggagaGGATGCCATGAAGTTTCTGG		
Ago2 T7R	ttaatacagactcactataggggagaCTCAGGCCATCTCGGTAGTAG		
Ago2 T7F2	ttaatacagactcactataggggagaTCAATGCCGATGATCGAATA		
Ago2 T7R2	ttaatacagactcactataggggagaGACGCAATGGTGACCTTCTT		
Mettl3 T7F	ttaatacagactcactataggggagaCAGCCTGGAGATGGTGAAC		
Mettl3 T7R	ttaatacagactcactataggggagaTCAGGCACTCGACTTTTGTG		
Dhx57 T7F	ttaatacagactcactataggggagaCCGACTGGAAAACAAGGTGT		
Dhx57 T7R	ttaatacagactcactataggggagaACGGATTCGATCAGTTCTGG		

Table 3. Oligos used in this study.

2. Materials and methods

Genotype	Category	Chr	Source
Dhx57 gRNA 1+8/CyO	gRNA line	II	this study
Alkbh6 gRNA 1+2/CyO	gRNA line	II	lab stock
Dhx57fs	Mutant allele	X	this study
Dhx57fs negative CTRL	Mutant allele CTRL	X	this study
Alkbh6Δ11/CyOGFP	Mutant allele	II	this study
Alkbh6Δ11 negative CTRL	Mutant allele CTRL	II	this study
Alkbh6Δ2/CyOGFP	Mutant allele	II	lab stock
Mettl3null/TM6c	Mutant allele	III	Lence et al., 2016
UAS-FlagMyc-Dhx57/CyO	Overexpression line	II	this study
UAS-Alkbh6-HA/CyOGFP	Overexpression line	II	lab stock
<i>Tub</i> GAL4/CyOGFP;Mettl3null/TM6c	Recombined line	II;III	lab stock
UAS-FlagMyc-Dhx57/CyO;Mettl3null/TM6b	Recombined line	II;III	this study
Dhx57fs;;Mettl3null/TM6c	Recombined line	X;III	this study
Dhx57fs; <i>Tub</i> GAL4/CyOGFP	Recombined line	X;II	this study
Dhx57fs; UAS-FlagMyc-Dhx57/CyO	Recombined line	X;II	this study
<i>Tub</i> GAL4, Alkbh6Δ11/CyOGFP	Recombined line	II	this study
UAS-Alkbh6-HA, Alkbh6Δ11/CyOGFP	Recombined line	II	this study
UAS-automiW; <i>GMR</i> GAL4 (w-)	Reporter line	X;II	Besnard-Guerin et al., 2015
Dhx57 RNAi	RNAi line		Bloomington (#55373)
Mettl3 RNAi	RNAi line		VDRC (GD 20968)
Ago2 RNAi	RNAi line		VDRC (KK 100356)
Def Dhx57/FM7c	Deficiency line		Bloomington (#26556)
CantonS	WT line		lab stock
<i>Tub</i> GAL4/CyOGFP	GAL4 driver	II	lab stock
sco/CyO;MKRS/TM6b	Balancer	II;III	lab stock
Fm7c RFP Tb	Balancer	X	Bloomington (#36337)
y2 cho2 v1; Sco/CyO	Balancer	X;II	NIG-FLY (TBX0007)
y1 v1 P(nos-phiC31\int.NLS)X; attP40 (II)	CRISPR/Cas9 line		NIG-FLY (TBX0002)
y2 cho2 v1/Yhs-hid; Sp/CyO	CRISPR/Cas9 line		NIG-FLY (TBX0008)
y2 cho2 v1; attP40(nos-Cas9)/CyO	CRISPR/Cas9 line		NIG-FLY (CAS0001)

Table 4. Flies generated and used in this study.

Name	Backbone	Promoter	Tag	Category
<i>Actin</i> -GAL4	pPac	actin5c	-	GAL4
Dhx57 gRNA 1-8	pBv-U6.2B	U6	-	CRISPR/Cas9
FlagMyc-cdAdar	pMTFMW	CuSO ₄ inducible	3xFlag+6xMyc N-term	TRIBE
FlagMyc-Dhx57-cdAdar	pMTFMW	CuSO ₄ inducible	3xFlag+6xMyc N-term	TRIBE
FlagMyc-Alkbh6	pPFMW	UASp	3xFlag+6xMyc N-term	OE
FlagMyc-Ythdf	pPFMW	UASp	3xFlag+6xMyc N-term	OE
FlagMyc-Dhx57	pPFMW attB	UASp	3xFlag+6xMyc N-term	Fly injection
Alkbh6-HA	pPWH	UASp	3xHA C-term	OE
GFP-HA	pPWH	UASp	3xHA C-term	OE
Myc-GFP	pPac-PuroMyc	actin5c	5xMyc N-term	OE
Myc-GFP-Dhx57	pPac-PuroMyc	actin5c	5xMyc N-term	OE
Myc-Ythdc1	pPac-PuroMyc	actin5c	5xMyc N-term	OE
Myc-Dhx57	pPac-PuroMyc	actin5c	5xMyc N-term	OE
Myc-Dhx57 frag1	pPac-PuroMyc	actin5c	5xMyc N-term	OE
Myc-Dhx57 frag2	pPac-PuroMyc	actin5c	5xMyc N-term	OE
Myc-Dhx57 frag3	pPac-PuroMyc	actin5c	5xMyc N-term	OE
Myc-Dhx57 frag1+2	pPac-PuroMyc	actin5c	5xMyc N-term	OE
Myc-Dhx57 frag2+3	pPac-PuroMyc	actin5c	5xMyc N-term	OE
Myc-Dhx36	pPac-PuroMyc	actin5c	5xMyc N-term	OE
Myc-Dhx34	pPac-PuroMyc	actin5c	5xMyc N-term	OE
Myc-Dhx9	pPac-PuroMyc	actin5c	5xMyc N-term	OE
GFP-barentz	pPGW	UASp	GFP N-term	OE
automiG	pMT	CuSO ₄ inducible	-	Reporter

Table 5: Plasmids generated and used in this study.

3. Aim of the work

m⁶A is the most prevalent modification on mRNA. Over the last decade, technical progress in biochemical detection methods together with numerous studies in different model organisms made m⁶A the best-characterized among all RNA modifications. Nevertheless, our understanding of the m⁶A biogenesis, molecular functions as well as biological relevance is far from being complete. The main aim of my PhD thesis is to expand our knowledge of this new layer of gene expression regulation with a focus on specific aspects of the m⁶A pathway that are still poorly investigated in *Drosophila*:

- **Aim I: Characterization of Hakai as a novel component of the m⁶A writer complex in flies.**

While the structure of the METTL3-METTL14 catalytic core of the methyltransferase complex has been extensively characterized (Śledź & Jinek, 2016; P. Wang et al., 2016; X. Wang et al., 2016), the exact composition and stoichiometry of the MACOM complex still needs to be completely elucidated. Hakai has been identified among the strongest interactors of some of the MACOM subunits in mammalian cells (Horiuchi et al., 2013; Wan et al., 2015) and recently reported as necessary for m⁶A mRNA deposition in plants (Růžička et al., 2017). In light of this, I aimed to 1) validate Hakai as a member of the m⁶A machinery in flies and 2) explore its molecular function within the m⁶A pathway.

- **Aim II: Identification and characterization of the proteins that mediate m⁶A functions in the fly nervous system.**

In flies, the YTH-domain protein family includes only two members: the nuclear Ythdc1 and the cytoplasmic Ythdf. While Ythdc1 has been already characterized as m⁶A reader in the context of splicing (Lence et al., 2016), Ythdf has been poorly studied so far. Furthermore, FMR1 has been recently identified as a sequence-context-dependent m⁶A reader in mammals (Arguello et al., 2017; Edupuganti et al., 2017) as well as in flies. Over the past years, it became increasingly clear that m⁶A plays a critical role during brain development. However, due to the difficulty of studying m⁶A *in vivo*, the molecular mechanisms by which m⁶A influence neurogenesis remain unclear. I therefore aimed to 1) identify the reader proteins mediating m⁶A functions specifically in the nervous system, 2) investigate the biological processes regulated by each reader and 3) characterize the interplay between different readers within the m⁶A pathway.

- **Aim III: Characterization of Alkbh6 as potential m⁶A eraser in flies.**

In vertebrates, m⁶A on mRNA can be reversed back to A by the ALKBH5 and FTO demethylases (Jia et al., 2011; Zheng et al., 2013). While ALKBH5 and FTO are absent in *Drosophila*, other members of the ALKBH family are expressed in flies. Among those, ALKBH6 has been recently shown to be able to bind both m⁶A-modified and unmodified RNA probes (Huong et al., 2020), but its endogenous targets have not been identified yet. In addition, ALKBH6 was reported to contribute to the maintenance of genome stability upon exposure to alkylating agents in human cancer cells (S. Zhao et al., 2021) as well as to be involved in the abiotic stress response in plants (Huong et al., 2020). One of the aims of my PhD work was to 1) investigate *Drosophila* Alkbh6 as possible m⁶A eraser, 2) screen other modifications on both RNA and DNA as potential targets of Alkbh6 and 3) explore its function within the cellular response to stress in flies.

4. Preliminary remarks

Parts of the results presented in this thesis have been published in peer-reviewed journals as research articles. Research articles 1 and 2 represent section 1 and 2 of the results, while section 3 and 4 covers unpublished data. *Contributions* as well as *Material and methods* are referred to the unpublished data only.

- **Research article 1:**

Bawankar P*, Lence T*, Paolantoni C*, Haussmann IU, Kazlauskienė M, Jacob D, Heidelberger JB, Richter FM, Nallasivan MP, Morin V, Kreim N, Beli P, Helm M, Jinek M, Soller M, Roignant JY. Hakai is required for stabilization of core components of the m⁶A mRNA methylation machinery. *Nat Commun.* 2021 Jun 18;12(1):3778

The project was initiated by another PhD student in the lab, Tina Lence. I worked on this project in collaboration with a post-doc in the lab, Praveen Bawankar. I performed immunostaining of Hakai isoforms in S2R+ (Fig 1C) and BG3 cells (Fig S3A) and I quantified Fl(2)d protein levels in S2R+ cells in different KD conditions (Fig 6D). I performed experiments for the Vir-dependent and Fl(2)d-dependent proteome in S2R+ cells (Fig S9A-C). Samples were then subjected to quantitative proteomic analysis. I prepared the corresponding figures and contributed to the writing of the manuscript.

- **Research article 2:**

Worpenberg L, Paolantoni C, Longhi S, Mulorz MM, Lence T, Wessels HH, Dassi E, Aiello G, Sutandy FXR, Scheibe M, Edupuganti RR, Busch A, Möckel MM, Vermeulen M, Butter F, König J, Notarangelo M, Ohler U, Dieterich C, Quattrone A, Soldano A, Roignant JY. Ythdf is a N⁶-methyladenosine reader that modulates Fmr1 target mRNA selection and restricts axonal growth in *Drosophila*. *EMBO J.* 2021 Feb 15;40(4):e104975

I worked on this project in collaboration with another PhD student in the lab, Lina Worpenberg. I performed the *in vitro* RNA probe pull-down in BG3 cells protein extract (Fig 2A). Samples were then subjected to quantitative proteomic analysis. I carried out all the NMJ experiments in the paper, including dissection, immunostaining, confocal microscopy, and analysis. More in details, I quantified NMJ bouton number, length and branching in larvae from different genotypes (Fig 1A-B, Fig 3A-D, Fig 3G, Fig EV1A and Fig EV4D), I quantified futsch protein levels at NMJ in larvae from different genotypes (Fig 7A-B) and I quantified NMJ bouton number for rescue experiments (Fig 7F). I prepared the corresponding figures and contributed to the writing of the manuscript.

Contributions

Stella Kanta

Generated and validated the *Dhx57^{fs}* mutant allele and provided help for the preparation of Dhx57 TRIBE libraries.

Tina Lence

Performed the staging experiment including sample collection and RNA extraction. Generated and validated the *Alkbh6^{Δ2}* mutant allele as well as the plasmids used for overexpression of Alkbh6 in S2R+ cells.

Athena Sklias

Performed bioinformatics analysis of the TGIRT-seq dataset.

Prof Christoph Dieterich

Performed bioinformatics analysis of the TRIBE dataset.

Dr Marion Scheibe, Dr Falk Butter

Carried out quantitative proteomics and data analysis (interactomes of Alkbh6 protein and m⁶A-interactomes).

Martina Schmidt-Dengler, Vishwaja Jhaveri, Prof Mark Helm

Performed LC-MS/MS quantification of m⁶A levels.

5. Results

5.1 Section 1: Research article 1



ARTICLE


<https://doi.org/10.1038/s41467-021-23892-5> OPEN

Hakai is required for stabilization of core components of the m⁶A mRNA methylation machinery

Praveen Bawankar^{1,11}, Tina Lence^{2,10,11}, Chiara Paolantoni^{3,11}, Irmgard U. Haussmann^{4,5}, Migle Kazlauskienė⁶, Dominik Jacob¹, Jan B. Heidelberger², Florian M. Richter¹, Mohanakarthik P. Nallasivan⁴, Violeta Morin², Nastasja Kreim⁷, Petra Beli^{2,8}, Mark Helm¹, Martin Jinek⁶, Matthias Soller^{4,9}✉ & Jean-Yves Roignant^{1,3}✉

N⁶-methyladenosine (m⁶A) is the most abundant internal modification on mRNA which influences most steps of mRNA metabolism and is involved in several biological functions. The E3 ubiquitin ligase Hakai was previously found in complex with components of the m⁶A methylation machinery in plants and mammalian cells but its precise function remained to be investigated. Here we show that Hakai is a conserved component of the methyltransferase complex in *Drosophila* and human cells. In *Drosophila*, its depletion results in reduced m⁶A levels and altered m⁶A-dependent functions including sex determination. We show that its ubiquitination domain is required for dimerization and interaction with other members of the m⁶A machinery, while its catalytic activity is dispensable. Finally, we demonstrate that the loss of Hakai destabilizes several subunits of the methyltransferase complex, resulting in impaired m⁶A deposition. Our work adds functional and molecular insights into the mechanism of the m⁶A mRNA writer complex.

¹Institute of Pharmaceutical and Biomedical Sciences, Johannes Gutenberg-University Mainz, Mainz, Germany. ²Institute of Molecular Biology (IMB), Mainz, Germany. ³Center for Integrative Genomics, Gépode Building, Faculty of Biology and Medicine, University of Lausanne, Lausanne, Switzerland. ⁴School of Biosciences, College of Life and Environmental Sciences, University of Birmingham, Birmingham, UK. ⁵Department of Life Science, Faculty of Health, Education and Life Sciences, Birmingham City University, Birmingham, UK. ⁶Department of Biochemistry, University of Zurich, Zurich, Switzerland. ⁷Bioinformatics core facility, Institute of Molecular Biology (IMB), Mainz, Germany. ⁸Institute of Developmental Biology and Neurobiology (IDN), Johannes Gutenberg-Universität, Mainz, Germany. ⁹Birmingham Centre for Genome Biology, University of Birmingham, Birmingham, UK. ¹⁰Present address: Institute for Molecular Infection Biology (IMIB), Faculty of Medicine, University of Würzburg, Würzburg, Germany. ¹¹These authors contributed equally: Praveen Bawankar, Tina Lence, Chiara Paolantoni. ✉email: M.Soller@bham.ac.uk; jean-yves.roignant@unil.ch

N⁶-methyladenosine (m⁶A) is one of the most abundant and well-studied mRNA modifications in eukaryotes^{1–4}. This modification plays a central role in almost every aspect of mRNA metabolism, and is essential for several biological processes such as cell differentiation^{1–8}, DNA repair⁹, circadian rhythm^{10–12}, neurogenesis¹³ and sex determination^{14–16}, among others. Its dysregulation in human is associated with numerous diseases, including metabolic alteration¹⁷, neuronal disorders^{18,19} and various types of cancers^{20–22}. The downstream effects of m⁶A are generally mediated by YTH domain RNA-binding proteins, known as “m⁶A readers” that preferentially bind m⁶A modified RNAs and affect their fate³.

m⁶A on mRNA is deposited co-transcriptionally by a conserved multiprotein complex that can be divided into two stable sub-complexes: the heterodimer METTL3/METTL14 also known as m⁶A-METTL Complex (MAC) that contains the catalytic activity, and the m⁶A-METTL Associated Complex (MACOM) that is required for full MAC activity and includes WTAP (Fl(2) d), VIRMA (Virilizer), RBM15/RBM15B (Spenito) and ZC3H13 (Flacc)^{23–25}. More recently, another factor named HAKAI was found associated with components of MACOM in plants and human cells and required to maintain m⁶A level^{26,27}.

The precise function of MAC and MACOM components has been the subject of intense research over the past years. Structural studies revealed that METTL3 and METTL14 form a stable heterodimer^{28–30} and that METTL3 is the only factor that contains the catalytic activity since METTL14 is unable to bind the methyl group donor S-Adenosylmethionine. Nevertheless, METTL14 is essential to support the interaction of the complex with its RNA targets and to enhance METTL3 activity. WTAP was shown to stabilize the interaction between METTL3 and METTL14 and to recruit the METTL3/METTL14 heterodimer into the nuclear speckles^{15,31}. RBM15/RBM15B is an RNA-binding protein that recognizes U-rich sequences on the mRNA and is suggested to recruit the m⁶A machinery in close proximity to these sites³². Furthermore, VIRMA was proposed to facilitate selective m⁶A installation near the stop codon and in the 3' UTR of mRNAs through its interaction with polyadenylation cleavage factors CPSF5 and CPSF6²⁷. Lastly, four recent studies identified ZC3H13 as part of MACOM^{24,27,33,34}. ZC3H13 was found to stabilize the interaction between WTAP and RBM15 in mouse embryonic stem cells as well as in flies and to contribute to the localization of the writer complex to the nucleus. The only m⁶A writer component whose function is still poorly explored is HAKAI.

HAKAI, also known as CBL1, is a RING-finger type E3 ubiquitin ligase that mediates ubiquitination and subsequent endocytosis of the E-cadherin complex, leading to cell-cell adhesion loss and increased cell motility³⁵. HAKAI can also regulate cell proliferation in an E-cadherin-independent manner by affecting the ability of the PTB-associated splicing factor to bind some of its RNA targets³⁶. During the last decades, HAKAI has been mostly studied in the context of epithelial-mesenchymal transitions and cancer progression³⁷. However, as aforementioned, it became increasingly clear that HAKAI is also a component of the m⁶A biogenesis machinery in vertebrates as well as in plants. HAKAI was identified as one of the strongest WTAP interactors in mammalian cells³⁸ and as part of an evolutionary conserved protein complex including WTAP, VIRMA and ZC3H13³⁹. Furthermore, *Hakai* mutant in *Arabidopsis thaliana* displayed mild developmental defects together with reduced m⁶A levels²⁶. Recently, we identified Hakai among the top enriched proteins in our Spenito (Nito) interactome in *Drosophila* S2R+ cells, suggesting its evolutionary conserved role within the m⁶A pathway²⁴.

Here we report that Hakai is a conserved member of MACOM and is essential for m⁶A deposition in flies. In line with its role in the m⁶A pathway, Hakai functions in the sex determination pathway and mediates splicing of *Sex lethal*. Moreover, its depletion results in altered gene expression and splicing changes that resemble the loss of other MACOM components. We find that Hakai in flies encodes short and long protein isoforms that display distinct subcellular localization. Its ubiquitin ligase domain is required for homodimerization and interaction with other MACOM components. Finally, we show that Hakai removal leads to a severe reduction of Virilizer (Vir), Fl(2)d and Flacc protein levels, indicating that Hakai is essential for maintaining the stability of MACOM components.

Results

***Drosophila* Hakai is a conserved MACOM subunit.** We previously found Hakai among highly enriched proteins in Nito and RBM15 interactomes in *Drosophila* S2R+ and mouse ES cells, respectively, suggesting it is a conserved member of MACOM (Fig. 1a)²⁴. In *Drosophila*, *Hakai* can generate four protein isoforms via alternative splicing: the two short and two long isoforms differ in the extension of the C-terminal region as a result of intron retention and in the length of the second exon due to alternative 3' splice sites in the first intron (Fig. 1b). All proteins share a RING-type E3 ubiquitin ligase domain and an adjacent C2H2-like zinc finger. This region is highly conserved and was shown in mammals to be required for Hakai dimerization and formation of the so-called “Hakai phosphotyrosine-binding domain” (HYB domain) (Supplementary Fig. 1)⁴⁰. Expression of RNA isoforms was monitored during development by real-time quantitative PCR (Supplementary Fig. 2). Both short and long isoforms greatly overlapped with the m⁶A profile, showing high enrichment during early embryogenesis and in ovaries, which is consistent with the transcript distribution of the other subunits of the m⁶A methyltransferase complex^{15,24}. In addition, the long isoforms were particularly elevated in males, suggestive of a possible function during spermatogenesis. Intriguingly, when we examined their subcellular localization in S2R+ cells we found that the short isoform (302 aa) was present exclusively in the cytoplasm with a strong signal at the cellular periphery, in contrast to the long isoform (473 aa) that was predominantly nuclear (Fig. 1c). A similar result was obtained in BG3 cells, which are cells derived from larval brains (Supplementary Fig. 3a). Furthermore the long isoform colocalized to sites of transcription on polytene chromosomes of salivary glands (Supplementary Fig. 3b). Altogether, since m⁶A is deposited co-transcriptionally, these results suggest that only the long isoform may be relevant with regards to m⁶A biogenesis.

To address if Hakai indeed interacts with MACOM components in *Drosophila*, we cloned Hakai cDNA encoding long (473 residues) isoform in a Myc-GFP-tagged expression vector and transfected the construct in *Drosophila* S2R+ cells to carry out Myc pull-down assay followed by mass spectrometry analysis. We found that the tagged Hakai was able to immunoprecipitate all MACOM components, even though the interaction with Nito was just below the cutoff (Fig. 1d, Supplementary Data 1). Furthermore, Mettl3 and Mettl14 were absent from the precipitated proteins, confirming our previous findings that the interaction between MAC and MACOM is either weak or transient.

To confirm these results, we performed co-immunoprecipitation assays in S2R+ cells. We found that Hakai can interact with other MACOM components, irrespective of the presence of RNA (Fig. 1e, f). Further confirmation of the interaction between Hakai and Fl(2)d/Nito was obtained via

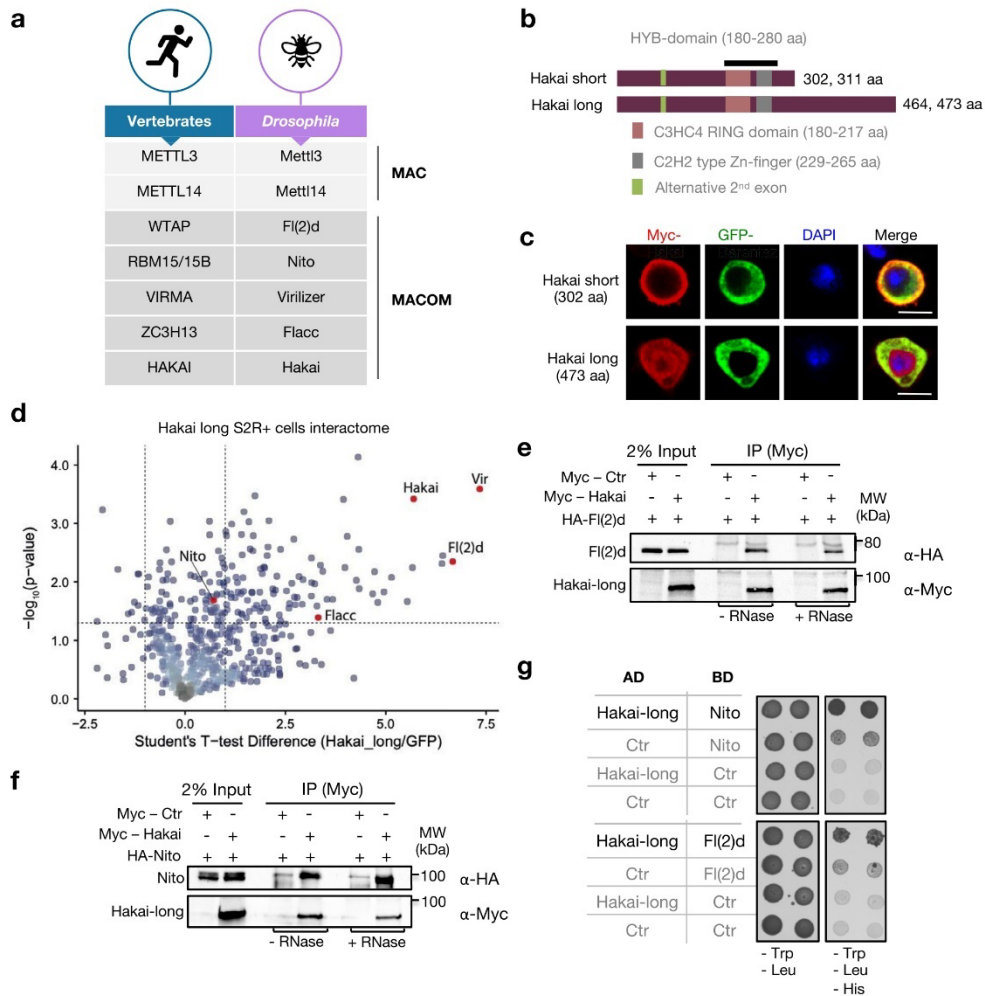


Fig. 1 Hakai interacts with MACOM components. **a** Table indicating the names of MAC and MACOM components in Vertebrates and *Drosophila*. **b** Schematic of the Hakai short and long protein isoforms depicting the RING domain (pink), the Zn-finger (grey) and the HYB domain (black). The green domain indicates the alternative region of the second exon that is included in isoforms 311 aa and 473 aa. **c** Immunostaining of Myc-tagged Hakai short and long protein isoforms overexpressed in S2R+ cells. GFP-tagged Barentsz protein served as a cytoplasmic marker. DAPI staining is shown in blue. The short Hakai isoform localizes strictly to the cytoplasm, whereas the long isoform localizes to both cellular compartments with the enrichment in the nucleus. Scale bars, 10 μ m. **d** Identification of proteins interacting with GFP-Hakai-long in S2R+ cells based on label-free analysis of two replicate experiments analyzed by quantitative MS-based proteomics. HAKAI immunoprecipitates alongside of all MACOM components. MACOM component proteins are highlighted in red. A complete list of quantified proteins can be found in Supplementary Data 2. **e, f** Co-immunoprecipitation experiments were carried out with lysates prepared from S2R+ cells transfected with Myc-tagged Hakai (long isoform) and HA-tagged Nito or FI(2)d. In control lanes, S2R+ cells were transfected with Myc alone and an identical HA-containing protein. Extracts were immunoprecipitated with anti-Myc antibody and immunoblotted using anti-Myc and anti-HA antibodies. Two percent of input was loaded. The same experiment was repeated in the presence of RNase T1. Nito and FI(2)d interact with Hakai in an RNase-independent manner. Blots shown are representative of one biological replicate. **g** Yeast-two-hybrid assay to investigate Hakai interaction with Nito and FI(2)d. Proteins were cloned in yeast expression vectors and fused with either Gal4-DNA binding domain (BD) or Gal4-DNA activation domain (AD). Indicated combinations of vectors were co-expressed in yeast and empty vectors encoding only activation or binding domain were used as control (Ctr). Recovered colonies were spotted on plates lacking Leucine and Tryptophan (-Leu, -Trp) as well as selection plates lacking amino acids Leucine, Tryptophan and Histidine (-Leu, -Trp, -His). AD-Hakai long isoform interacts with BD-FI(2)d and BD-Nito. Source data for Western blots and the yeast-two-hybrid assay are provided as a Source Data file.

yeast-two-hybrid (Y2H) assay (Fig. 1g). However, interaction between Hakai and Flacc was not detected in this assay and Vir could not be successfully expressed in yeast, probably due to its large size. Furthermore, in agreement with the human HAKAI structure⁴⁰, we observed that the Hakai fly orthologue could homodimerise, as well as Fl(2)d and Nito, which was not reported previously (Supplementary Fig. 4a, b).

Altogether our data indicate that Hakai is a component of the m⁶A machinery in flies, that it interacts with MACOM components, and that several subunits within this complex likely exist in more than one copy.

Vir functions as a scaffold for MACOM component interaction. To gain better mechanistic insights of Hakai within MACOM, we precisely mapped the intermolecular interactions between the different components of the complex. To do so, we performed co-immunoprecipitation experiments in the presence of RNase A using full length as well as fragments of MACOM subunits in different combinations (Fig. 2a). Results from these experiments revealed that Hakai N-terminal region (residues 1–295, common to both isoforms) interacts with the N-terminal region of Vir (residues 1–130) (Fig. 2b, c), while the middle region and C-terminus of Fl(2)d (residues 125–536) binds Vir C-terminal (residues 1501–1854) (Fig. 2d, e). The same region of Fl(2)d was also required for homodimerisation (Supplementary Fig. 4a). These data suggest that Vir may mediate the interaction between Fl(2)d and Hakai. To address this possibility, we tested whether Hakai and Fl(2)d still interact in the absence of Vir. The co-immunoprecipitation assay revealed that the interaction was strongly compromised upon *vir* KD (Fig. 2f and Supplementary Fig. 5a). Similarly, the interaction between Hakai and Nito was dramatically reduced (Supplementary Fig. 5a, b). In contrast, the lack of Hakai did not interfere with the association of Fl(2)d with Nito or Vir (Supplementary Fig. 5c–e). Therefore these results suggest that Vir likely stabilize the interaction between Fl(2)d, Hakai and Nito (Fig. 2g).

We next explored whether these interactions are conserved in the human MACOM. To this end, we overexpressed several human MACOM subunits (Supplementary Fig. 6a) in HEK293T cells and performed co-immunoprecipitation experiments in the presence of RNase A. We found that the interaction between HAKAI and the N-terminal domain of VIRMA (residues 1–130) is conserved between *Drosophila* (Fig. 2b, c) and humans (Supplementary Fig. 6b, c). We further showed that a region of HAKAI spanning residues 87–105, which is not present in the previously determined structure⁴⁰, is critical for this interaction (Supplementary Fig. 6c, lanes 11–12). Similarly, the predicted structured region of the Fl(2)d homologue WTAP (residues 1–249) co-immunoprecipitated with VIRMA (Supplementary Fig. 6d). In case of human VIRMA, we identified two distinct interaction domains. On one hand VIRMA interacts with WTAP through its C-terminal domain (residues 1575–1812) (Supplementary Fig. 6e), as shown for *Drosophila*. We also identified a second WTAP interacting site in the central region of the protein spanning residues 335–1130 (Supplementary Fig. 6e, lane 14). Interestingly, truncating this region further from either side abolished the interaction (Supplementary Fig. 6e, lanes 15–16), suggesting that WTAP binding involves multiple interaction sites or that the truncations disrupt the VIRMA protein fold. Altogether, these results demonstrate that VIRMA serves as an interaction platform for the assembly of HAKAI and WTAP into the MACOM complex in both *Drosophila* and humans (Fig. 2g, h).

Hakai is required for mRNA m⁶A methylation and alternative splicing of *Sex lethal* (*Sxl*). A key role for m⁶A in *Drosophila* has

been shown in alternative splicing of *Sex lethal* (*Sxl*), where it is required for autoregulation in females⁴¹. In females, *Sxl* binds to either side of an alternative exon containing a stop codon and blocks the splice sites to skip this exon, which is only included in males. In addition, *Sxl* also prevents expression of the dosage compensation factor *msl-2*, which is expressed only in males to upregulate transcription from the single X chromosome twofold. Loss of m⁶A interferes with sexual differentiation in females and increases female lethality due to aberrant dosage compensation^{14–16}. Hence, we wondered whether loss of *Hakai* is also required for mRNA m⁶A methylation and interferes with *Drosophila* sex determination and dosage compensation.

We obtained a previously characterized imprecise transposon excision line in the *Hakai* gene⁴². This *Hakai*¹ allele lacks the coding region covering the N-terminus and the RING-finger domain, and is considered to be a null loss of function (Fig. 3a). In addition, we used the CRISPR/Cas9 approach to generate *Hakai*, which encodes an early truncated product (first 57aa). When we crossed *Hakai*¹ to either of the two deficiency alleles (*Df(2L)Exel8041* or *Df(2L)Exel6044*) to normalize genetic background effects, we found that the mutants died in the pupal stage ($n = 240$). The m⁶A level of *Hakai*¹/*Df(2L)Exel8041* pupae was reduced compared to the control (Fig. 3b–d), but not completely absent as in *Mettl3*^{null} mutants¹⁴.

To test whether Hakai is required for *Sxl* autoregulation, we made use of a genetically sensitized background based on reduced *Sxl* levels by removal of one copy of *daughterless* (*da*), which is involved in *Sxl* transcription, and one copy of *Sxl* required for *Sxl* autoregulation. In the progeny of a cross between *da*^{Df/+}; *Mettl3*^{null/+} females and *Sxl*^{7B0} null males, most females died (Fig. 3e). Likewise, also removal of one copy of *Hakai* killed females (Fig. 3e).

Furthermore, when we crossed *Hakai*/CyO females, which harbours an early stop codon, to *Df(2L)Exel8041*/CyO males to normalize genetic background, we observed strong female lethality compared to CyO balancer-carrying control animals (149 females and 144 males, Fig. 3f). Although the two females we obtained did not show sexual transformation, all male flies were flightless ($n = 44$), as observed for *Mettl3*^{null} and *Mettl14*^{null} mutants^{14–16}.

To further confirm the involvement of Hakai in *Sxl* alternative splicing we made use of the female-lethal *vir*^{2F} allele¹⁴. We found that removal of one copy of *Hakai* restored female viability of *vir*^{2F}/*Df(2R)BSC778* females by correcting *Sxl* alternative splicing (Fig. 3g), as shown previously for other components of the methyltransferase complex^{14,24}.

Lastly, to demonstrate a role for Hakai in the sexual differentiation of *Drosophila* females we made use of the *vir*^{2F}/*vir*^{ts} genetically sensitized background, which occasionally shows patches of darkly pigmented male tissue in abdominal segments 5 and 6 in these females (Fig. 3j–l). Strikingly, removal of one copy of *Hakai* led to male pigmentation in the vast majority of these females (Fig. 3h, m) and a switch of *Sxl* alternative splicing to the male mode, including the otherwise skipped male exon (Fig. 3i, lane 5). Some females also displayed intersexual development of genitals (Fig. 3n). Intriguingly, loss of *Hakai* in the *vir*^{2F}/*vir*^{ts} genetically sensitized background revealed tissue-specificity in *Sxl* regulation as alternative splicing in the front part of females (head and thorax) was not altered, and also these females did not display male sex combs (Fig. 3h), suggesting the m⁶A pathways main function could be to guarantee robust *Sxl* alternative splicing across different tissues.

Hakai regulates the m⁶A pathway in *Drosophila*. To further corroborate Hakai as a genuine m⁶A writer in *Drosophila*, we

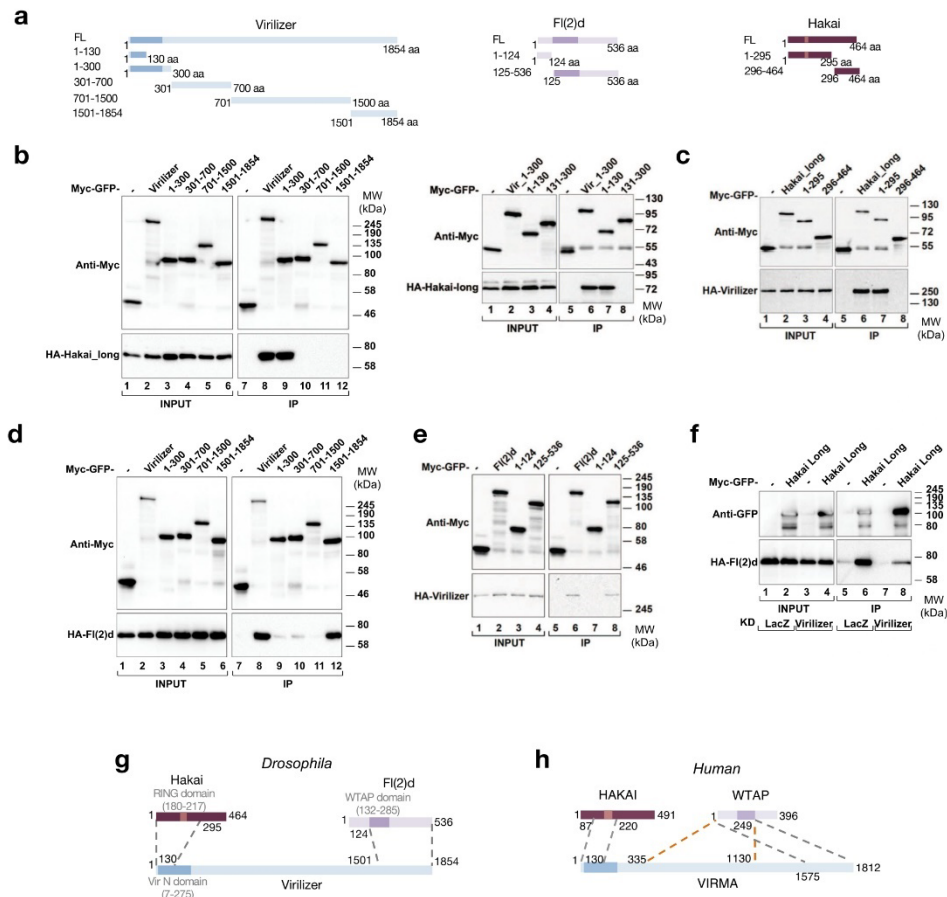


Fig. 2 Virilizer acts as a scaffold between Hakai and FI(2)d. **a** Schematic representation of proteins and protein fragments used for *Drosophila* co-immunoprecipitation assays. **b–e** Co-immunoprecipitation experiments were carried out with lysates prepared from S2R+ cells transfected with Myc-GFP-tagged Virilizer (full length or fragments) and HA-tagged Hakai-long (**b**), Myc-GFP-tagged Hakai-long (full length or fragments) and HA-tagged Virilizer (**c**), Myc-GFP-tagged Virilizer (full length or fragments) and HA-tagged FI(2)d (**d**), Myc-GFP-tagged FI(2)d (full length or fragments) and HA-tagged Virilizer (**e**). In control lanes, S2R+ cells were transfected with Myc-GFP alone and an identical HA-containing protein. Extracts were incubated with magnetic agarose GFP binder beads and immunoblotted using anti-Myc and anti-HA antibodies (**b–e**), as indicated. Two percent of input was loaded. The experiment was performed in the presence of RNase A. Images shown are representative of two biological replicates. **f** Co-immunoprecipitation experiments were carried out with lysates prepared from S2R+ cells transfected with Myc-GFP-tagged Hakai-long and HA-tagged FI(2)d upon control (LacZ) or *vir* KDs. In control lanes, S2R+ cells were transfected with Myc-GFP alone and an identical HA-containing protein. Extracts were incubated with magnetic agarose GFP binder beads and immunoblotted using anti-GFP and anti-HA antibodies. Two percent of input was loaded. **g, h** Schematic representing the interaction domains between Hakai, Vir and FI(2)d derived from co-IP experiments in *Drosophila* (**g**) or HEK393T cells (**h**). Orange dotted lines indicate the second interaction domain between Human WTAP and VIRMA. Source data for western blots are provided as a Source Data file.

depleted its product in S2R+ cells and compared its effect with the KD of other m⁶A pathway components. In agreement with Hakai being part of the m⁶A writer complex, its loss led to a significant reduction of m⁶A levels on mRNA as measured by mass spectrometry (Fig. 4a). However, this reduction (32%) was not as pronounced as the m⁶A reduction observed upon depletion of the Mettl3/Mettl14 heterodimer (59%), which is consistent with the results obtained by TLC from *Hakai¹/Df* mutant pupae (Fig. 3c, d). We next investigated its involvement in the regulation of m⁶A-dependent splicing events. We previously reported

changes in the splicing pattern of several transcripts upon KD of individual m⁶A writers^{15,24}. Splicing isoform quantification by RT-qPCR of two of the affected transcripts, *fl(2)d* and *Hairless*, resulted in a comparable isoform shift in *Hakai* KD and *Mettl3/Mettl14* KD in S2R+ cells (Fig. 4b). On a transcriptome-wide level, depletion of *Hakai* resulted in changes in gene expression and splicing that substantially overlap with changes occurring upon KD of other components of the m⁶A machinery (Fig. 4c; Supplementary Fig. 7). In particular, *Hakai* KD led to an increase of both alternative 5' splice site usage and intron retention,

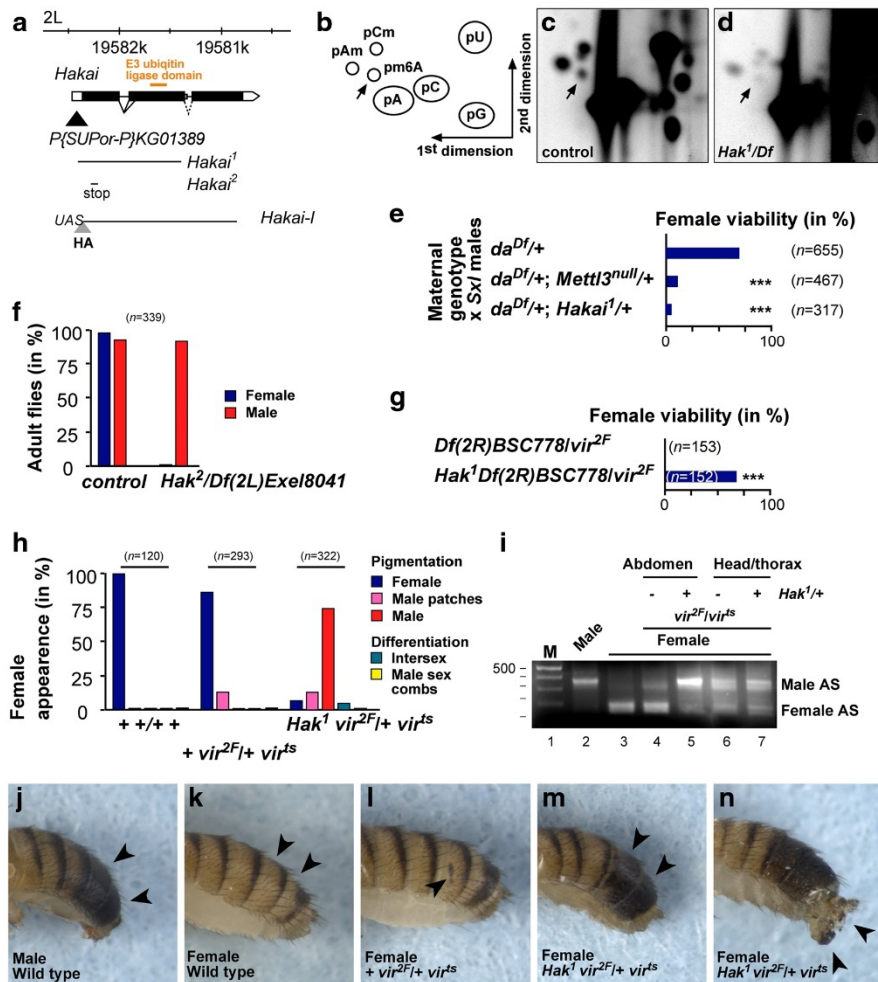


Fig. 3 *Hakai* is required for m^6A methylation and sex determination by regulating *Sex-lethal* alternative splicing. **a** Schematic of the *Hakai* genomic locus depicting the transposon (black triangle) used to generate the deletion in the *Hakai*¹ allele and the premature stop codon present in the *Hakai* allele, and the epitope-tagged UAS constructs of the short and long isoforms. Schematic diagram of a 2D thin-layer chromatography (TLC) depicting standard and methylated nucleotides (**b**), and TLCs depicting m^6A in control (**c**) and *Hakai*¹/*Df*(2L)*Exel8041* pupae (**d**). **e** Viability of female flies from a cross of the indicated genotypes mated with *Sxl*⁷⁸⁰ males. The loss of one copy of *Mettl3* or *Hakai* significantly reduces female survival in a genetic background where one copy of *Sxl* and *da* are absent. Viability was calculated from the numbers of females compared with males, and statistical significance was determined by a χ^2 test (Graphpad Prism). *** $P \leq 0.0001$. Unpaired two-tailed Student's *t*-test for unequal variances. **f** Viability of *Hakai*¹/*Df*(2L)*Exel8041* flies. The viability of female flies with homozygous *vir*^{2F} mutation can be rescued by the loss of a single copy of *Hakai*. Viability was calculated from the numbers of homozygous *vir*^{2F} females compared with heterozygous balancer-carrying siblings, and statistical significance was determined by a χ^2 test (Graphpad Prism). *** $P \leq 0.0001$. **h-n** External sexual differentiation (**h, j-n**) and *Sxl* alternative splicing in abdomen and head/thorax (i) of control, *vir*^{2F}/*vir*^{ts} and *Hakai*¹ *vir*^{2F}/*vir*^{ts} female flies. The gel shown in (i) is a representative of two biological replicates. The marker is a 100 bp DNA ladder with 500 bp indicated on top. Note that *Sxl* alternative splicing in *Hakai*¹ *vir*^{2F}/*vir*^{ts} female abdomens is switched to the male mode and that these females display male pigmentation (**h, m**), but no male sex combs (**h**). Source data for TLC, fly numbers and RT-PCR gels are provided as a Source Data file.

consistent with our previous findings on the individual MACOM component depletion (Fig. 4d²⁴). Note that depletion of MACOM components has a stronger impact on gene expression and splicing compared to the loss of MAC components. This is consistent with previous genetic data showing that *Mettl3* and *Mettl14* are

dispensable for fly viability while MACOM subunits are not^{14–16}, supporting additional function(s) for MACOM components. Altogether, these results demonstrate that *Hakai* is a bona fide component of MACOM and is required for m^6A biogenesis and function.

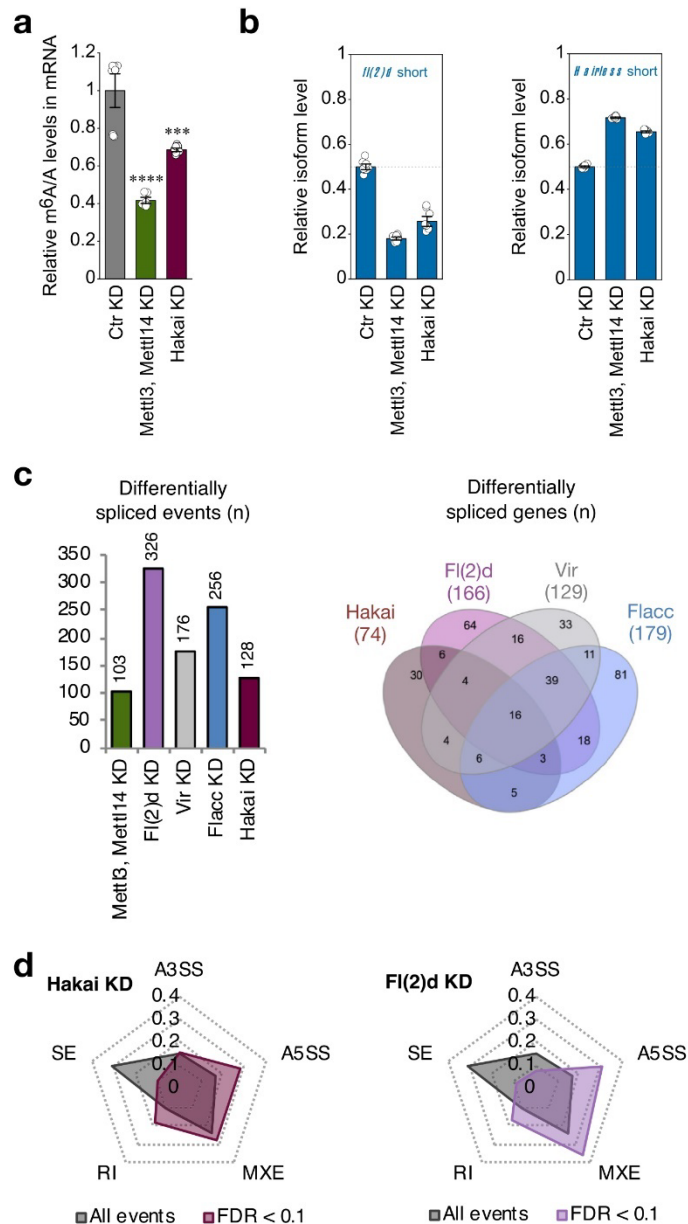


Fig. 4 Hakai regulates m⁶A levels and m⁶A-dependent splicing events. **a** LC-MS/MS quantification of m⁶A levels in either control samples or mRNA extracts depleted for the indicated proteins in S2R+ cells. The bar chart shows the mean with standard error (SE) of three biological replicates and three technical measurements. KD of *Hakai* results in substantial reduction of m⁶A levels. *** $P = 7.49E-04$ (Hakai KD), **** $P = 7.51E-06$ (Mettl13, Mettl14 KD). Unpaired two-tailed Student's *t*-test for unequal variances. **b** Relative isoform quantification of m⁶A-regulated genes (*fl(2)d* and *Hairless*) upon depletion of the indicated components. The bar chart shows the mean with standard error (SE) of three biological replicates and three technical measurements. *Hakai* is required for m⁶A-dependent splicing regulation. **c** Number of differentially spliced events upon knockdown of the indicated proteins (left) and common differentially spliced targets (right) (FDR < 0.1). **d** Radar charts display relative distribution of differentially spliced events upon knockdown of Fl(2)d and Hakai. Alternative 5' splice site (A5SS) selection and intron retention (RI) are overrepresented events upon loss of m⁶A writer components. Source data for m⁶A measurement, qPCR and RNA-seq are provided as a Source Data file.

The Hakai ubiquitination domain but not its activity is required for maintaining MACOM integrity. We next sought to address the molecular role of Hakai within MACOM. As Hakai is a well-studied E3 ubiquitin ligase in mammals, we wondered whether its ubiquitination activity plays any role within the m⁶A pathway. To address this possibility, we generated constructs expressing either the wild-type *Hakai* cDNA (*Hakai*^{WT}) or a cDNA containing point mutations in the RING domain (*Hakai*^{ΔRING}) that should abolish ubiquitination activity (see “Methods”). We then performed rescue experiments in our *Hakai* mutant flies and found that while the wild-type form was able to rescue the lethality, the mutated version failed to do so. This indicates that the RING domain is required for fly viability.

We therefore wondered if Hakai might regulate m⁶A levels by ubiquitination of MACOM components. To investigate this possibility we examined our previous ubiquitylome datasets from *Drosophila* S2 cells and found that Fl(2)d and Nito were among the ubiquitinated proteins⁴³. Thus, we cloned both proteins in a GFP-tag containing vector and expressed them in control and Hakai depleted S2R+ cells to monitor their ubiquitination. We immunoprecipitated both proteins under stringent 8 M Urea conditions and while we could not detect any ubiquitination signal for Nito, Fl(2)d appeared to be polyubiquitinated, as shown by a strong shift in molecular weight by more than 100 kDa (Supplementary Fig. 8a). Using mass spectrometry analysis, we could map two of the four previously identified sites (K236 and K245) in Fl(2)d (Supplementary Data 2), residing in the region required for homodimerization and interaction with Vir (Fig. 2e, Supplementary Fig. 4a). We noticed that Fl(2)d ubiquitination was reduced in the *Hakai* KD condition; however, the overall level of immunoprecipitated Fl(2)d was also diminished. We therefore repeated this experiment in control condition and after proteasome inhibition to prevent protein degradation. This experiment confirmed our previous observations; Fl(2)d was ubiquitinated and its protein intensity was strongly reduced upon *Hakai* KD. However, upon proteasome inhibition, levels of Fl(2)d as well as its ubiquitination remained unchanged despite efficient *Hakai* depletion (Supplementary Fig. 8b). This indicates that Hakai is not responsible for Fl(2)d ubiquitination, but is required for its stability.

To get better insight into the function of Hakai as an E3 ubiquitin ligase and find other putative targets, we next performed a ubiquitylome analysis in S2R+ cells in control versus *Hakai* KD condition. Cells isotopically labelled with heavy amino acids were depleted for *Hakai* and cells isotopically labelled with light amino acids served as a control in the forward experiment. A vice versa depletion was performed in the reverse experiment (Supplementary Fig. 8c). Proteins were digested with endo-proteinase Lys-C and peptides were further enriched with di-glycine-lysine remnant-recognizing antibody to identify ubiquitination sites via LC-MS/MS. We found over 3000 ubiquitination sites, but unexpectedly not a single site was reproducibly reduced in response to *Hakai* depletion and only one site in SesB was 1.5-fold increased (Fig. 5a, Supplementary Data 3). Therefore, this experiment suggests that Hakai does not act as an E3 ubiquitin ligase in *Drosophila* S2R+ cells. Alternatively, it is possible that its ubiquitination activity depends on specific external stimuli or that we have not quantified the ubiquitination sites that are regulated by Hakai due to the limited depth of the analysis.

We wondered what could explain the apparent discrepancy between our in vivo results, indicating the importance of the Hakai RING domain and the data obtained from S2R+ cells. Previous crystal structure in mammals showed that the RING domain is required for HAKAI dimerization⁴⁰. One possibility could be that the point mutations we generated in the RING

domain alter the ability of Hakai to dimerize and perhaps to interact with other MACOM components. To test this idea, we performed co-immunoprecipitation experiments by co-transfecting S2R+ cells with Myc-GFP-tagged Hakai either wild type or mutated in the RING domain and other components of MACOM, including Hakai itself. While WT Myc-GFP-Hakai strongly immunoprecipitated HA-Hakai, the RING mutant failed to do so, indicating that, like in mammals, the RING domain is required for Hakai homodimerization (Fig. 5b). More importantly, interactions with Fl(2)d and Vir were also strongly compromised (Fig. 5c, d). We interpret this result as an indication that Hakai dimerization is likely required for its association with other MACOM components.

Hakai is required for stabilization of MACOM components. Our results so far indicate that Hakai does not possess any ubiquitin activity towards MACOM components, and that it also does not serve as a scaffold to permit the assembly of these components. Nevertheless, as mentioned above, we found that *Hakai* depletion strongly destabilized Fl(2)d protein levels. In addition, we noticed in our co-immunoprecipitation experiments that the level of protein input for Fl(2)d and Vir was consistently reduced upon *Hakai* KD (Supplementary Fig. 5c, d), suggesting that Hakai may be required to stabilize these subunits. For this reason, we had to transfect twice the amount of these components to have comparable input level and therefore interpretable co-immunoprecipitation data. To confirm these observations, we took an unbiased approach by performing a global proteome analysis in S2R+ cells following *Hakai* depletion. As expected, Hakai levels were strongly reduced, indicating a successful KD (Fig. 6a). More strikingly, we identified seven additional proteins that were strongly down regulated, and among them three MACOM components: Fl(2)d, Flacc and Vir (Supplementary Data 4). The extent of downregulation for Vir was similar as for Hakai, indicating that Hakai loss has a particularly strong impact on Vir stability. In contrast, we did not detect any substantial changes in the protein levels of Nito, Mett13 and Mett14. We could confirm by western blot the specific reduction of the Fl(2)d level (Fig. 6b, c and Supplementary Fig. 9d). However, immunofluorescence assay showed that its nuclear localization was not affected (Supplementary Fig. 8d).

To examine whether the loss of Fl(2)d or Vir also impacts the stability of other m⁶A writer components, we repeated the S2R+ proteome analysis after depletion of these proteins. We found that Fl(2)d protein levels were significantly reduced upon *vir* KD and vice versa (Supplementary Fig. 9a-c). Similarly, as shown upon *Hakai* depletion, Flacc level was also decreased. However, in both cases, levels of Hakai and Nito were not affected. This was also confirmed by western blot (Fig. 6d and Supplementary Fig. 9e). Collectively, these results indicate that Hakai functions in stabilizing three MACOM components and this is likely the reason why m⁶A levels are reduced upon its depletion.

The role of Hakai in MACOM component stabilization is conserved in human. Given the high conservation of Hakai with its human ortholog and its interaction with Vir, we wondered if HAKAI function within MACOM is conserved in humans. To this end, we depleted human *HAKAI* and *VIRMA* in HeLa and U2OS cells and monitored the protein levels. We observed that the loss of *VIRMA* had no effect on HAKAI level (Fig. 6e), as also shown with the *Drosophila* homologues. In contrast, depletion of *HAKAI* strongly reduced *VIRMA* levels but not the levels of RBM15, the human ortholog of Nito. Altogether, these findings indicate that the role of HAKAI within MACOM is conserved in humans and that Hakai is indispensable for maintaining the

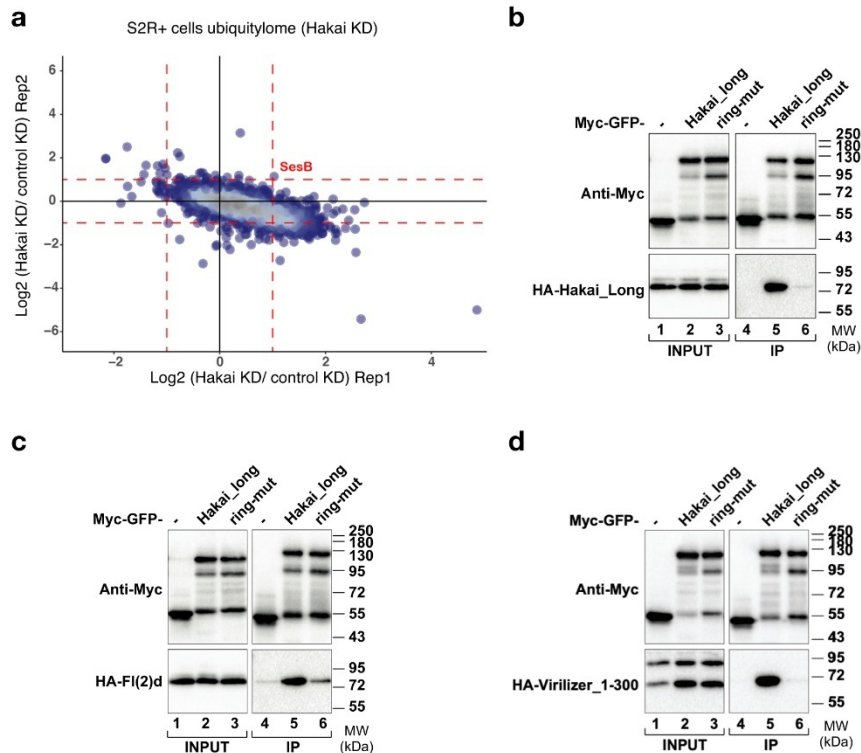


Fig. 5 Hakai RING domain is required for interaction with MACOM components. **a** Mass spectrometry analysis of Hakai-dependent ubiquitinated proteins in S2R+ cells. Scatter plot of normalized forward versus inverted reverse experiments plotted on a log₂ scale. The threshold was set to a twofold enrichment or depletion (red dashed line). One protein in the top right quadrant is enriched in both replicates. Hakai depletion does not affect global ubiquitination levels in *D. melanogaster* S2R+ cells. A complete list of quantified ubiquitylation sites after HAKAI depletion can be found in Supplementary Data 3. **b-d** Co-immunoprecipitation experiments were carried out with lysates prepared from S2R+ cells transfected with Myc-GFP-tagged Hakai-long (WT or RING mutant) and HA-tagged Hakai-long (**b**), HA-tagged Fl(2)d (**c**) and HA-tagged Virilizer fragment (**d**). In control lanes, S2R+ cells were transfected with Myc-GFP alone and an identical HA-containing protein. Extracts were incubated with magnetic GFP binder beads and immunoblotted using anti-Myc and anti-HA antibodies, as indicated. Two percent of input was loaded. The experiment was performed in the presence of RNase A. Images shown are representative of two biological replicates. Source data for Western blots are provided as a Source Data file.

functionality of m⁶A writer by ensuring the stability of MACOM components (Fig. 7).

Discussion

We recently showed that two conserved sub-complexes, MAC and MACOM interact to deposit m⁶A on mRNA in flies and mice²⁴. While the structure of the catalytic MAC, which consists of the heterodimer METTL3 and METTL14, has been thoroughly characterized^{28–30}, our knowledge of MACOM is limited. In particular, the full composition, assembly and exact function of each subunit have remained unclear. Our study identifies Hakai as an integral component of MACOM in *Drosophila* and human cells. In line with this function, we show that Hakai interacts with Vir and other MACOM components, and its depletion reduced m⁶A levels and led to altered gene expression, resembling loss of other MACOM subunits. Furthermore, flies lacking *Hakai* are lethal and display aberrant splicing of *Sex lethal*, consistent with the role of MACOM in sex determination and dosage

compensation pathways. The few individuals that escape lethality are flightless, as shown earlier in other mutants of the m⁶A pathway. Mechanistically, we found that Hakai is required to stabilize several MACOM components, likely explaining its requirement for m⁶A deposition.

The question that arises is whether all MACOM components have now been identified. We and others have validated five factors, which include Fl(2)d, Vir, Flacc, Nito and Hakai (this study and^{14–16,24,33}). Earlier biochemical studies estimated a molecular weight of 875 kDa for the large form of the human methyltransferase complex⁴⁴. The calculated total molecular weight of the combined five factors corresponds to 600 kDa, which suggests that the complex contains additional factors or multiple copies of the known factors. Our data show that Hakai, Fl(2)d and Nito have the ability to self-interact (Supplementary Fig. 4). If we assume that these three factors are present as dimers, the total weight reaches up to 868 kDa, which would be consistent with the predicted mass of MACOM. Nevertheless, additional

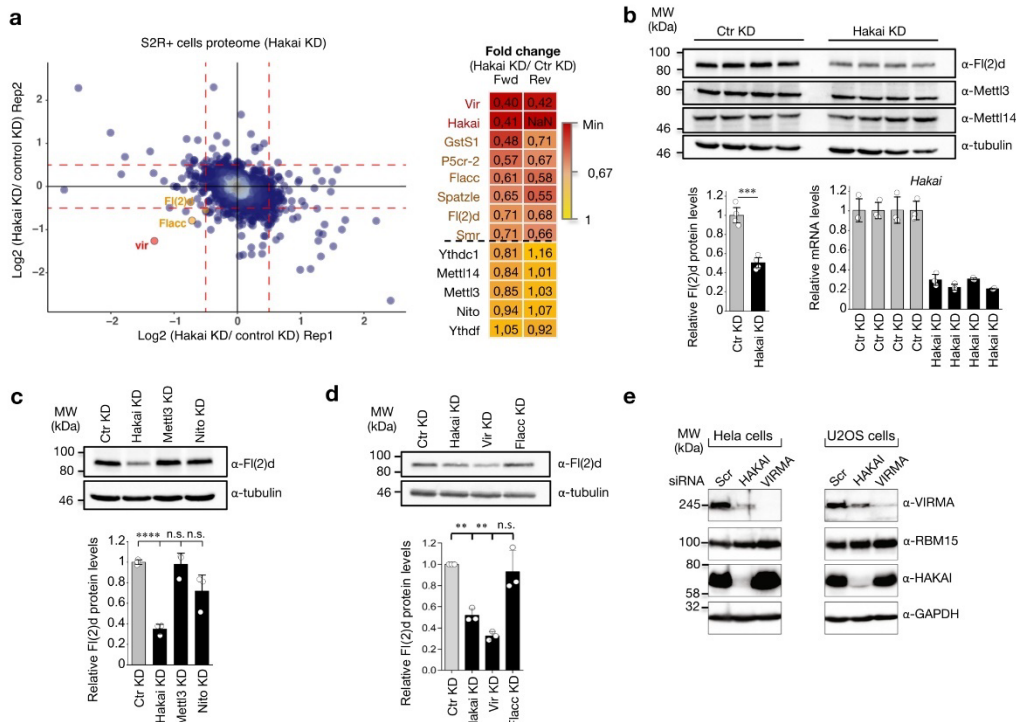


Fig. 6 Hakai regulates the stability of other MACOM components. **a** Mass spectrometry analysis of Hakai-dependent proteome in S2R+ cells. Scatter plot of normalized forward versus inverted reverse experiments plotted on a log₂ scale. The threshold was set to a 1.4-fold enrichment or depletion (red dashed line). Proteins in the bottom left quadrant are decreased in both replicates. Heat map of proteins whose levels were reduced by >1.4-fold in both replicates of the whole proteome analysis. Other components of the m⁶A writer complex and reader proteins are shown for comparison. A complete list of quantified proteins can be found in Supplementary Data 4. **b** Levels of endogenous FI(2)d, Mett13 and Mett14 proteins from control cells and cells depleted for Hakai were analyzed by western blot. Tubulin was used as a loading control. Quantification of FI(2)d, Mett13 and Mett14 levels from blots shown below (left). The bar chart shows the mean with standard error (SE) of four biological replicates. ****P* = 2.48E−04 (Hakai KD). Unpaired two-tailed Student's *t*-test for equal variances. Hakai depletion strongly destabilizes FI(2)d, but not Mett13 or Mett14 proteins. Relative expression levels of *Hakai* are shown as a validation of its KD efficiency. The bar chart shows the mean with standard error (SE) of three technical measurements (Bottom right). **c, d** Analysis of FI(2)d levels upon *Hakai*, *Mett13*, *nito* (**c**) or *Hakai*, *vir*, *Flacc* (**d**) depletion. Protein lysates from control and depleted cells were analyzed by western blot for levels of endogenous FI(2)d protein. Tubulin was used as a loading control. One representative experiment is shown and quantification of three biological replicates is shown below. The bar chart shows the mean with standard error (SE). (**c**) *****P* = 4.74E−05 (Hakai KD), ^{n.s.}*P* = 0.80029 (Mett13 KD) and ^{n.s.}*P* = 0.05398 (Nito KD). (**d**) ***P* = 0.0057 (Hakai KD), *P* = 0.0012 (Vir KD) (Hakai KD), and ^{n.s.}*P* = 0.6061 (Flacc KD). Unpaired two-tailed Student's *t*-test for equal variances. **e** Western blots were carried out with lysates prepared from HeLa and U2OS cells transfected with scrambled siRNA or siRNA against HAKAI or VIRMA. Extracts were immunoblotted using the indicated antibodies. Depletion of HAKAI reduced VIRMA levels while depletion of VIRMA had no impact on HAKAI levels. Images shown are representative of two biological replicates. Source data for western blots, measurement of protein levels and qPCR are provided as a Source Data file.

biochemical and structural characterization will be required to confirm the exact identity and stoichiometry of the different complex components.

While Hakai is undoubtedly a core component of the complex, it is surprising that its gene inactivation results in milder phenotypes in comparison to the inactivation of other MACOM components. Indeed, the few females that escaped developmental lethality in the *Hakai* loss-of-function mutant did not display male sex combs and this phenotype was also not observed in a sensitized background with reduced *Hakai* dosage. However, the females did show male pigmentation on their abdomen, indicating tissue-specific alteration of sex determination. These milder defects are consistent with our quantification of the m⁶A level in the *Hakai* mutant (Fig. 3), which appeared reduced but

not completely absent, as observed in the *Mett13* mutant¹⁴. Also, *Sxl* splicing showed tissue-specific alterations, indicative of local requirement for this factor. These results are consistent with a previous study in *Arabidopsis* showing less pronounced impact of Hakai on the m⁶A levels as well as on organismal development²⁶. This apparent discrepancy may be explained by the function we uncovered in this work. Our data show that upon depletion of *Hakai* the level of some of the other MACOM components is reduced but not completely lost (Fig. 6), which suggest that the remaining MACOM could still support methylation. In this case, tissue-specific requirement may be mediated through differential expression of factors that may impact on this residual interaction and could determine tissue-specific levels of m⁶A. Additional work would be required to test this hypothesis.

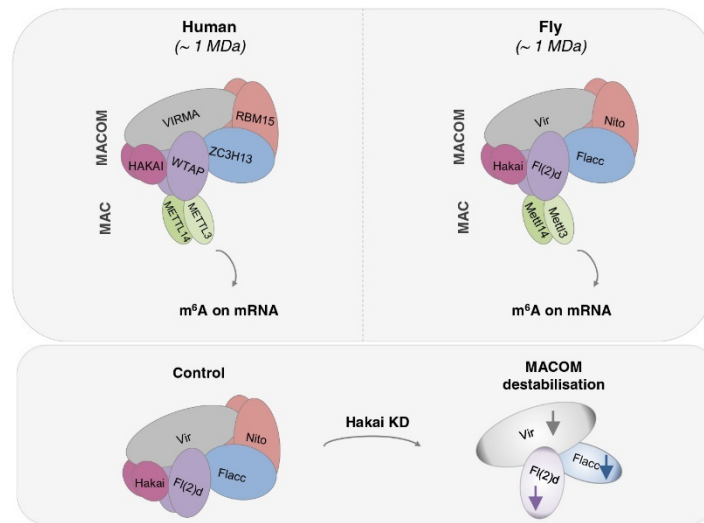


Fig. 7 Model showing the composition of the m⁶A methyltransferase complex in fly and human and the impact of Hakai on MACOM integrity. Top left and right represent the human and fly m⁶A methyltransferase complexes, respectively. (Bottom) The depletion of Hakai leads to a reduction in protein levels for Vir, Flacc and F(2)d.

In vertebrates, Hakai was shown to ubiquitinate E-cadherin and promote its degradation³⁵. In contrast, our data from *Drosophila* cells provide no evidence for ubiquitination activity towards MACOM components or any other proteins. Instead, our work strongly suggest that Hakai is required for the stability of three MACOM components, Vir, Fl(2)d and Flacc, independently of its enzymatic activity. The question that remains is how does Hakai exert this function. It was previously shown that the so-called “orphan proteins” are unstable and get degraded if their protein partners that constitute a common complex are absent. Destabilization can be triggered due to aberrant protein folding, altered localization or because of exposure of normally protected protein binding interfaces⁴⁵. It is therefore possible that Hakai stabilizes other MACOM components via one of these mechanisms. If this model is true, other components of the complex are also expected to stabilize each other. Indeed, we found that protein levels of Vir, Fl(2)d and Flacc were also strongly reduced upon loss of Vir or Fl(2)d (Fig. 6). Interestingly, in mES cells a strong reduction of Wtap levels was previously reported upon loss of Virma²⁷ and a strong destabilization of Zc3h13 was observed upon depletion of Virma, Wtap or Hakai³⁴, suggesting a conserved mechanism for Hakai-Vir-Fl(2)d-Flacc stabilization between flies and mice. We further demonstrated that protein levels of Hakai and Nito are unperturbed upon depletion of other MACOM components, suggesting that Hakai and Nito might function in additional processes not linked to MACOM or m⁶A-deposition. This is in agreement with observations that Hakai also localizes in the cytoplasm, and with a study that found Nito (RBM15) in an evolutionary conserved protein complex with proteins unrelated to remaining MACOM components³⁹.

Given our insights from the current study, we propose the following model of MACOM assembly: (i) Fl(2)d-Vir-Hakai form a minimal protein unit that is required for the assembly and functionality of the remaining methyltransferase complex. (ii) Stability of Fl(2)d and Vir depends on each other and Hakai, but is largely independent of Flacc and Nito. (iii) Fl(2)d-Vir-Hakai can interact with MAC, however, this is not sufficient for m⁶A

deposition. (iv) Joining of Flacc and Nito is essential for the formation of a complete MACOM complex that can bind and methylate its targets together with MAC.

In conclusion, our work revealed the requirement of Hakai for m⁶A deposition in *Drosophila*. The apparent dependency of Fl(2)d, Vir and Flacc for each other’s stability might be an important mechanism that maintains an equilibrium of protein stoichiometry for a complete complex assembly in order to prevent aberrant interactions of orphan subunits and unwanted m⁶A installation. Given the critical role of m⁶A in multiple physiological processes, it will be important to address whether perturbation of this equilibrium, for instance, by single nucleotide polymorphism, may impact the development or severity of pathological conditions.

Methods

Drosophila stocks and genetics. *Drosophila melanogaster* CantonS was used as the wild-type control. All *Hakai* alleles and corresponding chromosomal deficiencies (*Df(2L)Exel8041* and *Df(2L)Exel6044*) were re-balanced with a CyO balancer that is marked by *actinGFP* and *w+* to determine the lethal stage and collect homozygous *Hakai* null animals. Sexing at the larval stage was done by monitoring the presence of the male gonad.

The *P[VSH330548]attP40 Hakai* RNAi line was obtained from Vienna *Drosophila* Resource Center. *Hakai* was generated using the CRISPR-Cas9 system following the previously described procedure⁴⁶. Two independent guide RNAs were designed using the gRNA design tool: www.crisprflydesign.org (Supplementary Data 5). Oligonucleotides were annealed and cloned into pBFV-U6.2 vector (National Institute of Genetics, Japan). The vector was injected into embryos of TBX-0002 (*y1, v1, P[nos-phiC31]int.NLS.SX; attP40 (II)*) flies by Bestgene Inc. Flies were crossed with TBX-0008 (*y2 cho2 v1/Yhs-hid; Sp/CyO*) flies to identify positive recombinant flies by eye colour marker (Vermillion). Males were further crossed with CAS-0001 (*y2, cho2, v1; attP40(nos-Cas9)/CyO*) females. Males carrying *nos-Cas9* and U6-gRNA transgenes were screened for the expected deletion using oligos in Supplementary Data 5.

For genetic interaction studies, we used *Mettl3^{null}* and *vir* alleles as described²⁴. The *da* deficiency was *Df(2L)BSC209*.

Cloning. The plasmids used for immunohistochemistry and co-immunoprecipitation assays (shown in Fig. 1d, e) were constructed by cloning the corresponding cDNA in the pAC vector with the N-terminal Myc- tag (Hakai short and Hakai long) or N-terminal Myc-GFP tag (Fl(2)d and Nito)¹⁵. For plasmids

with the C-terminal HA tag, the corresponding cDNA was cloned in the Gateway-based vector (pPWH) obtained from Drosophila Genomics Resource Center (DGRC) at Indiana University as described in ref. 15. To generate the RING mutant construct the corresponding mutations were introduced: histidine at position 183 was replaced by alanine in combination with cysteine to alanine conversion for the residues 165, 168, 181, 186, 189, 198 and 201. The stability of the protein was not affected by these mutations. Hakai long and Ring mutant cDNA were cloned in the pUAST-eGFP-attB vector between BamHI and XbaI sites and the constructs were sent to BestGene for injections.

Myc-GFP construct was generated by cloning Myc tag in directional cloning within the KpnI restriction site in pAc5.1B-EGFP-V5-His vector. This construct also has V5-His in frame after EGFP. This construct was used as negative control for the experiment. Then all cDNAs were cloned in this vector for the subsequent experiments. For HA-tagged constructs all the cDNAs were cloned in pAc5.1B-lambdaN-HA vector in suitable restriction sites.

Cell culture, RNA interference and transfection. *Drosophila* S2R+ cells were grown in Schneider's medium (Gibco) supplemented with 10% FBS (Sigma) and 1% penicillin-streptomycin (Sigma). For RNA interference (RNAi) experiments, PCR templates for the dsRNA were prepared using T7 megascript Kit (NEB). dsRNA against bacterial β -galactosidase gene (*lacZ*) was used as a control for all RNA interference (RNAi) experiments. S2R+ cells were seeded at the density of 10^6 cells/ml in serum-free medium and 7.5 μ g of dsRNA was added to 10^6 cells. After 6 h of cell starvation, serum supplemented medium was added to the cells. dsRNA treatment was repeated after 48 and 96 h and cells were collected 24 h after the last treatment. Effectene (Qiagen) was used to transfect vector constructs in all overexpression experiments following the manufacturer's protocol.

For knockdown in HeLa and U2OS cells, siRNAs against VIRMA (catalogue no. s24832), HAKAI (catalogue no. s36537) as well as negative control siRNA were purchased from Ambion. siRNAs were transfected with Lipofectamine 2000 RNAi MAX (Invitrogen) according to the manufacturer's protocol.

Drosophila cell lines. *Drosophila* S2R+ cells were embryonic-derived cells obtained from the DGRC (at Indiana University; FlyBase accession FBtc0000150). *Drosophila* BG3 cells were derived from larval nervous system and also obtained from the DGRC (at Indiana University; FlyBase accession FBtc0000068). Both cell lines were tested for Mycoplasma infection by RNA-seq experiments.

Drosophila staging. The staging experiment was performed as described previously¹⁵ using *D. melanogaster w1118* flies. A total of three independent samples was collected for each *Drosophila* stage as well as for heads and ovaries. Samples from the staging experiment were used for RNA extraction to analyze m⁶A abundance in mRNA and expression levels of different transcripts during *Drosophila* development.

RNA isolation and mRNA purification. Total RNA from S2R+ cells was isolated using Trizol reagent (Invitrogen), and DNA was removed with DNase I treatment (New England Biolabs). Fly heads from 3- to 5-day-old flies were separated and homogenized in Trizol prior to RNA isolation. mRNA was isolated by two rounds of purification with Dynabeads Oligo d(T)25 (New England Biolabs).

RT-PCR. cDNA was prepared using M-MLV reverse transcriptase (Promega). Transcript levels were quantified using Power SYBR Green PCR master mix (Invitrogen) and the oligonucleotides indicated in Supplementary Data 5.

For Sxl quantification, Total RNA was extracted using Tri-reagent (SIGMA) and reverse transcription was done with Superscript II (Invitrogen) according to the manufacturer's instructions using an oligodT17V primer. PCR for Sxl was done for 40 cycles with 1 μ l of cDNA with primers Sxl F2 (ATGTACGGCAACAATAATCCGGGTAG) and Sxl R2 (CATTGTAAACACGACGCGACGATG). Experiments included three biological replicates.

LC-MS/MS analysis of m⁶A levels. mRNA samples for LC-MS/MS analysis were prepared as mentioned above. Three hundred nanograms of purified mRNA was digested with 0.3 U Nuclease P1 from Penicillium citrinum (Sigma-Aldrich, Steinheim, Germany) and 0.1 U Snake venom phosphodiesterase from *Crotalus adamanteus* (Worthington, Lakewood, USA) in 25 mM ammonium acetate, pH 5, supplemented with 20 μ M zinc chloride for 2 h at 37 °C. Remaining phosphates were removed by 1 U FastAP (Thermo Scientific, St Leon-Roth, Germany) in the manufacturer-supplied buffer, in a 1 h incubation at 37 °C. The resulting nucleoside mix was then spiked with 13C stable isotope labelled nucleoside mix from *Saccharomyces cerevisiae* RNA as an internal standard (SIL-IS) to a final concentration of 4 ng/ μ l for the sample RNA and 2 ng/ μ l for the SIL-IS. For the analysis, 10 μ l of the before mentioned mixture were injected into the LC-MS/MS machine. Generation of technical triplicates was obligatory. All mRNA samples were analyzed in biological triplicates. LC separation was performed on an Agilent 1200 series instrument, using 5 mM ammonium acetate buffer as solvent A and acetonitrile as buffer B. Each run started with 100% buffer A, which was decreased

to 92% within 10 min Solvent A was further reduced to 60% within another 10 min. Until minute 23 of the run, solvent A was increased to 100% again and kept at 100% for 7 min to re-equilibrate the column (Synergi Fusion, 4 μ M particle size, 80 Å pore size, 250 \times 2.0 mm, Phenomenex, Aschaffenburg, Germany). The ultraviolet signal at 254 nm was recorded via a DAD detector to monitor the main nucleosides. MS/MS was then conducted on the coupled Agilent 6460 Triple Quadrupole (QQQ) mass spectrometer equipped with an Agilent JetStream ESI source which was set to the following parameters: gas temperature, 350 °C; gas flow, 8 l/min; nebulizer pressure, 50 psi; sheath gas temperature, 350 °C; sheath gas flow, 12 l/min; and capillary voltage, 3,000 V. To analyze the mass transitions of the unlabelled m⁶A and all 13C m⁶A simultaneously, we used the dynamic multiple reaction monitoring mode.

Analysis of m⁶A methylation by TLC. Total RNA was extracted with Trizol (Invitrogen) and PolyA mRNA from oligo dT selection was prepared according to the manufacturer (Promega). For each sample, 50 ng of polyA mRNA was cut with RNase T1 (1000U, Fermentas) and 5'-end-labeled using 10 U of T4 PNK (NEB) and 0.5 μ l [³²P] ATP (6000 Ci/mmol, 25 μ M; Perkin-Elmer) in T4 PNK buffer for 2 h. The labelled RNA was precipitated, washed twice with 70% ethanol, resuspended in 10 μ l of 50 mM sodium acetate buffer (pH 5.5) and digested with P1 nuclease (SIGMA) for 1 h at 37 °C. Two microliters of each sample was loaded on cellulose F TLC plates (20 \times 20 cm; Merck) and run in a solvent system of isobutyric acid:0.5 M NH₄OH (5:3, v/v), as first dimension, and isopropanol:HCl:water (70:15:15, v/v/v), as the second dimension. TLCs were repeated from biological replicates. The identity of the nucleotide spots was determined as described¹⁴. For the quantification of spot intensities on TLCs, a storage phosphor screen (K-Screen; Kodak) and Molecular Imager FX in combination with QuantityOne software (BioRad) were used.

Immunostaining. For staining of *Drosophila* S2R+ and BG3 cells, cells were transferred to the eight-well chambers (Ibidi) at a density of 2×10^5 cells per well. After 30 min, cells were washed with 1 \times DPBS (Gibco), fixed with 4% formaldehyde for 10 min, and permeabilized with PBST (0.2% Triton X-100 in PBS) for 15 min. Cells were incubated with mouse anti-Myc (1:2000, Enzo, 9E10) or mouse anti-Flag (1:1000) in PBST supplemented with 10% donkey serum overnight at 4 °C. Cells were washed three times for 15 min in PBST and then incubated with secondary antibody and 1 \times DAPI solution in PBST supplemented with 10% donkey serum for 2 h at 4 °C. After three 15-min washes in PBST, cells were imaged with a Zeiss LSM 710 confocal microscope using a 63 \times oil immersion objective.

For polytene chromosome staining, the long Hakai isoform was expressed in salivary glands with *C155-GAL4* as described¹⁴. Briefly, larvae were grown at 18 °C under non-crowded conditions. Salivary glands were dissected in PBS containing 4% formaldehyde and 1% TritonX100, and fixed for 5 min, and then for another 2 min in 50% acetic acid containing 4% formaldehyde, before placing them in lactic acid (lactic acid:water:acetic acid, 1:2:3). Chromosomes were then spread under a siliconized cover slip and the cover slip removed after freezing. Chromosomes were blocked in PBT containing 0.2% BSA and 5% goat serum and sequentially incubated with primary antibodies (mouse anti-Pol II H5 IgM, 1:1000, Abcam, and rat anti-HA MAb 3F10, 1:50, Roche) followed by incubation with Alexa488- and/or Alexa647-coupled secondary antibodies (Molecular Probes) including DAPI (1 μ g/ml, Sigma).

Co-immunoprecipitation assay and western blot analysis of the *Drosophila* MACOM subunits. For the co-immunoprecipitation assays shown in Fig. 1e, f, different combinations of vectors with the indicated tags were co-transfected in S2R+ cells. Forty-eight hours after transfection, cells were collected, washed with DPBS, and pelleted by centrifugation at 400 \times g for 10 min. The cell pellet was lysed in 1 ml of lysis buffer (50 mM Tris-HCl at pH 7.4, 150 mM NaCl, 0.05% NP-40) supplemented with protease inhibitors and rotated head over tail for 15 min at 4 °C. Nuclei were collected by centrifugation at 1000 \times g for 10 min at 4 °C, resuspended in 300 μ l of lysis buffer, and sonicated with five cycles of 30 s on and 30 s off at the low power setting. Cytoplasmic and nuclear fractions were joined and centrifuged at 18,000 \times g for 10 min at 4 °C to remove the remaining cell debris. Protein concentrations were determined using Bradford reagent (Bio-Rad). For immunoprecipitation, 2 mg of proteins was incubated with 2 μ g of anti-Myc antibody coupled to protein A/G magnetic beads (Cell Signalling) in lysis buffer and rotated head over tail overnight at 4 °C. The beads were washed three times for 15 min with lysis buffer, and immunoprecipitated proteins were eluted by incubation in 1 \times NuPAGE LDS buffer (Thermo Fisher) for 10 min at 70 °C. Eluted immunoprecipitated proteins were removed from the beads, and DTT was added to 10% final volume. Immunoprecipitated proteins and input samples were analyzed by Western blot after incubation for an additional 5 min at 95 °C. For western blot analysis, proteins were separated on a 8% SDS-PAGE gel and transferred to a nitrocellulose membrane (Bio-Rad). After blocking with 5% milk in 0.05% Tween in PBS for 1 h at room temperature, the membrane was incubated with primary antibody in blocking solution overnight at 4 °C. Primary antibodies used were mouse anti-Myc 1:2000 (#9E10, Enzo); mouse anti-HA 1:1000 (#16B12, COVANCE); mouse anti-Tubulin 1:2000 (#903401, Biolegend); mouse anti-Fli(2)d 1:500

(#9G2, DSHB), guinea pig anti-Mettl13 1:500 and rabbit anti-Mettl14 (Lence et al. 2016) 1:250. The membrane was washed three times in PBST for 15 min and incubated for 1 h at room temperature with secondary antibody in blocking solution. Protein bands were detected using SuperSignalWest Pico chemiluminescent substrate (Thermo Scientific).

For the co-immunoprecipitation assays, shown in other figures, the following modifications were made: Cells were harvested 72 h after transfection and washed once with DPBS. The cell pellet was lysed in 0.5 ml of NET buffer (50 mM Tris-HCl pH 7.5, 150 mM NaCl, 0.1% Triton and 1 mM EDTA pH 8.0 supplemented with protease inhibitor and 10% glycerol) and sonicated for 3 cycles of 30 s at high power setting followed by incubation with RNase A at ice for 30 min. Lysate was centrifuged at 15,000 × g for 10 min at 4 °C. Ten percent of the samples were taken out as input samples and rest were incubated with GFP-magnetic beads on head to toe rotary mixer at 4 °C. The beads were washed three times for 15 min with NET buffer, and proteins were eluted by boiling the beads for 3 min at 95 °C in SDS-page loading dye supplemented with 100 mM DTT. Where applicable, depletion of indicated proteins was performed as described under “Cell culture, RNA interference and transfection”. Double amounts of constructs were transfected in several conditions, as indicated in corresponding figure legends.

Co-immunoprecipitation assay and western blot analysis of the human MACOM subunits. For co-immunoprecipitation assay of the human MACOM subunits, selected truncations of human MACOM components were cloned individually into pcDNA3-derived vectors with His₆-HA₃-mCherry- or His₆-FLAG₃-cGFP- tags. 0.25 mln. HEK293T cells were seeded into 2 ml media in 6-well plates, grown for ~24 h (reaching ~75% confluency) and transfected with corresponding plasmids, 1 µg each, using Xtreme[®] transfection agent (Roche) at 1:3 ratio. Cells were washed with PBS and harvested ~48 h after transfection using 250 µl of the lysis buffer (20 mM Tris-HCl, pH 7.5, 150 mM KCl, 1 mM EDTA, 0.1% Tween20), supplemented with Roche protease inhibitor. The cells were then flash frozen in liquid nitrogen and stored at -80 °C.

Upon thawing, the cells were further lysed by sonication for 30 s (0.5 s on/2 s off) at 10% amplitude. 2 µg RNase A was added to rule out RNA-mediated interactions. Soluble fraction was separated by centrifugation at full speed for 15 min and incubated with ~18 µl of magnetic anti-FLAG M2 beads (Sigma) for 1 h. The beads were washed 3-4 times with the lysis buffer. The resultant beads were mixed directly with the SDS loading dye and loaded onto 4-20% SDS gels (BioRad). The gels were scanned for GFP and mCherry signals using Typhoon FLA 9500 filters of 473 nm and 532 nm, respectively.

Immunoprecipitation and ubiquitination analysis of MycGFP-Fl(2)d and MycGFP-Nito. S2R+ cells were transfected with either MycGFP-tagged Nito or Fl(2)d proteins as described above. Forty-eight hours post-transfection attached cells in the 10-cm cell culture dish were washed 2x with cold PBS on ice. Cells were lysed with 1 ml of modified RIPA lysis buffer (50 mM Tris-HCl pH 7.5, 150 mM NaCl, 1 mM EDTA, 1% NP-40, 0.1% Na-deoxycholate), supplemented with complete protease inhibitor cocktail, 5 mM beta-glycerophosphate, 5 mM NaF, 1 mM Na-orthovanadate, 10 mM N-ethylmaleimide. Cells were then collected and incubated for 10 min on ice and centrifuged 15 min at 16,000 × g at 4 °C. Supernatant was transferred to a new tube and protein concentration measured using Bradford. 1.5 mg of proteins was incubated with 20 µl of washed GFPTrap-A beads (Chromotec) for 1 h at 4 °C end-over-end mixing. Beads were collected by centrifugation (3000 rpm, 1 min) and the supernatant removed. Beads were washed 1x with dilution buffer (10 mM Tris-HCl pH 7.5, 150 mM NaCl, 0.5 mM EDTA, 1x Protease Inhibitor (Sigma), 10 mM N-ethylmaleimide), 3x with stringent wash buffer (8 M Urea, 1% SDS in 1x PBS) and 1x with wash buffer (1% SDS in 1x PBS). Forty-microlitres of 2x LDS sample buffer (Invitrogen) supplemented with 1 mM DTT was added and beads were incubated for 10 min at 70 °C. Twenty-five percent of eluted proteins were analyzed by WB. Primary antibodies used were as follows: mouse anti-Myc 1:2000 (#9E10, Enzo) and mouse Ub antibody (P4D1, Santa Cruz).

The remaining 75% of eluted proteins were used for ubiquitinome and proteome analysis. Proteins were alkylated with 5.5 mM CAA for 30 min at RT in the dark, stained using the Colloidal Blue Staining Kit (Life Technologies) and digested in-gel using trypsin. Peptides were extracted from gel and desalted on reversed-phase C18 StageTIPS⁴⁷. Samples were then subjected to MS and peptide identification.

Stable isotope labelling by amino acids in cell culture (SILAC). For SILAC experiments (ubiquitinome and proteome of Hakai depleted cells), S2R+ cells were grown in Schneider medium (Dundee Cell) supplemented with either heavy (Arg10, Lys8) or light amino acids (Arg0, Lys0) (Sigma) for 6-8 passages and successful incorporation was confirmed by LC-MS/MS.

Ubiquitylome and proteome analysis in S2R+ cells. Ubiquitylome and proteome analysis of control and Hakai depleted SILAC S2R+ cells or Fl(2)d/Vir depleted S2R+ cells was performed as described previously^{43,48}. Following modifications were made: S2R+ cells were grown in Schneider medium (Dundee Cell) supplemented with either heavy (Arg10, Lys8) or light amino acids (Arg0, Lys0)

(Sigma) or without supplement for the label-free proteomes (Fl(2)d and Vir KD). Depletion of the different factors was performed with corresponding double-stranded RNA three times during 6 days and scaled up to obtain 50 mg of proteins per replicate (8-10, 15-cm cell culture dishes). Six hours prior to cell lysis, the MG132 proteasome inhibitor was added to a final concentration of 15 µM. Cells were lysed in modified RIPA lysis buffer (50 mM Tris-HCl pH 7.5, 150 mM NaCl, 1 mM EDTA, 1% NP-40, 0.1% Na-deoxycholate) supplemented with complete protease inhibitor cocktail (Roche), 5 mM -glycerophosphate, 5 mM NaF, 1 mM Na-orthovanadate, 10 mM N-ethylmaleimide. 1.5 ml of buffer was used per each 15-cm dish. All lysates of the same transfection were combined in a falcon and protein concentrations were measured by Bradford. Hundred micrograms of each protein sample was collected for WB analysis. For ubiquitylome and proteome analysis 25 mg of heavy and 25 mg of light labelled protein lysates were joined in a 1:1 ratio as follows: for forward experiment heavy labelled lysates with Hakai KD and light labelled lysates with control KD were joined, and vice versa for reverse experiment. 50 µg were then collected for proteome analysis. Finally, ice-cold acetone was added to 80% final conc. (4xV) and precipitated O/N at -20 °C and subjected to MS.

Label-free proteomes. A total of 15 × 10⁶ S2R+ cells were transfected with Myc-GFP-tagged HAKAI-long isoform in a 10-cm cell culture dish. In parallel, cells were transfected with Myc-GFP as negative control. After 72 h, the cells were harvested and washed with cold PBS. Cells were lysed with 1 ml of NET buffer (50 mM Tris-HCl pH 7.5, 150 mM NaCl, 0.1% Triton and 1 mM EDTA pH 8.0) and supplemented with 10% Glycerol and Protease inhibitor cocktail (Roche). Lysates were sonicated for 3 cycles of 30 s at a high power setting followed by incubation with RNase A on ice for 30 min. Lysate was centrifuged at 15,000 × g for 10 min at 4 °C. The cleared lysates were incubated with GFP-magnetic beads on a head-to-toe rotary mixer at 4 °C for 2 h. The beads were washed three times for 15 min with NET buffer, and proteins were eluted by incubating at 70 °C in NuPAGE buffer.

Proteome and ubiquitylome analyses. MS sample preparation, proteome analysis, MS, and peptide identification were performed as described previously in ref. ⁴⁸. For peptide identification in SILAC samples, raw data files were analyzed using MaxQuant (development version 1.5.2.8) to calculate the ratios between the different conditions⁴⁹. For the MaxQuant analysis, we used different parameter groups to define group-specific parameters to invert the SILAC ratios in replicate 2 (Reverse). As result of these settings H/L in both experiments represents HAKAI KD/Non-targeting control. The data with all quantified ubiquitylation sites (diglycine sites) and protein groups are provided as Supplementary_Data_3 (ubiquitylome analysis) and Supplementary_Data_4 (proteome analysis).

Analysis of label-free samples was performed using default setting for the LFQ analysis in MaxQuant (1.5.2.8) and the Perseus software version 1.5.6.0 to perform calculation of *p* value and Student's *t* test⁵⁰. Parent ion and MS2 spectra were searched against a database containing *D. melanogaster* protein sequences obtained from the UniProtKB released in May 2016 using Andromeda search engine⁵¹.

Yeast-two-hybrid assay (Y2H). Yeast-two-hybrid assay was performed using *S. cerevisiae* yeast strain [trp1-901, leu2-3,112, ura3-52, his3-200, gal4Δ, gal80Δ, LYS2::GAL1-HIS3, GAL2-ADE2, met2::GAL7-lacZ]. cDNAs of all tested genes (Mettl3, Mettl14, Fl(2)d, Vir, Nito, Flacc, Hakai) were cloned in vectors pGAD424-GW and pGBT9-GW, with Leu2 and Trp1 markers (kindly provided by Helle Ulrich Lab, IMB Mainz) to express all candidates with either the C-terminal Gal4-activation domain or the C-terminal Gal4-DNA binding domain, respectively. Briefly, yeast cells were grown in YPD medium until they reached OD = 0.6. Cells were centrifuged at 3500 rpm for 7 min at RT and washed 1x with water, 1x with 250 ml of SORB (100 mM LiOAc, 10 mM Tris pH 8.0, 1 mM EDTA pH 8.0, 1 M Sorbitol) and 1x with 100 ml of SORB. Pellets were resuspended in 3.6 ml of SORB and 400 ml of ssDNA carrier was added to competent cells. Fifty microlitres aliquots of cells were mixed with 100 ng of plasmid DNA. 6x volumes of PEG solution (10 mM Tris pH 8.0, 1 mM EDTA pH 8.0, 40 (w/v)-% PEG 3350) were then added to the cell-DNA mixture that was further incubated at RT for 30 min. Next, 1/9 of DMSO were added to cells that were subjected to 15 min heat shock at 42 °C. Following 2 min centrifugation at 1968 × g and RT, the cell pellet was resuspended in 500 µl of water and 100 µl of cell solution was plated onto Trp-/Leu- selection agar plates. After 3 days of incubation at 30 °C, 5 colonies of each transformation were resuspended in 500 µl of water and 4 µl were spotted on selection agar plates (Trp-/Leu- and Trp-/Leu-/His-). Plates were imaged in a 24-h interval.

RNA-seq analysis. Raw data processing, differential expression analysis and splicing analysis was done as described in ref. ²⁴. All samples from GSE105900 as well as the Hakai sample from GSE158663 were processed at the same time with the same tools and tool versions. The controls used as a reference for the differential splicing and the differential expression analysis are the same. In short the libraries were sequenced on a NextSeq500 with a read length of 85 bp single read and converted to fastq using bcl2fastq (v.2.19) and mapped against Ensembl release 90 of *D. melanogaster* using STAR (⁵², v. 2.5.10). Counts per gene were derived using featureCounts (⁵³, v. 2.5.1). Differential expression analysis was performed

using Bioconductor/DESeq2⁵⁴ (v1.16.1)) and filtered for an FDR < 5%, default independent filtering was used. Differential splicing analysis was performed using rMATS⁵⁵ (v. 3.2.5) and filtered for an FDR < 10%.

Statistics. For m⁶A level measurements datasets were compared using two-tailed Student's *t* test for unequal variances. F(2)d levels upon Control, Mettl3, Nito, Vir, Flacc and Hakai KD were compared using two-tailed Student's *t* test for equal variances. Normality was verified and homogeneity of variances was analyzed with Levene's test. Detailed descriptions of confidence intervals, effect sizes, degrees of freedom are shown in the Source data. Statistical tests used for RNAseq data analysis and mass spectrometry analysis are described in detail under relevant sections of "Methods" part.

Reporting summary. Further information on research design is available in the Nature Research Reporting Summary linked to this article.

Data availability

All data needed to evaluate the conclusions in the paper are present in the paper and/or Supplementary Materials. Additional data related to this paper may be requested from the authors. RNA-seq data are available in GEO: GSE158663. Proteomics data are available in PRIDE: PXD022294. Source data are provided with this paper.

Received: 21 October 2020; Accepted: 17 May 2021;

Published online: 18 June 2021

References

- Roignant J. Y., Soller M. m⁶A in mRNA: an ancient mechanism for fine-tuning gene expression. *Trends Genet.* **33**, 380–390 (2017).
- Shi, H., Wei, J. & He, C. Where, when, and how: context-dependent functions of RNA methylation writers, readers, and erasers. *Mol. Cell* **74**, 640–650 (2019).
- Zaccara, S., Ries, R. J. & Jaffrey, S. R. Reading, writing and erasing mRNA methylation. *Nat. Rev. Mol. Cell Biol.* **20**, 608–624 (2019).
- Anreiter I., Mir Q., Simpson J. T., Janga S. C., Soller M. New twists in detecting mRNA modification dynamics. *Trends Biotechnol.* **39**, 72–89 (2020).
- Batista, P. J. et al. m⁶A RNA modification controls cell fate transition in mammalian embryonic stem cells. *Cell Stem Cell* **15**, 707–719 (2014).
- Geula, S. et al. Stem cells. m⁶A mRNA methylation facilitates resolution of naive pluripotency toward differentiation. *Science* **347**, 1002–1006 (2015).
- Morena F., Argentati C., Bazzucchi M., Emiliani C., Martino S. Above the epitranscriptome: RNA modifications and stem cell identity. *Genes* **9**, 329 (2018).
- Malla, S., Melguizo-Sanchis, D. & Aguilo, F. Steering pluripotency and differentiation with N(6)-methyladenosine RNA modification. *Biochim Biophys. Acta Gen Regul. Mech.* **1862**, 394–402 (2019).
- Xiang, Y. et al. RNA m⁶A methylation regulates the ultraviolet-induced DNA damage response. *Nature* **543**, 573–576 (2017).
- Fustin, J. M. et al. RNA-methylation-dependent RNA processing controls the speed of the circadian clock. *Cell* **155**, 793–806 (2013).
- Wang, C. Y., Yeh, J. K., Shie, S. S., Hsieh, I. C. & Wen, M. S. Circadian rhythm of RNA N6-methyladenosine and the role of cryptochrome. *Biochem Biophys. Res Commun.* **465**, 88–94 (2015).
- Fustin, J. M. et al. Two Ck1delta transcripts regulated by m⁶A methylation code for two antagonistic kinases in the control of the circadian clock. *Proc. Natl Acad. Sci. USA* **115**, 5980–5985 (2018).
- Livneh, I., Moshitch-Moshkovitz, S., Amariglio, N., Rechavi, G. & Domimissini, D. The m⁶A epitranscriptome: transcriptome plasticity in brain development and function. *Nat. Rev. Neurosci.* **21**, 36–51 (2020).
- Haussmann, I. U. et al. m⁶A potentiates Sxl alternative pre-mRNA splicing for robust *Drosophila* sex determination. *Nature* **540**, 301–304 (2016).
- Lence, T. et al. m⁶A modulates neuronal functions and sex determination in *Drosophila*. *Nature* **540**, 242–247 (2016).
- Kan, L. et al. The m⁶A pathway facilitates sex determination in *Drosophila*. *Nat. Commun.* **8**, 15737 (2017).
- Zhong H., Tang H. F., Kai Y. N6-methyladenine RNA modification (m⁶A): an emerging regulator of metabolic diseases. *Curr. Drug Targets* **21**, 1056–1067 (2020).
- Angelova, M. T. et al. The emerging field of epitranscriptomics in neurodevelopmental and neuronal disorders. *Front. Bioeng. Biotechnol.* **6**, 46 (2018).
- Han, B. & Yao, H. H. N(6)-methyladenosine as a novel regulator of brain physiology and diseases. *Curr. Med. Sci.* **40**, 401–406 (2020).
- Chen, X. Y., Zhang, J. & Zhu, J. S. The role of m(6)A RNA methylation in human cancer. *Mol. Cancer* **18**, 103 (2019).
- He, L. et al. Functions of N6-methyladenosine and its role in cancer. *Mol. Cancer* **18**, 176 (2019).
- Wang, T., Kong, S., Tao, M. & Ju, S. The potential role of RNA N6-methyladenosine in Cancer progression. *Mol. Cancer* **19**, 88 (2020).
- Knuckles P., Buhler M. Adenosine methylation as a molecular imprint defining the fate of RNA. *FEBS Lett.* **592**, 2845–2859 (2018).
- Knuckles, P. et al. Zc3h13/Flacc is required for adenosine methylation by bridging the mRNA-binding factor Rbm15/Spenito to the m(6)A machinery component Wtap/Fl(2)d. *Genes Dev.* **32**, 415–429 (2018).
- Balacco, D. L. & Soller, M. The m(6)A writer: rise of a machine for growing tasks. *Biochemistry* **58**, 363–378 (2019).
- Ruzicka, K. et al. Identification of factors required for m(6) A mRNA methylation in Arabidopsis reveals a role for the conserved E3 ubiquitin ligase HAKAI. *N. Phytol.* **215**, 157–172 (2017).
- Yue, Y. et al. VIRMA mediates preferential m(6)A mRNA methylation in 3'UTR and near stop codon and associates with alternative polyadenylation. *Cell Discov.* **4**, 10 (2018).
- Sledz P., Jinek M. Structural insights into the molecular mechanism of the m(6)A writer complex. *Elife* **5**, e18434 (2016).
- Wang, P., Doxtader, K. A. & Nam, Y. Structural basis for cooperative function of Mettl3 and Mettl14 methyltransferases. *Mol. Cell* **63**, 306–317 (2016).
- Wang, X. et al. Structural basis of N(6)-adenosine methylation by the METTL3-METTL14 complex. *Nature* **534**, 575–578 (2016).
- Ping, X. L. et al. Mammalian WTAP is a regulatory subunit of the RNA N6-methyladenosine methyltransferase. *Cell Res.* **24**, 177–189 (2014).
- Patil, D. P. et al. m⁶A RNA methylation promotes XIST-mediated transcriptional repression. *Nature* **537**, 369–373 (2016).
- Guo, J., Tang, H. W., Li, J., Perrimon, N. & Yan, D. Xio is a component of the *Drosophila* sex determination pathway and RNA N(6)-methyladenosine methyltransferase complex. *Proc. Natl Acad. Sci. USA* **115**, 3674–3679 (2018).
- Wen, J. et al. Zc3h13 regulates nuclear RNA m(6)A Methylation and Mouse Embryonic Stem Cell Self-Renewal. *Mol. Cell* **69**, 1028–1038 e1026 (2018).
- Fujita, Y. et al. Hakai, a c-Cbl-like protein, ubiquitinates and induces endocytosis of the E-cadherin complex. *Nat. Cell Biol.* **4**, 222–231 (2002).
- Figueroa, A., Fujita, Y. & Gorospe, M. Hacking RNA: Hakai promotes tumorigenesis by enhancing the RNA-binding function of PSF. *Cell Cycle* **8**, 3648–3651 (2009).
- Aparicio, L. A., Valladares, M., Blanco, M., Alonso, G. & Figueroa, A. Biological influence of Hakai in cancer: a 10-year review. *Cancer Metastasis Rev.* **31**, 375–386 (2012).
- Horiuchi, K. et al. Identification of Wilms' tumor 1-associating protein complex and its role in alternative splicing and the cell cycle. *J. Biol. Chem.* **288**, 33292–33302 (2013).
- Wan, C. et al. Panorama of ancient metazoan macromolecular complexes. *Nature* **525**, 339–344 (2015).
- Mukherjee, M. et al. Structure of a novel phosphotyrosine-binding domain in Hakai that targets E-cadherin. *EMBO J.* **31**, 1308–1319 (2012).
- Schutt, C. & Nothiger, R. Structure, function and evolution of sex-determining systems in Dipteran insects. *Development* **127**, 667–677 (2000).
- Kaido, M., Wada, H., Shindo, M. & Hayashi, S. Essential requirement for RING finger E3 ubiquitin ligase Hakai in early embryonic development of *Drosophila*. *Genes Cells* **14**, 1067–1077 (2009).
- Schunter, S. et al. Ubiquitylation of the acetyltransferase MOF in *Drosophila melanogaster*. *PLoS ONE* **12**, e0177408 (2017).
- Bokar, J. A., Rath-Shambaugh, M. E., Ludwiczak, R., Narayan, P. & Rottman, F. Characterization and partial purification of mRNA N6-adenosine methyltransferase from HeLa cell nuclei. Internal mRNA methylation requires a multisubunit complex. *J. Biol. Chem.* **269**, 17697–17704 (1994).
- Juszkiewicz, S. & Hegde, R. S. Quality control of orphaned proteins. *Mol. Cell* **71**, 443–457 (2018).
- Kondo, S. & Ueda, R. Highly improved gene targeting by germline-specific Cas9 expression in *Drosophila*. *Genetics* **195**, 715–721 (2013).
- Rappsilber, J., Mann, M. & Ishihama, Y. Protocol for micro-purification, enrichment, pre-fractionation and storage of peptides for proteomics using StageTips. *Nat. Protoc.* **2**, 1896–1906 (2007).
- Heidelberger J. B. et al. Proteomic profiling of VCP substrates links VCP to K6-linked ubiquitylation and c-Myc function. *EMBO Rep.* **19**, e44754 (2018).
- Cox, J. & Mann, M. MaxQuant enables high peptide identification rates, individualized p.p.b. -range mass accuracies and proteome-wide protein quantification. *Nat. Biotechnol.* **26**, 1367–1372 (2008).
- Tyanova, S. et al. The Perseus computational platform for comprehensive analysis of (prote)omics data. *Nat. Methods* **13**, 731–740 (2016).
- Cox, J. et al. Andromeda: a peptide search engine integrated into the MaxQuant environment. *J. Proteome Res.* **10**, 1794–1805 (2011).
- Dobin, A. et al. STAR: ultrafast universal RNA-seq aligner. *Bioinformatics* **29**, 15–21 (2013).
- Liao, Y., Smyth, G. K. & Shi, W. The Subread aligner: fast, accurate and scalable read mapping by seed-and-vote. *Nucleic Acids Res.* **41**, e108 (2013).

54. Love, M. I., Huber, W. & Anders, S. Moderated estimation of fold change and dispersion for RNA-seq data with DESeq2. *Genome Biol.* **15**, 550 (2014).
55. Shen, S. et al. rMATS: robust and flexible detection of differential alternative splicing from replicate RNA-Seq data. *Proc. Natl Acad. Sci. USA* **111**, E5593–5601 (2014).

Acknowledgements

We thank the Bloomington, Kyoto and Vienna stock Center for fly lines and the *Drosophila* Genomics Resource Center at Indiana University for plasmids and cell lines. We are indebted to S. Hayashi for his effort to recover the *Hakai*¹ allele as well as BestGene and the University of Cambridge Department of Genetics Fly Facility for injections. We thank members of the Roignant and Soller lab for helpful discussion. We thank Christian Renz from the Ulrich group at IMB for sharing reagents and advices for the yeast-two-hybrid assay and Catia Igreja and Heike Budde from late Elisa Izaurralde lab for sharing plasmids used in this study. We thank the IMB Genomics core facility for their helpful support and the use of its NextSeq500 (INST 247/870-1 FUGG). Research in the laboratory of J.-Y.R. is supported by University of Lausanne, the Swiss National Science Foundation (310030_197906), the Deutsche Forschungsgemeinschaft RO 4681/9-1, RO 4681/12-1 and RO 4681/13-1. M.S. is funded by the BBSRC (BB/R002932/1) and the Leverhulme Trust. Research in the M.J. laboratory is supported by the Swiss National Competence Center for Research (NCCR) RNA & Disease. M.K. is supported by EMBO (ALTF 1087-2018) and Human Frontier Science Program (LT000248 2019-L) post-doctoral fellowships. M.J. is an International Research Scholar of the Howard Hughes Medical Institute and Vallee Scholar of the Bert L & N Kuggie Vallee Foundation. P.Beli is supported by the Emmy Noether Program (BE 5342/1-1 and BE 5342/1-2). C.P. in the lab of J.-Y.R. is supported by a Boehringer Ingelheim Fonds fellowship.

Author contributions

P. Bawankar, T.L., C.P., M.S. and J.-Y.R. conceived the project. P. Bawankar, T.L., C.P. contributed equally and are listed in the alphabetical order. All authors contributed to the experimental design, analysis, and interpretation of results. Experimental contributions were as follows: T.L. initiated the work, which was taken over by P. Bawankar and C.P. They performed all experiments except the following ones: I.U.H., M.P.N. and M.S. performed molecular biology, immunostaining of polytene chromosomes and genetic experiments. M.K. performed the HEK293T co-immunoprecipitation assays with help from M.J., J.B.H. and P. Beli performed MS-based proteomics for ubiquitylome, Hakai

interactomes and proteome analysis. D.J., F.M.R. carried out mass spectrometry measurement with the help of M.H. N.K. carried out the bioinformatic analysis. V.M. helped with the generation of *Hakai* mutants. P. Bawankar, T.L., C.P., M.S. and J.-Y.R. wrote the paper with input from all the other authors.

Competing interests

The authors declare no competing interests

Additional information

Supplementary information The online version contains supplementary material available at <https://doi.org/10.1038/s41467-021-23892-5>.

Correspondence and requests for materials should be addressed to M.S. or J.-Y.R.

Peer review information *Nature Communications* thanks the anonymous reviewers for their contribution to the peer review of this work. Peer reviewer reports are available.

Reprints and permission information is available at <http://www.nature.com/reprints>

Publisher's note Springer Nature remains neutral with regard to jurisdictional claims in published maps and institutional affiliations.



Open Access This article is licensed under a Creative Commons Attribution 4.0 International License, which permits use, sharing, adaptation, distribution and reproduction in any medium or format, as long as you give appropriate credit to the original author(s) and the source, provide a link to the Creative Commons license, and indicate if changes were made. The images or other third party material in this article are included in the article's Creative Commons license, unless indicated otherwise in a credit line to the material. If material is not included in the article's Creative Commons license and your intended use is not permitted by statutory regulation or exceeds the permitted use, you will need to obtain permission directly from the copyright holder. To view a copy of this license, visit <http://creativecommons.org/licenses/by/4.0/>.

© The Author(s) 2021

5. Results

Drosophila long isoform specific domain

```

H.sapiens 1 1MDTTEVKRGRGRGRTNARGRGRGRGK1DDSS1ADAALAASSCAALDDSPKRLD 60
D.melanogaster 1MDTTEVKRGRGRGRTNARGRGRGRGK1DDSS1ADAALAASSCAALDDSPKRLD 60
A.thaliana 1MDTTEVKRGRGRGRTNARGRGRGRGK1DDSS1ADAALAASSCAALDDSPKRLD 60

H.sapiens 31TD-N-ELQGTSSGS-GGIDVRRRIPIKLSKQANKAKPAPRTQR 46
D.melanogaster 61ASEDSVMQELDKDGELETTPGALLEPPLPHGALGANAASGM 48
A.thaliana 1ASEDSVMQELDKDGELETTPGALLEPPLPHGALGANAASGM 48

H.sapiens 4RTIIRNMPAKAPPGDEEGFDYHEERYDCGGELFANQ---RRFPGHLFWDFO---INILG 99
D.melanogaster 109VLQOVP---PVMVSIIDMEA--DISQLPFTTILSRGPEMLRLKWHK---VSLIG 100
A.thaliana 109VLQOVP---PVMVSIIDMEA--DISQLPFTTILSRGPEMLRLKWHK---VSLIG 100

H.sapiens 100EKDQTP-VVFDQKGLKIKYGMIFCKVFQYDCAIIEKKGDKKCPGSSPVQRIEQ 158
D.melanogaster 161EVLHPMIFCDQDKLIVYGMIFCKVFQYDCAIIEKKGDKKCPGSSPVQRIEQ 158
A.thaliana 62RKQLGERVHFVRRDIFKALAYRGLIYEDNARSLKAKRS---DSTLYLEDRIQKIQT 156

RING domain
H.sapiens 159T-RGSLFAGSI-----VQGCKRTYSQRDLQAHINRHRKAGKPVTRASLENVHPP 211
D.melanogaster 218G-LGVFMETNIGGSRYGSSGRRTIYSQRDLQAHINRHRKAGKPVTRASLENVHPP 211
A.thaliana 117KMMELICA-----APHCLSSEIKKLEFRHWVHDLKSLLQADAEKEDG 161

Zn finger
H.sapiens 212PTEPERFIIMPDKHHM-----HPKQHI-MMPPELQHVPEHYRQPHEDIKAPP 265
D.melanogaster 277KMTDLGG-VGLGLELHKQRKLSSESPPISSVASTASRPLSRLPLTGGV 328
A.thaliana 162NOSDWOSTM-----QSSSASEITL-----RA-----LHLSOLOQSRLELN 195

H.sapiens 266ELSMAPPPRSVSGEITFRISTRNKSHLITVPIQDQSSGAREPPPPAPARAHHP 325
D.melanogaster 329SIGSTIPPP-GSAAAQAHAI-HGHSTLTLAHLTRINANAG 372
A.thaliana 196-----R--SASTAKSOSGEGQVHPPDSD-KSRPGEETASPKGIRFPDYP 322

H.sapiens 326PVVSNPHNIMPQGHVAPP PPPPIISHPMHPQAASTMLVYS--QAPPMTSAPP 383
D.melanogaster 374ASLHN-----ILMGP-----PSLVPVPHNQ-NPGLPQDTLTKKSTHQSES--VADASY 397
A.thaliana 243M-----ILMGP-----PSLVPVPHNQ-NPGLPQDTLTKKSTHQSES--VADASY 397

H.sapiens 344ITPPGHIIAQMPVYMHNP-PGGPPRQHGPPVITAPRPHNYNINSLPQFTEDQGLSPFF 443
D.melanogaster 398-----SSYLASFGSAAGNPGSSG--PPGG-GATIAAQAHAN--SGSHSAVVGALIGST 446
A.thaliana 299MTRTES-GGSTLOSSLLEGVPPSPHMI--NLHFQGSYPPSWHGMAPHITQQVH 329

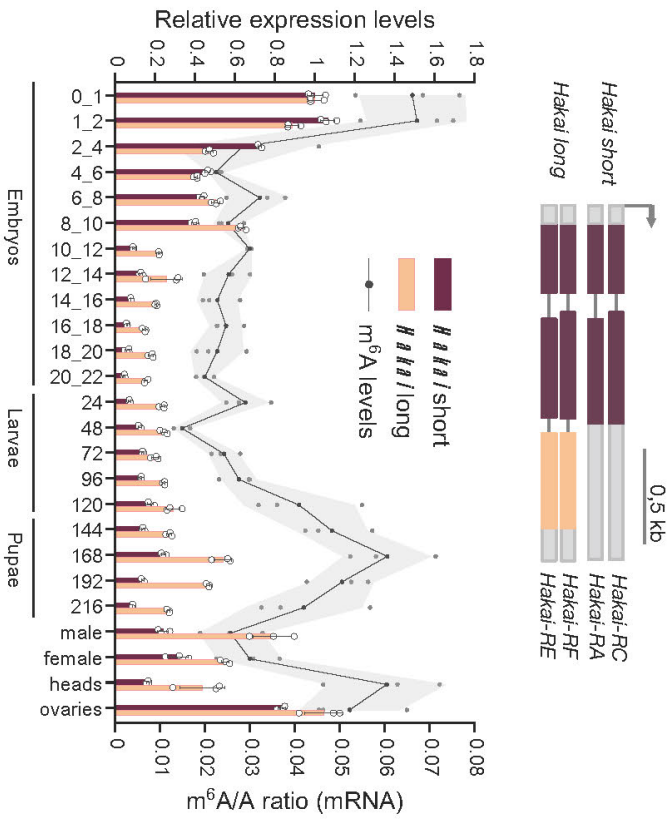
H.sapiens 441TORGGMSPGIPAPRGRPPPRRLGPPSQTPLPGPHHPDQTRVRYYY 491
D.melanogaster 447DAPITGGSSGHNQDSQ-----YYR 464
A.thaliana 340-RGRDGGSTGPPQELNRDGFQDE-----YYR 368

```

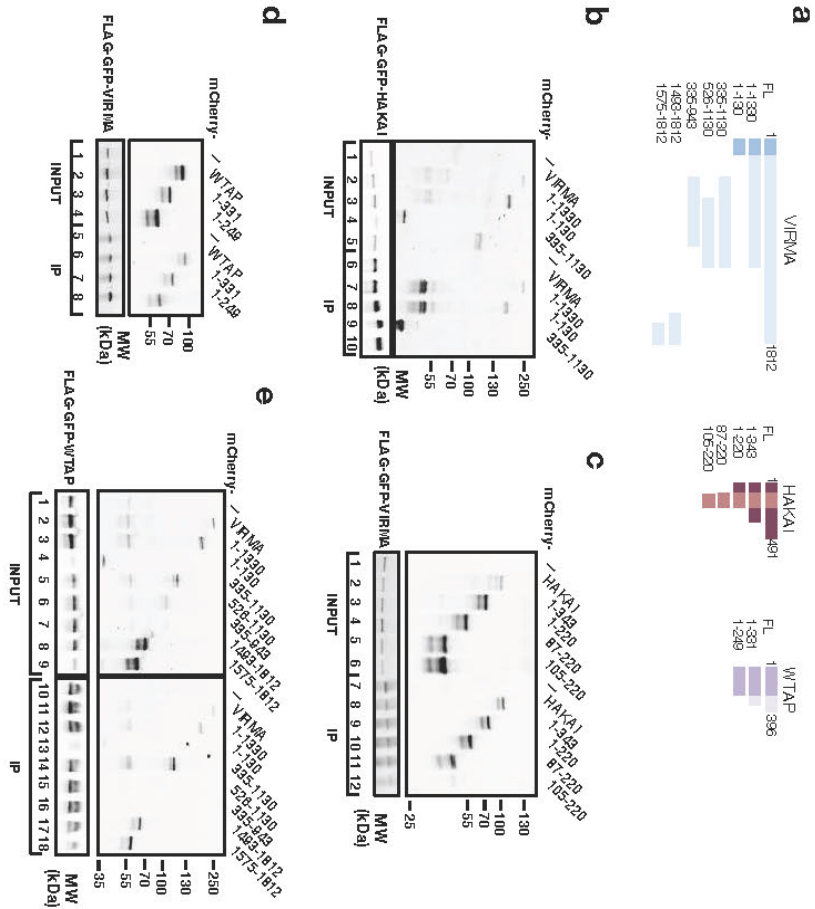
Supplementary Figure 1. Hakai protein alignment.

Alignment of Hakai protein sequences from *Drosophila melanogaster* (Hakai_Dm: M9PBE2-1), *Arabidopsis thaliana* (Hakai_At:Q9LFCO) and *Homo sapiens* (HAKAI_Hs: Q75N03-1) (6.4% identity, 64 aa similarities). Protein alignments were generated in Jalview 2.10.5 (Waterhouse et al. 2009) with ClustalO version 1.2.4 using default settings (Larkin et al. 2007). Colored by degree of amino acid conservation in each column with a 30 % cut off threshold. The orange line indicates the C-terminal region specific of the long isoforms.

5. Results



5. Results

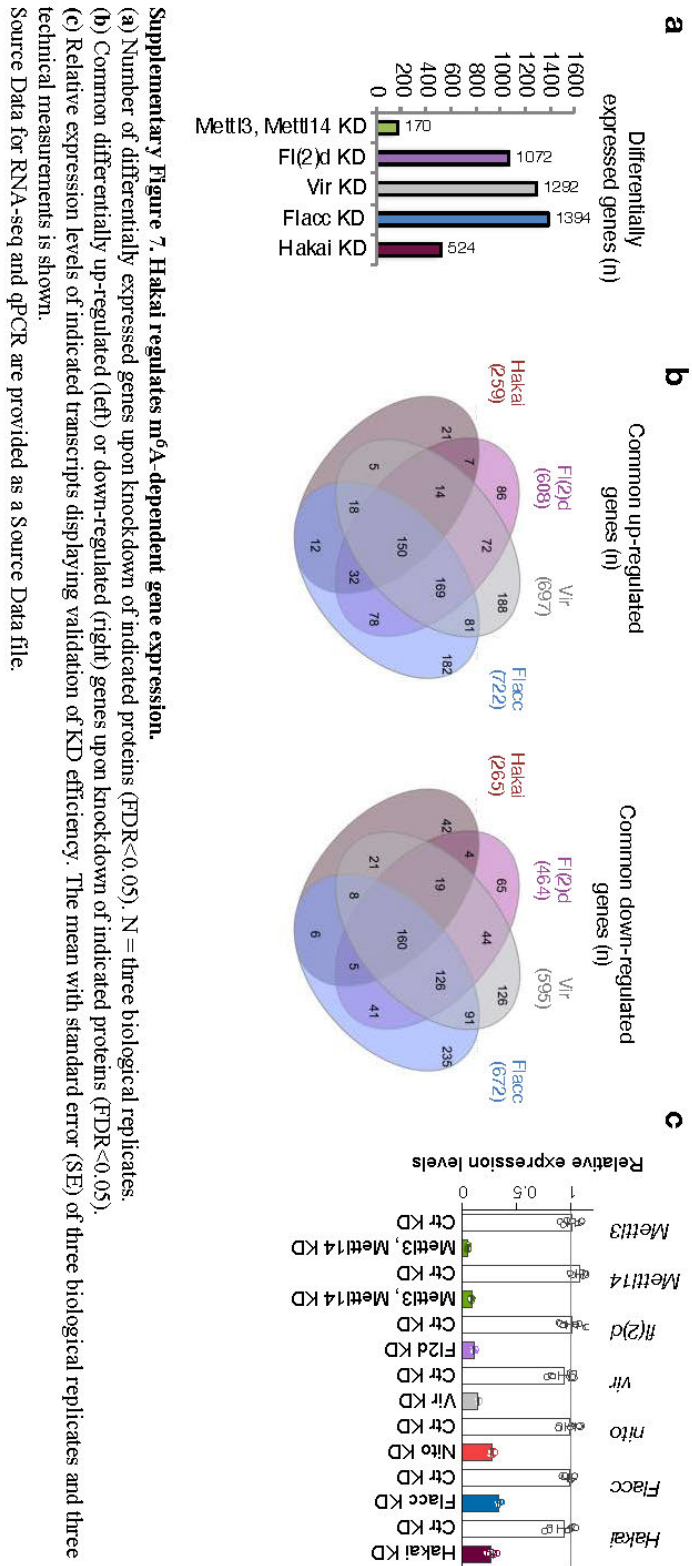


Supplementary Figure 6. VIRMA serves as an interaction platform for the assembly of HAKAI and WTAP into the MACOM complex in humans.

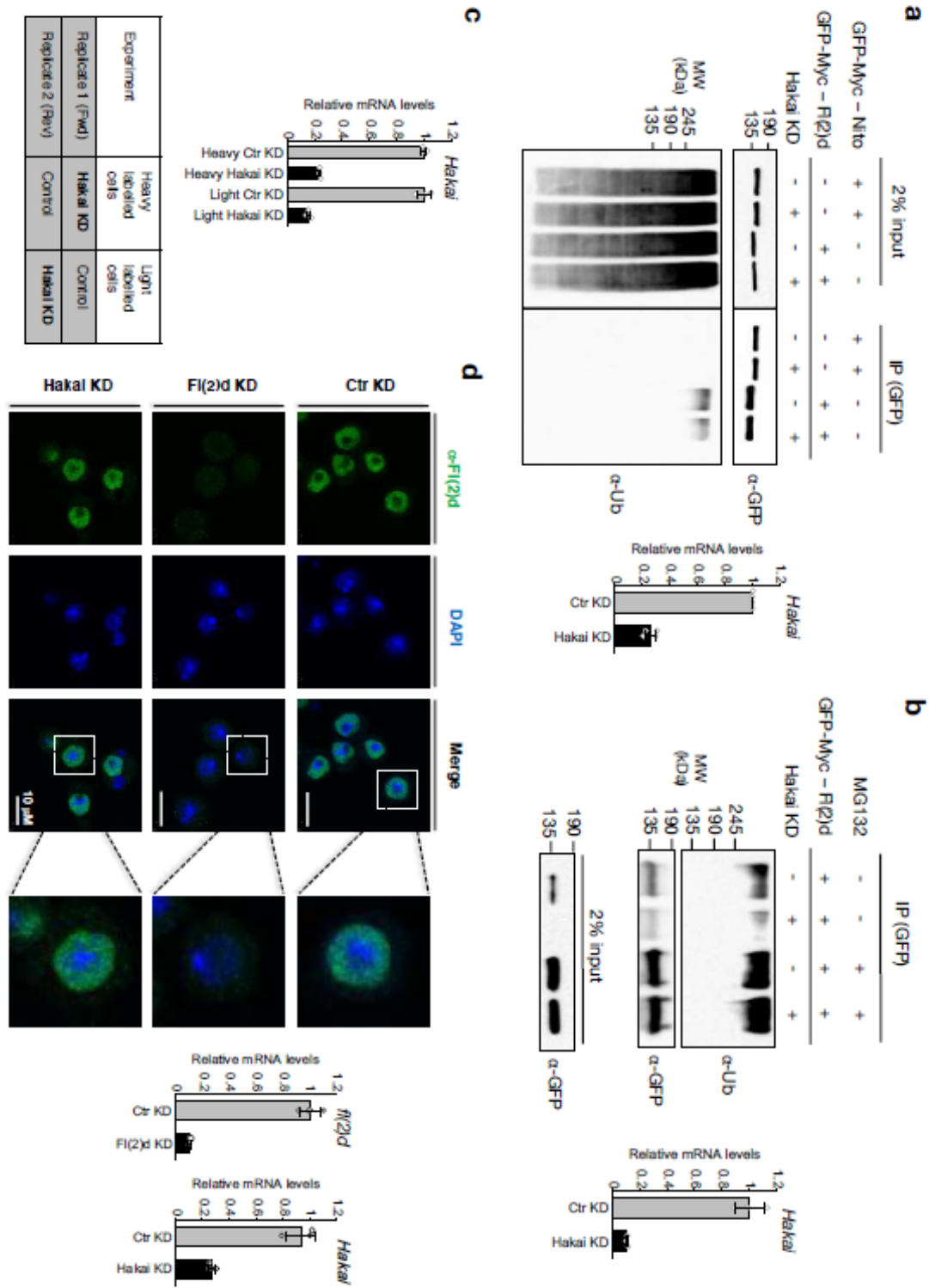
(a) Schematic representation of proteins and protein fragments used for human co-immunoprecipitation assays.

(b-e) Co-IP assays were carried out with lysates prepared from HEK293T cells transfected with (b) His6-FLAG3-eGFP-VIRMA (full-length) and His6-FLAG3-eGFP-HAKAI (full-length or indicated truncations); (c) His6-FLAG3-eGFP-VIRMA (full-length) and His6-FLAG3-eGFP-HAKAI (full-length or indicated truncations); (d) His6-FLAG3-eGFP-VIRMA (full-length) and His6-mCherry-WTAP (full-length or indicated truncations); (e) His6-FLAG3-eGFP-WTAP (full-length) and His6-FLAG3-eGFP-VIRMA (full-length or indicated truncations). Extracts were immunoprecipitated with magnetic anti-FLAG M2 beads and analysed based on fluorescence. 2% of input was loaded. (e) His6-FLAG3-eGFP-WTAP (full-length) and His6-FLAG3-eGFP-VIRMA (full-length or indicated truncations). The experiment was performed in the presence of RNase A.

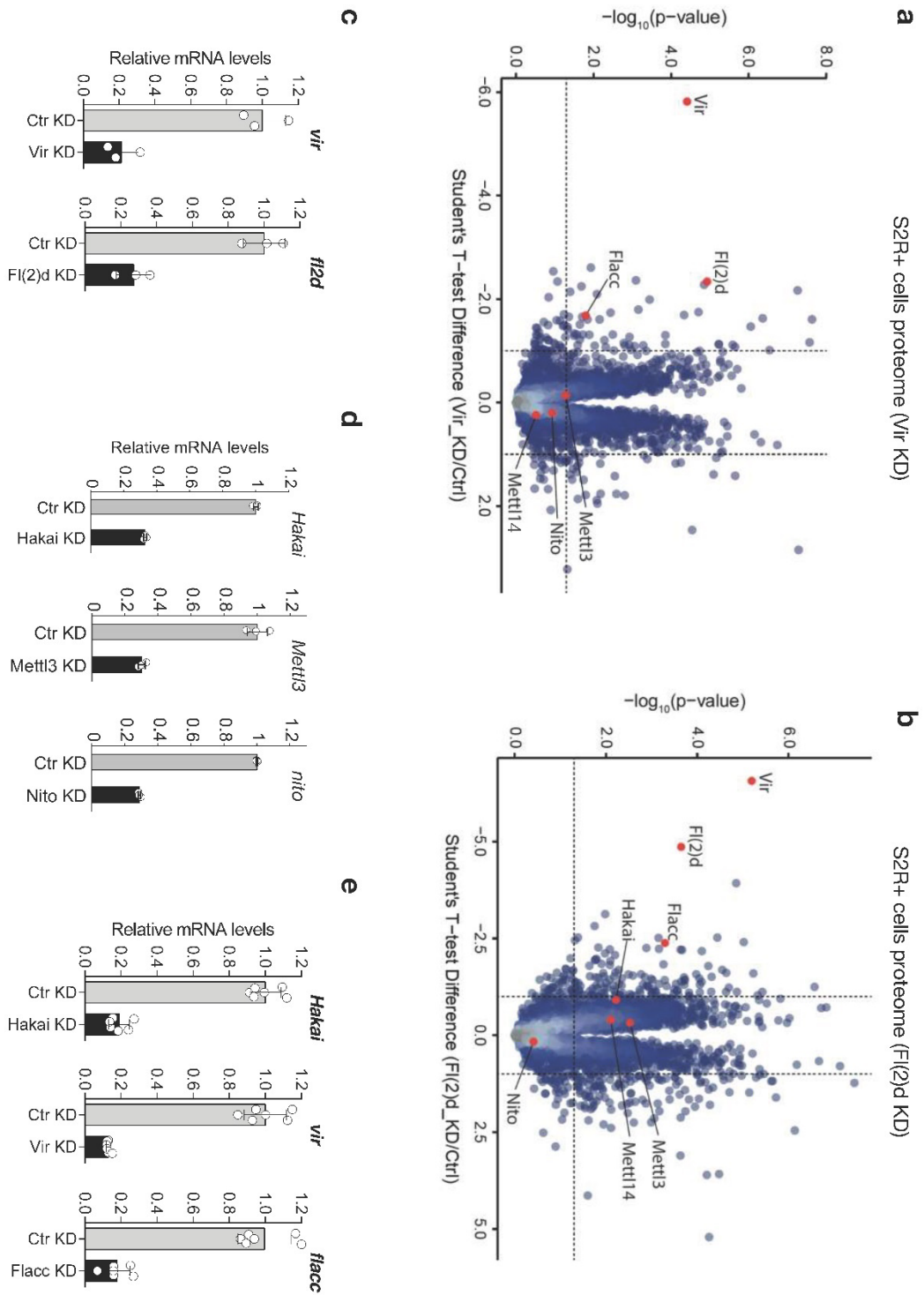
5. Results



5. Results



5. Results



Supplementary Figure 9. Vir and Fl(2)d control the stability of other MACOM components.

- (a-b) Quantitative mass spectrometry analysis of Vir-dependent proteome (A) or Fl(2)d-dependent proteome (B) in S2R+ cells. Label free quantification on four replicate experiments was performed to identify significantly upregulated and down regulated proteins. MACOM component proteins are highlighted in red. The threshold was set to a FDR of 0.05 (black dashed line y-axis) and to a T-test difference of ± 1 (black dashed line x-axis).
- (c) Relative expression levels of *Fl(2)d* and *vir* are shown as a validation of their KID efficiencies for the proteome in S2R+ cells. The mean with standard deviation of three technical measurements is shown.
- (d) Relative expression levels of *Hakai*, *Meth3* and *nro* are shown as a validation of their KID efficiencies for the analysis of Fl(2)d protein levels. The mean with standard error (SE) of three technical measurements is shown.
- (e) Relative expression levels of *Hakai*, *vir* and *Flacc* are shown as a validation of their KID efficiencies for the analysis of Fl(2)d protein levels. The mean with standard deviation of two biological replicates and three technical measurements is shown. Source Data for qPCR are provided as a Source Data file.

Supplementary References

1. Larkin MA, Blackshields G, Brown NP, Chenna R, McGettigan PA, McWilliam H, Valentin F, Wallace IM, Wilm A, Lopez R et al. 2007. Clustal W and Clustal X version 2.0. *Bioinformatics* **23**: 2947-2948.
2. Waterhouse AM, Procter JB, Martin DM, Clamp M, Barton GJ. 2009. Jalview Version 2--a multiple sequence alignment editor and analysis workbench. *Bioinformatics* **25**: 1189-1191.

5. Results

5.2 Section 2: Research article 2

Article

SOURCE
DATATRANSPARENT
PROCESSOPEN
ACCESS

Ythdf is a N6-methyladenosine reader that modulates Fmr1 target mRNA selection and restricts axonal growth in *Drosophila*

Lina Worpenberg¹, Chiara Paolantoni¹, Sara Longhi², Miriam M Mulorz³, Tina Lence³ , Hans-Hermann Wessels^{4,5} , Erik Dassi⁶, Giuseppe Aiello⁷ , F X Reymond Sutandy³, Marion Scheibe³, Raghu R Edupuganti⁸, Anke Busch⁹, Martin M Möckel¹⁰, Michiel Vermeulen⁸ , Falk Butter³ , Julian König³, Michela Notarangelo², Uwe Ohler^{4,5} , Christoph Dieterich^{11,12} , Alessandro Quattrone^{2,*} , Alessia Soldano^{2,**} & Jean-Yves Roignant^{1,13,***}

Abstract

N6-methyladenosine (m⁶A) regulates a variety of physiological processes through modulation of RNA metabolism. This modification is particularly enriched in the nervous system of several species, and its dysregulation has been associated with neurodevelopmental defects and neural dysfunctions. In *Drosophila*, loss of m⁶A alters fly behavior, albeit the underlying molecular mechanism and the role of m⁶A during nervous system development have remained elusive. Here we find that impairment of the m⁶A pathway leads to axonal overgrowth and misguidance at larval neuromuscular junctions as well as in the adult mushroom bodies. We identify Ythdf as the main m⁶A reader in the nervous system, being required to limit axonal growth. Mechanistically, we show that the m⁶A reader Ythdf directly interacts with Fmr1, the fly homolog of Fragile X mental retardation RNA binding protein (FMRP), to inhibit the translation of key transcripts involved in axonal growth regulation. Altogether, this study demonstrates that the m⁶A pathway controls development of the nervous system and modulates Fmr1 target transcript selection.

Keywords Fmr1; m⁶A; nervous system; RNA modification; Ythdf

Subject Categories Neuroscience; RNA Biology; Translation & Protein Quality

DOI 10.15252/emboj.2020104975 | Received 12 March 2020 | Revised 18 November 2020 | Accepted 30 November 2020 | Published online 11 January 2021

The EMBO Journal (2021) 40: e104975

Introduction

Chemical modifications on DNA and histones impact gene expression during cell differentiation, organismal development, and in several other biological programs (Jaenisch & Bird, 2003). Similarly, RNA modifications are an important, recently characterized layer of gene regulation but their functional characterization during development and in other biological/pathological processes is still in its infancy (Hsu *et al.*, 2017).

N6-methyladenosine (m⁶A) is the most prevalent modification found in mRNAs and long non-coding RNAs. The mark is widely conserved, enriched in mRNAs at the beginning of the last exons, in the sequence context RRACH (where R = A or G and H = A, C, or U) (Dominissini *et al.*, 2012; Meyer *et al.*, 2012; Ke *et al.*, 2015;

- 1 Center for Integrative Genomics, Génomopole Building, Faculty of Biology and Medicine, University of Lausanne, Lausanne, Switzerland
 - 2 Laboratory of Translational Genomics, Department of Cellular, Computational and Integrative Biology (CIBIO), University of Trento, Trento, Italy
 - 3 Institute of Molecular Biology (IMB), Mainz, Germany
 - 4 Max Delbrück Center for Molecular Medicine in the Helmholtz Association (MDC), Berlin Institute for Medical Systems Biology (BIMSB), Berlin, Germany
 - 5 Department of Biology, Humboldt University Berlin, Berlin, Germany
 - 6 Laboratory of RNA Regulatory Networks, Department CIBIO, University of Trento, Trento, Italy
 - 7 Armenise-Harvard Laboratory of Brain Disorders and Cancer, Department CIBIO, University of Trento, Trento, Italy
 - 8 Department of Molecular Biology, Faculty of Science, Radboud Institute for Molecular Life Sciences, Oncode Institute, Radboud University Nijmegen, Nijmegen, The Netherlands
 - 9 Bioinformatics Core Facility, IMB, Mainz, Germany
 - 10 Protein Production Core Facility, IMB, Mainz, Germany
 - 11 Klaus Tschira Institute for Integrative Computational Cardiology and Department of Internal Medicine III, University Hospital Heidelberg, Heidelberg, Germany
 - 12 German Center for Cardiovascular Research (DZHK), Partner site Heidelberg-Mannheim, Heidelberg, Germany
 - 13 Institute of Pharmaceutical and Biomedical Sciences, Johannes Gutenberg-University Mainz, Mainz, Germany
- *Corresponding author. Tel: +39 0461 283997; E-mail: alessandro.quattrone@unitn.it
 **Corresponding author. Tel: +39 0461 283096; E-mail: alessia.soldano@unitn.it
 ***Corresponding author. Tel: +41 21 692 3960; E-mail: jean-yves.roignant@unil.ch
 †These authors contributed equally to this work as senior authors.

Garcia-Campos *et al.*, 2019). m⁶A plays a central role in modulating RNA function, since it can influence many aspects of RNA life such as splicing, export, translation, and decay (Roignant & Soller, 2017; Zhao *et al.*, 2017). m⁶A deposition is operated by a multisubunit methyltransferase complex, composed of METTL3 and METTL14, as well as several associated components (reviewed in ref. Lence *et al.*, 2019). The m⁶A signature is subsequently recognized by “reader” proteins, among which the best described is the YTH domain family of proteins that decode the signal and mediate m⁶A biological effects (Liao *et al.*, 2018; Patil *et al.*, 2018).

Increasing evidence suggests a central role of m⁶A during nervous system development and functions (Angelova *et al.*, 2018; Jung & Goldman, 2018; Widagdo & Anggono, 2018; Du *et al.*, 2019; Li *et al.*, 2019; Livneh *et al.*, 2020). m⁶A is present at particularly high levels in the nervous system of different model animals (Meyer *et al.*, 2012; Lence *et al.*, 2016), and these levels can vary following behavioral stimuli or sensory experience (Widagdo *et al.*, 2016; Engel *et al.*, 2018; Koranda *et al.*, 2018; Yoon *et al.*, 2018). In mouse, m⁶A controls brain development (Li *et al.*, 2017; Li *et al.*, 2018; Ma *et al.*, 2018; Wang *et al.*, 2018; Chen *et al.*, 2019; Zhuang *et al.*, 2019) and is also required for axon regeneration (Weng *et al.*, 2018) and synaptic functions (Engel *et al.*, 2018; Koranda *et al.*, 2018; Merkurjev *et al.*, 2018; Shi *et al.*, 2018; Yu *et al.*, 2018). Similarly, in *Drosophila*, m⁶A promotes flight and locomotion via a neuronal function (Hausmann *et al.*, 2016; Lence *et al.*, 2016; Kan *et al.*, 2017; Lence *et al.*, 2017). A proper level of m⁶A appears critical for regulating axonal growth as *Mettl3* knock out (KO) in *Drosophila* has been associated with axonal overgrowth at neuromuscular junctions (NMJs) (Lence *et al.*, 2016), and conversely, higher m⁶A (or m⁶Am) produced by the loss of FTO, leads to shorter axonal length in mouse dorsal root ganglia neurons (Yu *et al.*, 2018). To date, the underlying mechanism of m⁶A in axonal growth has remained elusive.

Fragile X mental retardation protein (FMRP) is a polyribosome-associated RNA binding protein (RBP) that negatively regulates the translation of a subset of dendritic mRNAs (Laggerbauer *et al.*, 2001; Li *et al.*, 2001; Darnell *et al.*, 2011; Jacquemont *et al.*, 2018). Additional functions in splicing, export, and mRNA stability have also been reported for this RBP (Davis & Broadie, 2017). The loss of FMRP is the genetic cause of Fragile X syndrome (FXS), the most common inherited form of intellectual disability and autism, with an estimated prevalence of 1 in 4,000 males and 1 in 8,000 females (Garber *et al.*, 2006; Rousseau *et al.*, 2011; Bagni & Zukin, 2019). Previous high-throughput studies identified only short consensus sites for FMRP binding (ACUK, WGGGA, GAC sequences; K = G or U, W = A or U), suggesting that additional elements provide the binding specificity (Suhl *et al.*, 2014). Intriguingly, FMRP was recently identified as a putative m⁶A reader in mammalian cells via unbiased proteomics studies (Arguello *et al.*, 2017; Edupuganti *et al.*, 2017). Furthermore, FMRP target mRNAs were shown to largely overlap with methylated transcripts (Chang *et al.*, 2017), and FMRP was found to modulate their export to the cytoplasm (Edens *et al.*, 2019; Hsu *et al.*, 2019), as well as their stability (Zhang *et al.*, 2018). These studies indicate roles for FMRP in modulating m⁶A function in the nervous system. However, the physiological relevance of this crosstalk in the context of the FXS has yet to be evaluated. Moreover, it remains to be determined how FMRP interplays with other m⁶A readers.

In the present study, we seek to obtain mechanistic insights into the role of m⁶A in *Drosophila* neurodevelopment. We found that, in

addition to controlling axonal growth at neuromuscular junctions (NMJs), m⁶A prevents axonal crossing and β -lobe fusion of the neurons in the mushroom bodies (MBs), a higher hierarchy circuit of the central brain implicated in a wide range of fly behaviors, including learning and memory. By using an unbiased approach to identify m⁶A readers in the *Drosophila* nervous system, we demonstrate that Ythdf, the unique cytoplasmic YTH protein in *Drosophila*, recognizes methylated transcripts and mediates m⁶A function in restricting axonal growth. We further show that Ythdf directly interacts with Fmr1, the *Drosophila* FMRP homolog, and modulates its binding activity. Ythdf and Fmr1 share common targets related to nervous system development and act in concert to inhibit the translation of positive regulators of axonal growth. Thus, this study demonstrates that Fmr1 function in axonal growth is modulated by its interaction with the m⁶A reader Ythdf, providing mechanistic insight on this interplay and possibly novel avenues for therapeutic approaches of the FXS.

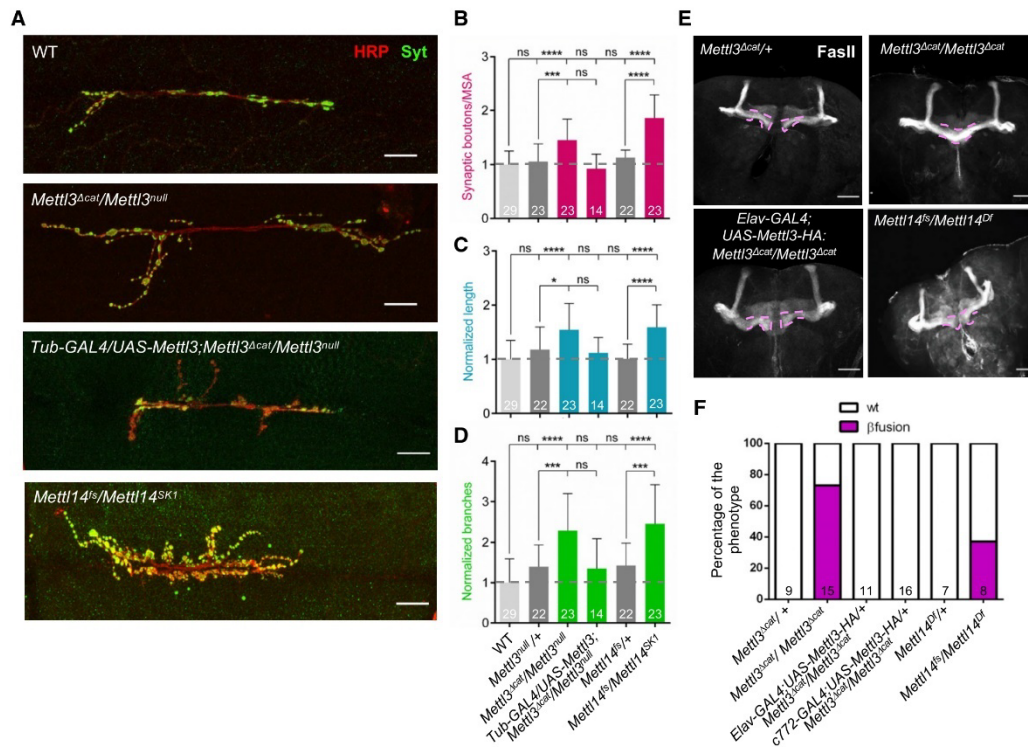
Results

m⁶A restricts axonal growth at the peripheral and central nervous system

Previous studies demonstrated that m⁶A controls several aspects of neuronal development and behavior in *Drosophila melanogaster* (Hausmann *et al.*, 2016; Lence *et al.*, 2016; Kan *et al.*, 2017). In particular, flies lacking *Mettl3* are flightless and have reduced speed and orientation defects (Lence *et al.*, 2016). Furthermore, an increased number of synaptic boutons was detected at mutant NMJs. To confirm and extend this initial analysis, we dissected additional alleles of *Mettl3*, as well as of *Mettl14*, and scored the number of synapses, branches, and the overall size of the axons. Consistent with our previous report, we observed an augmentation of synaptic bouton number of about 40% to 50%, depending on *Mettl3* allelic combinations (Fig EV1A and Appendix Fig S1). Furthermore, *Mettl3* mutants displayed significant axonal overgrowth and over-elaboration of synaptic terminals (Figs 1C and D, and EV1B and C). Importantly, all these defects were completely rescued upon ubiquitous expression of *Mettl3* cDNA. Consistent with *Mettl3* loss-of-function phenotypes, the *Mettl14* KO gave identical defects (Fig 1A–D). Thus, these results indicate that m⁶A is required for normal NMJ synaptic architecture in *Drosophila*.

We next asked whether m⁶A was also required for the integrity of the central nervous system (CNS). We dissected adult brains of control and fly mutants for the m⁶A pathway and examined the structure of MBs. Compared to wild-type flies, the MBs of *Mettl3* and *Mettl14* KOs exhibited midline crossing and fusion of the β lobes (Fig 1E). The penetrance varied from 37% to 73%, depending on the alleles (Fig 1F). A similar defect was observed upon inactivation of *Mettl3* or *Mettl14* specifically in the MB using RNAi (Fig EV1D and E), suggesting a cell-autonomous requirement of m⁶A. Furthermore, expression of *Mettl3* cDNA either ubiquitously, pan-neuronally, or in the MBs only, was sufficient to rescue the β lobe overgrowth, confirming the specificity and the cell-autonomous nature of the phenotype (Fig 1E and F). We conclude that m⁶A limits axonal growth in the peripheral and central nervous system.

5. Results



Fmr1 and Ythdf bind to methylated sites with different specificity

To decipher the mechanisms underlying the role of the m⁶A pathway in the nervous system, we aimed to identify the proteins that mediate m⁶A function in this tissue. We carried out RNA pulldowns in *Drosophila* neuronal cell lysates followed by quantitative mass spectrometry-based proteomics, as described before (Edupuganti *et al*, 2017). Briefly, a methylated RNA probe containing four repeats of the m⁶A consensus sequence GGACU was mixed with lysates from BG3 cells, which were derived from the larval CNS (Ui *et al*, 1994). As control, we used the same probe lacking the methylation. After pull-down, bound proteins were subjected to trypsin digestion and analyzed by liquid chromatography–tandem mass

spectrometry (LC-MS/MS). Using this approach, we identified eight proteins that were significantly enriched with the methylated probe (Fig 2A and Dataset EV1). As anticipated, the two YTH domain-containing proteins were among the most strongly enriched. Furthermore, we also found Fmr1, whose mammalian homolog was similarly shown to preferentially bind a methylated probe (Arguello *et al*, 2017; Edupuganti *et al*, 2017).

Given that binding of Ythdc1 to a methylated probe was already confirmed *in vitro* (Kan *et al*, 2017), we further aimed to address whether Ythdf and Fmr1 bear the same specificity. Therefore, we purified recombinant GST-tagged Ythdf as well as His-tagged Fmr1 lacking the first 219 N-terminal amino acids (as the full-length version is very unstable, also described in (Chen *et al*, 2014)) and tested their ability to bind the different probes. Consistent with our pull-down assay from

5. Results

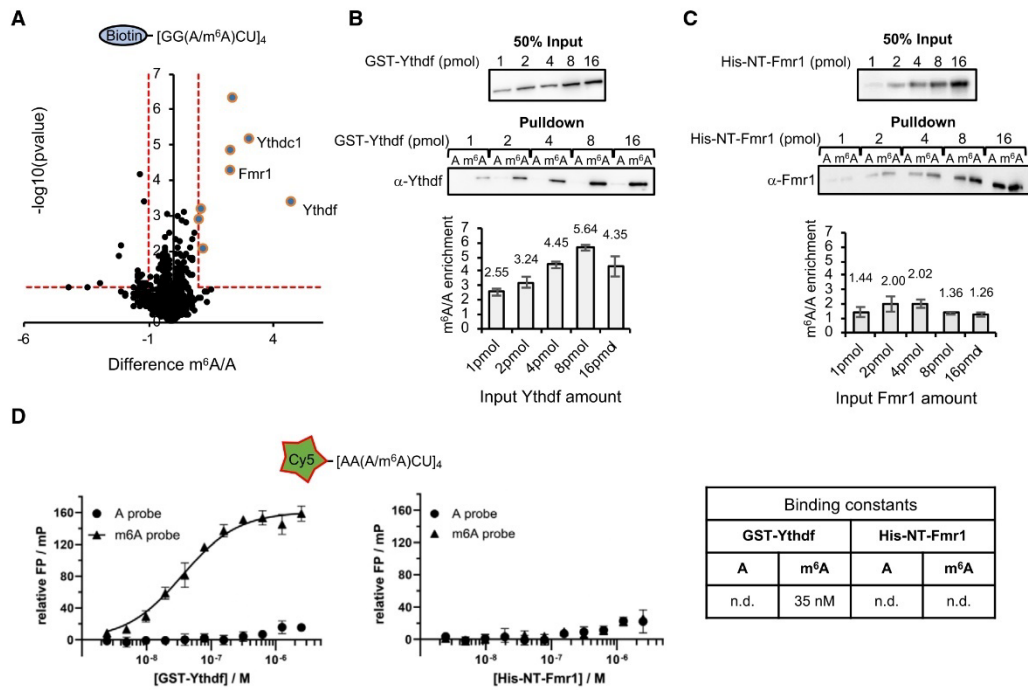


Figure 2. Ythdf and Fmr1 binding behavior to methylated RNA probes.

A Results of m⁶A RNA pull-down in BG3 protein cell extracts. Pull-down were performed using biotinylated probes containing four m⁶A consensus sites (GGACU), with or without the methylation. The *P*-value is calculated from a two-sided t-test with unequal variants (Welch t-test). Dashed lines represent $-\log_{10} P\text{-value} = 1$ as well as \log_2 enrichment = 1. m⁶A-enriched proteins ($-\log_{10} P\text{-value} > 1$ and \log_2 enrichment > 1) are depicted by bigger dots.

B, C Western blot showing the protein enrichments upon pull-down of the same probes as in (A) incubated with increasing concentrations of purified recombinant GST-Ythdf (B) and His-NT-Fmr1 (C). Quantification of the m⁶A/A signal intensity is shown below the blot as median \pm SEM of the triplicates. Both proteins bind more efficiently upon methylation.

D Results of fluorescence polarization (FP) assay using Cy5 labeled RNA probes containing four AAACU m⁶A consensus sites, with or without the methylation, incubated with GST-Ythdf and His-NT-Fmr1. The relative FP values from three independent experiments including standard deviation were plotted using GraphPad Prism 8. Binding constants (kd values) were determined by fitting a Michaelis–Menten non-linear regression onto the relative FP values in GraphPad Prism 8, if applicable. The respective binding constants are given in the table next to the graphs.

Source data are available online for this figure.

cell lysates, we found that both purified GST-Ythdf and His-Fmr1 bound preferentially to the methylated probe (Fig 2B and C). By incubating RNA probes with different concentrations of purified proteins, we found that the binding of Ythdf was highly specific at all used concentrations. In contrast, binding of Fmr1 was only slightly enriched in the m⁶A probe pull-down, as compared to the pulled down in the absence of methylation. Interestingly, the specificity for the m⁶A modified probe decreased with high level (16pmol) of either protein.

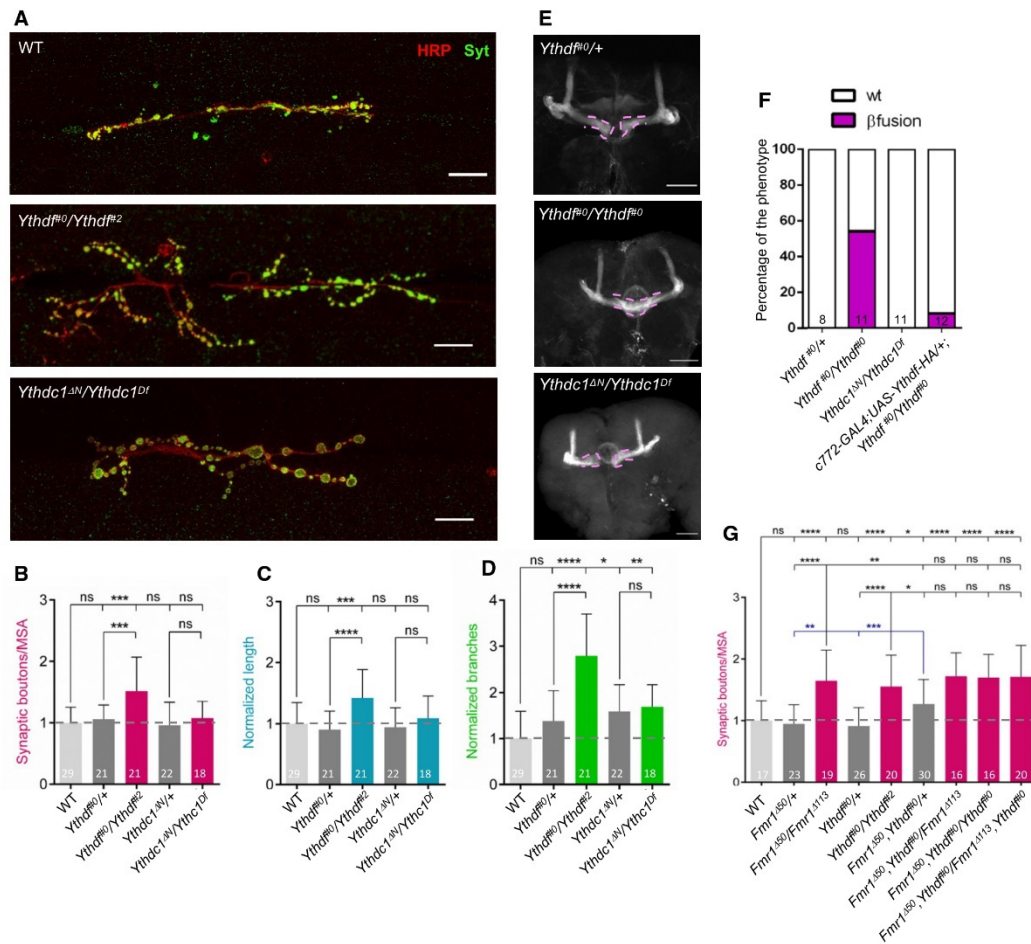
We also tested the binding behavior on RNA probes containing repeats of the alternative m⁶A consensus AAACU. In this case, Fmr1 displayed no specific binding to neither the methylated probe nor the non-methylated probe. Ythdf still bound with higher specificity the methylated probe, though a milder background binding to the unmethylated probe was also observed (Fig EV2). We confirmed this result by performing fluorescence polarization assays using Cy5

labeled RNA probes and calculated the binding constants of the Ythdf/Fmr1 RNA interaction (Fig 2D). While a strong binding of Ythdf to the m⁶A probe ($K_d = 35$ nM) could be determined, no binding to the unmethylated probe was observed. In line with the previous findings, Fmr1 did not bind any of the probes. We conclude that the binding of Fmr1 to m⁶A consensus sequences is largely sequence-dependent, which is in line with previous pull-down experiments in human cells (Edupuganti *et al.*, 2017) and with a recent study showing that only a fraction of methylated sites is recognized by human FMRP (Hsu *et al.*, 2019).

Fmr1 and Ythdf limit axonal growth

The *Fmr1* loss of function was previously shown to give overgrowth at NMJs, as well as fusion of MB β lobes (Appendix Fig

5. Results



S2 and Zhang *et al*, 2001; Michel *et al*, 2004), suggesting that it could mediate the $m^6\text{A}$ axonal growth function. To address whether Ythdc1 and/or Ythdf also control NMJ morphology, we dissected third instar larvae carrying mutations in the *Yth* genes.

Using our previously described *Ythdc1* allele combined over a deficiency line spanning the locus, we did not detect any gross morphological defect (Fig 3A–D). To address the contribution of Ythdf, we generated mutant alleles using the CRISPR/Cas9

5. Results

approach (Appendix Fig S1). Examination of the NMJs in the trans-heterozygote flies revealed significant overgrowth compared to control flies (Fig 3A–D). Thus, these results indicate that in addition to Fmr1, Ythdf may also contribute to the m⁶A-dependent regulation of NMJ morphology.

To address the role of YTH proteins in the CNS, we dissected adult brains of control and fly mutants for the respective *Yth* genes and examined the MB structure. Compared to control flies, *Ythdf* KO brains show a substantial fusion of the β lobes (55%), mimicking the loss of *Mettl3* and *Mettl14* (Fig 3E and F). This defect was rescued upon *Ythdf* re-expression. In contrast, the lack of *Ythdc1* displayed no visible defect. Altogether, these results indicate that the m⁶A pathway controls axonal growth, both at NMJs and MBs, possibly via Fmr1 and Ythdf.

Ythdf interacts physically and genetically with Fmr1

To address how Ythdf prevents overgrowth at NMJs and MBs, we searched for co-factors using stable isotope dimethyl labeling-based

quantitative proteomics upon immunoprecipitation of Flag-tagged Ythdf from S2R⁺ cells, which is an embryonic derived cell line. We identified 51 factors that showed more than two-fold enrichment in the Flag-Ythdf pulldown fraction in comparison to a control pulldown (Appendix Fig S3A and Dataset EV2). The co-purified proteins were especially enriched for RNA binding proteins and translation regulators (Appendix Fig S3B). Interestingly, Fmr1 was among the 20 most enriched proteins (Fig 4A). In fact, several proteins previously shown to interact with Fmr1 were also pulled down with Flag-Ythdf (Fig 4A, highlighted in bold; Ishizuka et al, 2002; Sahoo et al, 2018; Xu et al, 2013), suggesting that Ythdf may be part of a whole Fmr1 complex.

To validate the co-existence of Ythdf and Fmr1 in the same complex, we performed co-immunoprecipitation assays in S2R⁺ cells ectopically expressing Flag-Myc-tagged Ythdf and Myc-tagged Fmr1 in the presence of Benzonase. Notably, these experiments confirmed that Fmr1 and Ythdf co-precipitate, independently of RNA (Fig 4B). To next address whether these two proteins interact directly, we tested whether purified recombinant GST-tagged Ythdf and Fmr1

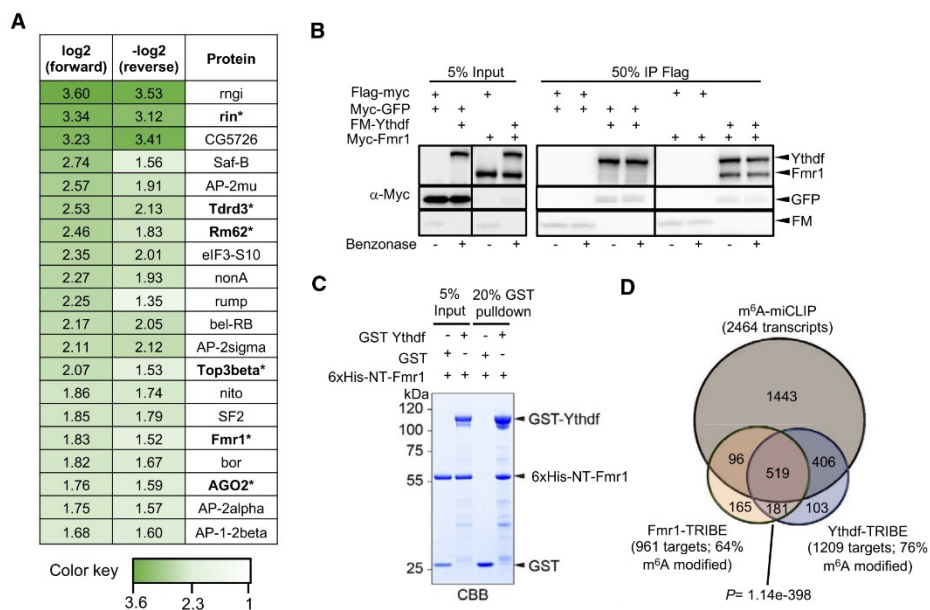


Figure 4. Fmr1 and Ythdf physically interact and share common targets.

A Heatmap indicating the normalized forward versus inverted reverse experiment enrichments on a log₂ scale of quantitative proteomics upon pulldown of Flag-tagged Ythdf in S2R⁺ cells. The threshold was set to a 1-fold enrichment. Fmr1 is co-purified with Ythdf. Known Fmr1 interacting proteins are highlighted in bold with asterisk.

B Co-immunoprecipitation experiment in S2R⁺ cells co-expressing Flag-Myc-tagged Ythdf and Myc-tagged Fmr1. Ythdf was used as a bait via its Flag tag. The lysate was treated with Benzonase as indicated to remove interactions enabled by RNA.

C GST pull-down of recombinant GST-Ythdf or GST alone mixed with recombinant 6xHis-NT-Fmr1. 2 μ M of recombinant proteins were used during the pulldown. The pulldown of the proteins was analyzed by CBB staining.

D Overlap of miCLIP dataset generated in S2R⁺ cells defining m⁶A modified transcripts with Fmr1 and Ythdf mRNA targets determined by TRIBES in S2R⁺ cells. The indicated P-value was determined by hypergeometric test.

Source data are available online for this figure.

proteins could pull down each other. As shown in Fig 4C, Fmr1 could be co-purified by pulling down GST-Ythdf but not GST alone, indicating that Ythdf and Fmr1 directly interact.

To address whether Ythdf and Fmr1 interact to regulate axonal growth at the NMJ, we performed epistasis experiments. While single heterozygote larvae displayed normal NMJ architecture, we found that double heterozygotes had a significant increase in the number of synaptic boutons (Fig 3G, compare lanes 2 and 4 with lane 6). Furthermore, the severity of the axonal growth defect observed in each homozygote mutants was not increased by removing one or two copies of the other genes (Fig 3G, compare lanes 2 and 5 with lanes 7, 8 and 9). These epistasis experiments thus suggest that both genes act in the same pathway to regulate the NMJ phenotype.

Ythdf and Fmr1 regulate translation of similar targets

In order to identify Ythdf and Fmr1 mRNA targets, we used the TRIBE approach, as previously described (Worpenberg et al, 2019). Briefly, metal-inducible fusion constructs expressing Ythdf-cdAdar, Fmr1-cdAdar, or cdAdar alone were transfected in S2R⁺ cells and RNA was isolated for sequencing 2 days after the induction of the constructs. Bound mRNA targets were identified by scoring A-I editing events obtained after comparison with unspecific events generated by cdAdar alone. Using a stringent cutoff, we identified 1209 Ythdf and 961 Fmr1 targets, with a significant degree of overlap ($n = 700$, $P = 1.14e-398$; Fig 4D, Dataset EV3). To address whether these targets were methylated, we performed miCLIP-seq using S2R⁺ cell extracts. We identified 2,464 methylated transcripts (about 34% of expressed genes), with strong enrichment of m⁶A sites within 5' UTR, in the sequence context AAACA (Fig EV3A and B; Dataset EV4). This profile is distinct from vertebrate and is consistent with an earlier report (Kan et al, 2017). Among methylated transcripts, 925 were common with Ythdf (76% of Ythdf targets) and 615 with Fmr1 (64% of Fmr1 targets; Fig 4D). Even though S2R⁺ cells do not have a neural origin, common methylated targets were enriched for axon regeneration (Fig EV3C). Moreover, consistent with the *in vivo* phenotypes, genes enriched for regulation of microtubule depolymerization were overrepresented. Altogether, these experiments identify common methylated targets for Ythdf and Fmr1, confirming they could act together to regulate gene expression.

To further understand the interplay between Ythdf and Fmr1 on RNA, we repeated pulldown experiments using the aforementioned biotinylated RNA probes. By combining a constant concentration of His-Fmr1 with an increasing amount of GST-Ythdf, we found a substantial increase of the Fmr1 binding to the methylated RNA probe with higher Ythdf protein concentrations in the GGACU sequence context (Fig 5A and B). Notably, the binding of Ythdf at the respective concentration was not changed by the presence of Fmr1 (Appendix Fig S4). The same trend could be observed for the alternative AAACU sequence context. Adding purified GST-Ythdf protein to His-Fmr1 protein enabled a specific enrichment of Fmr1 in the m⁶A probe pulldown fraction (Fig 5C). In addition, electrophoretic mobility shift assay (EMSA) using the Cy5 labeled AAACU RNA probes revealed a strong preference of Ythdf for the methylated RNA probe, while Fmr1 did interact with neither the methylated nor unmethylated probe (Fig 5D). Though, the

incubation of the RNA probe with a mixture of Fmr1 and Ythdf caused a shift of the RNA-protein complex signal in comparison with Ythdf alone, suggesting that Ythdf and Fmr1 bind together the methylated probe. Hence, these results indicate that Ythdf can facilitate binding of Fmr1 to methylated sites.

This result led us to investigate whether Fmr1 binding to mRNA is altered upon KO of Ythdf *in vivo*. To address this point, we performed a RNA immunoprecipitation assay (RIP) of endogenous Fmr1 from brain extracts of wt or *Ythdf* KO animals followed by sequencing. The RIP assay identified 584 significant target transcripts for the wild-type samples, corresponding to 487 genes (Fig 5E and Dataset EV5). These genes recapitulated the known functions associated with Fmr1, including nervous system development and regulation of RNA metabolism (Appendix Fig S5). The RIP assay in the *Ythdf* KO brains identified a similar number of target transcripts, 585, corresponding to 480 genes. The overlap between the two sets of targets is 57% (276 genes), with 211 and 204 genes, respectively, unique to wt and *Ythdf* KO samples (Fig 5E). This finding indicates that the binding specificity of Fmr1 is partially reprogrammed in the *Ythdf* mutant. Since our data suggest that Ythdf promotes Fmr1 binding to methylated transcripts, we expected in the *Ythdf* KO a loss of Fmr1 binding to the targets shared with Ythdf. We then analyzed the overlap between the genes lost in the *Ythdf* KO sample, with the previously identified Ythdf targets (Fig 4D), and we observed a significant overlap ($P = 3.04E-26$) (Fig 5F). Interestingly, the 211 lost genes are enriched in functions associated to neuronal development, including MB development, synapse assembly, and axon guidance (Appendix Fig S5).

Collectively, these experiments led to the identification of common methylated targets of Ythdf and Fmr1 and strongly suggest that these two factors directly interact to regulate gene expression.

Ythdf and Fmr1 control axonal growth at the MB and inhibit *chic* mRNA translation

Among the common targets of Fmr1 and Ythdf that are also methylated were *chickadee* (*chic*) transcripts (Fig EV4A). *chic* codes for Profilin, an actin-binding protein that modulates many processes depending on actin dynamics, among these neuronal growth and remodeling (Verheyen & Cooley, 1994). Importantly, previous work by Reeve and colleague demonstrated that Fmr1 controls axonal growth in the CNS via inhibition of *chic* translation (Reeve et al, 2005). We first performed an RNA immunoprecipitation assay (RIP) to confirm the binding of Fmr1 and Ythdf to *chic* mRNA in the adult fly brain using HA-tagged Ythdf and GFP-tagged Fmr1 driven by the neuronal driver *elav-GAL4*. As shown in Fig EV4B, both proteins were able to pulldown *chic* mRNA. To test whether the m⁶A pathway regulates *chic* expression in a similar manner as Fmr1, we examined Profilin protein levels using brain extracts from wild-type and *Ythdf* mutant. We found that the lack of Ythdf led to increased Profilin levels (Fig 6A and B). In contrast, *chic* mRNA levels remained unaffected (Fig 6C). These results prompted us to investigate whether the increased Profilin level was involved in the MB β -lobe fusion phenotype. We then crossed *Ythdf* mutant to *chic* mutant flies and scored for MB developmental defects. As shown in Fig 6D and E, loss of one copy of *chic* was sufficient to rescue the β -lobe fusion phenotype of *Ythdf* mutant flies. On the other hand, *chic* heterozygote mutant flies already showed β -lobe fusion per se,

5. Results

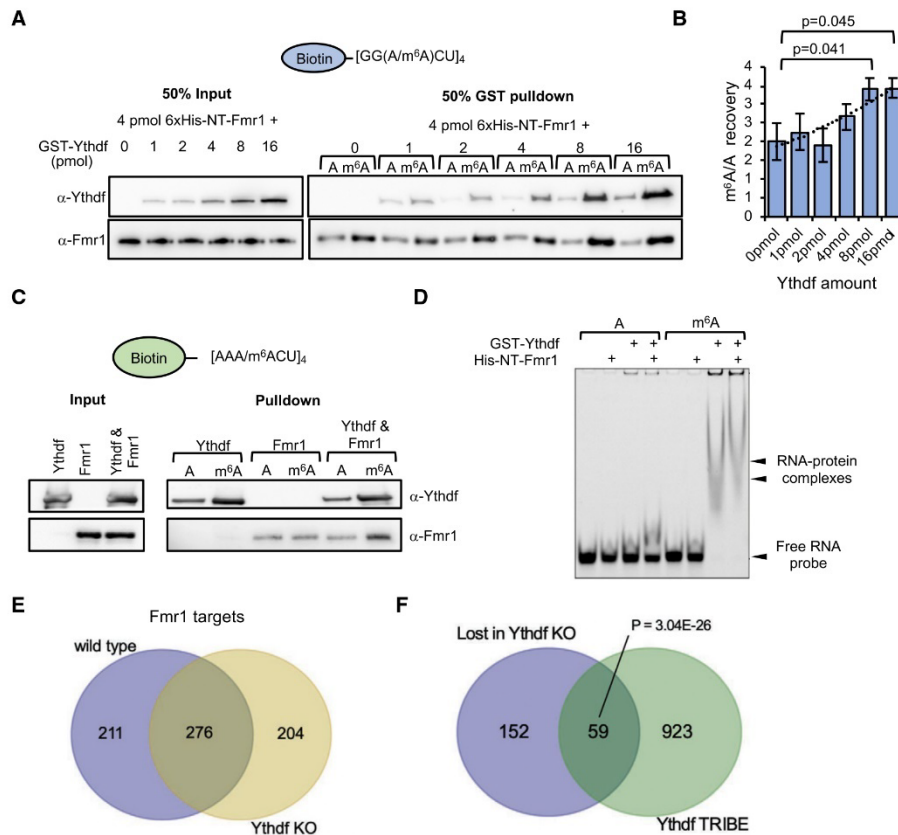


Figure 5. Ythdf modulates Fmr1 target selection.

A–D Pulldown of biotinylated RNA probes of (A) repetitive GGACU sequences incubated with 4 pmol His-NT-Fmr1 and increasing concentrations of GST-Ythdf and (B) the respective quantification plotted as the median of the m⁶A/A signal intensity ± SEM of three replicates. The indicated *P*-values were determined by unpaired, two-tailed Student's *t*-test. (C) AAACU sequences RNA probes incubated with either 32 pmol recombinant GST-Ythdf or/and 6xHis-NT-Fmr1. Pulled down proteins were analyzed by immunoblotting using α-Ythdf and α-Fmr1 antibodies. (D) EMSA assay using purified GST-Ythdf and His-NT-Fmr1 proteins and RNA probes in the AAACU sequence context.

E Intersection of Fmr1 RNA immunoprecipitation target genes for wild-type and *Ythdf* KO brains, displaying a considerable number of genes gained and lost with *Ythdf* loss.

F Intersection of genes lost (i.e., bound in wild-type but not in *Ythdf* KO) with *Ythdf* target genes determined by a TRIBE assay. *P*-value calculated with hypergeometric test.

Source data are available online for this figure.

suggesting that the level of Profilin has to be tightly regulated to ensure proper brain wiring. Hence, our results suggest that *Ythdf* interacts with *Fmr1* to limit the axonal growth at the MB and inhibit the translation of *chic* mRNA.

Ythdf and Fmr1 control axonal growth at the NMJ and inhibit *futsch* mRNA translation

We next investigated whether *chic* could also be common effector of *Fmr1* and *Ythdf* at the NMJ. As in the adult brain, we found that

both proteins interact with *chic* mRNA in the larval nervous system (Fig EV4C). However, in contrast to what we observed at the MB, removing one copy of *chic* had no effect on the NMJ phenotype produced by the loss of *Ythdf* (Fig EV4D). These results indicate that *chic* is not involved in the m⁶A-dependent phenotype at the NMJ and that other targets must be involved. To reveal their identity, we generated transgenic flies expressing *Ythdf*-cdAdar under the control of an UAS promoter. The construct was specifically expressed in the nervous system of third instar larvae using the *elav*-GAL4 driver and, after dissection, RNA was isolated and submitted for

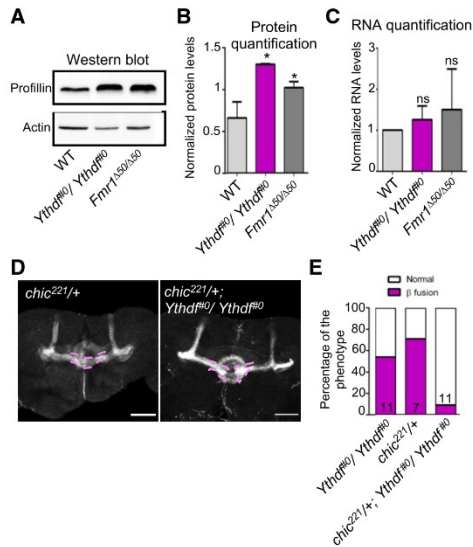


Figure 6. Fmr1 and Ythdf regulate CNS axonal growth and Profilin levels.

A Representative Western blot analysis of protein extracts of late pupae heads (85–95 h) from control, *Ythdf^{f0}/Ythdf^{f0}* and *Fmr1^{Δ50}/Fmr1^{Δ50}* flies. The membranes were probed with anti-Profilin or anti-Actin antibodies.

B Quantification of Profilin protein levels (mean ± SD) obtained from three independent protein extraction and Western blot analysis as in (A). Quantification was performed using Fiji. ** $P < 0.005$; * $P < 0.05$, measured with unpaired t-test.

C Quantification of *chic* mRNA levels (mean ± SD) obtained from six independent RNA extractions from control, *Ythdf^{f0}/Ythdf^{f0}* and *Fmr1^{Δ50}* late pupae heads, via real-time PCR analysis. Statistical analysis using unpaired t-test show no significant difference between the samples.

D Immunofluorescence analysis of adult *chic^{221/+}* and *chic^{221/+}; Ythdf^{f0}/Ythdf^{f0}* using anti-FasII antibody. Scale bar: 50 μm. Pink dashed lines highlight the normal and fused β-lobes.

E Quantification of the penetrance of β-lobe fusion phenotype for the indicated genotypes. Bars are labeled with the number of replicates.

Source data are available online for this figure.

high-throughput sequencing. Using this strategy, we identified 982 Ythdf target mRNAs in larval brains (Dataset EV6). We found a significant overlap with the Ythdf-TRIBE dataset produced in S2R⁺ cells ($n = 373$, $P = 1.32 \times 10^{-64}$, Fig EV4E), which includes the *chic* mRNA. Interestingly, we found that the *futsch* mRNA was scoring in the first 5% of the targets identified in the larval brain (53th highest TRIBE SumScore out of 982 mRNAs, Fig EV4F). *futsch* encodes a microtubule-associated protein that is a key target of Fmr1 in the regulation of axonal growth at the NMJ (Zhang et al, 2001). We confirmed the binding of Ythdf and Fmr1 to *futsch* mRNA in larval brains by immunoprecipitating HA-tagged Ythdf and GFP-tagged Fmr1 driven by the neuronal driver *elav-GAL4* (Fig EV4C). Remarkably, in *Mettl3* and *Ythdf* mutants *futsch* protein level was significantly upregulated at the larval NMJ and in larval brain extracts, which is reminiscent of the previously described upregulation observed in the *Fmr1* mutant (Fig 7A–C). In contrast, *futsch* mRNA

level was downregulated by two-fold (Fig 7D). To discriminate between a defect in translation inhibition and a defect in protein decay, we performed Translating Ribosome Affinity Purification (TRAP). By immunoprecipitation of a GFP-ribosomal fusion protein, TRAP enables the isolation of mRNAs associated with at least one ribosome, providing an estimation of the translation status of single transcripts. We expressed RPL10-GFP in neurons using the *elav-GAL4* driver and pulled down associated RNA using an anti-GFP antibody. Using this approach, we found that *futsch* mRNA was strongly enriched in the *Ythdf* mutant, demonstrating that its translation was likely increased (Fig 7E). Altogether, these experiments indicate that, like Fmr1, the m⁶A pathway restricts *futsch* mRNA translation in the larval nervous system.

To functionally address the relationship between the m⁶A pathway and *futsch* mRNA at the NMJ, we performed genetic experiments. As shown earlier, the number of synapses in the *Fmr1* mutant was restored to a normal level by removing *futsch* function (Fig 7F lanes 1–3, Zhang et al, 2001). Similar rescues were obtained in the *Mettl3* and *Ythdf* mutants (Fig 7F, lanes 1, 4–7). This indicates that the m⁶A pathway represses *futsch* mRNA translation, which contributes to the control of axonal growth at the NMJ.

Ythdf binding to *futsch* mRNA 5' UTR promotes translation inhibition

To functionally investigate the mechanism underpinning the influence of m⁶A and of the Ythdf/Fmr1 complex on *futsch* translation, we determined the location of the m⁶A sites on the *futsch* transcript. By analyzing our miCLIP-seq data, we found that *futsch* harbors two m⁶A sites in its 5' UTR, close to the start codon (Fig 8A). We verified the methylation of one of these sites *in vivo* by performing single-base elongation and ligation-based qPCR amplification (SELECT) (Xiao et al, 2018) using larval brain extract (Fig EV5A). To next define the influence of the methylation on *futsch* expression, we designed reporters containing the GFP coding sequence downstream of the WT *futsch* 5' UTR or a version containing A-T point mutations at the m⁶A sites (Fig 8B). We tested whether the binding of Ythdf and Fmr1 to the mutated reporter transcript was altered by immunoprecipitating Flag-tagged Ythdf and Fmr1 from S2R⁺ cell lysate co-transfected with the wt or mutated reporter constructs. While the wt *GFP* reporter was strongly enriched in the Ythdf and Fmr1 pulldown fractions, a significantly lower amount of the mutated *GFP* reporter transcript was recovered (Fig 8C), though the input protein and *GFP* transcript levels were similar (Fig EV5B and C). In addition, we found that the enrichment of the wt *futsch* 5' UTR reporter, but not the mutated version, was significantly increased in the Fmr1 pulldown fraction when Ythdf was co-expressed (Figs 8D and Fig EV5D), indicating that Ythdf increases the binding of Fmr1 to this reporter. We next analyzed whether mutations of the two m⁶A sites led to a change in the translation efficiency, similar to the observed increased translation of endogenous *futsch* in *Ythdf* mutants. As shown in Fig 8E and F, the GFP translation efficiency from the mutated reporter was significantly increased in comparison with the WT reporter. A similar increase of the translation efficiency could be observed for the wild-type reporter upon depletion of *Mettl3* (Fig 8E and F) or *Ythdf* (Fig 8G), while no significant difference was observed for the mutated reporter in the same conditions. Hence, we conclude that the

5. Results

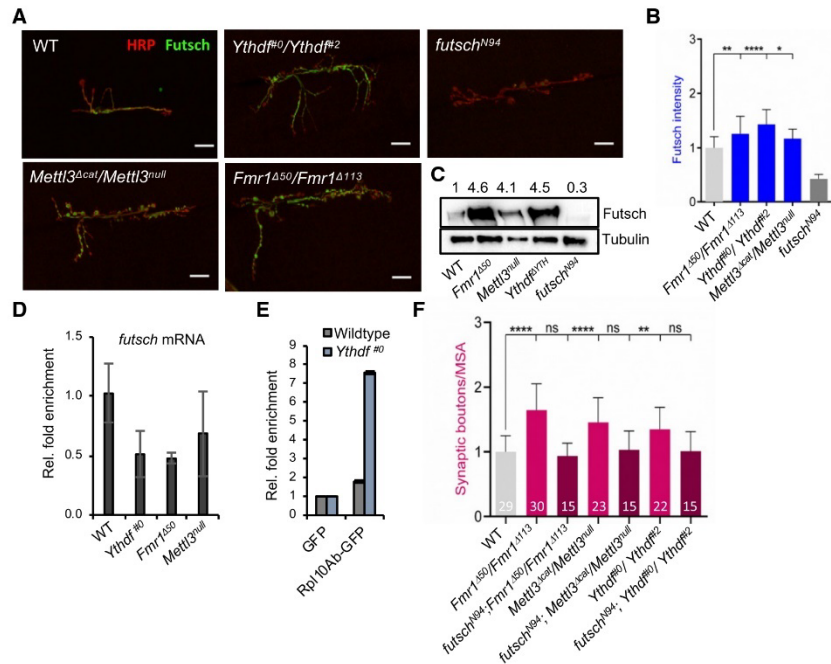


Figure 7. Fmr1 and Ythdf regulate CNS axonal growth and inhibit Futsch translation.

A Representative confocal images of muscle-6/7 NMJ synapses of abdominal hemisegment A2 for the indicated genotypes labeled with HRP (red) and α -futsch (green) to reveal the neuronal membrane and Futsch protein level. Scale bar: 20 μ m.

B Quantification of normalized Futsch protein level at NMJ 6/7 in A3 of the indicated genotypes ($n = 20$). Bars show mean \pm s.e.m. P values were determined with a Student's t -test. (* $P < 0.05$; ** $P < 0.01$; **** $P < 0.0001$).

C Western blot analysis of Futsch protein level in isolated third instar larval brains of different mutants compared to control. Numbers indicate normalized Futsch protein level in comparison to Tubulin levels.

D Quantification of *futsch* mRNA levels obtained from isolated 3rd instar larvae brains of the indicated genotypes via real-time PCR analysis. Bars show average \pm SD of biological triplicates.

E Translating Ribosome affinity purification assay. Quantification of *futsch* mRNA levels upon immunoprecipitation of GFP-tagged Rpl10Ab or GFP in wild-type and *Ythdf*^{#0} 3rd instar larvae with Real-time qPCR. Bars show average \pm SD of technical triplicates.

F Quantification of normalized bouton number (total number of boutons/muscle surface area (μ m² \times 1,000)) of NMJ 6/7 in hemisegment A3 of the indicated genotypes. Bars show mean \pm s.e.m. Multiple comparisons were performed using one-way ANOVA with a *post hoc* Sidak-Bonferroni correction (n.s. = not significant; ** $P < 0.01$; **** $P < 0.0001$). Bars are labeled with the number of replicates.

Source data are available online for this figure.

futsch 5' UTR harbors at least two m⁶A sites, which are required for Ythdf and Fmr1 binding and for the translational repression of *futsch* (Fig 8H).

Discussion

m⁶A on mRNA is emerging as a key modulator of nervous system biology (for recent review see (Livneh *et al*, 2020)). Despite the increasing amount of data associating m⁶A function to brain development, neuronal differentiation, regeneration, and synaptic function, the molecular mechanisms underlying these functions remain largely incomplete. Here we show that m⁶A is required for proper

neuronal development in both CNS and PNS, where it prevents MB β -lobes fusion and NMJ overgrowth, respectively. We further demonstrate a critical interplay between Ythdf and Fmr1 in the control of axonal growth. We show that Ythdf can interact with Fmr1 and inhibit the translation of critical targets that ensures proper axonal growth and homeostasis. Hence, our study reports that m⁶A can modulate Fmr1 target selectivity to influence the development of the nervous system in *Drosophila*.

m⁶A in axon growth and guidance

Previous work showed that flies lacking m⁶A are flightless and have reduced locomotion, due to impaired neuronal functions

5. Results

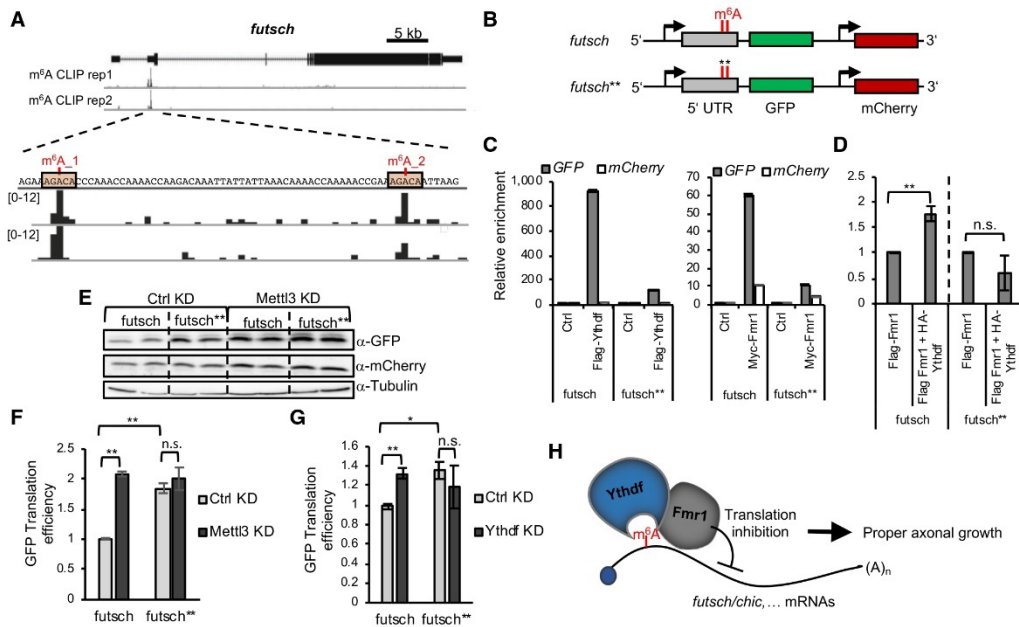


Figure 8. Ythdf recruits Fmr1 and repress Futsch translation via m⁶A.

A *futsch* genomic region (X1,408,435–1,454,00) and corresponding browser tracks from miCLIP-seq experiments in S2R⁺ cells. *futsch* transcripts contain two m⁶A peaks in its 5' UTR, as indicated.

B Schematic of GFP reporter constructs containing an *actin* promoter and either wild-type 5' UTR region of *futsch* or a mutated version (*futsch*^{**}) containing two-point mutations (A – T) at the identified m⁶A sites. mCherry is under the control of a same *actin* promoter.

C, D RNA immunoprecipitation assay. Quantification of GFP RNA levels upon immunoprecipitation of Myc-tagged Fmr1 or Flag-tagged Ythdf. Bars show average ± SD of technical triplicates (C) or Flag-tagged Fmr1 in the presence of overexpressed HA-tagged Ythdf. Bars show median ± s.e.m. of biological triplicates. P-values were determined with an unpaired, two-tailed Student's t-test. (n.s. = not significant; **P < 0.01) (D). *Rpl15* levels were used as a normalization control and the enrichment of mCherry is shown as a negative control for background binding.

E-G Representative Western blot analysis of the protein level (E) and quantification of the translation efficiency of S2R¹ cells transfected with the wild-type or mutated *futsch* reporter constructs upon control or *Mettl3* KD (F) or *Ythdf* KD (G). *LacZ* dsRNA was used for the control KD. The translation efficiency was calculated as the ratio of the relative GFP protein level and GFP mRNA level. mCherry served as a normalization control for both the protein and mRNA level. Bars show mean ± s.e.m. of biological triplicates. P values were determined with a Student's t-test. (n.s. = not significant; *P < 0.05; **P < 0.01).

H Model of the interplay between Ythdf and Fmr1 in translation control.

Source data are available online for this figure.

(Haussmann et al, 2016; Lence et al, 2016; Kan et al, 2017). In this study, we found that m⁶A controls axonal growth and guidance in the PNS and CNS, in part by regulating protein levels of two key components of the cytoskeleton, Futsch, and Profilin, respectively. Roles for m⁶A in axonal growth and guidance have been previously observed in mammals. For instance, depletion of FTO in axons of dorsal root ganglia neurons represses axon elongation in mouse (Yu et al, 2018). In this model, FTO depletion inhibits axon growth due to increased m⁶A levels on *growth-associated protein-43* (*GAP-43*) mRNA, resulting in reduced GAP-43 protein abundance. Accordingly, the growth defect can be rescued by expressing a deficient-m⁶A construct encoding GAP-43. However, how m⁶A inhibits GAP-43 translation is not understood. Perhaps a similar mechanism as described in our work, involving the recruitment of FMRP, is

operating (see also below). This would be consistent with the upregulation of GAP-43 observed at synapses of *Fmr1* KO mice (Klemmer et al, 2011). Upon injury of the same dorsal root ganglion neurons, it was shown that m⁶A levels increase dramatically, resulting in enhanced protein synthesis and eventually axon regeneration (Weng et al, 2018). A similar activity was also observed in the adult CNS. Thus, m⁶A plays a positive role in axonal growth upon injury, which seems in contradiction to its role in normal growth during development. Nevertheless in mouse embryonic dorsal spinal cord (DSC), m⁶A is required for axon growth and guidance by promoting *Robo3.1* translation via YTHDF1 (Zhuang et al, 2019). Thus, m⁶A has the ability to either promote or repress axon growth and guidance, which depends on the developmental and physiological contexts.

Ythdf controls axon growth and guidance and interacts with Fmr1

In mammals, there are three YTHDF proteins that were shown to control translation and mRNA decay. The current view is that YTHDF1 stimulates translation and YTHDF2 decreases mRNA stability, while YTHDF3 regulates both processes (Patil *et al.*, 2018; Zhao *et al.*, 2019), even though this model has been challenged recently (Lasman *et al.*, 2020; Zaccara & Jaffrey, 2020). Thus, more work is required to appreciate how the three YTH proteins interplay in the cytoplasm and how much of their functions overlap. In *Drosophila*, there is only one Ythdf protein but its function was not characterized prior to our work. In fact, the role of cytoplasmic m⁶A in this organism has remained enigmatic. Our attempt to demonstrate a role on mRNA stability in S2R⁺ cells was not conclusive, so it is unclear whether m⁶A regulates this process in flies (data not shown). The fact that most m⁶A sites resides in the 5' UTR, near the start codon, suggests instead that the main role of cytoplasmic m⁶A in *Drosophila* is to regulate translation. Consistent with this assumption, we found that m⁶A controls *futsch* and *chic* translation through Ythdf activity. However, in contrast to mammalian YTHDFs, *Drosophila* Ythdf does not activate their translation. It represses translation of these mRNAs likely via the recruitment of the translation inhibitor Fmr1. For future studies, it would be interesting to address whether translation inhibition is the major function of Ythdf in *Drosophila* or whether it has a broader role depending for instance on the nature of its interacting partners. Furthermore, whether such inhibitory role of YTHDFs in translation also exists in mammals awaits future investigations.

FMRP was recently shown to bind methylated mRNAs and to facilitate their export (Edens *et al.*, 2019; Hsu *et al.*, 2019), as well as to protect them from degradation by preventing YTHDF2 binding (Zhang *et al.*, 2018). It was proposed to be an m⁶A reader, acting in a sequence-dependent context. Indeed, *in vitro* pull down as well as FMR1 CLIP demonstrated association to GGACA/C/U sequence, with clear enrichment upon methylation (Arguello *et al.*, 2017; Edupuganti *et al.*, 2017; Hsu *et al.*, 2019). Whether this enrichment is due to direct recognition of the methyl group by FMR1 or to a change in RNA accessibility is still unclear. Replacing the first or the second G by A strongly decreased FMR1 association, while no effect was observed on YTH binding. Here we show that similar rules apply in *Drosophila*. In addition, our data further demonstrate that Ythdf interacts directly with Fmr1 and stabilizes its interaction to RNA. This direct interaction appears essential for both protein activities in the context of axonal growth. Of note, human YTHDF2 was recently shown to be in a same complex with FMR1, suggesting that this mode of interaction is conserved (Zhang *et al.*, 2018).

Relevance of this interplay in FXS

The absence of FMRP leads to the FXS, which is a severe inherited neuronal disorder that currently lacks efficient therapeutic treatment. The phenotype of the patients suffering from FXS is often complex, accompanied by an increase in autism spectrum disorder specific traits and other features like delayed motor development, hyperactivity, aggression, and epileptic seizures (reviewed in refs. Hagerman *et al.*, 2002; Garber *et al.*, 2008; Utari *et al.*, 2010; Santoro *et al.*, 2012; Hagerman *et al.*, 2014; Kidd *et al.*, 2014; Maurin *et al.*,

2014; Schaefer *et al.*, 2015; Dahlhaus, 2018). These abnormalities result from defects in neuronal development and maturation. Interestingly, the phenotypes of *Fmr1* mutants are reminiscent of the pathological symptoms of FXS patients and, consequently, *Drosophila* has been widely used to learn the basic mechanisms underlying FMRP functions and to test the efficacy of drug treatment (Drozd *et al.*, 2018). In particular, the increased synapse arborization and bouton number at the NMJ recall the dendritic spine overgrowth observed in FXS patients. Moreover, expressing human FMR1 in *Drosophila Fmr1* null mutants rescues the overgrowth at the NMJ and the defect in the brain, highlighting the functional conservation of the two orthologues (Coffee *et al.*, 2010). Since FMR1 is involved in different functions such as splicing, nuclear export, and translation, it remained unclear which activity was more relevant in the FXS etiology. A clue came when treatment with the translation inhibitor puromycin could rescue several aspects of FXS, including the locomotion phenotype and the overgrowth at the NMJ, suggesting that it was an excess of translation that yields these defects (Stefani *et al.*, 2004; Bolduc *et al.*, 2008; Kashima *et al.*, 2017). Accordingly, the first target identified for Fmr1 was *Futsch*, a microtubule-associated protein orthologue of mammalian MAP1B (Zhang *et al.*, 2001). Fmr1 negatively regulates *futsch* translation, and this is necessary to prevent NMJ overgrowth. Importantly, this function was also found in mice (Lu *et al.*, 2004). Our data showing that Fmr1 may repress translation via m⁶A activity links m⁶A to some aspects of the FXS studied in the fly model. It would be of critical importance to test whether a similar mechanism also applies to mammals. The FMR1-mediated nuclear export and stability of methylated RNA as recently uncovered may contribute as well to the disease (Zhang *et al.*, 2018; Edens *et al.*, 2019; Hsu *et al.*, 2019). It is worth mentioning that while our study mainly focuses on two key Fmr1 targets involved in the gross morphology of the nervous system, it is likely that m⁶A and Fmr1 regulate additional targets involved in more subtle processes such as synapse functionality and complex trait behaviors.

In conclusion, our study indicates that m⁶A modulates both CNS and PNS development by restricting axonal growth and promoting correct assembly of the neural circuits. These functions are reminiscent to the functions of Fmr1 in the nervous system, and our work shows that both m⁶A and Fmr1 tightly cooperate to regulate these processes. We foresee that this new knowledge will open new avenues for the design of complementary treatments of FXS.

Materials and Methods

Drosophila stocks

The stocks used are the following: *Fmr1*^{Delta50M}, *Fmr1*^{Delta113M}, *chic*²²¹, *futsch*^{N94}, *Mettl14*^{Df}, *Ythdc1*^{Df}, *Tub-GAL4*, *Elav-Gal4*, *c772Gal4:UAS-CD8-GFP*, *Elav-Gal4;UAS-FMR1-GFP/TM3* (Bloomington Stock Collection), *Mettl3*^{null}, *Mettl3*^{Deltaacat}, *UAS-Mettl3*, *Mettl14*^{Δ5}, *Ythdc1*^{DeltaN} (Lence *et al.*, 2016), *Mettl3*^{SK2}, *Mettl14*^{SK1} (kind gift from Eric Lai), *P(GD9882)v20969/TM3* (VDRC), *P(GD9882)v20968/TM3* (VDRC), *w1118;P(GD11887)v27577* (VDRC), *w1118;P(GD16300)v48560* (VDRC), and *w¹¹¹⁸* (kind gift from Paola Bellosta).

Drosophila melanogaster Canton-S with mutant alleles for *Ythdf* were generated using the CRISPR/Cas9 system, as described

5. Results

previously (Lence et al, 2016). Guide RNA sequences used were CTTCCGATAAATTCCTTCCGAATA and AACTATTCCGAAAGAATTTATCC as well as CTTCCGGCGAGTGGGGCAGGCGCG and AAACCGCGCTGCCCACTCGCCC. The first allele (*Ythdf^{Δ1}*) produces a deletion of 1,221 nucleotides in the coding sequence, deleting residues 172–557, that includes the whole YTH domain. The second allele (*Ythdf^{Δ2}*) is a deletion of 1319 nucleotides and removes residues 162–558.

Drosophila cell lines

Drosophila S2R⁺ are embryonically derived cells obtained from the *Drosophila* Genomics Resource Center (DGRC; Flybase accession FBtc0000150), while *Drosophila* BG3 cells are derived from central nervous system of third instar larvae (DGRC; Flybase accession FBtc0000068). Mycoplasma contamination was not detected (verified by analyzing RNA sequencing data).

Immunohistochemistry

For the immunohistochemistry in adult and pupal brains, the following protocol was used: Brains were collected in cold PBS and subsequently fixed for 10 min in 4% formaldehyde (in PBS 0.3% Triton X-100). Upon three washes in PBS 0.3% Triton X-100, the brains were blocked in 10% BSA (in PBS 0.3% Triton X-100) for 1 h rocking at RT. After this step, the brains were incubated overnight at 4°C with the primary antibody appropriately diluted in blocking solution. The second day, the samples were washed 3 times in PBS 0.3% Triton X-100 and then incubated with the appropriate secondary antibody diluted in blocking solution for 1 h at RT. Upon three washes in PBS 0.3% Triton X-100, the brains were mounted and kept at 4°C for imaging. Primary antibody used were as follows: anti-FasII 1/50 (ID4 Hybridoma Bank) and anti-GFP 1/500 (Invitrogen A11122). Secondary antibody used were Alexa Fluor 555 Donkey anti-Mouse and Alexa Fluor 488 Goat Anti-Rabbit at a dilution of 1/500. Images were acquired on a Leica TCS SP8 laser scanning confocal microscope or on a Leica DM6000CS confocal microscope and processed using Fiji™ software.

NMJ analysis

For NMJ staining, third instar larvae were dissected in cold PBS and fixed with 4% paraformaldehyde in PBS for 45 min. Larvae were then washed in PBS-T (PBS + 0.5% Triton X-100) six times for 30 min and incubated overnight at 4°C with the following primary antibodies: mouse anti-synaptotagmin, 1:200 (3H2 2D7, Developmental Studies Hybridoma Bank, DSHB) and TRITC-conjugated anti-HRP, 1:1,000. After six 30-min washes with PBS-T, secondary antibody anti-mouse conjugated to Alexa-488 was used at a concentration of 1:1,000 and incubated at room temperature for 2 h. Larvae were washed again six times with PBS-T and finally mounted in Vectashield.

Images from muscles 6–7 (segment A2–A3) were acquired with a Leica Confocal Microscope SP5. Serial optical sections at 1,024 × 1,024 pixels with 0.4 μm thickness were obtained with the ×40 objective. Bouton number was quantified using Imaris 9 software. ImageJ software was used to measure the muscles area and

the NMJ axon length and branching. Statistical tests were performed in GraphPad (PRISM 8).

RNA probe pulldown

For RNA probe pulldown in BG3 cells, cells were washed with DPBS, harvested, and pelleted for 10 min at 400 g. The cell pellet was resuspended in lysis buffer (10 mM Tris-HCl at pH 7.4, 150 mM NaCl, 2 mM EDTA, 0.5% NP-40, 0.5 mM DTT, protease inhibitor) and rotated head over tail for 15 min at 4°C. Nuclei were collected by 10-min centrifugation at 1,000 g at 4°C, resuspended in 300 μl of lysis buffer, and sonicated with 5 cycles of 30 s ON, 30 s OFF low power setting. Cytoplasmic and nuclear fractions were joined and centrifuged at 18000 g for 10 min at 4°C to remove the remaining cell debris. Protein concentration was determined by Bradford, and 1 mg lysate was used for the following pulldown procedure.

For RNA probe pulldown using purified recombinant proteins, the indicated amounts of purified proteins were resuspended in binding buffer (2% Triton X, 20 mM Tris-HCl, 10 mM EDTA, 120 mM NaCl, 50 mM KCl, 1 mM DTT, protease inhibitor) and used for the following pulldown procedure. Purified proteins were incubated with 1 μg of biotinylated RNA probe coupled to 20 μl Dynabeads MyOne Streptavidin C1 (Thermo Fisher) in 600 μl lysis buffer at 4°C for 1 h rotating head over tail. The beads were washed three times with lysis buffer and bound proteins eluted by incubation in 1x NuPage LDS supplemented with 100 mM DTT for 10 min at 70°C. Eluted proteins were analyzed by PAGE followed by Coomassie staining, immunoblotting using the corresponding antibodies or proceeded to quantitative proteomic analysis.

Expression and purification of recombinant proteins

N-His₆-tagged NT-Fmr1 (220-684) and N-GST-tagged Ythdf (full length) were expressed from pQIq-His6 and pGEX-6P-1, respectively, in *E. coli* BL21 (DE3) Rosetta™ 2pLys (Novagen). Cells were grown in LB-Luria at 37°C and 160 rpm to an OD₆₀₀ of 0.6–0.8 and chilled on ice, and expression was induced by addition of IPTG (1 mM). Cells were further incubated at 18°C and 160 rpm for 20 h, harvested by centrifugation for 15 min at 4,000 g at 4°C, and directly processed for purification: Cells were resuspended in lysis buffer (50 mM Tris-HCl pH 8.0, 500 mM NaCl, 15 mM imidazole, 5% glycerol, 1 mM DTT, 1 mM MgCl₂, Benzonase 1:2,500, protease inhibitors) and lysed by sonification. Lysates were cleared by centrifugation (45,000 g, 30 min, 4°C). For GST-Ythdf purification, additional 500 mM of NaCl and subsequently 0.2% of polyethyleneimine (40 kDa) was added to the cleared lysate, incubated for 10 min at 4°C, and centrifuged at 4000 g for 10 min in order to precipitate nucleic acids. Proteins were captured from cleared lysates using a HisTrap FF 5 ml (His-NT-Fmr) or GstTrap FF 5 ml column (GST-Ythdf; both GE Healthcare) according to the manufacturer's instructions and using a Biorad NGC Quest FPLC system. Fractions containing the respective recombinant proteins were pooled and concentrated using Amicon® Ultra-15 spin concentrators with 10 kDa cutoff (Merck Millipore). Concentrated protein pools were injected onto a Superdex 200 16/60 pg in gel filtration buffer (25 mM Tris-Cl pH 7.5, 500 mM NaCl, 1 mM DTT, 10% glycerol). Peak fractions containing the recombinant proteins were

5. Results

pooled, aliquoted, and snap-frozen in liquid nitrogen. Frozen aliquots were stored at -80°C .

TRIBE

TRIBE was performed as previously described (McMahon *et al*, 2016; Xu *et al*, 2018; Worpenberg *et al*, 2019). Briefly, for the identification of mRNA targets in S2R^+ cells, Flag-tagged Ythdf and Fmr1 versions fused to the catalytic domain of Adar (cdAdar) were ectopically expressed using a metal-inducible expression system. Forty-eight hours after protein expression induction, the cells were washed with DPBS and harvested.

For the identification of *in vivo* targets, 3rd instar larvae expressing a Flag-tagged version of Ythdf fused to cdAdar driven by *Elav-Gal4* were collected and the brains dissected and collected in PBS.

For protein expression analysis, 50% of the cells/brains were resuspended in lysis buffer (50 mM Tris-HCl at pH 7.4, 150 mM NaCl, 0.5% NP-40, protease inhibitor) and incubated for 30 min on ice. Cell debris was removed by centrifugation for 5 min at 12,000 g at 4°C and the expression analyzed by immunoblotting using anti-Flag antibody.

For the identification of editing events, the remaining 50% of cells were used for total RNA isolation using TRIzol reagent, mRNA was purified by two rounds of Oligo(dT) selection using Dynabeads, and the purified mRNA was used for Illumina Next-generation sequencing library preparation using NEBNext[®] Ultra[™] II RNA Library Prep Kit for Illumina according to manufacture protocol.

From the TRIBE data analysis, the score is defined as a log-likelihood ratio of two conditions and, therefore, describes how different conditions are (the higher the Score, the more different the A-I editing). The arbitrary SumScore cutoff used in this manuscript is 20 to exclude low confidence targets and background from our analysis.

Co-immunoprecipitation

S2R^+ cells were transfected using Effectene transfection reagent with plasmids expressing the indicated constructs. After 72 h, the cells were washed with DPBS, harvested, and pelleted by centrifugation for 3 min at 1,000 g. The cell pellet was resuspended in 1 ml lysis buffer (50 mM Tris-HCl at pH 7.4, 150 mM NaCl, 0.5% NP-40) supplemented with protease inhibitors and incubated for 30 min on ice. The cell debris was removed by centrifugation at 12,000 g for 5 min at 4°C, and the protein concentration of the cleared lysate was measured by Bradford. Two mg protein lysate was combined with 2 μl antibody coupled to 20 μl Protein G Dynabeads in lysis buffer and incubated rotating head over end at 4°C for 2 h. The beads were washed three times for 10 min with lysis buffer and the proteins eluted in 1 \times NuPage LDS buffer supplemented with 100 mM DTT by incubation for 10 min at 70°C. The eluted proteins were either analyzed by Western blot or conducted to quantitative proteomics analysis.

RNA immunoprecipitations (RIP)

For RIP from cell lysate, S2R^+ cells were transfected with the plasmids expressing the indicated constructs. After 72 h, the cells were washed with DPBS, harvested, and pelleted by centrifugation for 3 min at 1,000 g. The cell pellet was resuspended in 1 ml lysis

buffer (50 mM Tris-HCl at pH 7.4, 150 mM NaCl, 0.5% NP-40) supplemented with protease inhibitors and RNase inhibitor.

For RIP from *Drosophila* larvae, 30 larvae with the indicated genotype were collected in DPBS on ice, carefully washed by exchanging the DPBS two times, and lysed by squishing with a pestle in 1 ml lysis buffer. The resuspended cell pellet or larvae lysate was incubated for 30 min on ice. The cell debris was removed by centrifugation at 12,000 g for 5 min at 4°C, and the protein concentration of the cleared lysate was measured by Bradford. Two mg protein lysate was combined with 2 μl antibody coupled to 20 μl Protein G Dynabeads in lysis buffer and incubated rotating head over end at 4°C for 2 h. The beads were washed three times for 10 min with lysis buffer. 20% of the beads were used for the elution of protein-RNA complexes by incubation in 1 \times NuPage LDS buffer supplemented with 100 mM DTT for 10 min at 70°C. The eluted proteins were analyzed by Western blot. 80% of the beads were used to extract RNA using TRIzol reagent. The enrichment of the transcripts was analyzed by qPCR and the fold change calculated by normalizing the transcript levels in the pull-down fractions to the corresponding input and a control pull-down.

For RIP from pupal heads for endogenous Fmr1: 200 heads per each genotype were collected in PBS on ice and subsequently resuspended in 100 μl of lysis buffer (10 mM Tris-HCl pH 7.4, 140 mM NaCl, 0.5% Triton X-100, 1 mM DTT, 2 mM EDTA) supplemented with protease, phosphatase, and RNase inhibitors. The heads were lysed with a motor pestle and left on ice for 20'. The cell debris was removed by centrifugation at 12,000 g for 10 min at 4°C, and 1/10 of the volume was taken as an input and kept at -80°C , while the rest of the supernatant was divided in two and combined with either 20 μl of anti-Fmr1 5B6 and 20 μl of anti-Fmr1 5A11 or to 1.5 μl of mouse IgG together with 50 μl of Protein G Dynabeads in lysis buffer. The lysate was incubated with the beads antibody rotating head over end at 4°C overnight. The day after, the beads were washed three times for 10 min and subsequently resuspended in 100 μl of lysis buffer that were further treated with 40 μg of proteinase K for 30' at 55°C. Upon treatment, the supernatant was separated from the beads and RNA was extracted using TRIzol reagent. The enrichment of transcripts was analyzed by qPCR and the fold change calculated by normalizing the transcript levels in the pull-down fractions to the corresponding input and a control pull-down. For the RIP with overexpressed Ythdf-HA, 3 μg of anti-HA (Santa Cruz sc-805 rabbit polyclonal) was conjugated to 50 μl of Protein G Dynabeads and used to immunoprecipitate tagged Ythdf from 50 adult heads. For the RIP with overexpressed Fmr1-GFP, 25 μl of GFP Trap_MA beads (Chromtek) was used to immunoprecipitate tagged Fmr1 from 50 adult heads.

Sequencing and bioinformatics analysis of RNA immunoprecipitation from *Drosophila* heads

Strand-specific, rRNA-depleted libraries were generated with the Ovation[®] SoLo RNA-Seq System plus *Drosophila* AnyDeplete Probe Mix (Tecan Genomics). Each individual library was quantified and quality controlled using Qubit Fluorometer (Thermo Scientific), LabChip GX (Perkin Elmer). After libraries equimolar pooling, the final pool was quality checked again with Qubit, LabChip GX, and also qPCR (KAPA and BIORAD). The adaptor-tagged pool of libraries was sequenced in the Illumina Novaseq6000 in CIBIO NGS

5. Results

Core facility, using the Ovation SoLo Custom R1 primer and producing 960 million of reads. Reads were preprocessed (quality < Q30, adapters stripped) with TrimGalore (https://www.bioinformatics.babraham.ac.uk/projects/trim_galore/) and then aligned to the *Drosophila melanogaster* genome r6.28 with STAR (Dobin et al, 2013). Gene read counts were normalized by library size. RIP fold enrichment and *P*-value were computed for each condition with DESeq2 (Love et al, 2014) as (RIP / INPUT) or (IGG / INPUT). Genes and transcripts significantly enriched (adjusted *P*-value <= 0.05) in the RIP/INPUT and not in the corresponding IGG/INPUT were considered to be Fmr1 targets. Functional enrichment of Fmr1 targets was computed with Panther (Mi et al, 2019) and plotted with ReviGO (Supek et al, 2011). Overlap *P*-value was computed using hypergeometric test.

In vitro RNA interaction studies (Electro Mobility Shift Assay—EMSA and Fluorescence Polarization—FP)

Cy5-labeled RNA probes (Horizon Discovery, 10 nM in EMSA and 5 nM in the FP) were incubated with varying concentrations of His-NT-Fmr1 and/or GST-Ythdf (300 nM in EMSA and 2.5 nM to 2.5 μM in FP) at a total volume of 10 μl in interaction buffer (20 mM Tris-Cl pH 7.5, 150 mM NaCl, 10% glycerol, 1 mM EDTA, 1 mM DTT). The probes and proteins were incubated for 10 min at room temperature. For EMSA, the samples were mixed with 2 μl of 6 × loading buffer (60% Glycerol, 20 mM Tris-Cl pH 8.0, 60 mM EDTA) and loaded onto a 12% TBE-PA-Gel. The gel was run for 45 min at 200 V in TBE buffer and scanned using a Typhoon FLA 9000 @ 635 nm to visualize the fluorescence of the Cy5-labeled RNA probes. For FP measurements, samples were transferred to a 384-well plate (Corning™, Low-Volume, Polystyrene, black) and fluorescence polarization of the Cy5-labeled oligos was analyzed on a Tecan Spark 20M plate reader at 20°C (excitation wavelength: 625 nm, emission wavelength: 665 nm, gain: 125, flashes: 15, integration time: 40 μs). Relative fluorescence polarization was calculated by subtracting the FP value of the oligo-only conditions from all conditions that contained variable amounts of His-NT-Fmr1 and/or GST-Ythdf. The relative FP values from three independent experiments including standard deviation were plotted using GraphPad Prism 8. Binding constants (kd values) were determined by fitting a Michaelis-Menten non-linear regression onto the relative FP values in GraphPad Prism 8, if applicable.

Cell culture

Drosophila melanogaster S2R⁺ and BG3 cells were cultured in Schneider's *Drosophila* media (PAN BIOTECH) supplemented with 10% FBS and 1% penicillin-streptomycin. The culture medium for BG3 cells was additionally supplemented with 10 μg/ml insulin. Plasmid transfections were achieved using Effectene transfection reagent (Qiagen) according to the manufacturer's protocol. The knockdown was achieved using dsRNA. The PCR templates for the dsRNA were prepared using T7 megascript Kit (NEB). 2 Mio S2R⁺ cells were seeded in 6-well plates and treated 6h in serum-free medium with 15 μg of dsRNA. Afterward, medium containing 10% FBS and 1% penicillin-streptomycin was added to the cells. dsRNA treatment was repeated after 48 and 96 h.

Reporter assay

2 Mio cells were seeded 24 h before the transfection of the indicated reporter plasmids. Twenty-four h after transfection, the cells were harvested. One half was used for RNA extraction followed by RT-qPCR to determine the relative *GFP* level normalized to the *mCherry* level. The second half was used for Western blot analysis as described. The relative *GFP* protein level was determined by normalization to the mCherry protein level. The translation efficiency was determined by normalizing the relative *GFP* protein level to the relative *GFP* mRNA level.

RNA isolation and quantitative real-time PCR analysis

Total RNA from S2R⁺ cells or larval brains was isolated using TRIzol reagent according to the manufacturer protocol, DNA contamination removed by DNase-I (NEB) treatment and reverse-transcribed using M-MLV reverse transcriptase (Promega). The transcript levels were quantified by real-time PCR using Power SYBR green Master Mix. *Rpl15* mRNA and *18S* rRNA were used as housekeeping control genes.

Total RNA from head lysates was isolated using TRIzol reagent according to the manufacturer protocol and reverse-transcribed using RevertAid First Strand cDNA Synthesis Kit. The transcript levels were quantified by real-time PCR using Power SYBR green Master Mix. *RP49* and *Tubulin* RNA were used as housekeeping control genes.

Western blot analysis

Proteins were extracted for 30 min on ice, the lysates were centrifuged at 12,000 g for 5 min at 4°C, and protein concentration in the supernatant was determined by Bradford. For Futsch protein detection, lysates were additionally dephosphorylated using Lambda protein phosphatase (NEB) following manufacturer's instructions. Protein samples were separated on SDS-PAGE gels. Wet transfer to nitrocellulose membrane (Whatman) was performed for 90 min at 100 V. Membranes were blocked for 30 min in 5% non-fat dry milk and PBS-0.5% Tween 20 (PBS-T) and incubated with primary antibodies overnight at 4°C: anti-Profilin chi1J 1/500 (Hybridoma Bank), anti-Actin I-19 (Santa Cruz sc-1616), and anti-Futsch 22C10 (Hybridoma Bank). Signal was detected with corresponding HRP-conjugated secondary antibodies and ECL™ Prime Western Blotting Detection Reagent or ECL™ Select Western Blotting Detection Reagent (Amersham).

GST pulldown

Recombinant GST-tagged Ythdf or GST (2 μM final) were mixed with recombinant His6-tagged NT-Fmr1 (2 μM final) in 100 μl binding buffer (20 mM Tris-Cl pH 7.5, 150 mM NaCl, 10% glycerol, 0.1% Triton X-100, 1 mM DTT) and incubated for 1 h rotating head over end at 4°C with 20 μl Glutathione Sepharose beads. The beads were washed once with binding buffer +1% Triton X-100 and two subsequent times with binding buffer. Bound proteins were eluted by incubation in 50 μl 1× NuPage LDS supplemented with 100 mM DTT for 5 min at 95°C. Input and pulldown samples were analyzed by SDS-PAGE and subsequent coomassie brilliant blue staining.

5. Results

TRAP

TRAP was performed as previously described (Thomas *et al*, 2012). Briefly, *Drosophila melanogaster* 3rd instar larvae expressing *Elav-Gal4* driven GFP-tagged Rpl10Ab or cytoplasmic GFP in a wild-type and *Ythdf* mutant background were collected and lysed in extraction buffer (20 mM HEPES, pH 7.5, 150 mM KCl, 5 mM MgCl₂, 1% Triton X-100, 0.5 mM DTT, 100 µg/ml Cycloheximide, 100 U/ml Rnase inhibitor, Protease Inhibitor). Cell debris was removed by centrifugation at 12,000 g for 5 min at 4°C and the protein amount determined by Bradford. Two mg lysate was combined with 20 µl Protein G Dyna-beads conjugated to anti-GFP antibody and incubated at 4°C for 2 h followed by three washing steps in Wash Buffer (150 mM NaCl, 0.05% Triton X-100, 50 mM Tris, 5 mM MgCl₂, and 40 U/ml RNase inhibitor) at 4°C. RNA was extracted using TRIzol reagent following manufacturer's protocol and the enrichment of the transcripts analyzed by qPCR.

m⁶A-miCLIP

miCLIP was performed following previously described method (Linder *et al*, 2015) using 10 µg of purified mRNA from *Drosophila* S2R⁺ cells and 5 µg of anti-m⁶A antibody (Synaptic Systems, Lot# 202003/2-82). Immunoprecipitations were performed in quadruplicates, and as a control, one immunoprecipitation was performed where UV-crosslinking was omitted. Of note, this sample produced a library of limited complexity, reflecting a low amount of background mRNA binding. Briefly, total RNA was isolated using Trizol reagent (Invitrogen) and DNA was removed with DNase-I treatment (NEB). Polyadenylated RNA was purified by two rounds of binding to Oligo (dT)25 magnetic beads (NEB), and mRNA was fragmented with RNA fragmentation solution (Ambion) using 1 µl of solution per 2 µg of mRNA and with 7-min incubation at 70°C. Immunoprecipitation was performed at 4°C in 500 µl of binding buffer (BB) (50 mM Tris-HCl pH 7.4, 150 mM NaCl, 0.5 % NP-40). First, isolated mRNA and antibody were incubated for 2 h. Samples were then transferred to individual well of a 12-well cell culture plate and crosslinked on ice (two times at 150 mJ/cm²). Next, 60 µl of magnetic ProteinG beads (Invitrogen) was resuspended in 500 µl of BB and added to the IP sample. Samples were then incubated for additional 2 h at 4°C, before washing with ice-cold solutions was performed: 1x with BB, 2x with high salt buffer (50 mM Tris-HCl pH 7.4, 1 M NaCl, 1% NP-40, 0.1% SDS), 1x BB, 2x with PNK buffer (20 mM Tris-HCl pH 7.4, 10 mM MgCl₂, 0.2% Tween). All washes were performed by gentle pipetting and with 1-min incubation on ice. Washes with HSB were additionally rotated for 2 min at 4°C. Finally, beads were resuspended in 900 µl of PNK buffer. Forty µl was used for WB analysis to evaluate immunoprecipitation efficiency. Remaining 860 µl was used for library preparation. All steps of library preparation were performed as previously described in (Sutandy *et al*, 2016). Libraries were sequenced on an Illumina NextSeq500.

For the miCLIP fragmented input control library, fragmented mRNA, that was also used for miCLIP IP, was first purified using the 1.8× volume of RNAClean XP beads (Beckman Coulter). Following the 20-min incubation at RT, captured RNA was washed 3x with 80% EtOH and eluted in 20 µl of RNase-free water. The library was prepared using ~ 50 ng of cleaned, fragmented mRNA using the NEBNext Ultra Directional RNA Library Prep Kit for Illumina (NEB),

by omitting the RNA fragmentation step and following the manufacturer's protocol. For library amplification, 11 PCR cycles were used and indicated primer and adaptor sequences: NEBNext Index 27 Primer for Illumina: 5'-CAAGCAGAAGACGGCATACGAGATAAAG GAATGTGACTGGAGTTCAGACGTGTGCTCTTCCGATC-s-T-3' (Expected index read: ATTCTT), NEBNext Adaptor for Illumina: 5'-/5Phos/GAT CGG AAG AGC ACA CGT CTG AAC TCC AGT CUA CAC TCT TTC CCT ACA CGA CGC TCT TCC GAT C-s-T-3'. Libraries were sequenced on an Illumina NextSeq500.

m⁶A-miCLIP analysis

Sequencing qualities were checked for all reads using FastQC (version 0.11.5; <https://www.bioinformatics.babraham.ac.uk/projects/fastqc/>). Afterward, reads were filtered based on sequencing qualities (Phred score) of the barcode region. Reads with more than one position with a Phred score < 20 in the experimental barcode (positions 4 to 7 in the reads) or any position with a Phred score < 10 in the random barcode (positions 1 to 3 and 8 to 9) were excluded from the subsequent analysis. Remaining reads were de-multiplexed based on the experimental barcode (positions 4-7) using Flexbar (v3.0.0) (Dodt *et al*, 2012) without allowing any mismatch.

Individual samples were processed using the CLIP Tool Kit (CTK) v1.0.9. (Shah *et al*, 2017). We largely followed recommended user guide lines specific to CTK iCLIP data analysis as described here (https://www.zhnglab.c2b2.columbia.edu/index.php/ICLIP_data_analysis_using_CTK). Briefly, 3'adapter sequences [AGATCGGAAGAGCGGTTCAG] were trimmed using cutadapt v1.8. [overlap = 5; -m 29] (Martin, 2011). PCR duplicates were removed using a custom perl script, followed by the extraction of the 9 nucleotide miCLIP barcode and its addition to the read name. All cDNA libraries were filtered for common *Drosophila* virus sequences (Webster *et al*, 2016) using bowtie v1.1.2 [-p 4 -q (-X 1000) -fr best]. Next, to avoid sequencing read alignment software biases, we decided to map sequencing reads to the *Drosophila melanogaster* dm6 genome assembly (ensemble v81) using novoalign (<http://www.novocraft.com/>), bwa (Li & Durbin, 2009), and STAR v2.4.2a (Dobin *et al*, 2013). For STAR alignments, we used a custom python script to transform sam files into the expected format for downstream CITS identification. For STAR alignments, we did not consider spliced reads, soft-clipped reads, mismatches and indels near read start and read end, and reads with more than one indel or mismatch. Then, unique tags were identified using *parseAlignment.pl* [-v --map-quality 1 --min-len 18 --indel-to-end 2] to extract unique tags, followed by read collapsing using *tag2collapse.pl*. [-v -big --random-barcode -EM 30 --seq-error-model alignment -weight --weight-in-name --keep-max-score --keep-tag-name]. Crosslinking induced mutation sites (CIMS) indicative for the antibody-m⁶A interaction were identified running *CIMS.pl* [-big -n 10], and CIMS with FDR < 0.001 were retained. Crosslinking induced truncations sites were identified using *CITS.pl* [-big -p 0.001 --gap 25]. Sites spanning more than 1 nucleotide were removed.

We further filtered identified CIMS and CITS to be reproducible in at least 2 out of 4 replicate m⁶A immunoprecipitation samples and not present in identified CITS from the input control sample for each aligner separately. Moreover, CIMS were filtered to have a minimum of 6 unique tags [k > 5], at least three unique substitutions [m > 2], and be prevalent in less than 20% of the coverage [m/k < 0.2] to avoid calling homozygous and heterozygous single nucleotide

5. Results

variants. CIMS sites were found to be almost exclusive C-to-T conversions ($n = 6,225$, $88\% \pm 5.8\%$) independent of the alignment software used (3 aligners $n = 2677$, 2 $n = 2411$, 1 $n = 1137$). For a stringent CITS set, we filtered CITS sites ($n = 22,917$) that mostly truncated at A residues ($n = 11,897$, 52%) and were followed by C residues (CITS-AC; $n = 6,799$, 57%). Two thousand three hundred and two (37%) of C-to-T CIMS overlapped within a 1nt window to CITS-AC sites, suggesting that in many cases the same nucleotide was identified. Together, we considered a set of 13,024 C-to-T conversions CIMS and AC truncation CITS across 2,464 genes for our final S2 cell miCLIP data set. CITS sites were annotated as described before (Wessels et al, 2019). For representation purposes, we simplified the annotation categories. All CITS not annotated to 5'UTR, CDS, 3'UTR, or intron were summarized in the category "other". Enrichments were calculated relative to median feature proportions (5'UTR = 0.08 (131nt), CDS = 0.78 (1309.5nt), 3'UTR = 0.14 (234nt)) determined previously for S2 cells (Wessels et al, 2019). Enrichments for sites annotated as intronic were set to 1.

SELECT

SELECT was performed as described previously (Mao et al, 2019). Briefly, 1 μg total RNA of isolated 3rd instar larval brains of the indicated genotypes was diluted in 5 μM dNTPs, 40 nM up and 40 nM down primers (m^6A_1 up: TAGCCAGTACCGTAGTGCCTGGTTGGTTT TGGTTTGGGTG; m^6A_1 down: CTTTCTTTGGTTTGGTTAATAAC TCAGAGGCTGAGTCGCTGCAT; m^6A_2 up: TAGCCAGTACCGTAGT GCCTGGTTTTCGACTTTGCTTAATTG; m^6A_2 down: CTTTC GGTTTTGGTTTTCAGAGGCTGAGTCGCTGCAT; Control up: TAGCCAGTACCGTAGTGCCTGGTTTTCGACTTTGCTTAATTGT; Control down: TTTTCGGTTTTCGACTTTGCTTAATTGTCGCTGCAT), targeting the m^6A or a control site one nucleotide upstream of the m^6A_2 site on *futsch*, and 1 \times CutSmart buffer (NEB) to 17 μl . Annealing of primers was performed for 1 min at each 90°C, 80°C, 70°C, 60°C, 50°C, and 6 min at 40°C. Afterward, 0.01U Bst 2.0 DNA polymerase, 0.5U SplintR ligase and 10 nmol ATP was added in a total volume of 3 μl and incubated for 20 min at 40°C and 80°C. qPCR for quantification was carried out using 4 μl of SELECT reaction in a 20 μl reaction volume using SYBR green. Relative SELECT products were calculated by normalization to the RNA abundance determined by the control site and the wild-type control.

Statistics

Multiple comparisons of the NMJ phenotypes were performed using one-way ANOVA with a *post hoc* Sidak-Bonferroni correction (n.s. = not significant; * $P < 0.05$; ** $P < 0.01$; *** $P < 0.001$; **** $P < 0.0001$). *P* values of Western blot quantification, RIP experiments, and SELECT were determined with an unpaired, two-tailed Student's *t*-test. (n.s. = not significant; * $p < 0.05$; ** $p < 0.01$; *** $p < 0.001$; **** $p < 0.0001$). The significance of the overlap of the TRIBE and miCLIP datasets was determined by a hypergeometric test.

Data availability

TRIBE-seq: <https://www.ncbi.nlm.nih.gov/bioproject/?term=PRJNA605328>.

miCLIP-seq: <https://www.ncbi.nlm.nih.gov/geo/query/acc.cgi?acc=GSE145342>

RIP-seq: <https://www.ncbi.nlm.nih.gov/geo/query/acc.cgi?acc=GSE161655>

Expanded View for this article is available online.

Acknowledgements

We thank the Bloomington *Drosophila* Stock Center, the Vienna *Drosophila* Resource Center and the *Drosophila* Genomics Resource Center at Indiana University for stocks, plasmids and cell lines; members of the Quattrone and Roignant labs for helpful discussion. We thank the IMB Genomics core facility for their helpful support and the use of its NextSeq500 (INST 247/870-1 FUGG), the advanced Imaging Facility and the Next Generation Sequencing at CIBIO Department for great support. Support by IMB Proteomics Core Facility is gratefully acknowledged (instrument is funded by DFG INST 247/766-1 FUGG). In particular, we wish to thank Anja Freiwald from IMB Proteomics core facility for sample preparation and Dr. Mario Dejung from Proteomics core facility for data processing. We thank Prof. Bassem Hassan and Prof. Paola Bellosta for kindly sharing *Drosophila* stocks and Dr. Fabian Feiguin for sharing stocks and the anti-Futsch antibody. We thank Tobias Jakobi for help with loading TRIBE datasets. Research in the laboratory of J.-Y.R. is supported by the University of Lausanne, the Deutsch-Israelische Projektkooperation (DIP) RO 4681/6-1, the Deutsche Forschungsgemeinschaft RO 4681/9-1, RO 4681/12-1, RO 4681/13-1 and the Epitranscriptome COST action (CA16120). Research in the laboratory of A. Q. is supported by the AIRC Foundation, The CARITRO Foundation, a private donation by the Zobebe family and the Epitranscriptome COST action (CA16120). The Vermeulen lab is part of the OncoCode Institute, which is partly funded by the Dutch Cancer Society (KWF). This project (Alessia Soldano in the A.Q. lab) has received funding from the European Union's Horizon 2020 research and innovation programme under the Marie Skłodowska Curie grant agreement No 752621. Chiara Paolantoni in the lab of J.Y.R. is supported by a Boehringer Ingelheim Fonds fellowship.

Author contributions

AS, LW, AQ, and J-YR conceived the study. AS, LW, CP, SL, MMMu, TL, H-HW, MN, GA, FXRS, MS, RRE, AB, MMMö, MV, FB, JK, UO, CD, ED, AQ, and J-YR performed the methodology. AS and LW wrote the draft of the manuscript. All authors reviewed and edited the manuscript. AS, AQ, and J-YR supervised the study and overall contributed equally.

Conflict of interest

The authors declare that they have no conflict of interest.

References

- Angelova MT, Dimitrova DG, Dinges N, Lence T, Worpenberg L, Carre C, Roignant JY (2018) The emerging field of epitranscriptomics in neurodevelopmental and neuronal disorders. *Front Bioeng Biotechnol* 6: 46
- Arguello AE, DeLiberto AN, Kleiner RE (2017) RNA chemical proteomics reveals the N(6)-methyladenosine (m(6)A)-regulated protein-RNA interactome. *J Am Chem Soc* 139: 17249–17252
- Bagni C, Zukin RS (2019) A synaptic perspective of fragile X syndrome and autism spectrum disorders. *Neuron* 101: 1070–1088
- Bolduc FV, Bell K, Cox H, Broadie KS, Tully T (2008) Excess protein synthesis in *Drosophila* fragile X mutants impairs long-term memory. *Nat Neurosci* 11: 1143–1145

5. Results

- Chang M, Lv H, Zhang W, Ma C, He X, Zhao S, Zhang ZW, Zeng YX, Song S, Niu Y et al (2017) Region-specific RNA m(6A) methylation represents a new layer of control in the gene regulatory network in the mouse brain. *Open Biol* 7: 170166
- Chen E, Sharma MR, Shi X, Agrawal RK, Joseph S (2014) Fragile X mental retardation protein regulates translation by binding directly to the ribosome. *Mol Cell* 54: 407–417
- Chen J, Zhang YC, Huang C, Shen H, Sun B, Cheng X, Zhang YJ, Yang YG, Shu Q, Yang Y et al (2019) m(6A) regulates neurogenesis and neuronal development by modulating histone methyltransferase Ezh2. *Genomics Proteomics Bioinformatics* 17: 154–168
- Coffee Jr RL, Tessier CR, Woodruff III EA, Broadie K (2010) Fragile X mental retardation protein has a unique, evolutionarily conserved neuronal function not shared with FXR1P or FXR2P. *Dis Model Mech* 3: 471–485
- Dahlhaus R (2018) Of Men and Mice: Modeling the Fragile X Syndrome. *Front Mol Neurosci* 11: 41
- Darnell JC, Van Driesche SJ, Zhang C, Hung KY, Mele A, Fraser CE, Stone EF, Chen C, Fak JJ, Chi SW et al (2011) FMRP stalls ribosomal translocation on mRNAs linked to synaptic function and autism. *Cell* 146: 247–261
- Davis JK, Broadie K (2017) Multifarious functions of the fragile X mental retardation protein. *Trends Genet* 33: 703–714
- Dobin A, Davis CA, Schlesinger F, Drenkow J, Zaleski C, Jha S, Batut P, Chaisson M, Gingeras TR (2013) STAR: ultrafast universal RNA-seq aligner. *Bioinformatics* 29: 15–21
- Dotd M, Roehr JT, Ahmed R, Dieterich C (2012) FLEXBAR-flexible barcode and adapter processing for next-generation sequencing platforms. *Biology* 1: 895–905
- Dominissini D, Moshitch-Moshkovitz S, Schwartz S, Salmon-Divon M, Ungar L, Osenberg S, Cesarkas K, Jacob-Hirsch J, Amariglio N, Kupiec M et al (2012) Topology of the human and mouse m⁶A RNA methylomes revealed by m⁶A-seq. *Nature* 485: 201–206
- Drozdz M, Bardoni B, Capovilla M (2018) Modeling fragile X syndrome in *Drosophila*. *Front Mol Neurosci* 11: 124
- Du K, Zhang L, Lee T, Sun T (2019) m(6A) RNA methylation controls neural development and is involved in human diseases. *Mol Neurobiol* 56: 1596–1606
- Edens BM, Vissers C, Su J, Arumugam S, Xu Z, Shi H, Miller N, Rojas Ringeling F, Ming GL, He C et al (2019) FMRP modulates neural differentiation through m(6A)-dependent mRNA nuclear export. *Cell Rep* 28: 845–854
- Edupuganti RR, Geiger S, Lindeboom RGH, Shi H, Hsu PJ, Lu Z, Wang SY, Baltissen MPA, Jansen P, Rossa M et al (2017) N(6)-methyladenosine (m(6)A) recruits and repels proteins to regulate mRNA homeostasis. *Nat Struct Mol Biol* 24: 870–878
- Engel M, Eggert C, Kaplick PM, Eder M, Roh S, Tietze L, Namendorf C, Arloth J, Weber P, Rex-Haffner M et al (2018) The Role of m(6A)/m-RNA Methylation in Stress Response Regulation. *Neuron* 99: 389–403
- Garber K, Smith KT, Reines D, Warren ST (2006) Transcription, translation and fragile X syndrome. *Curr Opin Genet Dev* 16: 270–275
- Garber KB, Visootsak J, Warren ST (2008) Fragile X syndrome. *Eur J Hum Genet* 16: 666–672
- Garcia-Campos MA, Edelheit S, Toth U, Safra M, Shachar R, Viukov S, Winkler R, Nir R, Lasman L, Brandis A et al (2019) Deciphering the "m(6A) Code" via Antibody-Independent Quantitative Profiling. *Cell* 178(3): 731–747
- Hagerman RJ, Des-Portes V, Gasparini F, Jacquemont S, Comez-Mancilla B (2014) Translating molecular advances in fragile X syndrome into therapy: a review. *J Clin Psychiatry* 75: e294–e307
- Hagerman RJ, Miller LJ, McGrath-Clarke J, Riley K, Goldson E, Harris SW, Simon J, Church K, Bonnell J, Ognibene TC et al (2002) Influence of stimulants on electrodermal studies in Fragile X syndrome. *Microsc Res Tech* 57: 168–173
- Hausmann IU, Bodi Z, Sanchez-Moran E, Mongan NP, Archer N, Fray RG, Soller M (2016) m(6A) potentiates Sxl alternative pre-mRNA splicing for robust *Drosophila* sex determination. *Nature* 540: 301–304
- Hsu PJ, Shi H, He C (2017) Epitranscriptomic influences on development and disease. *Genome Biol* 18: 197
- Hsu PJ, Shi H, Zhu AC, Lu Z, Miller N, Edens BM, Ma YC, He C (2019) The RNA-binding protein FMRP facilitates the nuclear export of N(6)-methyladenosine-containing mRNAs. *J Biol Chem* 294: 19889–19895
- Ishizuka A, Siomi MC, Siomi H (2002) A *Drosophila* fragile X protein interacts with components of RNAi and ribosomal proteins. *Genes Dev* 16: 2497–2508
- Jacquemont S, Pacini L, Jonch AE, Cencelli G, Rozenberg I, He Y, D'Andrea L, Pedini G, Eldeeb M, Willemsen R et al (2018) Protein synthesis levels are increased in a subset of individuals with fragile X syndrome. *Hum Mol Genet* 27: 2039–2051
- Jaenisch R, Bird A (2003) Epigenetic regulation of gene expression: how the genome integrates intrinsic and environmental signals. *Nat Genet* 33 (Suppl): 245–254
- Jung Y, Goldman D (2018) Role of RNA modifications in brain and behavior. *Genes Brain Behav* 17: e12444
- Kan L, Grozhik AV, Vedanayagam J, Patil DP, Pang N, Lim KS, Huang YC, Joseph B, Lin CJ, Despic V et al (2017) The m(6A) pathway facilitates sex determination in *Drosophila*. *Nat Commun* 8: 15737
- Kashima R, Redmond PL, Ghatpande P, Roy S, Kornberg TB, Hanke T, Knapp S, Lagna G, Hata A (2017) Hyperactive locomotion in a *Drosophila* model is a functional readout for the synaptic abnormalities underlying fragile X syndrome. *Sci Signal* 10: eaa18133
- Ke S, Alemu EA, Mertens C, Gantman EC, Fak JJ, Mele A, Haripal B, Zucker-Scharff I, Moore MJ, Park CY et al (2015) A majority of m⁶A residues are in the last exons, allowing the potential for 3' UTR regulation. *Genes Dev* 29: 2037–2053
- Kidd SA, Lachiewicz A, Barbooth D, Blitz RK, Delahunty C, McBrien D, Visootsak J, Berry-Kravis E (2014) Fragile X syndrome: a review of associated medical problems. *Pediatrics* 134: 995–1005
- Klemmer P, Meredith RM, Holmgren CD, Klychnikov OI, Stahl-Zeng J, Loos M, van der Schors RC, Wortel J, de Wit H, Spijker S et al (2011) Proteomics, ultrastructure, and physiology of hippocampal synapses in a fragile X syndrome mouse model reveal presynaptic phenotype. *J Biol Chem* 286: 25495–25504
- Koranda JL, Dore L, Shi H, Patel MJ, Vaasjo LO, Rao MN, Chen K, Lu Z, Yi Y, Chi W et al (2018) Mettl14 Is Essential for Epitranscriptomic Regulation of Striatal Function and Learning. *Neuron* 99: 283–292
- Laggerbauer B, Ostareck D, Keidel EM, Ostareck-Lederer A, Fischer U (2001) Evidence that fragile X mental retardation protein is a negative regulator of translation. *Hum Mol Genet* 10: 329–338
- Lasman L, Krupalnik V, Viukov S, Mor N, Aguilera-Castrejón A, Schneir D, Bayerl J, Mizrahi O, Peles S, Tawil S et al (2020) Context-dependent functional compensation between Ythdf m(6A) reader proteins. *Genes Dev* 34: 1373–1391
- Lence T, Akhtar J, Bayer M, Schmid K, Spindler L, Ho CH, Kreim N, Andrade-Navarro MA, Poeck B, Helm M et al (2016) m(6A) modulates neuronal functions and sex determination in *Drosophila*. *Nature* 540: 242–247
- Lence T, Paolantoni C, Worpenberg L, Roignant JY (2019) Mechanistic insights into m(6A) RNA enzymes. *Biochim Biophys Acta Gene Regul Mech* 1862: 222–229

5. Results

- Lence T, Soller M, Roignant JY (2017) A fly view on the roles and mechanisms of the m(6)A mRNA modification and its players. *RNA Biol* 14: 1232–1240
- Li H, Durbin R (2009) Fast and accurate short read alignment with Burrows-Wheeler transform. *Bioinformatics* 25: 1754–1760
- Li J, Yang X, Qi Z, Sang Y, Liu Y, Xu B, Liu W, Xu Z, Deng Y (2019) The role of mRNA m(6)A methylation in the nervous system. *Cell Biosci* 9: 66
- Li L, Zang L, Zhang F, Chen J, Shen H, Shu L, Liang F, Feng C, Chen D, Tao H et al (2017) Fat mass and obesity-associated (FTO) protein regulates adult neurogenesis. *Hum Mol Genet* 26: 2398–2411
- Li M, Zhao X, Wang W, Shi H, Pan Q, Lu Z, Perez SP, Suganthan R, He C, Bjoras M et al (2018) Ythdf2-mediated m(6)A mRNA clearance modulates neural development in mice. *Genome Biol* 19: 69
- Li Z, Zhang Y, Ku L, Wilkinson KD, Warren ST, Feng Y (2001) The fragile X mental retardation protein inhibits translation via interacting with mRNA. *Nucleic Acids Res* 29: 2276–2283
- Liao S, Sun H, Xu C (2018) YTH domain: a family of N(6)-methyladenosine (m(6)A) readers. *Genomics Proteomics Bioinformatics* 16: 99–107
- Linder B, Grozhik AV, Olarerin-George AO, Meydan C, Mason CE, Jaffrey SR (2015) Single-nucleotide-resolution mapping of m⁶A and m⁵Am throughout the transcriptome. *Nat Methods* 12: 767–772
- Livneh I, Moshitch-Moshkovitz S, Amariglio N, Rechavi G, Dominissini D (2020) The m(6)A epitranscriptome: transcriptome plasticity in brain development and function. *Nat Rev Neurosci* 21: 36–51
- Love MI, Huber W, Anders S (2014) Moderated estimation of fold change and dispersion for RNA-seq data with DESeq2. *Genome Biol* 15: 550
- Lu R, Wang H, Liang Z, Ku L, O'Donnell WT, Li W, Warren ST, Feng Y (2004) The fragile X protein controls microtubule-associated protein 1B translation and microtubule stability in brain neuron development. *Proc Natl Acad Sci USA* 101: 15201–15206
- Ma C, Chang M, Lv H, Zhang ZW, Zhang W, He X, Wu G, Zhao S, Zhang Y, Wang D et al (2018) RNA m(6)A methylation participates in regulation of postnatal development of the mouse cerebellum. *Genome Biol* 19: 68
- Mao Y, Dong L, Liu XM, Guo J, Ma H, Shen B, Qian SB (2019) m(6)A in mRNA coding regions promotes translation via the RNA helicase-containing YTHDC2. *Nat Commun* 10: 5332
- Martin M (2011) Cutadapt removes adapter sequences from high-throughput sequencing reads. *EMBnet Journal* 17: 10–12
- Maurin T, Zongaro S, Bardoni B (2014) Fragile X Syndrome: from molecular pathology to therapy. *Neurosci Biobehav Rev* 46(Pt 2): 242–255
- McMahon AC, Rahman R, Jin H, Shen JL, Fieldsend A, Luo W, Rosbash M (2016) TRIBE: hijacking an RNA-editing enzyme to identify cell-specific targets of RNA-binding proteins. *Cell* 165: 742–753
- Merkurjev D, Hong WT, Iida K, Oomoto I, Goldie BJ, Yamaguti H, Ohara T, Kawaguchi SY, Hirano T, Martin KC et al (2018) Synaptic N(6)-methyladenosine (m(6)A) epitranscriptome reveals functional partitioning of localized transcripts. *Nat Neurosci* 21: 1004–1014
- Meyer KD, Saletore Y, Zumbo P, Elemento O, Mason CE, Jaffrey SR (2012) Comprehensive analysis of mRNA methylation reveals enrichment in 3' UTRs and near stop codons. *Cell* 149: 1635–1646
- Mi H, Muruganujan A, Huang X, Ebert D, Mills C, Guo X, Thomas PD (2019) Protocol update for large-scale genome and gene function analysis with the PANTHER classification system (v.14.0). *Nat Protoc* 14: 703–721
- Michel CI, Kraft R, Restifo LL (2004) Defective neuronal development in the mushroom bodies of *Drosophila* fragile X mental retardation 1 mutants. *J Neurosci* 24: 5798–5809
- Patil DP, Pickering BF, Jaffrey SR (2018) Reading m(6)A in the transcriptome: m(6)A-binding proteins. *Trends Cell Biol* 28: 113–127
- Reeve SP, Bassetto L, Genova GK, Kleyner Y, Leyssen M, Jackson FR, Hassan BA (2005) The *Drosophila* fragile X mental retardation protein controls actin dynamics by directly regulating profilin in the brain. *Curr Biol* 15: 1156–1163
- Roignant JY, Soller M (2017) m(6)A in mRNA: an ancient mechanism for fine-tuning gene expression. *Trends Genet* 33: 380–390
- Rousseau F, Labelle Y, Bussieres J, Lindsay C (2011) The fragile x mental retardation syndrome 20 years after the FMR1 gene discovery: an expanding universe of knowledge. *Clin Biochem Rev* 32: 135–162
- Sahoo PK, Lee SJ, Jaiswal PB, Alber S, Kar AN, Miller-Randolph S, Taylor EE, Smith T, Singh B, Ho TS et al (2018) Axonal G3BP1 stress granule protein limits axonal mRNA translation and nerve regeneration. *Nat Commun* 9: 3358
- Santoro MR, Bray SM, Warren ST (2012) Molecular mechanisms of fragile X syndrome: a twenty-year perspective. *Annu Rev Pathol* 7: 219–245
- Schaefer TL, Davenport MH, Erickson CA (2015) Emerging pharmacologic treatment options for fragile X syndrome. *Appl Clin Genet* 8: 75–93
- Shah A, Qian Y, Weyn-Vanhenenryck SM, Zhang C (2017) CLIP Tool Kit (CTK): a flexible and robust pipeline to analyze CLIP sequencing data. *Bioinformatics* 33: 566–567
- Shi H, Zhang X, Weng YL, Lu Z, Liu Y, Lu Z, Li J, Hao P, Zhang Y, Zhang F et al (2018) m(6)A facilitates hippocampus-dependent learning and memory through YTHDF1. *Nature* 563: 249–253
- Stefani G, Fraser CE, Darnell JC, Darnell RB (2004) Fragile X mental retardation protein is associated with translating polyribosomes in neuronal cells. *J Neurosci* 24: 7272–7276
- Suhl JA, Chopra P, Anderson BR, Bassell GJ, Warren ST (2014) Analysis of FMRP mRNA target datasets reveals highly associated mRNAs mediated by G-quadruplex structures formed via clustered WCGA sequences. *Hum Mol Genet* 23: 5479–5491
- Supek F, Bošnjak M, Škunca N, Šmuc T (2011) REVIGO summarizes and visualizes long lists of gene ontology terms. *PLoS One* 6: e21800
- Sutandy FX, Hildebrandt A, König J (2016) Profiling the binding sites of RNA-binding proteins with nucleotide resolution using iCLIP. *Methods Mol Biol* 1358: 175–195
- Thomas A, Lee PJ, Dalton JE, Nomie KJ, Stoica L, Costa-Mattioli M, Chang P, Nuzhdin S, Arbeitman MN, Dierick HA (2012) A versatile method for cell-specific profiling of translated mRNAs in *Drosophila*. *PLoS One* 7: e40276
- Ui K, Nishihara S, Sakuma M, Togashi S, Ueda R, Miyata Y, Miyake T (1994) Newly established cell lines from *Drosophila* larval CNS express neural specific characteristics. *Vitro Cell Dev Biol Anim* 30A: 209–216
- Utari A, Adams E, Berry-Kravis E, Chavez A, Scaggis F, Ngotran L, Boyd A, Hessl D, Gane LW, Tassone F et al (2010) Aging in fragile X syndrome. *J Neurodev Disord* 2: 70–76
- Verheyen EM, Cooley L (1994) Profilin mutations disrupt multiple actin-dependent processes during *Drosophila* development. *Development* 120: 717–728
- Wang CX, Cui GS, Liu X, Xu K, Wang M, Zhang XX, Jiang LY, Li A, Yang Y, Lai WY et al (2018) METTL3-mediated m⁶A modification is required for cerebellar development. *PLoS Biol* 16: e2004880
- Webster CL, Longdon B, Lewis SH, Obbard DJ (2016) Twenty-five new viruses associated with the *Drosophilidae* (Diptera). *Evol Bioinform Online* 12: 13–25
- Weng YL, Wang X, An R, Cassin J, Vissers C, Liu Y, Liu Y, Xu T, Wang X, Wong SZH et al (2018) Epitranscriptomic m(6)A regulation of axon regeneration in the adult mammalian nervous system. *Neuron* 97: 313–325
- Wessels HH, Lebedeva S, Hirsekorn A, Wurmus R, Akalin A, Mukherjee N, Ohler U (2019) Global identification of functional microRNA-mRNA interactions in *Drosophila*. *Nat Commun* 10: 1626

5. Results

- Widagdo J, Anggono V (2018) The m⁶A-epitranscriptomic signature in neurobiology: from neurodevelopment to brain plasticity. *J Neurochem* 147: 137–152
- Widagdo J, Zhao QY, Kempen MJ, Tan MC, Ratnu VS, Wei W, Leighton L, Spadaro PA, Edson J, Anggono V et al (2016) Experience-dependent accumulation of N⁶-methyladenosine in the prefrontal cortex is associated with memory processes in mice. *J Neurosci* 36: 6771–6777
- Worpenberg L, Jakobi T, Dieterich C, Roignant JY (2019) Identification of methylated transcripts using the TRIBES approach. *Methods Mol Biol* 1870: 89–106
- Xiao Y, Wang Y, Tang Q, Wei L, Zhang X, Jia G (2018) An elongation- and ligation-based qPCR amplification method for the radiolabeling-free detection of locus-specific N(6)-methyladenosine modification. *Angew Chem Int Ed Engl* 57: 15995–16000
- Xu D, Shen W, Guo R, Xue Y, Peng W, Sima J, Yang J, Sharov A, Srikantan S, Yang J et al (2013) Top3beta is an RNA topoisomerase that works with fragile X syndrome protein to promote synapse formation. *Nat Neurosci* 16: 1238–1247
- Xu W, Rahman R, Rosbash M (2018) Mechanistic implications of enhanced editing by a HyperTRIBES RNA-binding protein. *RNA* 24: 173–182
- Yoon KJ, Ming GL, Song H (2018) Epitranscriptomes in the adult mammalian brain: dynamic changes regulate behavior. *Neuron* 99: 243–245
- Yu J, Chen M, Huang H, Zhu J, Song H, Zhu J, Park J, Ji SJ (2018) Dynamic m⁶A modification regulates local translation of mRNA in axons. *Nucleic Acids Res* 46: 1412–1423
- Zaccara S, Jaffrey SR (2020) A Unified Model for the Function of YTHDF Proteins in Regulating m(6)A-Modified mRNA. *Cell* 181: 1582–1595
- Zhang F, Kang Y, Wang M, Li Y, Xu T, Yang W, Song H, Wu H, Shu Q, Jin P (2018) Fragile X mental retardation protein modulates the stability of its m⁶A-marked messenger RNA targets. *Hum Mol Genet* 27: 3936–3950
- Zhang YQ, Bailey AM, Matthies HJ, Renden RB, Smith MA, Speese SD, Rubin GM, Broadie K (2001) *Drosophila* fragile X-related gene regulates the MAP1B homolog Futsch to control synaptic structure and function. *Cell* 107: 591–603
- Zhao BS, Roundtree IA, He C (2017) Post-transcriptional gene regulation by mRNA modifications. *Nat Rev Mol Cell Biol* 18: 31–42
- Zhao YL, Liu YH, Wu RF, Bi Z, Yao YX, Liu Q, Wang YZ, Wang XX (2019) Understanding m(6)A function through uncovering the diversity roles of YTH domain-containing proteins. *Mol Biotechnol* 61: 355–364
- Zhuang M, Li X, Zhu J, Zhang J, Niu F, Liang F, Chen M, Li D, Han P, Ji SJ (2019) The m⁶A reader YTHDF1 regulates axon guidance through translational control of Robo3.1 expression. *Nucleic Acids Res* 47: 4765–4777



License: This is an open access article under the terms of the Creative Commons Attribution-NonCommercial-NoDeriv 4.0 License, which permits use and distribution in any medium, provided the original work is properly cited, the use is non-commercial and no modifications or adaptations are made.

Expanded View Figures

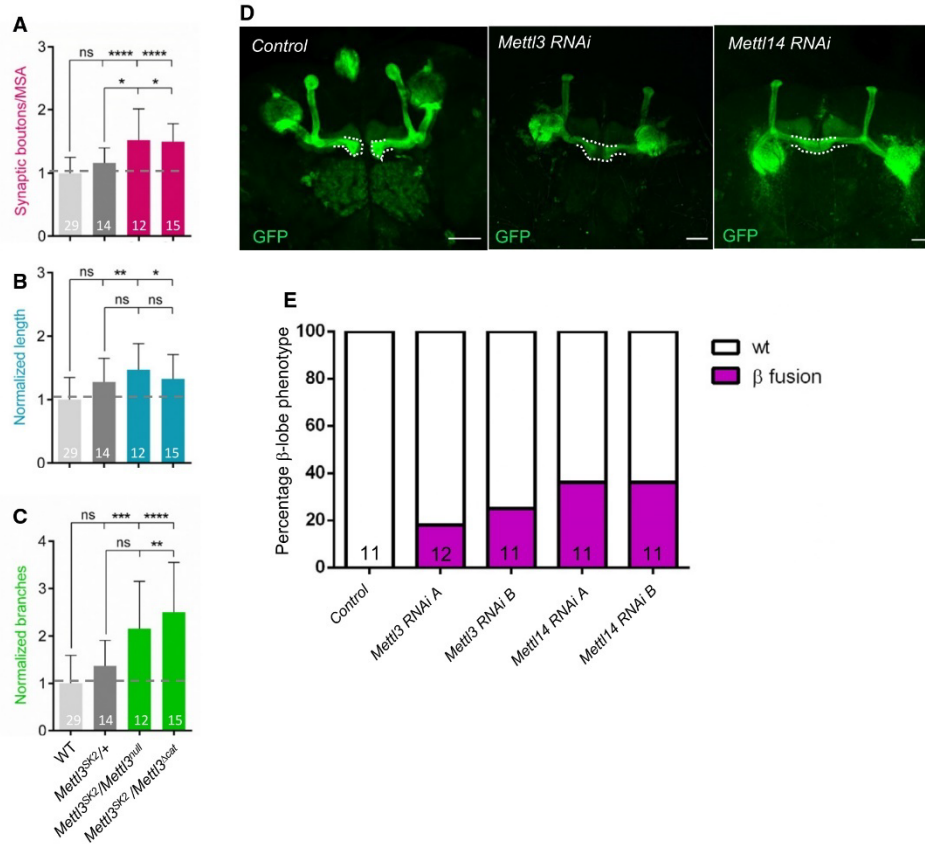


Figure EV1. m⁶A writer components control axonal growth at NMJ and MB.

A–C Quantification of normalized bouton number (A, total number of boutons/muscle surface area ($\mu\text{m}^2 \times 1,000$)), normalized axon length (B), and normalized branching (C) of muscle-6/7 NMJ in hemisegments A2–A3 of the indicated genotypes. Bars show mean \pm s.e.m. Multiple comparisons were performed using one-way ANOVA with a *post hoc* Sidak–Bonferroni correction (n.s. = not significant; * $P < 0.05$; ** $P < 0.01$; *** $P < 0.001$; **** $P < 0.0001$).

D Analysis of adult control *c772Gal:UAS-CD8,GFP*, *c772Gal:UAS-CD8,GFP:Mettl3 RNAi* (*u20969*) and *c772Gal:UAS-CD8,GFP:Mettl14 RNAi* (*u48560*) MB in the brains by visualization of the membrane GFP autofluorescence. White dashed lines highlight the normal and fused β -lobes. Scale bar 50 μm .

E Quantification of the penetrance of β -lobe fusion phenotype in the following genotypes: control (*c772Gal:UAS-CD8,GFP/+*), *c772Gal:UAS-CD8,GFP:Mettl3 RNAi* (*u20968*) indicated as RNAi A, *c772Gal:UAS-CD8,GFP:Mettl3 RNAi* (*u20969*) indicated as RNAi B, *c772Gal:UAS-CD8,GFP:Mettl14 RNAi* (*u13542*) indicated as RNAi A and *c772Gal:UAS-CD8,GFP:Mettl14 RNAi* (*u48560*) indicated as RNAi B.

Data information: In (A–C, E), bars are labeled with the number of replicates.

5. Results

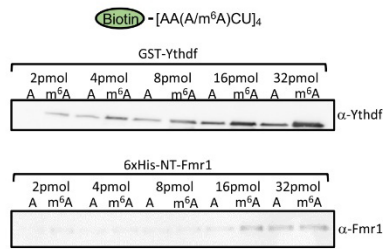


Figure EV2. Binding behavior of Ythdf and Fmr1 on RNA probe in the AAACU sequence context.
Results of m⁶A RNA pulldown using RNA probes. Pulldown were performed using biotinylated probes containing four AAACU m⁶A consensus sites, with or without the methylation and recombinant purified GST-Ythdf and His-NT-Fmr1 proteins. Ythdf binds more efficiently upon methylation, while Fmr1 does not show specificity for any of the probes.

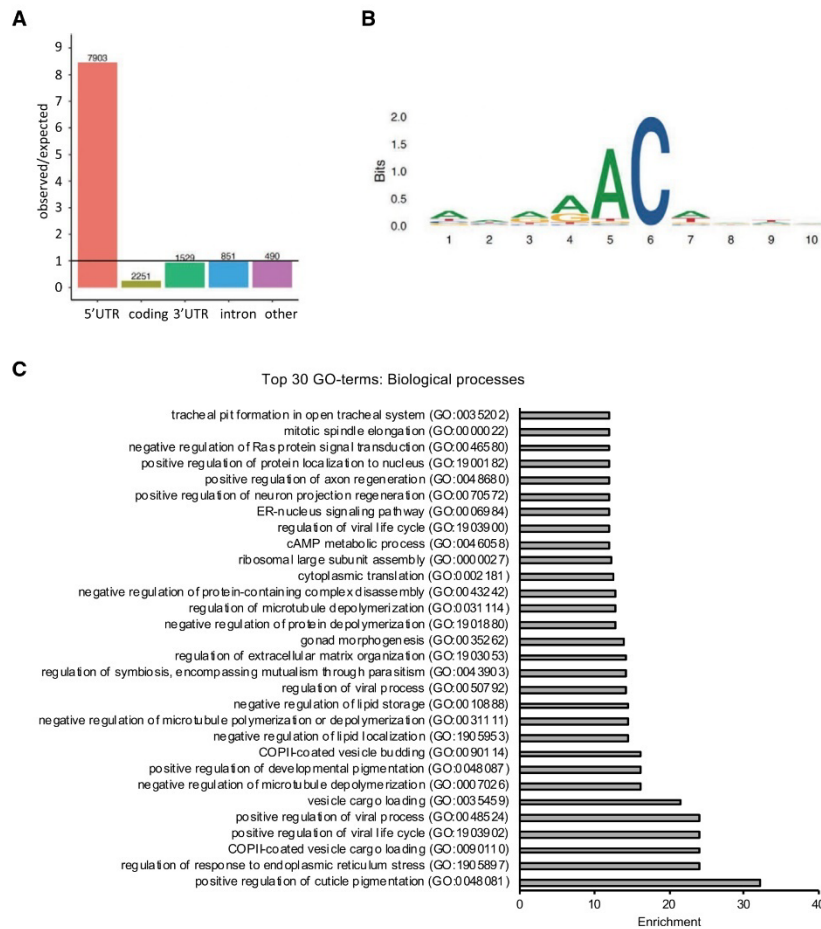


Figure EV3.

5. Results

Figure EV3. miCLIP analysis from S2R⁺ cells.
 A Relative enrichment of m⁶A peaks across transcript segments identified by miCLIP. The numbers above the bars correspond to the number of m⁶A sites determined as described in the Materials and Methods section. In total, a set of 13024 C-to-T conversions and AC truncation CITS across 2464 genes was identified.
 B Sequence logo of deduced consensus motif for m⁶A peaks centered on the modified adenosine.
 C Top 30 enriched Gene ontology (GO)-terms of biological processes for the gene set of m⁶A modified and Fmr1- and Ythdf-bound transcripts.

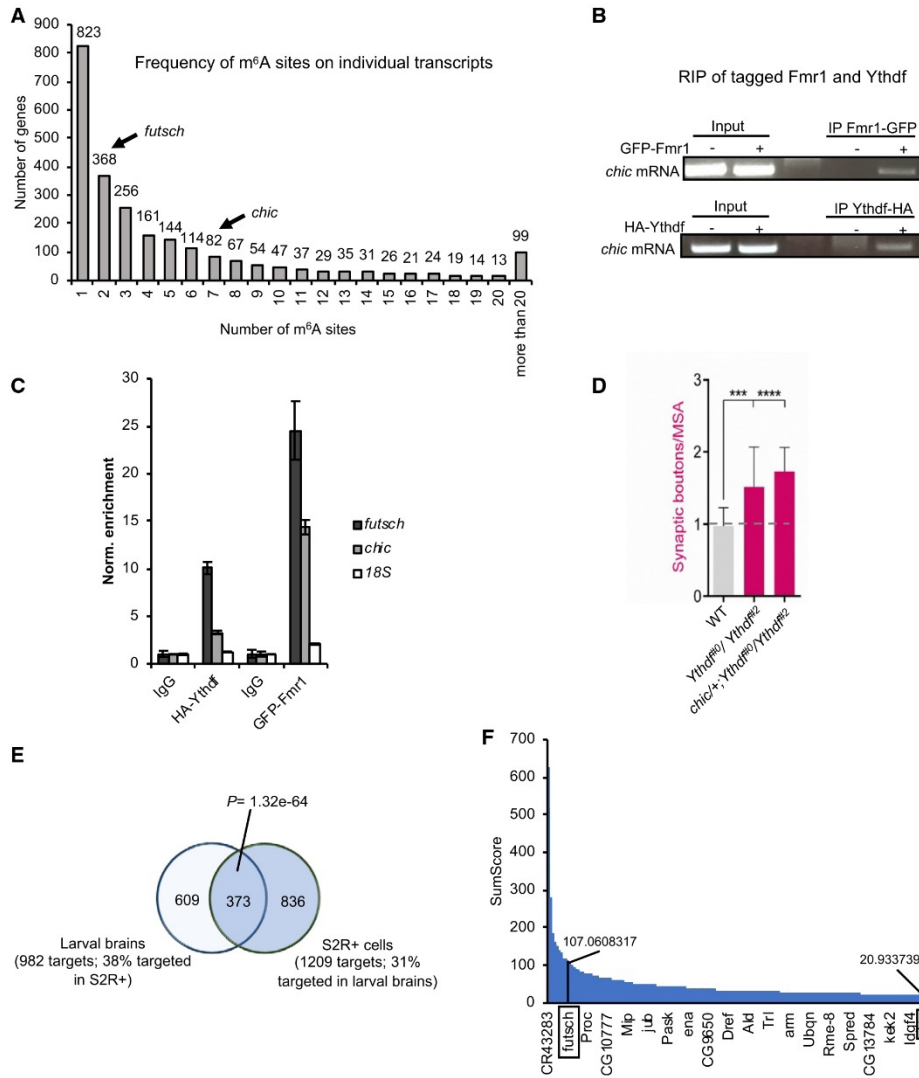


Figure EV4.

5. Results

Figure EV4. Fmr1 and Ythdf bind *chic* and *futsch* transcripts.

A Graph showing the frequency of m⁶A sites on individual transcripts identified by miCLIP-seq.
 B RNA Immunoprecipitation of GFP-tagged Fmr1 (*Elav-Gal4; UAS-Fmr1-GFP*) or HA-tagged Ythdf (*Elav-Gal4; UAS-Ythdf-HA*) from 50 adult heads. The RNA was then reverse-transcribed and analyzed via PCR with primers designed on *chic* transcript.
 C RNA immunoprecipitation assay. Quantification of *futsch* and *chic* RNA levels upon immunoprecipitation of pan-neuronally expressed GFP-tagged Fmr1 or HA-tagged Ythdf in 3rd instar larvae. *I85* mRNA serves as a negative control for unspecific enrichment.
 D Quantification of normalized bouton number (total number of boutons/muscle surface area (μm² × 1,000)) of muscle-6/7 NMJ in hemisegments A2–A3 of the indicated genotypes (n = 20). Bars show mean ± s.e.m. Multiple comparisons were performed using one-way ANOVA with a *post hoc* Sidak–Bonferroni correction (***P < 0.001; ****P < 0.0001).
 E Vein diagram showing the overlap of Ythdf-TRIBE datasets produced in S2R+ cells and in larval brain. The P-value is calculated by hypergeometric test.
 F Graph showing the distribution of SumScores of all identified Ythdf mRNA targets by TRIBE in the larval nervous system. The position and SumScores of *futsch* and *chic* are marked in the graph.

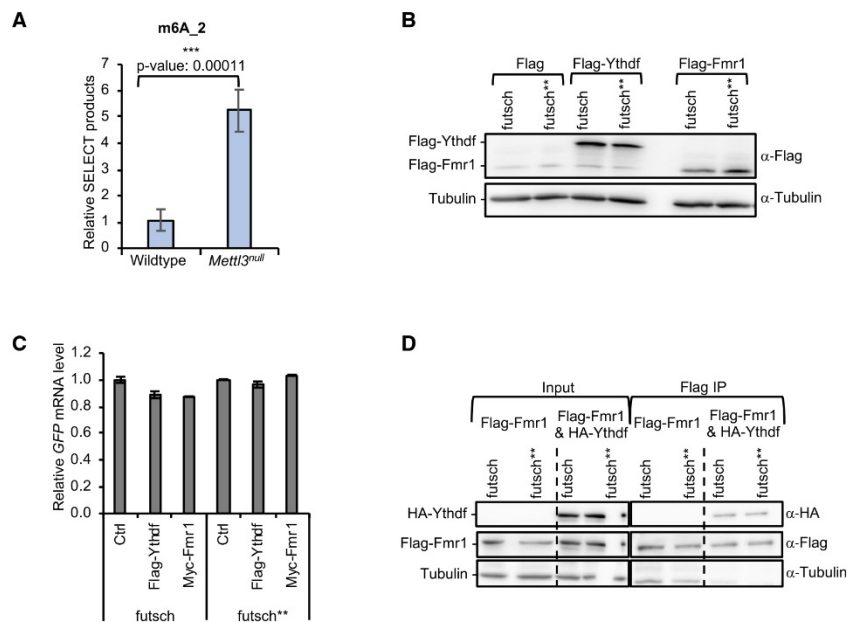
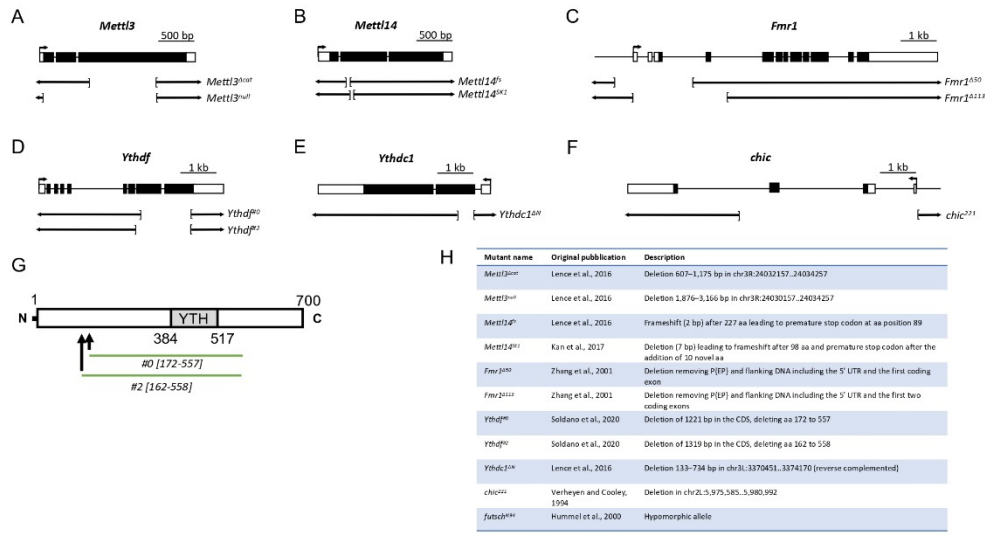


Figure EV5. Controls for assay with the *futsch* 5'UTR reporter.

A Relative amount of SELECT qPCR products targeting the m⁶A_2 site on *futsch* using total RNA of Wild-type or *Mett13^{null}* larval brains. Bars show average ± SD of biological triplicates. P values were determined with a Student's t-test. (***P < 0.001).
 B Representative Western blot analysis showing the protein input level for RNA immunoprecipitation experiment of *futsch* 5'UTR GFP reporter.
 C Relative GFP mRNA input level for RNA immunoprecipitation experiment of *futsch* 5'UTR GFP reporter. *Rpl15* served as a normalization control. Experiments were performed in triplicates. Bars show average ± SD.
 D Representative Western blot analysis showing the protein input level and IP efficiencies for RNA immunoprecipitation experiment of *futsch* 5'UTR GFP reporter in the presence of HA-Ythdf and Flag-Fmr1.

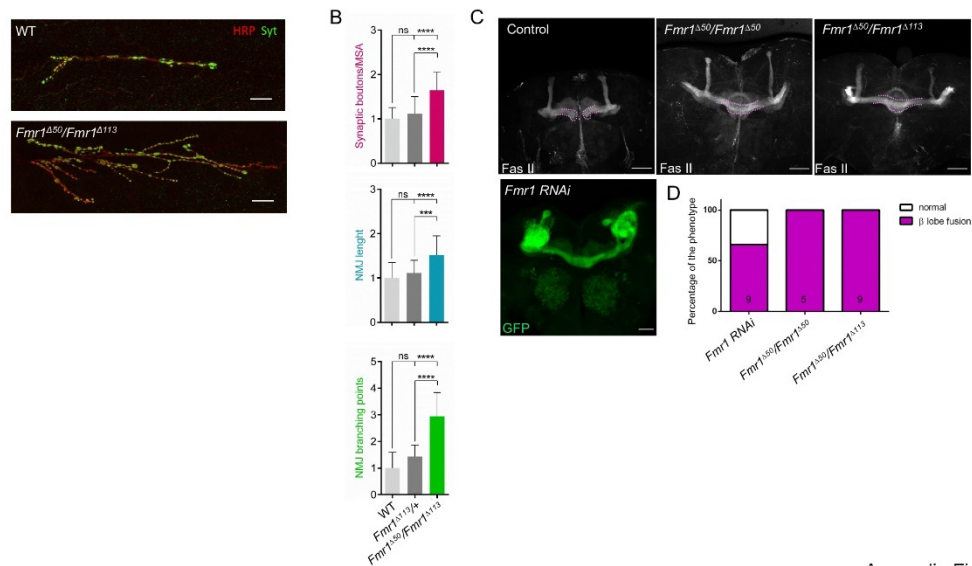
5. Results



Appendix Figure S1: Molecular information of the alleles used in this study

(A-F) *Mettl3* (A), *Mettl14* (B), *Fmr1* (C), *Ythdf* (D), *Ythdc1* (E) and *chic* (F) loci with indicated deletions. (G) Schematic showing the deleted parts (in green) of the *Ythdf* protein (H) Table recapitulating the information about the origins and molecular deletions of the alleles used in this study.

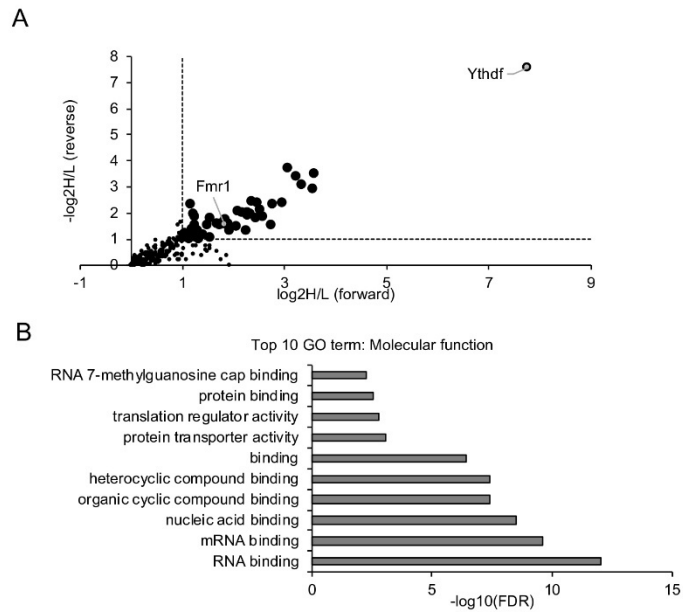
5. Results



Appendix Figure S2: *Fmr1* loss of function is reminiscent to the *m⁶A* loss

(A) Representative confocal images of muscle-6/7 NMJ synapses of abdominal hemisegments A2-A3 for the indicated genotypes labelled with anti-Synaptotagmin (green) and HRP (red) to reveal the synaptic vesicles and the neuronal membrane. Scale bar: 20 μ m. (B) Quantification of normalized bouton number, normalized axon length and normalized branching of NMJ 6/7 in A2-A3 of the indicated genotypes. Error bars show mean \pm s.e.m. Multiple comparisons were performed using one-way ANOVA with a post-hoc Sidak-Bonferroni correction. (n.s. = not significant; $p < 0.001 = **$; $p < 0.0001 = ****$). (C) Immunofluorescence analysis of adult control, *Fmr1^{Δ50}/Fmr1^{Δ50}* and *Fmr1^{Δ50}/Fmr1^{Δ113}* with anti FasII antibody. The *Fmr1^{Δ50}/Fmr1^{Δ50}* brains were dissected few hours prior to eclosion since no homozygote viable adults were obtained. For *c772Gal:UAS-CD8,GFP:Fmr1 (8833) RNAi* brain, MBs are marked by membrane GFP (autofluorescence). Scale bar 50 μ m. (D) Quantification of the penetrance of β -lobe fusion phenotype for the indicated genotypes.

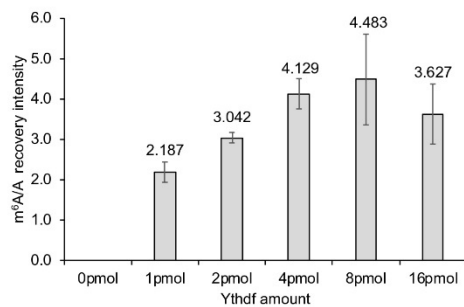
5. Results



Appendix Figure S3: Ythdf interactome

(A) Quantitative proteomics upon pulldown of Flag-tagged Ythdf in S2R+ cells. Scatter plot of normalized forward versus inverted reverse experiments plotted on a \log_2 scale. The threshold was set to a 1-fold enrichment (dashed line). (B) Top 10 enriched Gene ontology (GO)-terms of Molecular function for Ythdf interactors.

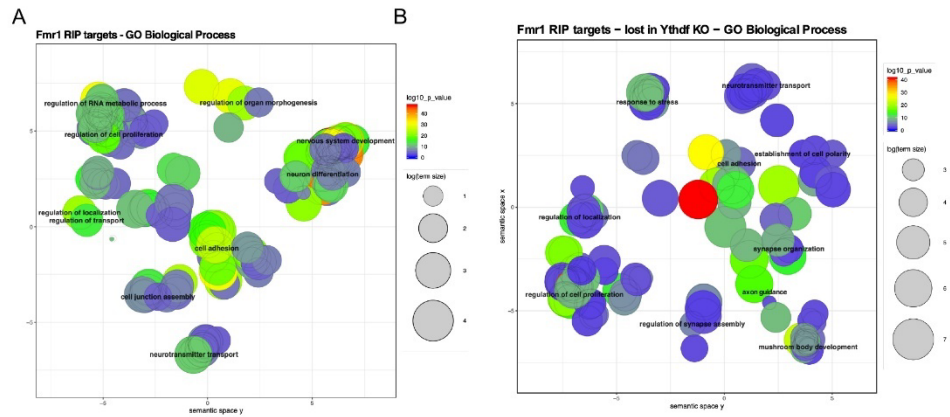
5. Results



Appendix Figure S4: Enrichment of Ythdf in m⁶A probe pulldown fraction is not influenced by Fmr1

Quantification of the enrichment of GST-Ythdf upon pulldown of GGACU RNA probes incubated with 4 pmol of His-NT-Fmr1 and increasing amounts of GST-Ythdf, plotted as the median of the m⁶A/A signal intensity +/- SEM of all replicates.

5. Results



Appendix Figure S5: Gene ontology analysis of FMR1-bound mRNAs

(A) Plot of significantly enriched Gene Ontology Biological Process terms in wild type Fmr1 RNA immunoprecipitation targets. Terms are plotted in semantic space, with functionally closer terms closer to one another in the plot. Representatives for each term group are indicated by their name. Adjusted p-values are indicated by the color scale, while term plot size is a function of the corresponding number of genes. (B) Plot of significantly enriched Gene Ontology Biological Process terms in genes lost in *Ythdf* KO samples. Terms are plotted in semantic space, with functionally closer terms closer to one another in the plot. Representatives for each term group are indicated by their name. Adjusted p-values are indicated by the color scale, while term plot size is a function of the corresponding number of genes.

5.3 Section 3

5.3.1 Identification of m⁶A readers in *Drosophila melanogaster*

As described in section 2 of the results, we sought to identify the reader proteins mediating m⁶A functions in the nervous system of flies. To this aim, we performed *in vitro* RNA pull-down assays by incubating biotinylated RNA probes containing four repeats of the m⁶A consensus sequence GG(A/m⁶A)CU with protein extracts from larval CNS-derived BG3 cells. After pull-down with streptavidin beads and stringent washes, the bound proteins were identified by mass spectrometry. In addition to the two *Drosophila* YTH proteins, Ythdc1 and Ythdf, and the fly orthologue of FMR1, the RNA helicase CG1582 was identified among the factors showing preferential binding to the methylated RNA probe.

CG1582 belongs to the family of DExD/H box RNA helicases. RNA helicases are evolutionary conserved enzymes that bind and remodel RNA or ribonucleoprotein complexes (RNPs) via ATP hydrolysis taking part in nearly all aspects of RNA metabolism from transcription to decay. The human homologue of CG1582 is DHX57, however neither of the two proteins were mechanistically linked to any aspect of RNA metabolism so far, underlying the necessity for further investigation. In *Drosophila melanogaster*, the *CG1582* gene (hereafter renamed to *Dhx57*) codes for a 146 kDa protein containing two recombinase A (RecA)-like domains (DExD/H box and helicase C-term domains) arranged in tandem, which are involved in RNA binding as well as ATP hydrolysis and are typical of proteins belonging to the helicase superfamilies 1-2, a helicase-associated domain (HA2) and an OB fold, which collaborate with the N-terminal RecA domains for the binding of RNA substrates, and a RWD domain of unknown function (Figure 6A).

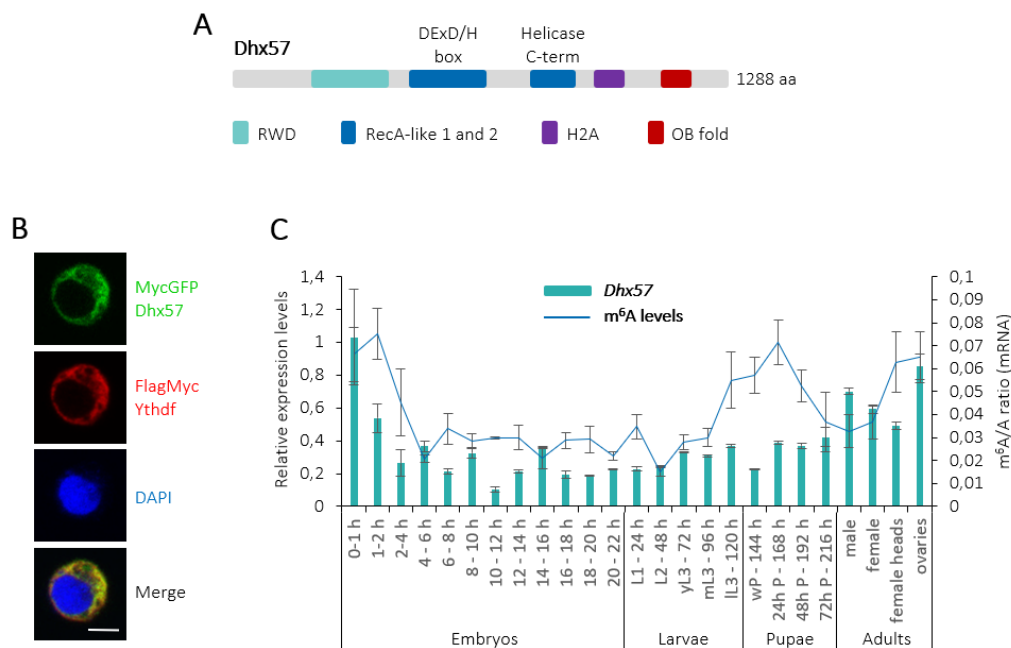


Figure 6. Dhx57 localizes to the cytoplasm and its expression correlates with m⁶A profile during fly development.

5. Results

A) Schematic representation of the Dhx57 protein with known protein domains. **B)** Immunostaining of MycGFP-Dhx57 (green) overexpressed in S2R+ cells. FlagMyc-Ythdf (red) served as cytoplasmic marker. DAPI staining is shown in blue. Scale bar: 10 μ m. **C)** Relative expression of the *Dhx57* transcript during *Drosophila* development (*w1118* flies) analyzed by RT-qPCR. Levels of m⁶A modification were analyzed in the same mRNA samples using LC-MS/MS. Bars represent the mean \pm standard deviation of three technical measurements from three biological replicates.

Firstly, we inspected the subcellular localization of the Dhx57 protein by cloning the corresponding cDNA in an expression vector with a N-terminal MycGFP-tag and co-expressed it in S2R+ cells along with FlagMyc-tagged Ythdf as cytoplasmic marker. The Dhx57 protein displayed a strict cytoplasmic localization (**Figure 6B**), suggesting that it might exert its helicase function during the steps of RNA metabolism taking place in the cell cytosol. We next examined the expression profile of *Dhx57* over the course of the fly development monitoring its mRNA abundance during *Drosophila* developmental stages by RT-qPCR. Interestingly, *Dhx57* transcript levels were highest during early embryogenesis and in ovaries, which is consistent with transcript distribution of other proteins involved in the m⁶A pathway and with the m⁶A profile during fly development (Lence et al., 2016) (**Figure 6C**).

5.3.2 Dhx57 preferentially binds to m⁶A-modified RNA

In light of Dhx57 localization to the cytoplasm, we next decided to explore whether the cytoplasmic m⁶A reader Ythdf had an effect on the enrichment of Dhx57 in the methylated probe pull-down fraction. To this aim, RNA pull-down experiments were repeated in S2R+ cells upon control and Ythdf depletion. We found that Dhx57 preferential binding to the m⁶A-modified probe was not affected in the absence of Ythdf, suggesting that Ythdf does not mediate the binding of Dhx57 to methylated sites (**Figure 7A-B**).

We also tested the binding of Dhx57 to RNA probes containing four repeats of the alternative m⁶A consensus sequence AA(A/m⁶A)CU identified in *Drosophila* miCLIP datasets (Kan et al., 2017, 2021; Worpenberg et al., 2021). While both Ythdc1 and Ythdf displayed enrichment for binding to the m⁶A-modified AAACU probe over the non-modified one, Dhx57 was not detected in the methylated probe pull-down fraction (**Figure 7D**). To further validate the results obtained via quantitative proteomics, additional RNA pull-down experiments were performed incubating protein lysates from S2R+ cells expressing Myc-tagged Dhx57 with the same m⁶A-modified or unmodified RNA probes used previously. Probes were pulled-down with streptavidin-coupled magnetic beads and recovered proteins were analysed by western blot. Lysate containing the Myc-GFP protein was used as negative control and, as expected, the protein did not bind any of the probes. Consistently with the results of the RNA pull-downs performed in BG3 and S2R+ cells, Dhx57 recognized the m⁶A-modified GGACU probe considerably better than the unmethylated one, with a binding selectivity comparable to that of the known m⁶A reader Ythdc1, while it did not show preferential binding to m⁶A within the AAACU motif (**Figure 7E**).

In summary, these results indicate that *Drosophila* Dhx57 preferentially binds to m⁶A-modified RNA in the GGACU sequence context and that m⁶A recognition is not mediated by Ythdf.

5. Results

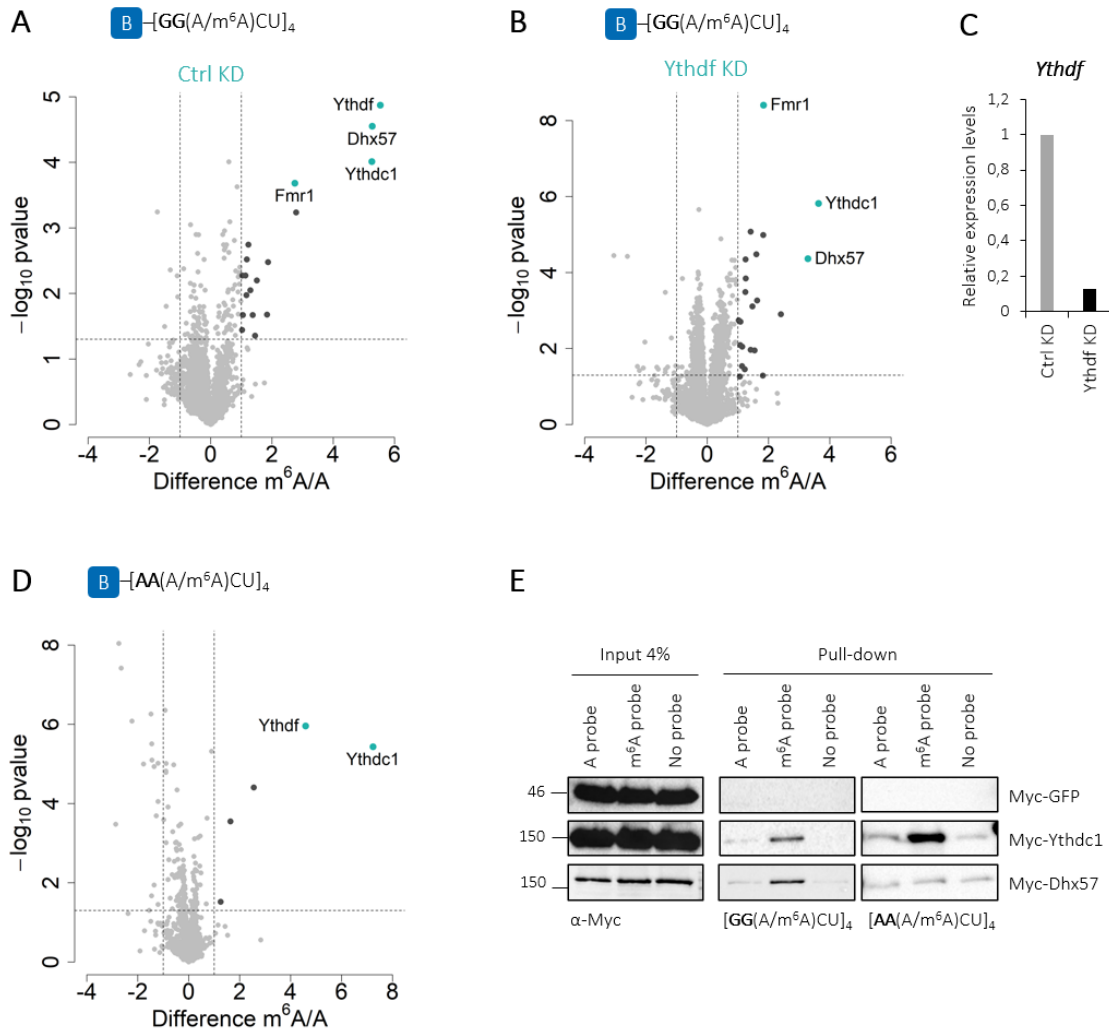


Figure 7. Dhx57 protein preferentially binds m⁶A-modified RNA in the GGACU sequence context.

A-B-D) Mass spectrometry analysis of RNA pull-downs in S2R+ protein cell extracts. Pull-downs were performed using biotinylated probes containing four m⁶A consensus sites [GG(A/m⁶A)CU] (**A-B**) or [AA(A/m⁶A)CU] (**D**) upon control (**A**) or Ythdf (**B**) depletion. P-value is calculated from a two-sided t-test with unequal variants (Welch t-test). Dashed lines represent -log₁₀ P-value = 1 as well as log₂ enrichment = 1. Significantly enriched proteins are depicted in black and highlighted in light blue when the name is shown. **C)** Relative expression levels of *Ythdf* as validation of its KD efficiency. Average of three technical measurements is shown. **E)** RNA pull-down using biotinylated probes of repetitive [GG(A/m⁶A)CU] sequences and protein extracts from S2R+ cells transfected with either Myc-GFP, Myc-Ythdc1 or Myc-Dhx57. Western blot using anti-Myc antibody.

Next, to investigate whether the preferential binding to m⁶A-modified RNA was specific to Dhx57 or a feature shared with other RNA helicases belonging to the DEAH box family, affinity of Dhx57's paralogs (**Figure 8A**) to methylated/unmethylated GGACU RNA probes was analyzed in S2R+ cells. While the closest paralog to Dhx57, Dhx36, was efficiently pulled-down by both RNA probes and showed a slight preference for the m⁶A-modified one, Dhx34 and Dhx9 proteins displayed no clear binding to neither methylated nor unmethylated probe (**Figure 8B**). These results suggest that m⁶A binding is not common to *Drosophila* DEAH box helicases but it is a peculiar ability of Dhx57. To better understand the molecular basis of such specificity, we aimed to narrow down the region of Dhx57 required for binding to m⁶A-

5. Results

modified RNA. To do so, we performed RNA pull-down assays using full-length as well as fragments of Dhx57 in different combinations (**Figure 8C**). Unfortunately, neither single fragments nor combination of them was able to reproduce the strong binding preference for the m⁶A-modified probe of the full-length Dhx57 protein (**Figure 8D**). This could be due to the artificial truncations interfering with proper folding of Dhx57 or could reflect the fact that the N-terminal and C-terminal regions are both required for binding to m⁶A sites.

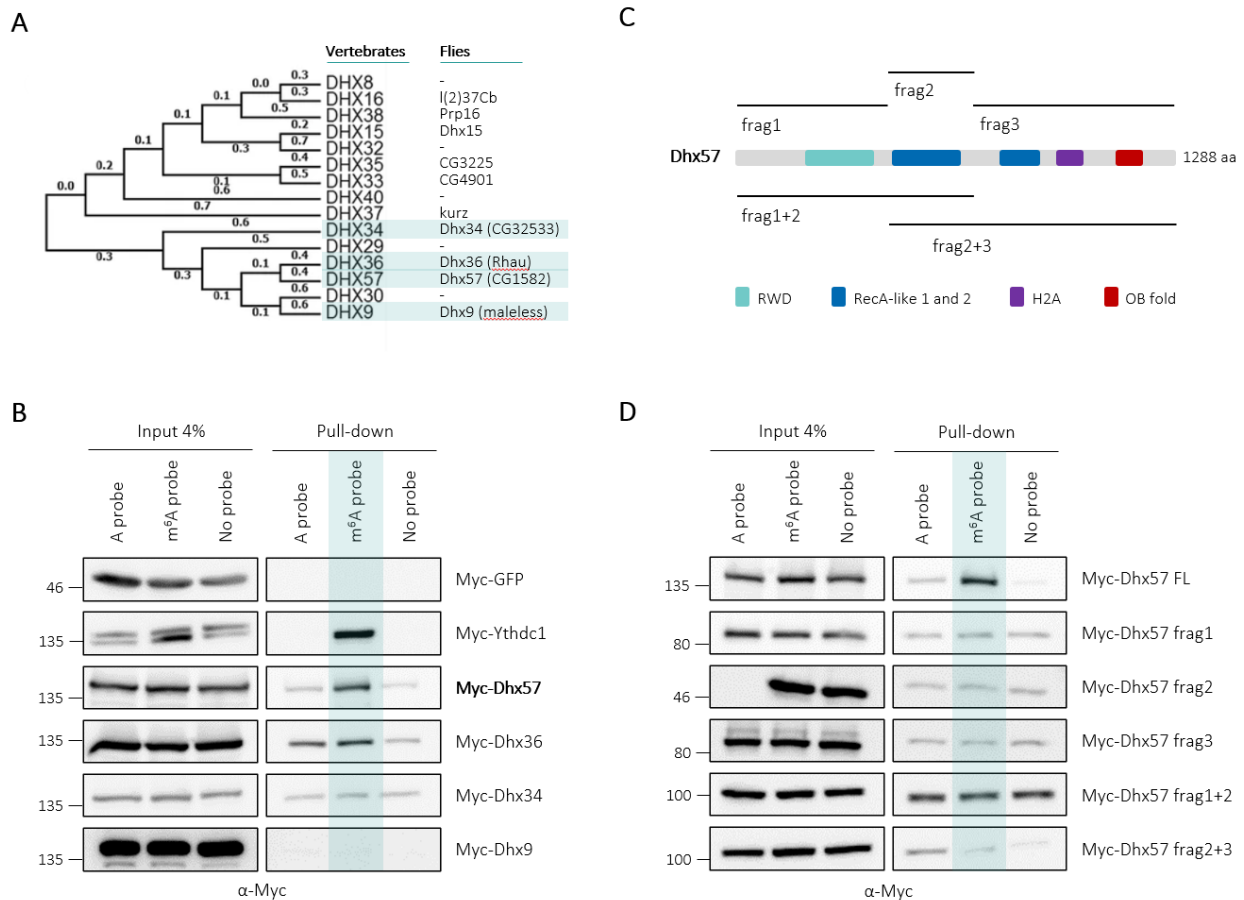


Figure 8. Preferential binding to m⁶A-modified RNA is specific to Dhx57 among *Drosophila* DEAH box helicases.

A) Phylogenetic analysis of vertebrate DEAH helicases with corresponding *D. melanogaster* homologs (adapted from (Suthar et al., 2016)). Closest paralogs to Dhx57 in flies that were selected for RNA pull-down experiments are highlighted in light blue. **B**) RNA pull-down using biotinylated probes of repetitive [GG(A/m⁶A)CU] sequences and protein extracts from S2R+ cells transfected with either Myc-GFP, Myc-Dhx57, Myc-Dhx36, Myc-Dhx34 or Myc-Dhx9. Western blot using anti-Myc antibody. **C**) Schematic representation of Dhx57 protein and protein fragments used for RNA pull-down experiments. **D**) RNA pull-down using biotinylated probes of repetitive [GG(A/m⁶A)CU] sequences and protein extracts from S2R+ cells transfected with either Myc-Dhx57 full-length (FL) or Myc-Dhx57 fragments (frag) 1/2/3/1+2/2+3. Western blot using anti-Myc antibody.

5.3.3 mRNA targets of Dhx57 are mostly methylated

In order to investigate a potential role as m⁶A reader protein for Dhx57, we took advantage of the TRIBE method (Worpenberg et al., 2019) to identify the mRNA targets bound by Dhx57. Briefly, the

5. Results

catalytic domain of the editing enzyme Adar (cdAdar) was fused to Dhx57, transfected in S2R+ cells and mRNA isolated for high-throughput sequencing. As a version of the Adar protein lacking the RNA-binding domain was used, bound mRNA targets were determined by the RNA-binding ability of Dhx57 and identified comparing A-to-I editing events with unspecific events generated by cdAdar alone. Expression of the FlagMyc-tagged Dhx57-cdAdar fusion protein was verified via western blot (**Figure 9A**). Using the TRIBE approach with a stringent cutoff (SumScore ≥ 30), we identified 301 Dhx57 mRNA targets in S2R+ cells (**Figure 9B**). To address whether those targets were methylated, we overlapped the obtained dataset with our miCLIP dataset from S2R+ cells (Worpenberg et al., 2021) and found that 89.3% of Dhx57 targets were also m⁶A-modified (**Figure 9B**). We next analyzed the gene ontology (GO) of Dhx57 methylated targets and found that they showed enrichment for many distinct biological processes, such as cellular response to virus, long-term strengthening of NMJs and integrated stress response signaling (**Figure 9C**).

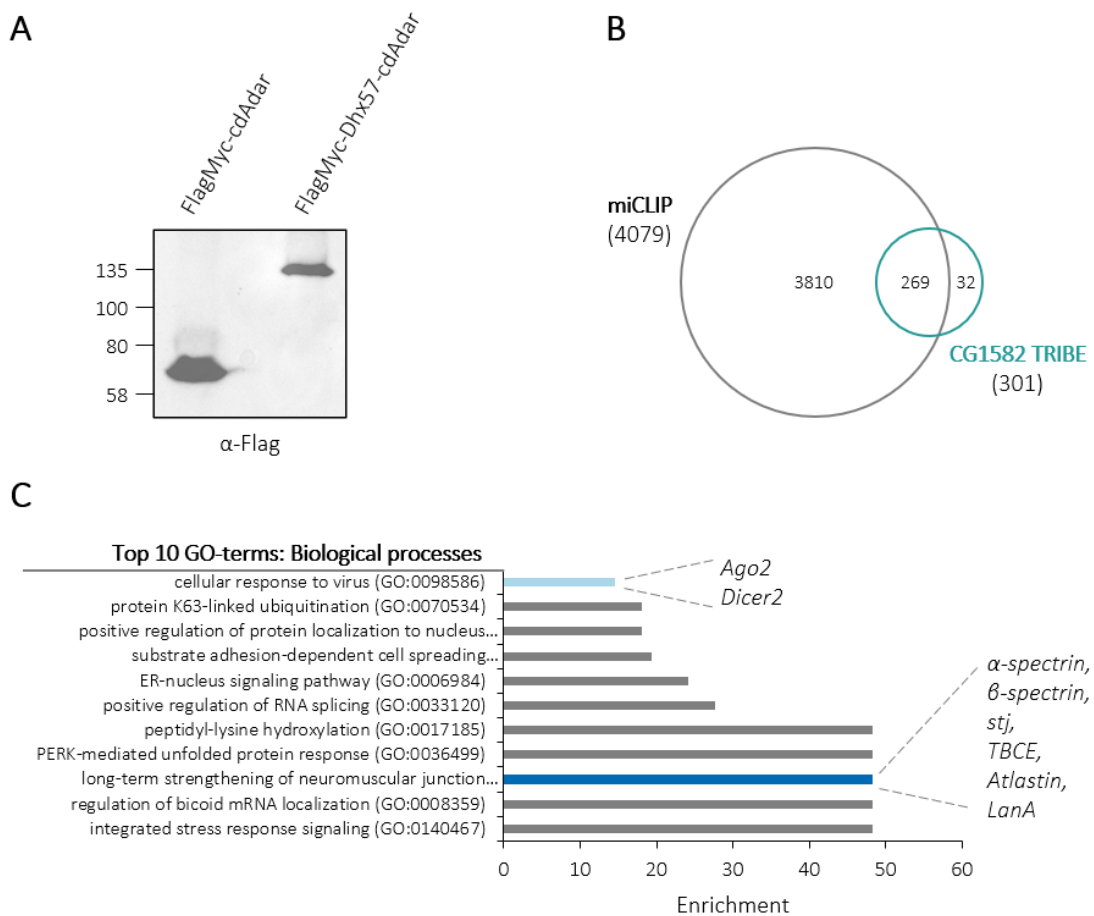


Figure 9. mRNA targets of Dhx57 are mostly methylated.

A) Verification of the expression of FlagMyc-cdAdar and FlagMyc-Dhx57-cdAdar via western blot using anti-Flag antibody. **B)** Overlap of miCLIP dataset (Worpenberg et al., 2021) with Dhx57 mRNA targets determined by TRIBE in S2R+ cells (SumScore ≥ 30). **C)** Gene ontology (GO) analysis of Dhx57 methylated TRIBE targets. Top ten terms for biological process are sorted by their fold enrichment. Targets related to cellular response to virus (light blue) and long-term strengthening of NMJs (blue) are listed on the right.

5. Results

To demonstrate that binding of Dhx57 to its mRNA targets is dependent on the presence of m⁶A sites, we performed RNA immunoprecipitation (RIP) experiments in flies overexpressing FlagMyc-tagged Dhx57 under the control of the ubiquitous *Tubulin*-GAL4 driver in a WT or *Mettl3* mutant background. The driver alone in WT or *Mettl3* mutant background was used as negative control. Western blot analysis showed that the anti-Myc antibody efficiently immunoprecipitated FlagMyc-tagged Dhx57 and, as expected, no Mettl3 protein was detected in *Mettl3*^{null} mutant flies (**Figure 10A**). The expression levels of some of the methylated mRNA targets of Dhx57 identified by TRIBE were quantified via RT-qPCR and enrichment was calculated normalizing transcript levels in the RIP fractions to the corresponding input and to the negative control. We found that loss of Mettl3 drastically reduced the interaction between Dhx57 and the selected transcripts (**Figure 10B-C**), showing that Dhx57 binding to mRNA depends on the presence of m⁶A sites.

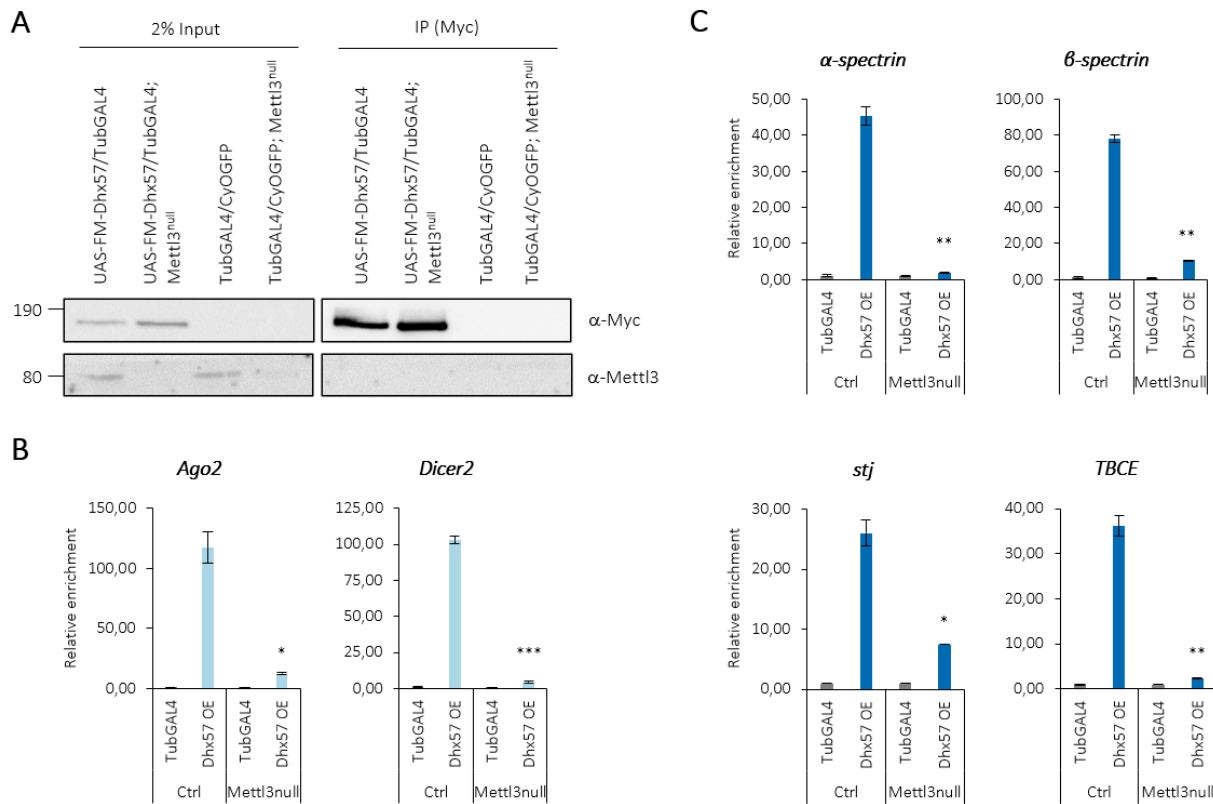


Figure 10. Dhx57 binding to its mRNA targets is m⁶A-dependent.

A-C) Dhx57 RIP *in vivo*. UAS-FlagMyc-Dhx57 was overexpressed in flies under the control of the *Tubulin*-GAL4 driver in WT or *Mettl3* mutant background. Proteins were immunoprecipitated using anti-Myc antibody. **A)** Western blot of the RIP experiment using anti-Myc and anti-Mettl3 antibodies. **B-C)** RT-qPCR analysis of the RIP experiment. Fold enrichment over input of selected Dhx57 methylated transcripts was quantified relative to the driver alone negative control. Bars represent the mean ± standard deviation of three technical measurements.

5.3.4 Loss of Dhx57 has no significant effect on small RNA-directed silencing pathways

On account of *Ago2* and *Dicer2* being identified as Dhx57's methylated targets related to the "cellular response to virus" process found among the most enriched GO terms in our analysis, we decided to investigate the involvement of Dhx57 and Mettl3 in the biogenesis and activity of small silencing RNAs.

In *Drosophila*, siRNAs generated from the genome of RNA viruses by the *Dicer2* ribonuclease and loaded into *Ago2* play an essential role in antiviral defense (Schneider & Imler, 2021). Although fly miRNAs derive from processing of precursor transcripts by *Dicer1* and are preferentially loaded into *Ago1*, a subset of miRNAs and some miRNA passenger strands were found to associate to *Ago2* (Czech et al., 2009; Ghildiyal et al., 2010; Tomari et al., 2007), suggesting the existence of crosstalk and collaboration between different small silencing RNA pathways.

To examine whether loss of Dhx57 would affect small RNA-mediated silencing in flies, we took advantage of the self-silencing automiG reporter (Carré et al., 2013) (Figure 11A). Briefly, the automiG vector simultaneously expresses *GFP* and two artificial miRNAs targeting *GFP* mRNA (*miG1* and *miG2*), allowing screening and identification of factors required for *Ago2*-mediated miRNA silencing. After KD of either *Ago2*, *Mettl3* or *Dhx57*, S2R+ cells were transfected with the automiG reporter and GFP expression was assessed via western blot as a readout of small RNA-mediated silencing. As expected, *Ago2* KD strongly suppressed the self-silencing ability of automiG, while depletion of either *Mettl3* or *Dhx57* failed to induce GFP expression (Figure 11B).

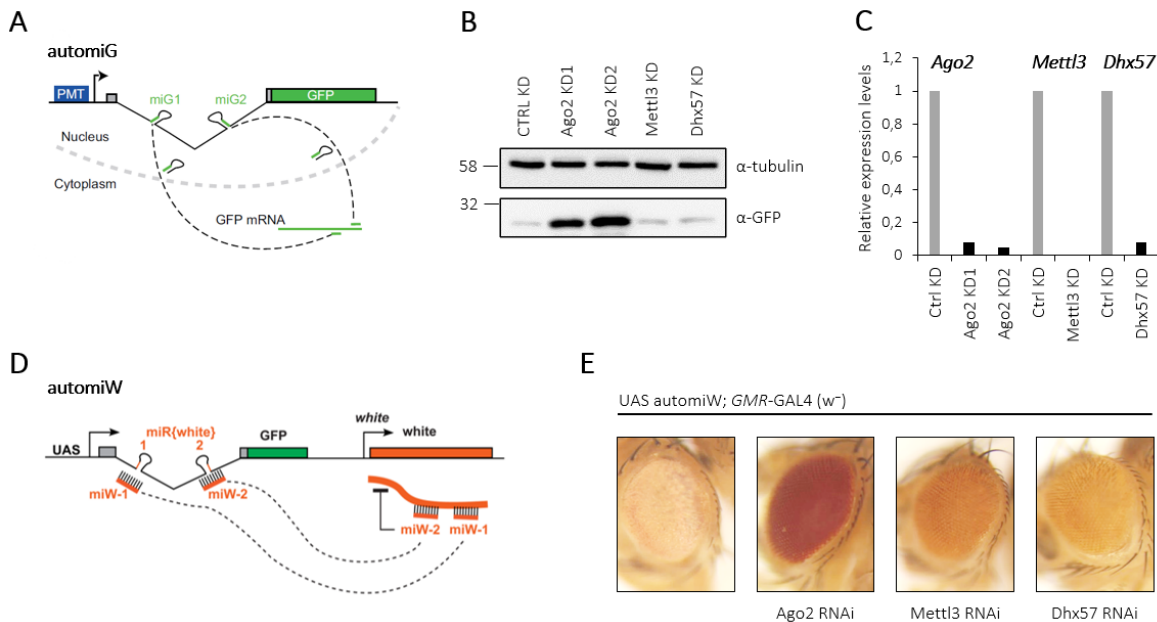


Figure 11. Loss of Dhx57 has no significant effect on small RNA-directed silencing pathways.

A) Schematic representation of the automiG reporter (Carré et al., 2013). **B)** Analysis of the automiG silencing in S2R+ cells depleted of *Ago2*, *Mettl3* or *Dhx57*. Western blot using anti-GFP antibody. Tubulin was used as loading control. **C)** Relative expression levels of *Ago2*, *Mettl3* and *Dhx57* as validation of their KD efficiency. Average of three technical measurements is shown. **D)** Schematic representation of the automiW genetic sensor (Besnard-Guérin et al., 2015). **E)** Analysis of the automiW silencing in adult fly eyes. Silencing of the *white* transgene of automiW was under the control of the eye-specific *GMR-GAL4* driver and analyzed upon *Ago2*, *Mettl3* or *Dhx57* RNAi.

5. Results

Conceptually very similar to automiG, the automiW self-silencing reporter (Besnard-Guérin et al., 2015) (**Figure 11D**) can be used to evaluate Ago2-mediated miRNA silencing *in vivo*. The automiW construct includes a UAS promoter driving the expression of the *white* gene, whose protein product is responsible for red pigment deposition in fly eyes, as well as two artificial miRNAs targeting *white* mRNA (*miW-1* and *miW-2*). Expression of automiW under the control of the eye-specific *GMR-GAL4* (*w⁻*) driver, which does not carry a functional *white* gene, results in flies with white eyes as *miW-1* and *miW-2* efficiently silence the expression of the *white* transgene (**Figure 11E**). Combining expression of the automiW reporter with RNAi-mediated depletion of either Ago2, Mettl3 or Dhx57, we observed that only Ago2 KD strongly inhibited silencing of the *white* transgene (red eyes), while depletion of either Mettl3 or Dhx57 had just a mild effect on eye pigmentation (pale orange eyes) (**Figure 11E**). These results are in line with what we observed with the automiG reporter *in vitro*, suggesting that both Mettl3 and Dhx57 are dispensable for efficient Ago2-mediated miRNA silencing in this context.

5.3.5 Dhx57 regulates axonal growth at larval NMJs

Among the most enriched terms resulting from the GO enrichment analysis of Dhx57 methylated targets, “long-term strengthening of NMJs”, caught our attention in consideration of the NMJ synaptic overgrowth phenotype that we previously described for most m⁶A mutants (Worpenberg et al., 2021).

In order to analyze larval NMJ morphology upon loss of Dhx57, we generated *Dhx57* mutant flies using the CRISPR-Cas9 approach with two gRNAs targeting the entire gene region of *Dhx57*. A deletion of approximately 2 kb within the C-terminal part of the *Dhx57* gene targeted by the second gRNA was obtained and confirmed by PCR (**Figure 12A-B**). As the mutation almost completely removes the RecA-like helicase domains, we can assume that the mutant Dhx57 protein lacks its helicase function. We found that *Dhx57^{fs}* homozygous mutant flies were viable and fertile and did not show any significant morphological defects.

Interestingly, we observed that *Dhx57^{fs}* homozygous mutant larvae showed a phenotype very similar to the synaptic overgrowth displayed by most of the m⁶A mutants, characterized by a significant increase in the number of synaptic boutons per muscle surface compared to WT or *Dhx57^{fs}* heterozygous mutant larvae (**Figure 12C-D**). Consistent with our previous results, *Dhx57^{fs}* mutants also displayed significantly increased axonal length and branching of synaptic terminals (**Figure 12C and 12E-F**). Of note, all the NMJ defects observed in *Dhx57^{fs}* homozygous larvae were recapitulated combining the mutant allele with a deficiency line spanning the *Dhx57* locus and were completely rescued upon ubiquitous expression of *Dhx57* cDNA (**Figure 12 C-F**).

These results, together with the above-described preferential binding to methylated RNAs, indicate that Dhx57 may contribute to the regulation of NMJ morphology in an m⁶A-dependent manner. To address this possibility, we performed genetic interaction experiments examining larval NMJs in different combinations of *Dhx57* and *Mettl3* mutants. Mapping genetic interactions by simultaneously perturbing pairs of genes has been extensively used to identify genes whose products are functionally related. Double mutants giving rise to a phenotype that cannot be predicted by simply adding or multiplying the single-locus effects indicates functional relationship between genes and pathways, while a phenotype

5. Results

equal to the sum of the two mutated genes' individual effect suggests that the two mutations act independently.

Quantification of NMJ synapses, length and branches in single or double *Dhx57* and *Mettl3* mutants revealed that the overgrowth phenotype observed upon loss of *Dhx57* or *Mettl3* was not aggravated by removing one or two copies of the other genes (**Figure 13A-C**), suggesting that they act in the same pathway and co-regulate axonal growth at larval NMJs.

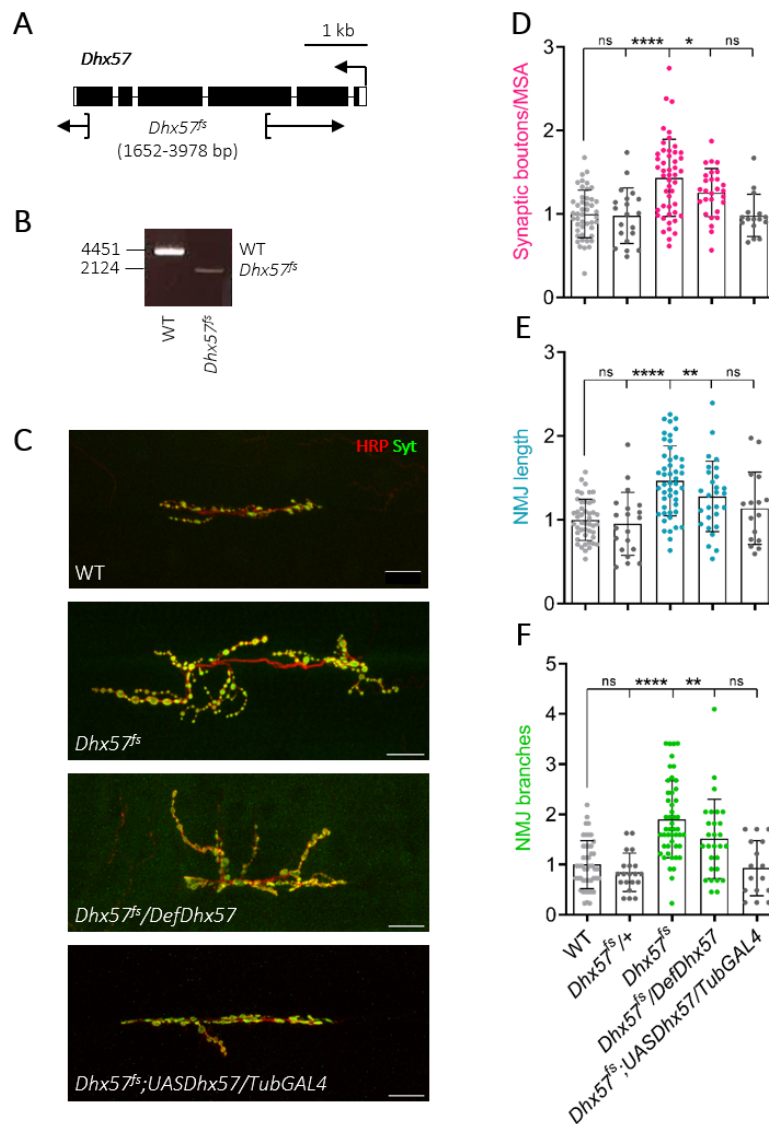


Figure 12. *Dhx57* contributes to the regulation of axonal growth in the *Drosophila* larval NMJ system.

A) Schematic of the *Dhx57* locus with indicated deletion generated by CRISPR-Cas9. **B)** PCR validation of loss of function allele using genomic DNA from WT and homozygous *Dhx57^Δ* mutant flies. **C)** Representative confocal images of muscle 6/7 NMJ (hemisegments A2-A3) for the indicated genotypes labelled with anti-Synaptotagmin (green) and HRP (red) to reveal the synaptic vesicles and the neuronal membrane. Scale bar: 20 μ m. **D-F)** Quantification of normalized bouton number (**D**), axon length (**E**) and branching (**F**) of NMJ 6/7 of the indicated genotypes. Error bars show mean \pm s.e.m. Multiple comparisons were performed using one-way ANOVA with a *post hoc* Sidak-Bonferroni correction (ns = not significant; **P* < 0.05; ***P* < 0.01; *****P* < 0.0001).

5. Results

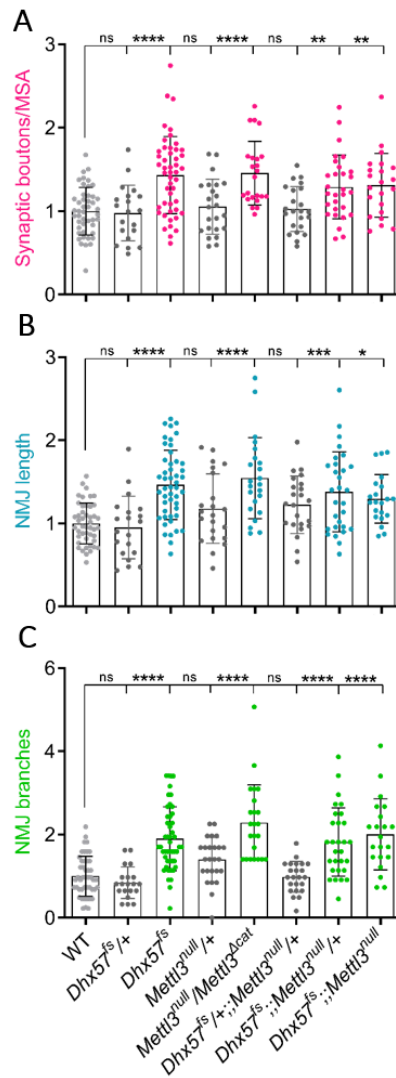


Figure 13. Dhx57 and Mett13 interact genetically to control axonal growth in the *Drosophila* larval NMJ system.

Quantification of normalized bouton number (A), axon length (B) and branching (C) of NMJ 6/7 of the indicated genotypes. Error bars show mean \pm s.e.m. Multiple comparisons were performed using one-way ANOVA with a *post hoc* Sidak-Bonferroni correction (ns = not significant; *P < 0.05; **P < 0.01; ***P < 0.001; ****P < 0.0001).

5.4 Section 4

5.4.1 No obvious m⁶A erasers acting on mRNA in *Drosophila melanogaster*

More than half of the enzymes belonging to the ALKBH family of demethylases target m⁶A on different nucleic acid substrates. Although they appear to have a limited role under physiological conditions, ALKBH5 and FTO catalyze m⁶A demethylation on mRNA both *in vitro* and *in vivo*. In addition, ALKBH3 demethylates m⁶A on tRNA, while ALKBH1 and ALKBH4 act on 6mA on DNA (see chapter 1.4.3).

Since ALKBH5 and FTO are only found in vertebrates, previous work in the lab investigated whether any of the other ALKBH proteins whose homologs are present in *Drosophila* (**Figure 14A**) might target m⁶A on mRNA in flies. To this aim, fly homologs of ALKBH1, ALKBH4, ALKBH6, ALKBH7 and ALKBH8 were depleted in S2R+ cells and m⁶A levels on mRNA quantified via mass spectrometry. However, none of these depletions, of single ALKBH proteins or combination of them, affected mRNA m⁶A levels in a significant way (unpublished data), indicating that there is no obvious m⁶A eraser acting on mRNA in flies.

Within the ALKBH family, ALKBH6 is one of the least investigated proteins and the only member whose molecular targets are still unknown. In light of this, we decided to focus our work on the functional characterization of CG6144 (hereafter renamed to *Alkbh6*) in flies. In addition to a mutant allele already available in our lab (*Alkbh6^{Δ2}*, unpublished), we generated a second mutant (*Alkbh6^{Δ11}*) using the CRISPR-Cas9 approach and the same gRNAs previously designed to target the entire *Alkbh6* gene. Both mutant alleles are characterized by a large deletion removing 95% (*Alkbh6^{Δ2}*) or 60% (*Alkbh6^{Δ11}*) of the *Alkbh6* CDS starting from the translation start site, and can be considered null alleles (**Figure 14B-C**).

Aiming to address whether any mRNA modification might be the substrate of *Alkbh6* catalytic activity, we purified mRNA from both *Alkbh6* mutant fly lines as well as from flies expressing HA-tagged *Alkbh6* under the control of the ubiquitous *Tubulin*-GAL4 driver and subjected it to mass spectrometry analysis. Comparable to what was previously observed in cells depleted of *Alkbh6*, neither loss nor overexpression of *Alkbh6* in flies altered global levels of m⁶A (**Figure 14D**) or of any of the other modifications detected on mRNA (data not shown). Nevertheless, these results do not exclude that *Alkbh6* might act on a restricted subset of methylated mRNA targets or on other RNA species.

Interestingly, *Arabidopsis* ALKBH6 (At4g20350) was recently reported to bind both m⁵C- and m⁶A labeled RNA probes (Huong et al., 2020). Of note, electrophoretic mobility shift assay (EMSA) experiments showed that recombinant plant ALKBH6 retarded the migration of both modified and unmodified probes, with no clear evidence of preferential binding to methylated RNAs. To test the binding behaviour of *Alkbh6* to m⁶A-modified RNA in flies, we performed pull-down experiments using our AA(A/m⁶A)CU RNA probes. In line with what was reported for *Arabidopsis* ALKBH6, western blot analysis showed that FlagMyc-tagged *Drosophila* *Alkbh6* was efficiently pulled down by both the m⁶A-modified and unmodified probe. However *Alkbh6* was detected with the same intensity also in the control experiment with no probe added to the protein lysate (**Figure 14E**). Similar results were observed in pull-down experiments performed with HA-tagged *Alkbh6* or more stringent washes (data not shown), making it impossible to conclude from these data whether *Alkbh6* is able to specifically recognize m⁶A or, in general, to bind to RNA at all.

5. Results

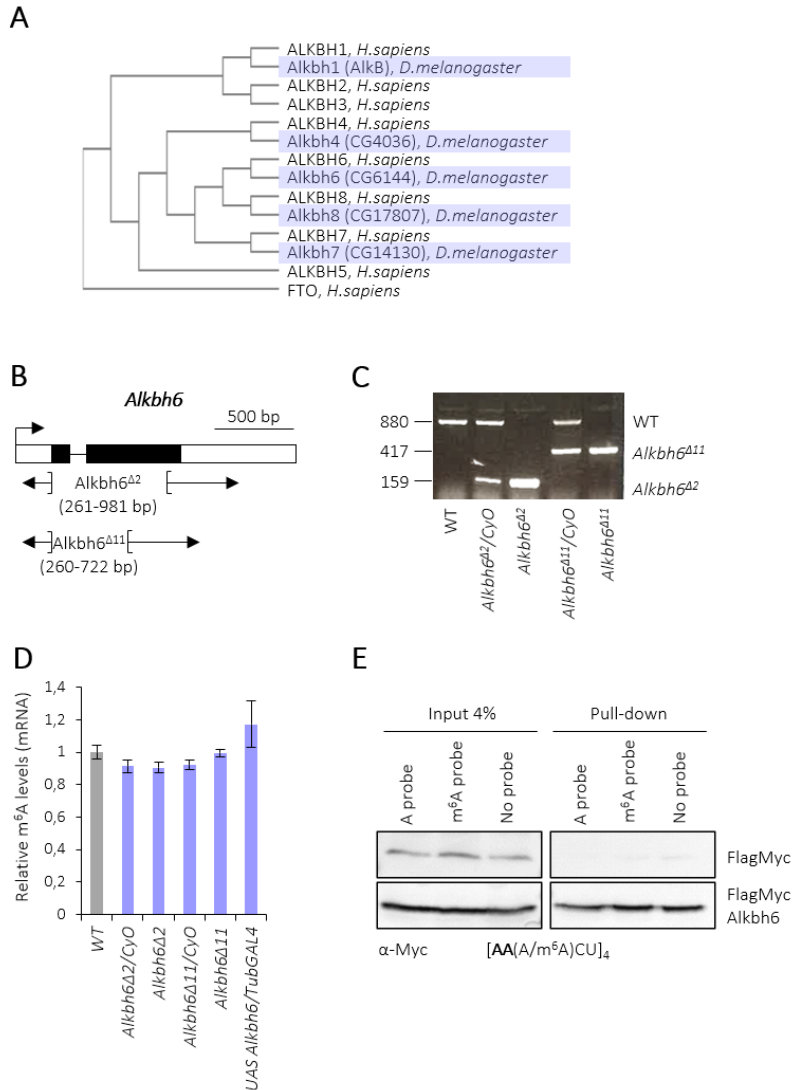


Figure 14. No obvious mRNA m⁶A erasers in flies.

A) Phylogenetic tree of the ALKBH family generated using Simple Phylogeny (EMBL-EBI). Each fly (*D.melanogaster*) protein clusters with the corresponding human (*H.sapiens*) homolog. **B**) Schematic of the *Alkbh6* locus with indicated deletions generated by CRISPR-Cas9. **C**) PCR validation of loss of function alleles using genomic DNA from WT and heterozygous or homozygous *Alkbh6 Δ 2/Alkbh6 Δ 11* mutant flies. **D**) LC-MS/MS quantification of m⁶A levels in mRNA extracts from WT, heterozygous or homozygous *Alkbh6 Δ 2/Alkbh6 Δ 11* mutants flies and flies overexpressing UAS-*Alkbh6*-HA under the control of the *Tubulin*-GAL4 driver. Bars represent the mean \pm standard deviation of three technical measurements. **E**) RNA pull-down using biotinylated probes of repetitive [AA(A/m⁶A)CU] sequences and protein extracts from S2R+ cells transfected with either FlagMyc, or FlagMyc-*Alkbh6*. Western blot using anti-Myc antibody.

5.4.2 The expression profile of *Alkbh6* follows m⁶A levels during fly development

In *Drosophila melanogaster*, the *Alkbh6* gene codes for a 26 kDa protein, which is characterized, like all proteins belonging to the ALKBH family, by the presence of a Fe(II)- and α -ketoglutarate-dependent dioxygenase domain (**Figure 15A**). Fe(II)- and α -ketoglutarate-dependent dioxygenases (α KGDs) represent one of the largest classes of mononuclear non-heme iron enzymes, which catalyze a wide range of

5. Results

reactions, including hydroxylation, dealkylation, demethylation, desaturations as well as ring expansion/contraction. The catalytic core of all α KGDs is characterized by a double-stranded β -helix fold that binds ferrous iron and the co-substrate α KG with evolutionary conserved residues. α KGDs catalyze oxidation reactions by incorporating a single oxygen atom from molecular oxygen (O_2) into their substrates, while the second oxygen atom is used for oxidation of the co-substrate α KG into succinate and carbon dioxide (Fedeles et al., 2015).

Expression of *Alkbh6* with a C-terminal HA-tag, together with GFP-tagged Barentsz as cytoplasmic marker, was used to evaluate the subcellular localization of the *Alkbh6* protein in S2R+ cells. As previously reported for human ALKBH6 (Tsujikawa et al., 2007), with whom it shares ~50% identity, *Drosophila* *Alkbh6* was detected ubiquitously throughout the cells with enrichment in the cytoplasm (**Figure 15B**).

In addition, we analysed the expression profile of *Alkbh6* during *Drosophila* development and observed that it was remarkably similar to the trend of m^6A abundance on mRNA. Highest levels were observed in the early stages of embryogenesis, during pupation and in adults as well as fly heads (**Figure 15C**). Differently from the profile of m^6A during fly development, *Alkbh6* is not particularly enriched in ovaries (**Figure 15C**), which is in line with data from human tissues showing significantly higher expression in testis than ovaries (Tsujikawa et al., 2007).

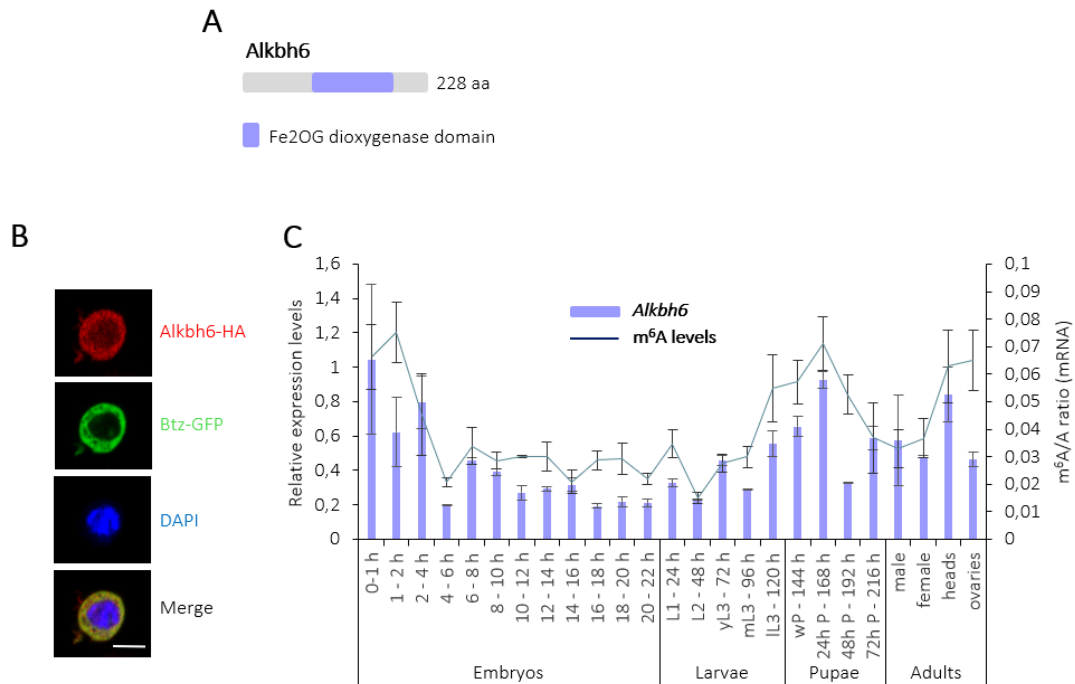


Figure 15. *Alkbh6* localizes ubiquitously in the cell and its expression correlates with m^6A profile during fly development.

A) Schematic representation of the *Alkbh6* protein with known protein domains. **B)** Immunostaining of *Alkbh6*-HA (red) overexpressed in S2R+ cells. Barentsz-GFP (green) served as cytoplasmic marker. DAPI staining is shown in blue. Scale bar: 10 μ m. **C)** Relative expression of *Alkbh6* transcript during *Drosophila* development (*w1118* flies) analyzed by RT-qPCR. Levels of m^6A modification were analyzed in the same mRNA samples using LC-MS/MS. Bars represent the mean \pm standard deviation of three technical measurements from three biological replicates.

5.4.3 Expression of *Alkbh6* is upregulated in response to abiotic stress

As previously mentioned, catalytic activity and substrates as well as interacting partners of ALKBH6 are still largely unknown and only a few reports addressed its functions so far. Recently, the biological function of ALKBH6 was partially characterized in the context of the abiotic stress response in *Arabidopsis thaliana* (Huong et al., 2020). Huong and colleagues reported that expression of *Arabidopsis* ALKBH6 was upregulated in response to high salinity and that plants mutant for *ALKBH6* showed a much lower survival rate under salt, drought or heat stress compared to WT (Huong et al., 2020).

In light of this, we decided to quantify expression levels of *Alkbh6* in response to abiotic stress in flies. To this aim, we subjected S2R+ cells to different conditions of stress, ranging from temperature shock and oxidative stress to starvation and salt stress (Figure 16A). For heat or cold shock, cells were incubated at 37°C or 4°C, respectively. Exposure to H₂O₂ or the herbicide paraquat (PQ) (Hosamani & Muralidhara, 2013) was used to induce oxidative stress. Starvation was achieved incubating cells in serum-free medium, while salt stress derived from NaCl addition to the cell culture medium. According to existing literature, stress stimuli were induced for different amounts of time (short/long exposure) and with or without a period of recovery before RNA isolation and transcript levels quantification via real-time qPCR. Notably, we observed that *Alkbh6* expression was significantly increased in all stress conditions except for cold shock, while levels of *Alkbh8*, which is the closest paralog to *Alkbh6* (Figure 14A), remained substantially unaltered in cells exposed to any type of stress (Figure 16B). Highest levels of *Alkbh6* were observed upon starvation and heat shock as well as paraquat-induced oxidative stress (Figure 16B). In addition, expression of *Alkbh6* was not upregulated further by longer exposure to stress (heat shock and starvation) and remained significantly higher than control levels also after a period of recovery (heat shock, oxidative and salt stress) (Figure 16B).

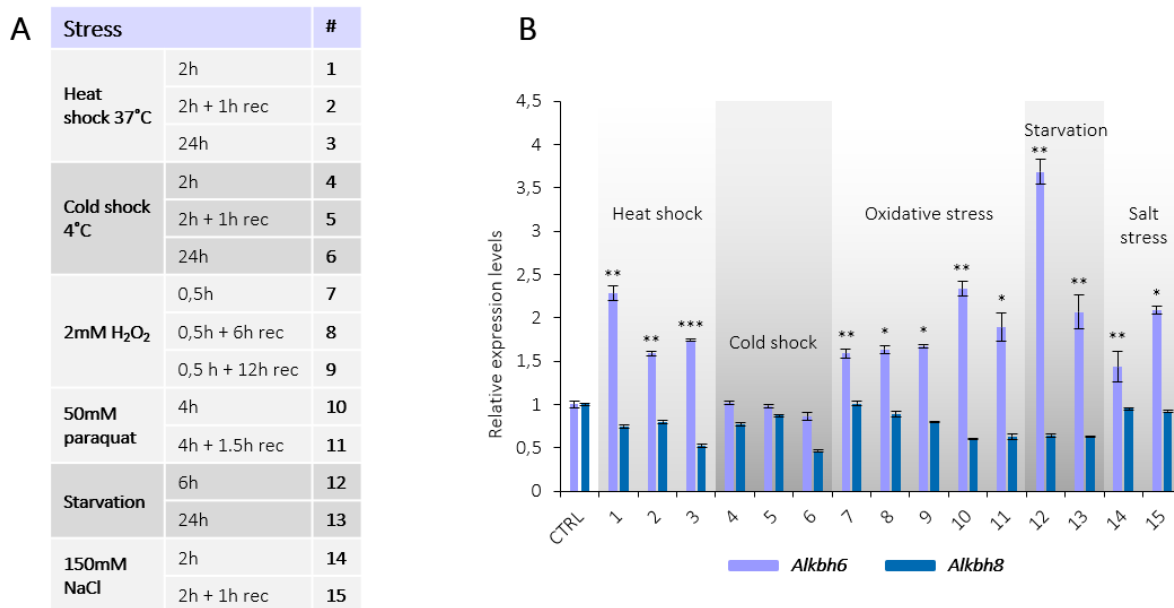


Figure 16. *Alkbh6* is upregulated in response to abiotic stress.

5. Results

A) Table displaying the different conditions of abiotic stress to which S2R+ cells were exposed, including type and duration of the stress stimulus as well as recovery (rec) period. **B)** Relative expression of *Alkbh6* and *Alkbh8* transcripts analyzed by RT-qPCR in S2R+ cells exposed to different types of stress. Stress conditions from 1 to 15 refer to summary table (**A**). Bars represent the mean \pm standard deviation of three technical measurements from three biological replicates.

Next, confocal microscopy analysis was used to evaluate any changes in the subcellular localization of *Alkbh6* in cells exposed to stress compared to control ones. With the exception of cold shock, we chose the settings that previously gave rise to the strongest upregulation of *Alkbh6* for each different type of stress stimulus, reducing the number of experimental conditions from fifteen to five. Since antibody for *Alkbh6* detection was not available in *Drosophila*, exposure to stress was performed in S2R+ cells overexpressing *Alkbh6* with a N-terminal FlagMyc-tag. In unstressed S2R+ cells, *Alkbh6* localized to both nucleus and cytoplasm (**Figure 17A**), resembling the localization pattern observed upon expression of HA-tagged *Alkbh6* (**Figure 15B**). A similar ubiquitous localization was observed also in S2R+ cells exposed to heat shock, H₂O₂-induced oxidative stress and salt stress (**Figure 17A**). Differently, we found that the presence of *Alkbh6* in the nucleus appeared to be increased and enriched at the nuclear periphery upon paraquat-induced oxidative stress as well as starvation (**Figure 17A**).

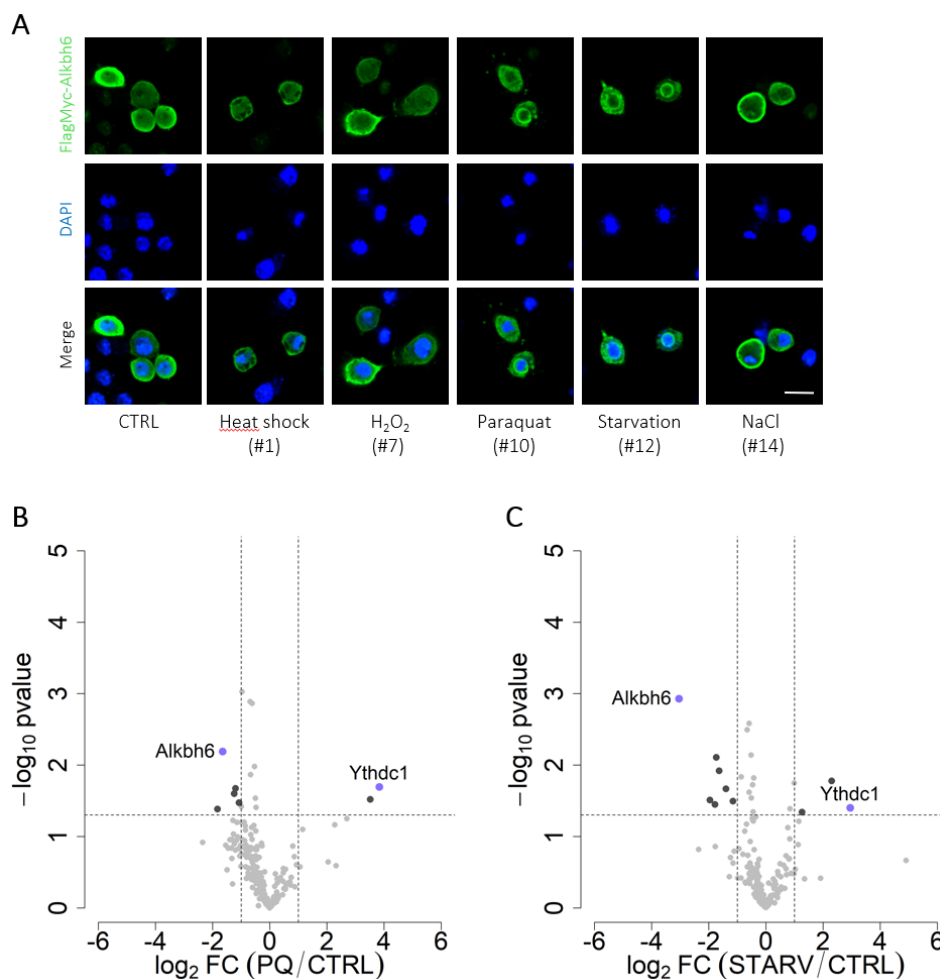


Figure 17. *Alkbh6* is enriched in the nucleus and interacts with *Ythdc1* upon oxidative stress and starvation.

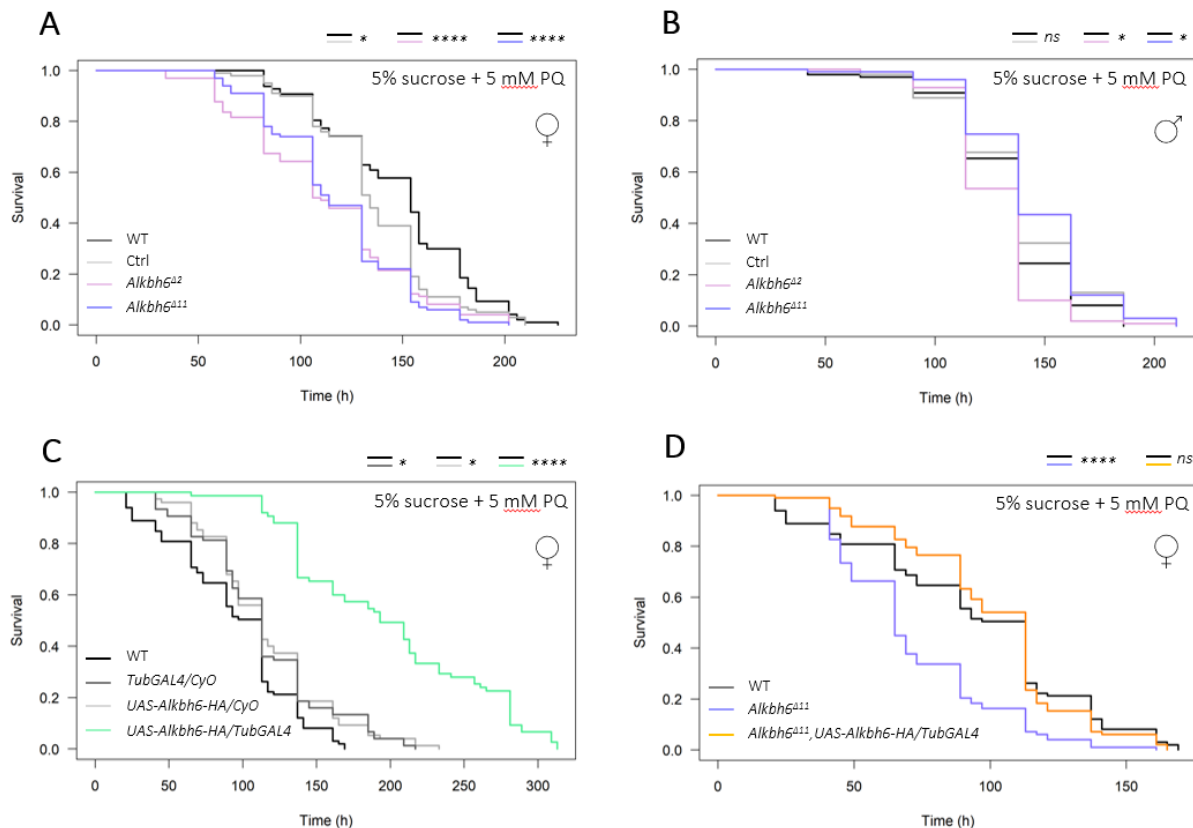
5. Results

A) Immunostaining of FlagMyc-Alkbh6 (green) overexpressed in S2R+ cells. DAPI staining is shown in blue. Scale bar: 10 μ m. Numbering of stress conditions refers to summary table (Fig 16A). **B-C)** Mass spectrometry analysis of Alkbh6's interactors in S2R+ protein cell extracts. IP was performed using Alkbh6-HA as bait upon control and paraquat (**B**) or starvation (**C**) exposure. P-value is calculated from a two-sided t-test with unequal variants (Welch t-test). Dashed lines represent $-\log_{10}$ P-value = 1 as well as \log_2 enrichment = 1. Significantly enriched proteins are depicted in black and highlighted in purple when the name is shown.

Aiming to gain a better insight into the possible function of Alkbh6 in the context of cellular stress, we decided to perform Alkbh6 interactome analysis in physiological as well as stress conditions. HA-tagged Alkbh6 protein was overexpressed in S2R+ cells exposed to paraquat, starvation or no treatment and enriched using an anti-HA antibody coupled to magnetic beads. Following stringent washing, the recovered proteins were subjected to mass spectrometry analysis. Only a few proteins were found to be enriched in the stress conditions compared to control in all replicates. Surprisingly, Ythdc1 was identified as interactor of Alkbh6 in both cells exposed to paraquat and starvation, while the m⁶A nuclear reader was not pulled down together with Alkbh6 under non-stress conditions (**Figure 17B-C**).

5.4.4 *Alkbh6* mutants are more sensitive to oxidative stress and starvation

In summary, we showed that expression of the *Alkbh6* transcripts is upregulated in response to different types of abiotic stress in S2R+ cells. Additionally, paraquat-induced oxidative stress and starvation resulted in increased localization of Alkbh6 to the nucleus and triggered its interaction with the m⁶A nuclear reader Ythdc1. In light of these observations, we next evaluated the response of *Alkbh6* mutant flies to prolonged exposure to paraquat as well as starvation.



5. Results

Figure 18. *Alkbh6* mutant flies are more sensitive to paraquat-induced oxidative stress.

A-D) Survival curves of female (**A, C-D**) and male (**B**) flies of the indicated genotype upon exposure to 5 mM paraquat in 5% sucrose. Results represent the pooled data of five replicates. Multiple comparisons were performed using log-rank test with a *post hoc* Bonferroni-Holm correction (ns = not significant; *P < 0.05; ****P < 0.0001).

To induce oxidative stress, adult flies were fed daily with 5 mM paraquat using the filter paper disc method and mortality was scored three times a day. Paraquat was diluted in a 5% sucrose solution to promote feeding. Mortality of flies fed only with 5% sucrose was monitored in parallel to exclude effects of the only-sucrose diet on survivability (data not shown). Analysis of the lifespan of paraquat-treated flies revealed that both *Alkbh6^{Δ2}* and *Alkbh6^{Δ11}* mutant flies were more sensitive to paraquat exposure and died significantly faster than WT and flies with the same genetic background (Ctrl) (**Figure 18A-B**). This phenotype was more pronounced in female flies (**Figure 18A**), while the difference between the survival curves of male flies from different genotypes upon paraquat feeding was less significant (**Figure 18B**). The sex-specific effect of paraquat on the lifespan of *Alkbh6* mutants might be explained by the fact that *Alkbh6* protein levels are considerably higher in adult female flies compared to males (Flybase developmental proteome, (Casas-Vila et al., 2017)), although this difference could be absent in case of stress. Next, we examined how flies overexpressing *Alkbh6* responded to paraquat treatment. Compared to WT flies, the *Tubulin*-GAL4 driver alone or UAS-*Alkbh6* alone did not affect the mortality rate in a significant way, while ubiquitous overexpression of UAS-*Alkbh6* under the control of *Tubulin*-GAL4 greatly extended the lifespan of flies exposed to paraquat (**Figure 18C**). In line with this, ubiquitous expression of *Alkbh6* was able to rescue the paraquat sensitivity phenotype of *Alkbh6^{Δ11}* female flies returning their lifespan back to WT duration (**Figure 18D**).

To induce starvation, adult flies were kept in vials with wet filter paper (wet starvation) or in empty vials (dry starvation). Analysis of the mortality rate revealed that both female and male *Alkbh6^{Δ11}* mutant flies had a shorter lifespan compared to WT and control flies upon wet starvation (**Figure 19A-B**). Upon dry starvation, a similar phenotype was observed in *Alkbh6^{Δ11}* females, while the duration of *Alkbh6^{Δ11}* males' lifespan was comparable to WT (**Figure 19C-D**). Ubiquitous overexpression of *Alkbh6* considerably extended the lifespan of starved flies of both sexes (**Figure 19C-D**) and efficiently rescued the increased sensitivity to dry starvation of *Alkbh6^{Δ11}* females (**Figure 19C**).

5. Results

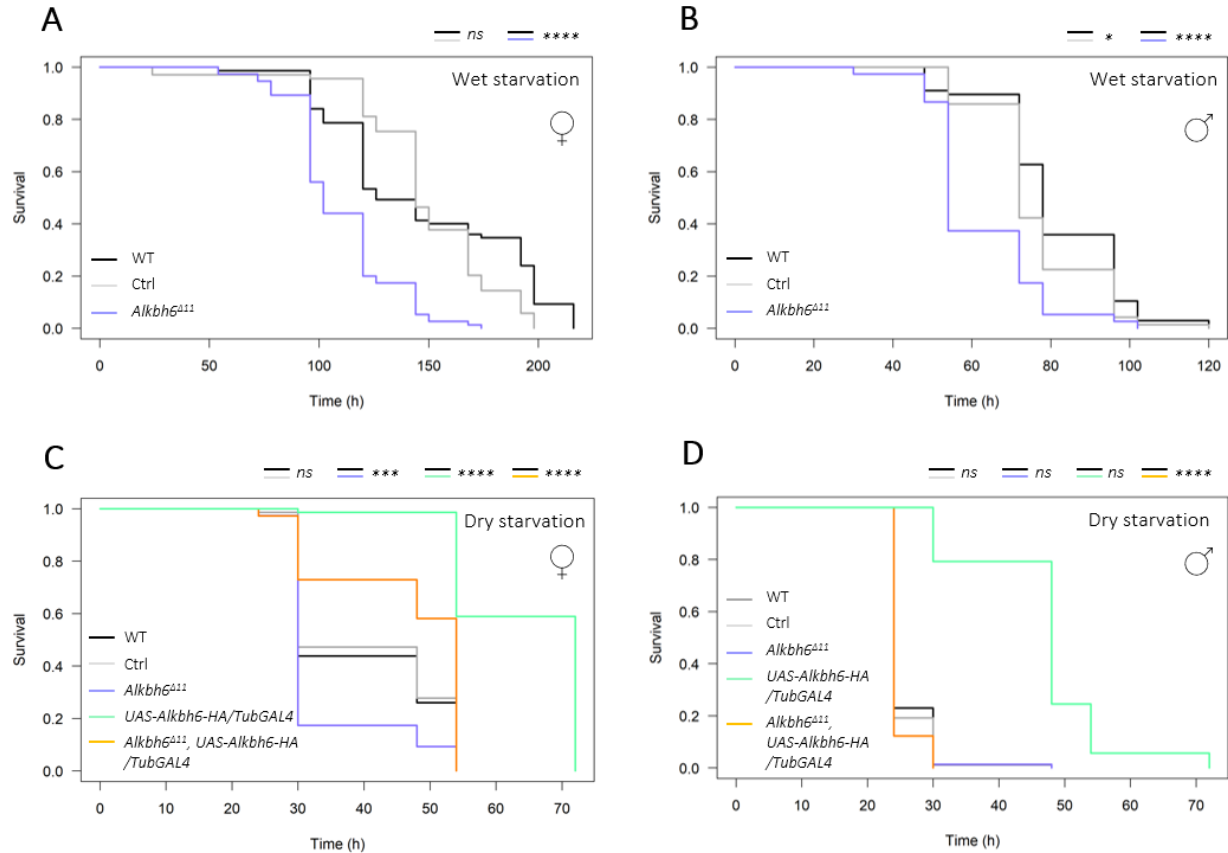


Figure 19. *Alkbh6* mutant flies are more sensitive to starvation.

A-D Survival curves of female (**A,C**) and male (**B,D**) flies of the indicated genotype upon exposure to wet (**A-B**) or dry (**C-D**) starvation. Results represent the pooled data of five replicates. Multiple comparisons were performed using log-rank test with a *post hoc* Bonferroni-Holm correction (ns = not significant; *P < 0.05; ***P < 0.001; ****P < 0.0001).

5.4.5 Loss of *Alkbh6* aggravates the effects of oxidative stress on flies

To investigate the impact of *Alkbh6* on gene expression in response to paraquat-induced oxidative stress, we carried out transcriptome analysis in WT and *Alkbh6*^{Δ11} female flies after 24 h of feeding with paraquat diluted in a sucrose solution or with sucrose alone. Taking into account the scarcity of reports describing *Alkbh6* targets and functions, we decided to perform TGIRT sequencing in order to cover as many different RNA biotypes as possible in an unbiased way. Differently from polyA-enriched RNA-seq, TGIRT-seq relies on the highly processive thermostable group II intron reverse transcriptase (TGIRT) enzyme and allows simultaneous detection of both coding and noncoding RNAs independently of length, secondary structure and modifications as well as faithful estimation of abundance within each class of RNA (Boivin et al., 2018). Combining TGIRT-seq to ribodepletion and chemical fragmentation, we analyzed all non-ribosomal RNA species above 50 bp, including mRNAs, ncRNAs, snRNAs, snoRNAs and tRNAs.

Read distribution of different classes of RNA detected by TGIRT-seq was reproducible between sample replicates (**Figure 20A**) and, as expected (Boivin et al., 2018), the majority of reads corresponded to tRNAs, followed by snoRNAs and protein-coding RNAs. Nevertheless, relative abundance of the different RNA species was not affected in *Alkbh6* mutants compared to WT (**Figure 20A**). In flies fed with

5. Results

sucrose alone (control condition), loss of *Alkbh6* altered the expression of only a few genes (n=130, 57 upregulated and 73 downregulated), which were for the vast majority protein coding genes (**Figure 20B**) not enriched for any specific biological process by GO-term analysis (data not shown). By comparing flies fed with paraquat diluted in a sucrose solution and flies fed with sucrose alone, we observed that exposure to paraquat altered the expression of many genes (n=900, 393 upregulated and 507 downregulated) (**Figure 20C** and **20E**). Approximately half of the upregulated genes were common between WT and *Alkbh6* mutants (n=204) (**Figure 20D**) and were enriched for biosynthesis of glutathione, which is a tripeptide produced in response to oxidative stress to prevent cellular damage. No enrichment for specific biological processes was found performing GO-term analysis on the genes upregulated in WT flies only (n=87), while upregulated genes specific to *Alkbh6* mutants (n=102), in line with increased susceptibility to paraquat of flies lacking *Alkbh6* (**Figure 18A**), were enriched for processes linked to the cellular stress response (**Figure 20C-D**). Similarly, ~50% of the downregulated genes were shared between WT and *Alkbh6* mutant (n=232) (**Figure 20F**) and mostly reflected a reduction in oogenesis and a general slowdown of cellular metabolic processes. While the downregulated genes specific to WT (n=151) were not enriched for any biological process, the ones specific for *Alkbh6* mutants (n=124) were enriched for hormone biosynthetic processes and ecdysteroid metabolism (**Figure 20E-F**).

5. Results

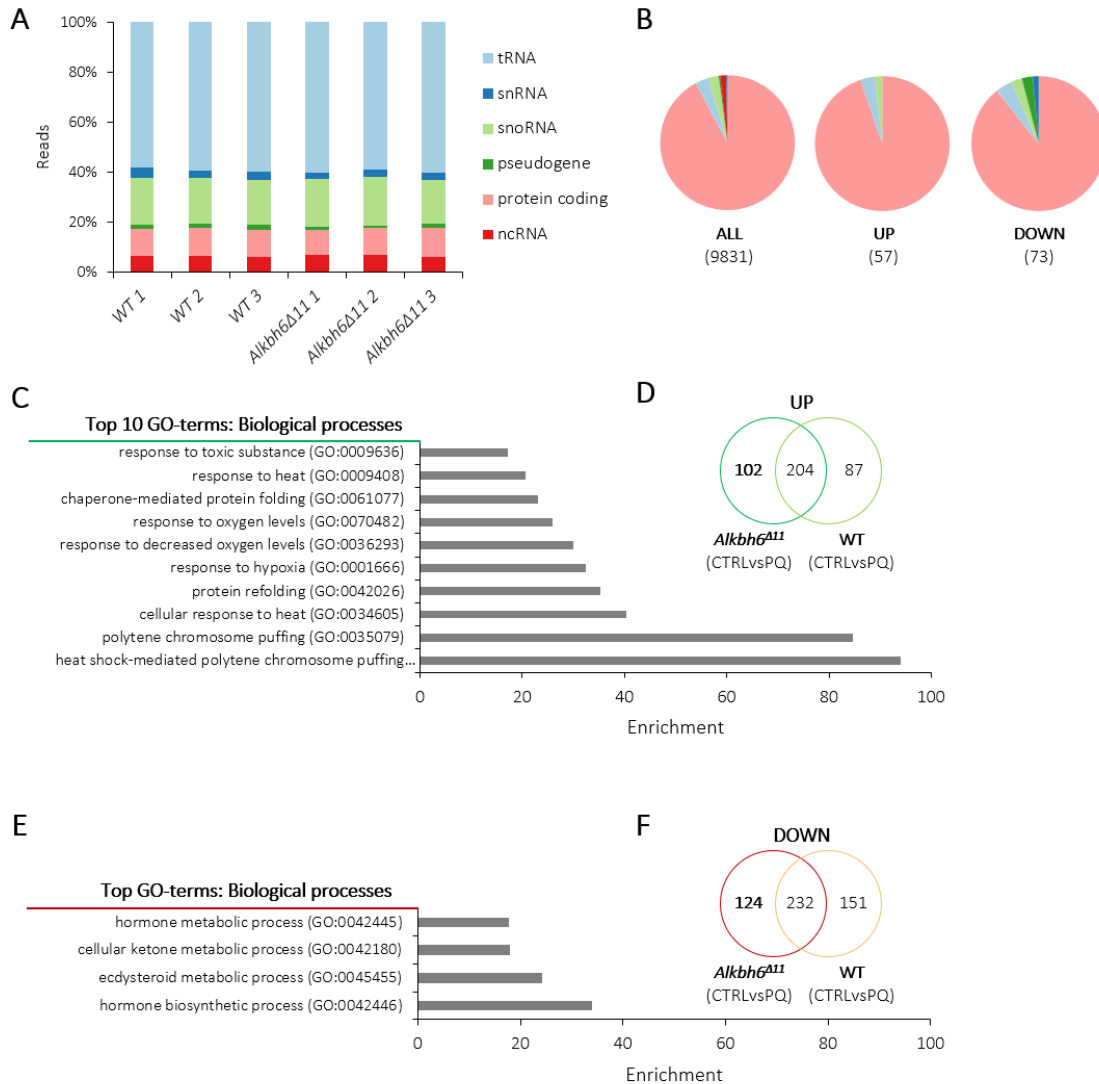


Figure 20. Loss of *Alkbh6* aggravates the effects of paraquat-induced oxidative stress on flies.

A) Stacked bar plot illustrating read distribution of different classes of RNA detected by TGIRT-seq in all expressed genes (TPM ≥ 1 in $n \geq 3$) in WT and *Alkbh6* Δ 11 mutant female flies in control condition. The color legend for the different RNA classes is shown on the right. **B**) Pie charts illustrating gene distribution in different classes of RNA detected by TGIRT-seq in all expressed genes (CPM ≥ 1 in $n \geq 3$, left), upregulated (FDR < 0.05 and logFC ≥ 1 , middle) and downregulated (FDR < 0.05 and logFC ≤ -1 , right) in *Alkbh6* Δ 11 mutant compared to WT female flies in control condition. **C-D**) Overlap of upregulated genes (CPM ≥ 1 in $n \geq 3$, FDR < 0.05 and logFC ≥ 1) in control versus oxidative stress (5 mM PQ) conditions between *Alkbh6* Δ 11 mutant and WT female flies (**D**) and gene ontology (GO) analysis of upregulated genes specific to *Alkbh6* Δ 11 mutant flies (**C**). **E-F**) Overlap of downregulated genes (CPM ≥ 1 in $n \geq 3$, FDR < 0.05 and logFC ≤ -1) in control versus oxidative stress (5 mM PQ) conditions between *Alkbh6* Δ 11 mutant and WT female flies (**F**) and gene ontology (GO) analysis of downregulated genes specific to *Alkbh6* Δ 11 mutant flies (**E**).

6. Discussion

The identity of a single cell is determined by the selection of genes it expresses starting from the exact same genome common to all cells of a multicellular organism. Although gene expression is heavily controlled at the level of transcript synthesis, transcription does not represent the only chance for regulation. Post-transcriptional regulation is the control of gene expression at the level of RNA and can occur at any processing step after transcription, including alternative splicing, localization, stability and ultimately translation. In recent years, the biochemical modifications of RNA have emerged as an additional layer of gene expression regulation that powerfully impacts transcription as well as post-transcriptional RNA metabolism and fate. RNA modifications, collectively known as epitranscriptome, decorate every known RNA species and alterations in their levels have been linked to a wide range of diseases including neurological disorders and multiple cancers. Methylation of adenosine at the N6 position (m⁶A) is the most prevalent modification on mRNA and the best characterized RNA modification overall. Despite being known since the 1970s, only in the last decade a combination of technological progress and renewed scientific interest allowed characterization of m⁶A enzymatic machinery, transcriptome-wide distribution as well as cellular and biological functions. Accumulating evidence indicates that m⁶A methylation represents an important regulatory system that influences almost every aspects of RNA metabolism allowing for fast and dynamic regulation of gene expression in physiological as well as stress conditions.

In this study, we used *Drosophila melanogaster* as model organism to investigate specific aspects of the m⁶A pathway that are still poorly characterized and in general to expand our knowledge of this important new layer of gene expression regulation. Discussion of our main findings is organized in four different sections. Characterization of Hakai as novel component of the m⁶A writer complex in flies is discussed in chapter 6.1. Our observations about Alkbh6 and its possible role within the cellular response to stress are discussed in chapter 6.2. Chapter 6.3 covers identification as well as characterization of the proteins that mediate m⁶A functions in the fly nervous system. Special focus is given to the Ythdf-Fmr1 interplay in the context of the m⁶A-dependent regulation of axonal growth at larval NMJs. Finally, discussion of all our results related to the RNA helicase Dhx57 as possible new m⁶A-binding protein in *Drosophila* are presented in chapter 6.4.

6.1 Writing m⁶A in *Drosophila*

The effectors of the m⁶A pathway include writers and erasers, which respectively deposit and remove the modification, and readers that specifically recognize it and mediate its functions. During the 1990's, pioneer work by Bokar, Rottman and colleagues (Bokar et al., 1994, 1997) discovered that HeLa cell nuclear extracts were able to *in vitro* methylate RNA in a SAM-dependent way within the previously established A/GAC m⁶A consensus sequence (C. M. Wei et al., 1976). Although a large multiprotein methyltransferase complex composed of two sub-complexes of different sizes had already been identified as responsible for m⁶A deposition on mRNA at that time, its exact composition remained a mystery for more than two decades. Nowadays, we know that the small subunit of the m⁶A writer complex (MAC) consists of the catalytic heterodimer METTL3-METTL14, while the large one (MACOM)

6. Discussion

includes the other five elements of the complex: WTAP, VIRMA, RBM15, ZC3H13 and HAKAI. The assembly of MAC and MACOM in one single entity is mostly mediated by interactions between METTL3 and WTAP (Su et al., 2022). WTAP (Ping et al., 2014; Schöller et al., 2018), together with ZC3H13 (Wen et al., 2018), is also required for the proper localization of the writer complex to the nucleus. Despite its multimeric nature, the enzymatic activity of the m⁶A writer complex is restricted to the METTL3 component. In fact, structural and biochemical studies revealed that METTL14 is catalytically inactive because of its inability to bind the methyl group donor SAM but is nevertheless crucial to enhance METTL3 activity and to act as RNA-binding scaffold (Śledź & Jinek, 2016; P. Wang et al., 2016; X. Wang et al., 2016). Altogether, MACOM components have been shown in various species to enhance m⁶A writing activity and to provide support for RNA target selectivity and binding.

HAKAI, also known as CBLL1, is the latest identified and least characterized m⁶A writer. HAKAI is a RING-finger type E3 ubiquitin ligase known to target the tyrosine-phosphorylated intracellular domain of E-cadherin for ubiquitination (Fujita et al., 2002). Once ubiquitinated, E-cadherin undergoes endocytosis and degradation, which consequently leads to disruption of cell-cell contacts and increase in cell motility. In light of this, HAKAI has been mainly studied in the context of epithelia-mesenchymal transitions (EMT) and cancer progression (Aparicio et al., 2012). More recently, its identification as part of a protein complex including WTAP, VIRMA and ZC3H13 in mammalian cells (Wan et al., 2015) combined with mild developmental defects and reduced m⁶A levels observed in *Arabidopsis* HAKAI mutant (Růžička et al., 2017) opened the way to its characterization as evolutionary conserved component of the m⁶A biogenesis machinery. In line with what was previously reported in vertebrates as well as in plants, previous work from our lab identified Hakai among the strongest interactors of Nito in *Drosophila* S2R+ cells (Knuckles et al., 2018). *In vitro*, loss of Hakai resulted in reduced mRNA m⁶A levels as well as altered gene expression and splicing patterns analogous to those observed upon depletion of other MACOM components, validating Hakai as an integral component of the m⁶A writer complex in flies.

6.1.1 Internal architecture of the MACOM complex

In *Drosophila*, the *Hakai* gene codes for two short and two long protein isoforms only differing in the extension of the C-terminal region. All Hakai proteins possess two N-terminal domains that have high sequence identity (~60%) with human HAKAI: a RING-type zinc finger domain, which is commonly found in E3 ubiquitin ligases, and a C2H2-type zinc finger domain. Crystal structure of the two zinc-finger domains of human HAKAI revealed that an atypical pTyr-binding domain is formed at the interface between two anti-parallel intertwined HAKAI monomers (Mukherjee et al., 2012). The so-called HYB domain (Hakai pTyr-binding) specifically recognizes single pTyr residues flanked by acidic amino acids in proteins phosphorylated by the Src kinase, such as E-cadherin, cortactin and DOK1 (Mukherjee et al., 2012). In agreement with the human HAKAI structure, we showed that *Drosophila* Hakai also dimerizes regardless of isoform identity and that the RING domain is required for homodimerization and interaction with other members of MACOM.

Using full-length as well as fragments of MACOM components in different combinations, we precisely mapped the intermolecular interactions between the different elements of the complex in fly as well as human cells. Although HAKAI was first identified among the interactors of WTAP (Horiuchi et al., 2013), we propose that their interaction is likely indirect. Particularly, we observed that the N-terminal region of Hakai interacts with the N-terminal domain of Vir, while Fl(2)d binds to the C-terminus at the opposite

end of Vir. In addition, interaction between Hakai and Fl(2)d is greatly compromised upon depletion of Vir, indicating that Vir acts as a scaffold for the assembly of Hakai and Fl(2)d into the MACOM complex. Notably, several predicted tyrosine phosphorylation sites flanked by at least one acidic amino acid can be found within the N-terminal region of Vir (Y195, Y245, Y263, Y307). This, together with the fact that mutations in the RING domain of Hakai not only prevent its dimerization but also weaken its binding to Vir, corroborate a model of Hakai-Vir direct interaction that is dependent on Hakai homodimerization and consequential recognition of Vir pTyr residues.

Recently, first-time resolution of the structure of human MACOM via cryo-EM shed light on its internal architecture and elucidated how it assembles in a single complex with MAC (Su et al., 2022). Although HAKAI could be co-purified together with the other MACOM components via SDS-PAGE, only WTAP, VIRMA, and ZC3H13 were found in the cryo-EM structure and HAKAI was hypothesized not to be visible on account of its high flexibility. Intriguingly, the N-terminal domain of VIRMA, which we propose constitutes the site of direct interaction between HAKAI and the rest of MACOM, is also missing from the structure and its absence might explain why HAKAI could not be resolved together with the other MACOM components in the cryo-EM structure.

6.1.2 Function of Hakai within the MACOM complex

As previously mentioned, MACOM components have been shown to enhance activity as well as to contribute to specificity of the m⁶A writer complex. However, removing HAKAI from the complex does not affect the catalytic activity of MAC nor weaken the binding affinity of MACOM to mRNA substrates *in vitro* (Su et al., 2022), and the function of HAKAI within the methyltransferase complex has long remained unclear. We found that *Drosophila* Hakai is crucial for the stabilization of some of the other MACOM elements. Our results show that depletion of Hakai leads to severe reduction of the protein levels of Vir, Fl(2)d and Flacc, while it does not affect levels of the two MAC components and Nito. In agreement with the high evolutionary conservation of Hakai, its stabilizing effect on MACOM components is conserved in human cells. Notably, the fact that not all subunits of the writer complex are affected by depletion of Hakai and that the affected ones are strongly destabilized but not completely lost might be one of the reasons why loss of Hakai give rise to milder phenotypes in regard to m⁶A levels and sex determination compared to loss of other MACOM components in flies as well as plants (Růžička et al., 2017).

HAKAI is characterized by the presence of a conserved RING domain and in virtue of this was promptly classified as E3 ubiquitin ligase (Fujita et al., 2002). Nevertheless, lack of Hakai causes reduction rather than increase in the protein levels of other MACOM components in *Drosophila* cells, suggesting that it may not act as an E3 ubiquitin ligase in this context. In agreement with this hypothesis, we observed that Fl(2)d is ubiquitinated at two sites (K236 and K245), but its ubiquitination is independent of Hakai in flies. In addition, by performing an unbiased ubiquitylome analysis in control versus Hakai KD conditions, we found that none of the thousands of ubiquitination sites identified in S2R+ cells were negatively impacted by depletion of Hakai, not even E-cadherin, which is the only protein target known to be bound and presumably ubiquitinated by HAKAI in mammalian cells (Fujita et al., 2002). As a matter of fact, while HAKAI undoubtedly interacts with E-cadherin in a tyrosine phosphorylation-dependent manner (Fujita et al., 2002; Mukherjee et al., 2012) and levels of ubiquitinated E-cadherin are increased upon overexpression of HAKAI (Fujita et al., 2002), clear evidence of direct ubiquitination of E-cadherin by HAKAI is currently not available. Over the years, several studies showed that the E-cadherin complex can

6. Discussion

be ubiquitinated in a p-Tyr dependent way by other E3 ubiquitin ligases, such as MDM2 (J.-Y. Yang et al., 2006), SKP2 (Inuzuka et al., 2012) and RNF43 (Y. Zhang et al., 2019), so it is possible that HAKAI acts only as bridging factor mediating the transfer of phosphorylated protein recognized by its HYB domain to other E3 ligases. Nonetheless, it is still possible that Hakai directly ubiquitinates its protein targets only in particular cell types or that its ubiquitination activity depends on specific external stimuli.

Besides ubiquitination, many other post-translational modifications (PTMs), such as methylation, acetylation, sumoylation and neddylation, are known to be involved in the regulation of protein stability and intramolecular interactions (J. M. Lee et al., 2023). For instance, arginine methylation has been shown to weaken the association of Arg-containing proteins to nucleic acids and to increase the concentration threshold at which multivalent protein-RNA complexes undergo liquid-liquid phase separation (LLPS) (Q. Wu et al., 2021). Unlike the other MACOM components, VIRMA appears to be heavily Arg-methylated in its C-terminal region and two of the arginine residues that have been identified as methylated (R1773 and R1775) are conserved in the *Drosophila* Vir protein. In addition, we observed that Art1, which is the *Drosophila* homolog of the protein arginine methyltransferase 1 (PRMT1) enzyme, was found among the strongest interactors of the Hakai protein in S2R+ cells. Taking into account that the m⁶A writer complex has been hypothesized to undergo LLPS to increase local concentration and enzymatic activity (D. Han et al., 2022), it would be interesting to investigate whether arginine methylation of MACOM components has perhaps an influence on localization and functioning of the m⁶A writer complex and secondly if Hakai plays a role in this context. HAKAI is also known as CBL1 (CBL-like-1) because of its sequence and structure similarity with the well characterized E3 ubiquitin ligase CBL (Casitas B-lineage Lymphoma). Of interest, previous studies reported that CBL-mediated neddylation of the TGF- β Type II receptor antagonizes its ubiquitination and degradation promoting the antiproliferative effect of TGF- β on blood cells (Zuo et al., 2013), whereas HAKAI has been shown to regulate turnover of the scaffold protein Ajuba via neddylation in hepatocellular carcinoma cells (M. Liu et al., 2018). Keeping all these observations in mind, it would be interesting to investigate whether Hakai might mediate dynamic changes in the PTM landscape of MACOM in order to regulate m⁶A methylation in response to environmental and cellular signals.

6.1.3 Do the short and long Hakai isoforms have different functions in flies?

In a similar way to all other components of the m⁶A writer complex, HAKAI displays strict nuclear localization in plants (Růžička et al., 2017) as well as in most mammalian cell lines (Horiuchi et al., 2013). However, in addition to predominant localization in the nucleus, weak but widespread cytoplasmic signal was detected using anti-HAKAI antibody in cancerous epithelial cell lines (Díaz-Díaz et al., 2020; Figueroa et al., 2009) as well as in epithelial cells treated with HGF to induce cell-cell contacts dissociation and promote cell motility (Figueroa et al., 2009). Peculiarly, the *Drosophila* Hakai protein exists in short and long isoforms with distinct subcellular localization. As previously reported in S2 cells (Kaido et al., 2009), we observed that the Hakai long isoform localized ubiquitously in the cell with noticeable enrichment in the nucleus. Contrastingly, localization of the short isoform appeared to be exclusively cytoplasmic and strongly enriched at the cellular membrane. Notably, we observed differential localization between Hakai isoforms in both S2R+ and BG3 cells. Despite referring to ectopically expressed Myc-tagged Hakai isoforms, the localization pattern we observed raises the possibility that the two isoforms might be involved in different cellular processes and have distinct functions. Since m⁶A deposition happens co-

transcriptionally in the nucleus, the nuclear-localized long isoform of Hakai seems to be likely the one involved in the process of m⁶A writing. However, we observed in yeast-two-hybrid assays that Hakai isoforms can homo- as well as hetero-dimerize and that they are both able to bind Fl(2)d and Nito. In addition, the lethality of our *Hakai*^{null} mutant flies can be rescued by ectopic expression of both Hakai long and short. Taken together, our observations suggest that the two *Drosophila* Hakai isoforms might act redundantly. Additional work is needed to clarify whether the localization of short and long isoforms in different cellular compartments can be observed also analyzing the distribution of the endogenously expressed Hakai proteins and if so, whether the difference is biologically relevant. To this aim, it would be important to generate *Hakai* long-specific mutant flies to evaluate whether lack of the long isoform is sufficient to give rise to MACOM components destabilization and m⁶A level reduction or whether its loss can be compensated by Hakai short *in vivo*. Additionally, resolution of the structure of the *Drosophila* m⁶A writer complex would also be helpful to uncover which Hakai isoform (or heterodimers of Hakai short and long?) is part of it as well as to better understand how exactly Hakai exert its stabilizing function within the MACOM complex.

6.2 Can m⁶A be erased in *Drosophila*?

A very important discovery that reignited interest in the m⁶A field was the identification of two enzymes that can demethylate m⁶A: FTO (Jia et al., 2011) and ALKBH5 (Zheng et al., 2013). Nevertheless, FTO has been later shown to display a strong preference for m⁶Am within the 5' cap of mRNAs (Mauer et al., 2017) and snRNAs (Mauer et al., 2019) as well as to target m⁶A on the U6 snRNA and m¹A on tRNAs in addition to internal m⁶A on mRNAs (J. Wei et al., 2018). Unlike FTO, ALKBH5 has no activity toward m⁶Am and is selective for m⁶A on mRNA (Mauer et al., 2017). Except for tissue specific defects, mice lacking either FTO or ALKBH5 are mostly normal indicating that m⁶A demethylation is not essential for development or viability (Hess et al., 2013; Mauer et al., 2017). In addition, although changes in m⁶A levels on mRNA were detected in cells that either overexpressed or were depleted of FTO/ALKBH5 (Jia et al., 2011; Z. Li et al., 2017; J. Wei et al., 2018; Zheng et al., 2013), only a limited amount of m⁶A sites have been validated as direct targets of demethylation activity. These observations, together with the fact that m⁶A levels are quite stable throughout the life cycle of mRNA (Ke et al., 2017), suggest that further studies are needed to determine whether demethylation has a predominant role in regulating the global distribution of m⁶A on mRNA.

FTO and ALKBH5 belong to the ALKBH family of Fe(II)- and α -ketoglutarate-dependent dioxygenases that includes the nine human homologs of bacterial AlkB named ALKBH1-8 and FTO (Gerken et al., 2007; Kurowski et al., 2003). ALKBH proteins can target a wide range of modifications on nucleic acids as well as proteins (Table 1) and some members of the family recognize m⁶A on substrates different from mRNA: ALKBH1 and ALKBH4 demethylate 6mA on DNA (Kweon et al., 2019), while ALKBH3 reverses m⁶A on tRNAs (Ueda et al., 2017). FTO and ALKBH5 are found solely in vertebrate species and the *Drosophila* ALKBH family only includes homologs of ALKBH1 (AlkB), ALKBH4 (CG4036), ALKBH6 (CG6144), ALKBH7 (CG14130) and ALKBH8 (CG17807). Previous work from our lab revealed that depletion of none of the *Drosophila* ALKBH proteins altered global levels of m⁶A on mRNA in a significant way (unpublished data). Even though we cannot exclude that ALKBH proteins might act on a restricted subset of methylated mRNA targets or on other RNA species, it appears that there are no obvious m⁶A demethylases in flies.

6.2.1 m⁶A on mRNA is probably not the main substrate of Alkbh6

Within the ALKBH family, ALKBH6 represents the least characterized member of the group. Although the biological relevance of ALKBH6 has been partially addressed in plants (Huong et al., 2020) and human pancreatic cancer cells (S. Zhao et al., 2021), no direct evidence of ALKBH6 activity towards any type of substrates is currently available. Thus, given the lack of knowledge about ALKBH6 and the availability of a mutant allele for the *Drosophila Alkbh6* gene previously generated in our lab, we decided to explore functions and targets of this poorly characterized member of the ALKBH family in flies.

All ALKBH proteins display a similar double-stranded β -helix (DSBH) fold at their catalytic core, but different nucleotide recognition lids (NRLs) for substrate binding and specificity. NRLs consist of two looped structures (named “Flip1” and “Flip2”) forming a lid over the active site that is involved in nucleic acid recognition and “flipping” of methylated bases out of the helix for oxidative demethylation (Sundheim et al., 2008). Crystal structure of human ALKBH6 revealed that its Flip1 and Flip2 differ from the ones of other ALKBH proteins in both sequence and conformation and that ALKBH6 is able to discriminate against double-stranded nucleic acids thanks to a unique long Flip3 (L. Ma et al., 2022). Residues of the catalytic core that have been previously reported to be important for nucleotide recognition in other members of the ALKBH family are mostly conserved in ALKBH6 suggesting that it might act as a DNA/RNA demethylase. Indeed, purified human ALKBH6 was shown to bind RNA and ssDNA as well as bubble or bulge DNA but not dsDNA *in vitro* (L. Ma et al., 2022).

As previously mentioned, ALKBH6’s function has been to some extent investigated in *Arabidopsis thaliana* (Huong et al., 2020). Although neither m⁶A nor m⁵C levels were significantly affected in ALKBH6 mutant plants, Huong and colleagues tested the binding affinity of the *Arabidopsis* ALKBH6 protein to methylated RNA probes via EMSA assay. Two of the RNA probes used in the experiment were derived from known m⁶A-modified sequences of *Arabidopsis SOS3* or human *MAT2A* transcripts, while the third one consisted of the m⁵C consensus sequence previously identified in plants. Results of the assay showed that ALKBH6 was able to bind to m⁶A/m⁵C-labeled RNA probes with the same affinity as to unmodified ones, indicating that *Arabidopsis* ALKBH6 can efficiently bind to both methylated and unmethylated RNA substrates *in vitro* (Huong et al., 2020). Nonetheless, enzymatic activity of ALKBH6 towards m⁶A or m⁵C was not tested. On our side, we observed that m⁶A levels on mRNA were not affected in flies that either overexpressed or were depleted of Alkbh6 (**Figure 14D**). In addition, RNA pull-down experiments performed with protein lysate from S2R+ cells expressing FlagMyc-tagged Alkbh6 did not show specific binding of Alkbh6 to AA(A/m⁶A)CU RNA probes regardless of their methylation status (**Figure 14E**). Taken together, our data suggests that m⁶A distribution on mRNA is not globally regulated by Alkbh6 in *Drosophila*.

6.2.2 What is the function of Alkbh6 in flies?

Interestingly, Huong and colleagues also reported that expression levels of *ALKBH6* mRNA were increased up to fourfold in plants grown in conditions of high salinity and that ALKBH6 mutants showed significantly lower survival rate under salt, drought or heat stress compared to WT plants (Huong et al., 2020). Taking a cue from these observations, we subjected S2R+ cells to different types of abiotic stress and quantified expression levels of *Alkbh6* via RT-qPCR. Remarkably, *Alkbh6* resulted to be significantly

6. Discussion

overexpressed upon heat, oxidative and salt stress as well as starvation but not in response to cold stress (**Figure 16**). Notably, expression of *Alkbh8*, which is the member of the ALKBH family displaying highest homology to *Alkbh6*, was not affected by any of the stress stimuli we tested. In line with these results, we found that flies lacking *Alkbh6* are highly sensitive to oxidative stress as well as starvation and die significantly faster than WT flies when deprived of food or exposed to the oxidative stress inducer paraquat (**Figure 18A-B** and **19**). In addition, ectopic expression of UAS-*Alkbh6* cDNA driven by the ubiquitous *Tubulin*-GAL4 driver was sufficient to rescue the sensitivity to oxidative stress of *Alkbh6* mutants and, when expressed in a WT background, considerably extended the lifespan of flies exposed to paraquat (**Figure 18C-D**). To investigate the mechanism underlying this phenotype, we carried out transcriptome analysis in WT and *Alkbh6* mutant flies after a 24h exposure to paraquat (**Figure 20**). As could be expected, we found that the differentially expressed genes common between the two genotypes reflected a general slowdown of cellular metabolic processes and gametogenesis as well as an increase in the biosynthesis of the antioxidant glutathione. Furthermore, genes that were upregulated and downregulated specifically in *Alkbh6* mutants were enriched for processes linked to the cellular stress response and for ecdysteroid metabolism, respectively (**Figure 20C-F**). Thus, in agreement with increased susceptibility to paraquat of flies lacking *Alkbh6*, our transcriptomic data show that, for identical exposure time, the physiological response to paraquat-induced oxidative stress was significantly stronger in *Alkbh6* mutants than in WT flies. Given that we assessed only the effects of a 24h paraquat treatment so far, transcriptomic analysis at different time points after paraquat exposure should help to validate a model according to which loss of *Alkbh6* results in hypersensitivity and accelerated response to oxidative stress in *Drosophila*. It would also be interesting to evaluate whether the involvement of *Alkbh6* in the oxidative stress response is conserved in higher organisms. Oxidative stress can be defined as the imbalance between the production of reactive oxygen species (ROS) and the ability of the cells to clear them. Alterations in the normal redox state of cells can generate different types of DNA lesions, which, if left unrepaired, can become cytotoxic as well as mutagenic. Among the DNA lesions induced by oxidative stress, exocyclic ϵ -adducts are the result of the reaction between DNA bases and the by-products of oxidatively-damaged unsaturated lipids (Blair, 2001). Notably, human ALKBH2 was reported to repair all three types of ϵ -adducts (ϵ A, ϵ C and 1,N²- ϵ G) in dsDNA and only ϵ A and ϵ C in ssDNA, while ALKBH3 repaired exclusively ϵ C in ssDNA (Zdzalik et al., 2015). Although only ALKBH2 and ALKBH3 were shown to target this type of oxidative DNA damage so far, we cannot exclude that other members of the ALKBH family might also be able to repair ϵ -adducts. In light of this, it would be interesting to investigate which proteins are responsible for the repair of ϵ -adducts in *Drosophila* — which lacks homologs of ALKBH2 and ALKBH3 — and whether the inefficient removal of ϵ -adducts might explain the sensitivity to paraquat-induced oxidative stress of our *Alkbh6* mutant flies.

Besides oxidative stress, alkylative stress also constitutes a major source of DNA damage. Alkylating agents generate different types of DNA lesions, such as O6mG, 3mA, 1mA and 3mC, and are commonly used as chemotherapeutics in the treatment of various type of cancer (D. Fu et al., 2012). Alkylating agent-induced DNA damage is recognized and repaired by different cellular mechanisms, including base excision repair and direct repair by ALKBH enzymes. Both ALKBH2 and ALKBH3 are able to repair 1mA and 3mC in dsDNA and ssDNA/RNA, respectively (Aas et al., 2003; Duncan et al., 2002). Interestingly, human ALKBH6 has been recently reported to be required to maintain genome stability and to promote survival in pancreatic cancer cells exposed to alkylating agents (S. Zhao et al., 2021). Particularly, Zhao and

colleagues showed that pancreatic cancer cells depleted of ALKBH6 accumulated DNA damage in the form of DSBs and displayed reduced viability when exposed to the alkylating agent methyl methane sulfonate (MMS). Therefore, in parallel to the efficiency of ϵ -adducts repair, it would be also important to test if alkylative stress-induced DNA methylation is correctly repaired in *Alkbh6* mutants or if lack of *Alkbh6* makes flies more sensitive to alkylative stress as it does for oxidative stress.

As previously reported for human ALKBH6 (TsujiKawa et al., 2007), we showed that *Drosophila* *Alkbh6* localizes ubiquitously in S2R+ cells (**Figure 15B**). Intriguingly, the distribution of *Alkbh6* appeared to be enriched at the nuclear periphery in response to paraquat-induced oxidative stress as well as starvation (**Figure 17A**). In addition, we performed *Alkbh6* interactome analysis and surprisingly identified the m⁶A nuclear reader *Ythdc1* in S2R+ cells exposed to paraquat or starvation, but not in unstressed cells (**Figure 17B-C**). Of note, m⁶A-modified mRNAs were shown to rapidly and transiently accumulate at sites of DNA damage and to contribute to regulation of the UV-induced DNA damage response (Xiang et al., 2017). In light of this, we can speculate that accumulation of *Ythdc1*-bound m⁶A-modified transcripts at sites of DNA damage might facilitate recruitment of *Alkbh6* to the nucleus for the repair of oxidative stress-induced DNA methylation.

6.3 Reading m⁶A in the nervous system of *Drosophila*

The two major mechanisms by which m⁶A exerts its functions are recruitment of proteins that specifically recognize and bind the modification (m⁶A readers) or alteration of local RNA structures that indirectly affects the binding of classical RBPs (m⁶A switch). Among the best characterized m⁶A readers we find the YTH domain-containing proteins that can specifically accommodate m⁶A inside an aromatic cage of the YTH domain. Vertebrate species possess five YTH m⁶A readers: YTHDC1, YTHDC2 and the three paralogs YTHDF1, YTHDF2 and YTHDF3. In *Drosophila*, the YTH family of m⁶A readers is limited to two members: the nuclear *Ythdc1* and the cytoplasmic *Ythdf* protein. While *Ythdc1* was shown to be the main mediator of m⁶A-dependent splicing (Hausmann et al., 2016; Kan et al., 2017; Lence et al., 2016), the function of *Ythdf* was still largely uncharacterized at the time this project started.

6.3.1 Loss of m⁶A affects adult locomotion and larval NMJ morphology

Multiple lines of evidence indicate that m⁶A plays a central role in controlling both development and function of the nervous system (Angelova et al., 2018). Previous work from our lab (Lence et al., 2016) and others (Hausmann et al., 2016; Kan et al., 2017) revealed that flies lacking *Mettl3*-deposited m⁶A are flightless and display locomotion defects including slow walking speed and disorientation. Notably, all phenotypes were rescued by ubiquitous as well as neuronal expression of *Mettl3* cDNA, but not if *Mettl3* was expressed exclusively in muscles. The larval neuromuscular junction (NMJ) system of *Mettl3* mutants was also analyzed to investigate potential neurological defects underlying the locomotion phenotype observed in flies. Interestingly, *Mettl3* mutants displayed a significant increase in the number of synaptic boutons and active zones per bouton — which are the sites of neurotransmitter release — compared to WT larvae. In this study, we validated the results of previous NMJ analysis and, in addition to increased boutons number, we also observed increased axonal length and branching of synaptic terminals in both *Mettl3* and *Mettl14* mutant larvae. Once again, complete rescue of the NMJ phenotype of *Mettl3* mutants could be achieved by ubiquitous expression of *Mettl3* cDNA. Although we cannot assume a

cause-effect relationship between the synaptic overgrowth phenotype at larval NMJ and the locomotion defects at the adult stage of *Mettl3* mutant flies, our data clearly indicate that m⁶A modification is important for larval NMJ morphology and potentially synaptic transmission. In the future, it will be important to perform electrophysiological analysis in order to assess functionality of the oversized NMJs of *Mettl3* mutant larvae and to investigate whether they display locomotion defects similar to the ones we observed in adult flies lacking *Mettl3*. Vice versa, NMJ analysis in adult *Mettl3* mutants would allow us to verify whether the morphological defects observed in mutant larvae persist even after metamorphosis to adult flies.

6.3.2 Ythdf and Fmr1 interplay to regulate axonal growth at larval NMJs

In light of the NMJ phenotype of *Mettl3* mutants, we aimed to identify and characterise the proteins that can decode m⁶A in the *Drosophila* nervous system. To this aim, we performed *in vitro* RNA pull-down assays by incubating biotinylated RNA probes containing four repeats of the m⁶A consensus sequence GG(A/m⁶A)CU with protein extracts from larval CNS-derived BG3 cells. In addition to Ythdc1 and Ythdf, *Drosophila* Fmr1 was also identified among the most enriched proteins in the pull-down lysate with the m⁶A-modified probe. Our observations are in line with the results of similar pull-down experiments performed in mammalian cells, which previously identified FMR1 as a sequence-context-dependent m⁶A-binding protein (Arguello et al., 2017; Edupuganti et al., 2017). We also showed that Fmr1 co-immunoprecipitated with Ythdf and vice versa and that the two proteins directly interact with each other in an RNA-independent manner. Of note, loss of function or overexpression of *Drosophila* Fmr1 was previously shown to give rise to either enlarged or shrunken larval NMJs, respectively (Y. Q. Zhang et al., 2001). In light of this, we decided to test whether the two YTH domain-containing proteins also contributed to the regulation of NMJ morphology. Remarkably, while *Ythdc1* mutants did not display any morphological defects, loss of *Ythdf* resulted in a phenotype of synaptic overgrowth, indicating that Ythdf plays a role in the m⁶A-dependent regulation of NMJ morphology together with Fmr1. Consistently with this model, quantitative analysis of double-mutant genetic interactions showed that the NMJ overgrowth phenotype observed in either *Ythdf* or *Fmr1* homozygous mutant larvae was not aggravated by removing one or two copies of the other genes, indicating that Ythdf and Fmr1 act in the same pathway and co-regulate axonal growth at larval NMJ.

Mechanistically, we found that the m⁶A pathway controls larval NMJ morphology, primarily via the Ythdf/Fmr1-mediated repression of *futsch* mRNA translation. *Futsch*, which is the *Drosophila* homolog of the microtubule-associated protein MAP1B, controls assembly and organization of the microtubule cytoskeleton during axonal growth and synaptogenesis. Notably, Fmr1 was already known for twenty years to act as a negative regulator of *futsch* translation to tightly control synaptic growth and function at larval NMJs (Y. Q. Zhang et al., 2001). In this study, we validated and expanded those previous findings showing that binding of Ythdf to two m⁶A sites in the 5'UTR of *futsch* mRNA is necessary to guide Fmr1 for efficient translational repression of *futsch*. In light of this, our results are in contrast with the known role of mammalian YTHDF proteins as mediators of m⁶A-dependent translation enhancement. Interestingly, FMR1 was reported to co-immunoprecipitate with YTHDF2 in an RNA-independent manner (F. Zhang et al., 2018). Differently from our findings showing that *Drosophila* Fmr1 and Ythdf act in concert to repress translation, Zhang and colleagues proposed a model in which mammalian FMR1 and YTHDF2 compete for binding to a common set of methylated targets whose stability is enhanced or reduced upon binding by

6. Discussion

FMR1 or YTHDF2, respectively. Nevertheless, FMR1 was recently identified among the proteins possibly repressing translation of m⁶A-modified transcripts in the quantitative trait locus (QTL) analysis of m⁶A peaks in human lymphoblastoid cells (Z. Zhang et al., 2020; Z. Zou et al., 2022). Therefore, it would be interesting to investigate whether an interplay between YTHDF2 and FMR1 to promote m⁶A-dependent translation repression exists also in mammals. In addition, how common translation inhibition by Fmr1-Ythdf is in *Drosophila*? The possibility that other methylated transcripts besides *futsch* are regulated by this mechanism has not been addressed in our current work and will be the subject of future investigations. Finally, as FMR1 was implicated in mediating the nuclear export of m⁶A-modified mRNAs (Edens et al., 2019; Hsu, Shi, et al., 2019), it is also possible that a similar mechanism is conserved in flies. Considering that Fmr1 was found enriched in the interactome of MACOM components (Bawankar et al., 2021; Knuckles et al., 2018) as well as of Ythdc1 (Lence et al., 2016), it would be interesting to examine whether Fmr1 binds to *futsch* already in the nucleus and contributes to its efficient export to the cytoplasm together with Ythdc1 in *Drosophila* cells.

6.3.3 Possible link between m⁶A and FXS

The Fragile X syndrome (FXS) is the most common inherited form of mental retardation and the prime monogenic cause of autism. FXS is caused by expansion (≥ 200) of the CGG repeats normally present (5-45) in the 5'UTR of the *FMR1* gene on the X-chromosome. In FXS patients, the abnormally expanded CGG segment is hypermethylated resulting in epigenetic inactivation of the *FMR1* gene and consequent loss of the FMR1 protein (also known as FMRP). FXS is named after the evident constriction at the end of the long arm of the X chromosome that corresponds to the expanded trinucleotide repeats of *FMR1* and makes the chromosome look like “broken” or “fragile” when examined under the microscope.

Over the years, numerous animal models based on mutations or KO of *FMR1* homologs have been used to characterize its function as well as to screen drug candidates for the pharmacological therapy of FXS. Remarkably, *Fmr1* mutant flies recapitulate most of the pathological symptoms of FXS patients, including learning and memory deficits, autism-like behaviors (abnormal grooming and impaired social behavior), irregular circadian rhythm in constant darkness, locomotion defects and decreased male courtship activity (Trajković et al., 2023). Most interestingly for us, FXS is considered to be a synaptic disorder. FXS patients (Irwin et al., 2001) as well as adult *FMR1* KO mice (Comery et al., 1997; Nimchinsky et al., 2001) often display abnormal development of dendritic spines, which appear to be increased in density and morphologically closer to immature (long and thin) than mature (stubby or mushroom-shaped) spines in several regions of the brain cortex. These abnormalities of the dendritic spines — which constitute the postsynaptic site of most excitatory synapses in the mammalian brain — closely resemble the overgrowth phenotype we observed at the excitatory NMJ synapses of most m⁶A mutants. Notably, ectopic expression of human FMR1 can fully rescue the NMJ phenotype of *Fmr1* mutant larvae (Coffee Jr et al., 2010). In addition, as Fmr1 represses *futsch* translation in *Drosophila*, FMR1 was shown to negatively regulate translation of MAP1B during active synaptogenesis in the mouse brain (Lu et al., 2004). Considering this functional conservation together with the fact that numerous m⁶A sites were identified on human and mouse *MAP1B* mRNA, it would be very interesting to test whether m⁶A methylation is necessary for efficient translational repression of mammalian MAP1B. The existence of a similar mechanism would pave the way for potential new treatments of FXS lifelong symptoms.

6.4 Dhx57 is a potential new m⁶A binding protein in *Drosophila*

During our search for the reader proteins that mediate m⁶A functions in the nervous system of flies, we observed that the cytoplasmic RNA helicase Dhx57 was reproducibly enriched in the pull-down fraction with the m⁶A-modified RNA probe in BG3 (Worpenberg et al., 2021) as well as S2R+ cells (**Figure 7A**). Dhx57 preferential binding to methylated RNA resulted to be independent from the presence of the known cytoplasmic reader Ythdf (**Figure 7B**) and restricted to the GGACU sequence context (**Figure 7D-E**). Dhx57, which is a DEXD/H box RNA helicase homologue to human DHX57, belongs to the large group of RNA helicases that are still completely uncharacterized across the eukaryotic tree of life.

To investigate whether the ability to bind m⁶A was unique to Dhx57 or shared with other RNA helicases of the DEXD/H box family, we tested Dhx57 paralogs' binding affinity to methylated/unmethylated GGACU RNA probes in S2R+ cells. Only Dhx36, which is the closest paralog to Dhx57, showed a slight preference for the m⁶A-modified RNA probe, while Dhx34 and Dhx9 displayed no clear binding to either of the probes (**Figure 8A-B**). These results suggest that m⁶A binding is not a common feature of *Drosophila* DEXH box helicases but it is a peculiar ability of Dhx57. Pull-down experiments with the exact same GG(A/m⁶A)CU RNA probes were previously performed to screen for m⁶A interactors in mammalian cell lines (Edupuganti et al., 2017). Interestingly, DHX57 was found a little below the 1.5-fold enrichment threshold in pull-downs performed with either HeLa or mESC cytoplasmic lysates, while it did not show any enrichment in binding to a methylated GAACU probe. Differently from our results, a similar enrichment could be observed for DHX9, whereas other paralogs of DHX57 were either found among background proteins (DHX30 and DHX36) or undetected (DHX29 and DHX34). In the future, additional pull-down experiments upon overexpression of these proteins in different mammalian cell lines will have to be performed in order to clarify whether or not preferential binding to m⁶A-modified RNA is an evolutionary conserved ability of DHX57 (and other DEXD/H box helicases).

6.4.1 What are the targets of Dhx57?

To identify the mRNA targets of Dhx57, we performed TRIBE sequencing on polyA-enriched RNA and found that a subset of ~300 transcripts was bound by Dhx57 in S2R+ cells (**Figure 9**). Overlap of the Dhx57 TRIBE dataset with the list of m⁶A-modified transcripts identified via miCLIP in S2R+ cells (Worpenberg et al., 2021) revealed that the great majority (~89%) of Dhx57 mRNA targets are methylated (**Figure 9B**). Of note, unlike the vertebrate m⁶A profile, the m⁶A sites identified in *Drosophila* via miCLIP are mostly located in the 5'UTR rather than in the CDS and 3'UTR and are enriched in the AAACA rather than in the GGACU sequence context (underlined A is targeted for methylation) (Kan et al., 2017, 2021; Worpenberg et al., 2021). Since we observed that Dhx57 preferentially binds to m⁶A exclusively in the GGACU sequence context, we decided to examine whether this motif was enriched at the m⁶A sites of Dhx57 mRNA targets. To overcome the lack of nucleotide resolution of TRIBE, we performed motif enrichment analysis considering all miCLIP m⁶A sites found within ±0.5 or 1kb from the A-to-I editing events identified in the Dhx57 TRIBE dataset. In contrast with our hypothesis, we found that the classic m⁶A consensus sequence was enriched in the selected regions but mostly within the AAACU motif (data not shown). However, it is important to keep in mind that the editing range of the Dhx57-Adar fusion protein is rather difficult to predict as it might be affected by both sequence and secondary structure of the target RNAs. Thus, although binding of Dhx57 to selected mRNA targets resulted to be

severely compromised in flies lacking *Mettl3* (**Figure 10**), mapping of Dhx57's binding sites at single-nucleotide-resolution via iCLIP is of critical importance to unequivocally validate the RNA targets of Dhx57 as well as to clarify whether its binding sites overlap with known sites of m⁶A methylation on mRNA. In addition, reporter constructs containing A-T point mutations at the m⁶A sites of selected Dhx57 targets could be used to unambiguously confirm that Dhx57 binds to at least some of its RNA targets in an m⁶A-dependent manner. Since Dhx57 does not possess a YTH domain and preferential binds to m⁶A-modified RNA independently from Ythdf, it would also be interesting to investigate if m⁶A-mediated structural switches can explain its substrate preference.

6.4.2 What is the function of Dhx57 in flies?

GO term analysis of the methylated targets of Dhx57 identified via TRIBE showed enrichment for many distinct biological processes, such as cellular response to virus, long-term strengthening of NMJs and integrated stress response signaling (**Figure 9C**). Enrichment of the cellular response to virus is consistent with the role that DExD/H box RNA helicases are known to play at the virus-host interface (Ranji & Boris-Lawrie, 2010). On the one hand, some RNA helicases (RIG-I-like receptors or RLRs) can function as cellular sensors that recognize non-self RNA molecules and contribute to the activation of the innate antiviral response. On the other hand, some viruses are able to hijack cellular RNA helicases of the host to promote replication of their genome. Like in plants and other invertebrates, RIG-I-like receptors are absent in *Drosophila*, but Dicer2, which belongs to the same DExD/H box helicase family as RLRs, can sense viral infection and trigger antiviral gene expression as RLRs do in mammals (Schneider & Imler, 2021). Briefly, Dicer2 is an RNase III enzyme that can process long dsRNAs typically produced as intermediates during viral replication into short interfering RNA (siRNA) duplexes. Those siRNA duplexes are then loaded onto Ago2, where one strand (passenger strand) is discarded and the other one (guide strand) is used to guide Ago2 towards its target RNA for translation inhibition or degradation in a process known as RNA interference (RNAi). Although viral infection causes specific activation of the siRNA pathway in *Drosophila*, a subset of miRNAs and some miRNA passenger strands were found to associate to Ago2 (Czech et al., 2009; Ghildiyal et al., 2010; Tomari et al., 2007). Thus, to examine whether loss of Dhx57 or alteration of m⁶A levels would affect the RNAi process, we expressed self-silencing reporters designed to estimate the efficiency of Ago2-mediated miRNA silencing in both S2R+ cells and flies depleted of Dhx57 or *Mettl3*. Our results showed that both Dhx57 and *Mettl3* seem to be dispensable for efficient Ago2-mediated miRNA silencing (**Figure 11**), however we cannot exclude that they might be still involved in the antiviral response based on the siRNA pathway. Considering that the 5'UTR-biased m⁶A profile of *Drosophila* suggests that its main cytoplasmic function is to regulate translation, we can speculate that m⁶A-dependent target recognition by Dhx57 might provide the means for rapid and selective translational activation of antiviral factors such as Dicer2 and Ago2 upon viral infection. To address this possibility, it would be important to evaluate the response of *Dhx57* and *Mettl3* mutant flies to exposure to *Drosophila* viruses as well as to perform transcriptomic and proteomic analysis of WT and *Dhx57/Mettl3* mutant flies in control vs viral infection conditions. Alternatively, recognition of m⁶A on viral RNA by Dhx57 as cellular mechanism to detect viral infection represents another intriguing possibility. In support of this model, human DHX57 was shown to display strong and specific binding to an RNA G-quadruplex (G4) probe (Murat et al., 2018) and colocalization between m⁶A and G4-forming sequences was observed in different RNA viruses (e.g. HIV, Zika, Hepatitis B, SV40) (Fleming et al., 2019).

6. Discussion

Whether *Drosophila* Dhx57 can bind to RNA G4s and its relevance *in vivo* awaits future investigations. Finally, it would be also interesting to explore the role of Dhx57 in the cellular response to other types of stress besides viral infection (e.g. heat shock, oxidative stress, starvation).

Taking a cue from the results of the GO term analysis of Dhx57 methylated targets, we also analyzed NMJ morphology upon loss of Dhx57 and found that *Dhx57* mutant larvae displayed increased synaptic boutons number as well as axonal length and branching, mimicking the NMJ defects of most m⁶A mutants (**Figure 12C-F**). Even though the phenotype was fully rescued by ubiquitous expression of *Dhx57* cDNA, it would be informative to perform additional rescue experiments using the pan-neuronal *elav*-GAL4 driver as well as drivers expressed only in motoneurons (*BG380*-GAL4), glia cells (*repo*-GAL4) or muscle fibers (*24B*-GAL4) in order to explore the possible tissue-specific requirement of Dhx57 for proper NMJ development. In addition, *Dhx57* catalytic-dead mutants should be generated in order to evaluate whether or not its helicase activity is required for m⁶A recognition and NMJ morphology regulation.

Dhx57 methylated targets that are related to the long-term strengthening of NMJs encode for proteins whose loss has already been shown to result in NMJ overgrowth (atlastin (M. Lee et al., 2009) and TBCE (S. Jin et al., 2009)) or impaired synaptic transmission (α -/ β -spectrin (Featherstone et al., 2001) and stj (Ly et al., 2008)). Of note, activity-dependent long-lasting changes in neuronal function and connectivity of *Drosophila* larval NMJs were shown to be mediated by local subsynaptic protein synthesis of the postsynaptic glutamate receptor subunit DGluR-IIA (Sigrist et al., 2000, 2003). In light of this, it would be interesting to analyze the larval PNS-specific proteome of WT and *Dhx57/Mettl3* mutant larvae as well as to investigate if the activity-dependent long-term strengthening of NMJs is impaired upon loss of *Dhx57* or Mettl3-dependent m⁶A.

6.5 Conclusions

The main aim of this PhD thesis was to expand our knowledge of the m⁶A pathway with a focus on specific aspects that are still poorly investigated in *Drosophila*. Results published in the form of research articles substantially improved our understanding of the composition of the m⁶A writer machinery (Bawankar et al., 2021) as well as highlighted the importance of this modification for proper neuronal development of flies (Worpenberg et al., 2021). In addition, unpublished findings represent an important resource of data and tools for further characterization of Dhx57 as potential m⁶A reader and Alkbh6 as potential eraser of stress-induced DNA methylation. Main findings of this study are divided according to the three original aims and summarized below.

- **Aim I: Characterization of Hakai as a novel component of the m⁶A writer complex in flies.**
 - Hakai is a core component of the m⁶A writer complex in *Drosophila* and human cells.
 - The RING domain of Hakai is required for homodimerization and interaction with other members of the MACOM complex.
 - Hakai plays a key role in the stabilization of other MACOM components (Vir, Fl(2)d and Flacc) but independently of its ubiquitination activity.

- **Aim II: Identification and characterization of the proteins that mediate m⁶A functions in the fly nervous system.**
 - Most m⁶A mutants display a phenotype of axonal overgrowth at larval NMJs.
 - Ythdf is the main m⁶A reader in the nervous system of flies and it directly interacts with Fmr1 in an RNA-independent manner.
 - The m⁶A pathway controls larval NMJ morphology primarily via the Ythdf/Fmr1-mediated repression of *futsch* mRNA translation.
 - The uncharacterized RNA helicase Dhx57 preferentially binds to m⁶A-modified RNA in the GGACU sequence context independently from Ythdf.
 - *Dhx57* mutants mimic the NMJ overgrowth phenotype of most m⁶A mutants.

- **Aim III: Characterization of Alkbh6 as potential m⁶A eraser in flies.**
 - There are no obvious m⁶A erasers in flies.
 - m⁶A on mRNA is probably not the main substrate of Alkbh6.
 - Alkbh6 expression increases in response to different types of abiotic stress.
 - *Alkbh6* mutants are hypersensitive to oxidative stress and starvation.

8. References

- Aas, P. A., Otterlei, M., Falnes, P. Ø., Vågbø, C. B., Skorpen, F., Akbari, M., Sundheim, O., Bjørås, M., Slupphaug, G., Seeberg, E., & Krokan, H. E. (2003). Human and bacterial oxidative demethylases repair alkylation damage in both RNA and DNA. *Nature*, *421*(6925), 859–863. <https://doi.org/10.1038/nature01363>
- Abakir, A., Giles, T. C., Cristini, A., Foster, J. M., Dai, N., Starczak, M., Rubio-Roldan, A., Li, M., Eleftheriou, M., Crutchley, J., Flatt, L., Young, L., Gaffney, D. J., Denning, C., Dalhus, B., Emes, R. D., Gackowski, D., Corrêa, I. R., Garcia-Perez, J. L., ... Ruzov, A. (2020). N6-methyladenosine regulates the stability of RNA:DNA hybrids in human cells. *Nature Genetics*, *52*(1), 48–55. <https://doi.org/10.1038/s41588-019-0549-x>
- Abbas, Y. M., Laudenbach, B. T., Martínez-Montero, S., Cencic, R., Habjan, M., Pichlmair, A., Damha, M. J., Pelletier, J., & Nagar, B. (2017). Structure of human IFIT1 with capped RNA reveals adaptable mRNA binding and mechanisms for sensing N1 and N2 ribose 2'-O methylations. *Proceedings of the National Academy of Sciences*, *114*(11), E2106–E2115. <https://doi.org/10.1073/pnas.1612444114>
- Adams, M. D., Celniker, S. E., Holt, R. A., Evans, C. A., Gocayne, J. D., Amanatides, P. G., Scherer, S. E., Li, P. W., Hoskins, R. A., Galle, R. F., George, R. A., Lewis, S. E., Richards, S., Ashburner, M., Henderson, S. N., Sutton, G. G., Wortman, J. R., Yandell, M. D., Zhang, Q., ... Venter, J. C. (2000). The Genome Sequence of *Drosophila melanogaster*. *Science*, *287*(5461), 2185–2195. <https://doi.org/10.1126/science.287.5461.2185>
- Agarwala, S. D., Blitzblau, H. G., Hochwagen, A., & Fink, G. R. (2012). RNA Methylation by the MIS Complex Regulates a Cell Fate Decision in Yeast. *PLOS Genetics*, *8*(6), e1002732-. <https://doi.org/10.1371/journal.pgen.1002732>
- Aguilo, F., Zhang, F., Sancho, A., Fidalgo, M., Di Cecilia, S., Vashisht, A., Lee, D. F., Chen, C. H., Rengasamy, M., Andino, B., Jahouh, F., Roman, A., Krig, S. R., Wang, R., Zhang, W., Wohlschlegel, J. A., Wang, J., & Walsh, M. J. (2015). Coordination of m6A mRNA Methylation and Gene Transcription by ZFP217 Regulates Pluripotency and Reprogramming. *Cell Stem Cell*, *17*(6), 689–704. <https://doi.org/10.1016/J.STEM.2015.09.005>
- Aguilo, F., Zhang, F., Sancho, A., Fidalgo, M., di Cecilia, S., Vashisht, A., Lee, D. F., Chen, C. H., Rengasamy, M., Andino, B., Jahouh, F., Roman, A., Krig, S. R., Wang, R., Zhang, W., Wohlschlegel, J. A., Wang, J., & Walsh, M. J. (2015). Coordination of m6A mRNA Methylation and Gene Transcription by ZFP217 Regulates Pluripotency and Reprogramming. *Cell Stem Cell*, *17*(6), 689–704. <https://doi.org/10.1016/J.STEM.2015.09.005>
- Aik, W., Scotti, J. S., Choi, H., Gong, L., Demetriades, M., Schofield, C. J., & McDonough, M. A. (2014). Structure of human RNA N6-methyladenine demethylase ALKBH5 provides insights into its mechanisms of nucleic acid recognition and demethylation. *Nucleic Acids Research*, *42*(7), 4741–4754. <https://doi.org/10.1093/nar/gku085>
- Akhtar, J., Renaud, Y., Albrecht, S., Ghavi-Helm, Y., Roignant, J. Y., Silies, M., & Junion, G. (2021). m6A RNA methylation regulates promoter-proximal pausing of RNA polymerase II. *Molecular Cell*, *81*(16), 3356–3367.e6. <https://doi.org/10.1016/J.MOLCEL.2021.06.023>
- Akichika, S., Hirano, S., Shichino, Y., Suzuki, T., Nishimasu, H., Ishitani, R., Sugita, A., Hirose, Y., Iwasaki, S., Nureki, O., & Suzuki, T. (2019). Cap-specific terminal N6-methylation of RNA by an RNA polymerase II-associated methyltransferase. *Science*, *363*(6423), eaav0080. <https://doi.org/10.1126/science.aav0080>
- Alarcón, C. R., Goodarzi, H., Lee, H., Liu, X., Tavazoie, S., & Tavazoie, S. F. (2015). HNRNPA2B1 Is a Mediator of m6A-Dependent Nuclear RNA Processing Events. *Cell*, *162*(6), 1299–1308. <https://doi.org/10.1016/J.CELL.2015.08.011>
- Anders, M., Chelysheva, I., Goebel, I., Trenkner, T., Zhou, J., Mao, Y., Verzini, S., Qian, S.-B., & Ignatova, Z. (2018). Dynamic m⁶A methylation facilitates mRNA triaging to stress granules. *Life Science Alliance*, *1*(4), e201800113. <https://doi.org/10.26508/lsa.201800113>
- Anderson, B. R., Chopra, P., Suhl, J. A., Warren, S. T., & Bassell, G. J. (2016). Identification of consensus binding sites clarifies FMRP binding determinants. *Nucleic Acids Research*, *44*(14), 6649–6659. <https://doi.org/10.1093/nar/gkw593>
- Angelova, M. T., Dimitrova, D. G., Dinges, N., Lence, T., Worpenberg, L., Carré, C., & Roignant, J.-Y. (2018). The Emerging Field of Epitranscriptomics in Neurodevelopmental and Neuronal Disorders. *Frontiers in Bioengineering and Biotechnology*, *6*. <https://www.frontiersin.org/articles/10.3389/fbioe.2018.00046>
- Aoyama, T., Yamashita, S., & Tomita, K. (2020). Mechanistic insights into m6A modification of U6 snRNA by human METTL16. *Nucleic Acids Research*, *48*(9), 5157–5168. <https://doi.org/10.1093/nar/gkaa227>
- Aparicio, L. A., Valladares, M., Blanco, M., Alonso, G., & Figueroa, A. (2012). Biological influence of Hakai in cancer: a 10-year review. *Cancer and Metastasis Reviews*, *31*(1), 375–386. <https://doi.org/10.1007/s10555-012-9348-x>
- Arango, D., Sturgill, D., Alhusaini, N., Dillman, A. A., Sweet, T. J., Hanson, G., Hosogane, M., Sinclair, W. R., Nanan, K. K., Mandler, M. D., Fox, S. D., Zenggeya, T. T., Andresson, T., Meier, J. L., Coller, J., & Oberdoerffer, S. (2018). Acetylation of Cytidine in mRNA Promotes Translation Efficiency. *Cell*, *175*(7), 1872–1886.e24. <https://doi.org/10.1016/J.CELL.2018.10.030>
- Arango, D., Sturgill, D., Yang, R., Kanai, T., Bauer, P., Roy, J., Wang, Z., Hosogane, M., Schiffrers, S., & Oberdoerffer, S. (2022). Direct epitranscriptomic regulation of mammalian translation initiation through N4-acetylcytidine. *Molecular Cell*, *82*(15), 2797–2814.e11. <https://doi.org/10.1016/J.MOLCEL.2022.05.016>
- Arguello, A. E., DeLiberto, A. N., & Kleiner, R. E. (2017). RNA Chemical Proteomics Reveals the N6-Methyladenosine (m6A)-Regulated Protein–RNA Interactome. *Journal of the American Chemical Society*, *139*(48), 17249–17252. <https://doi.org/10.1021/jacs.7b09213>

8. References

- Ascano, M., Mukherjee, N., Bandaru, P., Miller, J. B., Nusbaum, J. D., Corcoran, D. L., Langlois, C., Munschauer, M., Dewell, S., Hafner, M., Williams, Z., Ohler, U., & Tuschl, T. (2012). FMRP targets distinct mRNA sequence elements to regulate protein expression. *Nature*, *492*(7429), 382–386. <https://doi.org/10.1038/nature11737>
- Astigarraga, S., Hofmeyer, K., Farajian, R., & Treisman, J. E. (2010). Three *Drosophila* Liprins Interact to Control Synapse Formation. *The Journal of Neuroscience*, *30*(46), 15358. <https://doi.org/10.1523/JNEUROSCI.1862-10.2010>
- Athanasiadis, A., Rich, A., & Maas, S. (2004). Widespread A-to-I RNA Editing of Alu-Containing mRNAs in the Human Transcriptome. *PLOS Biology*, *2*(12), e391-. <https://doi.org/10.1371/journal.pbio.0020391>
- Azzam, S. K., Alsafar, H., & Sajini, A. A. (2022). FTO m6A Demethylase in Obesity and Cancer: Implications and Underlying Molecular Mechanisms. *International Journal of Molecular Sciences*, *23*(7). <https://doi.org/10.3390/ijms23073800>
- Bailey, A. S., Batista, P. J., Gold, R. S., Chen, Y. G., de Rooij, D. G., Chang, H. Y., & Fuller, M. T. (2017). The conserved RNA helicase YTHDC2 regulates the transition from proliferation to differentiation in the germline. *ELife*, *6*, e26116. <https://doi.org/10.7554/eLife.26116>
- Barbieri, I., Tzelepis, K., Pandolfini, L., Shi, J., Millán-Zambrano, G., Robson, S. C., Aspris, D., Migliori, V., Bannister, A. J., Han, N., De Braekeleer, E., Pongstingl, H., Hendrick, A., Vakoc, C. R., Vassiliou, G. S., & Kouzarides, T. (2017). Promoter-bound METTL3 maintains myeloid leukaemia by m6A-dependent translation control. *Nature*, *552*(7683), 126–131. <https://doi.org/10.1038/nature24678>
- Bartoli, K., Schaening, C., Carlile, T., & Gilbert, W. (2018). *Conserved Methyltransferase Spb1 Targets mRNAs for Regulated Modification with 2'-O-Methyl Ribose*. bioRxiv. <https://doi.org/10.1101/271916>
- Bartosovic, M., Molares, H. C., Gregorova, P., Hrossova, D., Kudla, G., & Vanacova, S. (2017). N6-methyladenosine demethylase FTO targets pre-mRNAs and regulates alternative splicing and 3'-end processing. *Nucleic Acids Research*, *45*(19), 11356–11370. <https://doi.org/10.1093/nar/gkx778>
- Batista, P. J., Molinie, B., Wang, J., Qu, K., Zhang, J., Li, L., Bouley, D. M., Lujan, E., Haddad, B., Daneshvar, K., Carter, A. C., Flynn, R. A., Zhou, C., Lim, K. S., Dedon, P., Wernig, M., Mullen, A. C., Xing, Y., Giallourakis, C. C., & Chang, H. Y. (2014). m6A RNA Modification Controls Cell Fate Transition in Mammalian Embryonic Stem Cells. *Cell Stem Cell*, *15*(6), 707–719. <https://doi.org/10.1016/j.stem.2014.09.019>
- Bawankar, P., Lence, T., Paolantoni, C., Haussmann, I. U., Kazlauskienė, M., Jacob, D., Heidelberger, J. B., Richter, F. M., Nallasivan, M. P., Morin, V., Kreim, N., Beli, P., Helm, M., Jinek, M., Soller, M., & Roignant, J.-Y. (2021). Hakai is required for stabilization of core components of the m6A mRNA methylation machinery. *Nature Communications*, *12*(1), 3778. <https://doi.org/10.1038/s41467-021-23892-5>
- Beemon, K., & Keith, J. (1977). Localization of N6-methyladenosine in the Rous sarcoma virus genome. *Journal of Molecular Biology*, *113*(1), 165–179. [https://doi.org/10.1016/0022-2836\(77\)90047-X](https://doi.org/10.1016/0022-2836(77)90047-X)
- Bélanger, F., Stepinski, J., Darzynkiewicz, E., & Pelletier, J. (2010). Characterization of hMTr1, a Human Cap1 2'-O-Ribose Methyltransferase. *Journal of Biological Chemistry*, *285*(43), 33037–33044. <https://doi.org/10.1074/JBC.M110.155283>
- Bertero, A., Brown, S., Madrigal, P., Osnato, A., Ortman, D., Yiangou, L., Kadiwala, J., Hubner, N. C., de los Mozos, I. R., Sadée, C., Lenaerts, A.-S., Nakanoh, S., Grandy, R., Farnell, E., Ule, J., Stunnenberg, H. G., Mendjan, S., & Vallier, L. (2018). The SMAD2/3 interactome reveals that TGFβ controls m6A mRNA methylation in pluripotency. *Nature*, *555*(7695), 256–259. <https://doi.org/10.1038/nature25784>
- Berulava, T., & Horsthemke, B. (2010). The obesity-associated SNPs in intron 1 of the FTO gene affect primary transcript levels. *European Journal of Human Genetics*, *18*(9), 1054–1056. <https://doi.org/10.1038/ejhg.2010.71>
- Besnard-Guérin, C., Jacquier, C., Pidoux, J., Deddouche, S., & Antoniewski, C. (2015). The cricket paralysis virus suppressor inhibits microRNA silencing mediated by the *Drosophila* Argonaute-2 protein. *PLoS One*, *10*(3), e0120205. <https://doi.org/10.1371/journal.pone.0120205>
- Birkedal, U., Christensen-Dalsgaard, M., Krogh, N., Sabarinathan, R., Gorodkin, J., & Nielsen, H. (2014). Profiling of ribose methylations in RNA by high-throughput sequencing. *Angewandte Chemie*, *54*(2), 451–455.
- Blair, I. A. (2001). Lipid hydroperoxide-mediated DNA damage. *Experimental Gerontology*, *36*(9), 1473–1481. [https://doi.org/10.1016/S0531-5565\(01\)00133-4](https://doi.org/10.1016/S0531-5565(01)00133-4)
- Bluhm, A., Casas-Vila, N., Scheibe, M., & Butter, F. (2016). Reader interactome of epigenetic histone marks in birds. *PROTEOMICS*, *16*(3), 427–436. <https://doi.org/10.1002/pmic.201500217>
- Boccalletto, P., Stefaniak, F., Ray, A., Cappannini, A., Mukherjee, S., Purta, E., Kurkowska, M., Shirvanizadeh, N., Destefanis, E., Groza, P., Avşar, G., Romitelli, A., Pir, P., Dassi, E., Conticello, S. G., Aguilo, F., & Bujnicki, J. M. (2022). MODOMICS: a database of RNA modification pathways. 2021 update. *Nucleic Acids Research*, *50*(D1), D231–D235. <https://doi.org/10.1093/nar/gkab1083>
- Boivin, V., Deschamps-Francoeur, G., Couture, S., Nottingham, R. M., Bouchard-Bourelle, P., Lambowitz, A. M., Scott, M. S., & Abou-Elela, S. (2018). Simultaneous sequencing of coding and noncoding RNA reveals a human transcriptome dominated by a small number of highly expressed noncoding genes. *RNA (New York, N.Y.)*, *24*(7), 950–965. <https://doi.org/10.1261/rna.064493.117>
- Boivin, V., Reulet, G., Boisvert, O., Couture, S., Elela, S. A., & Scott, M. S. (2020). Reducing the structure bias of RNA-Seq reveals a large number of non-annotated non-coding RNA. *Nucleic Acids Research*, *48*(5), 2271–2286. <https://doi.org/10.1093/nar/gkaa028>
- Bokar, J. A., Rath-Shambaugh, M. E., Ludwiczak, R., Narayan, P., & Rottman, F. (1994). Characterization and partial purification of mRNA N6-adenosine methyltransferase from HeLa cell nuclei. Internal mRNA methylation requires a multisubunit complex. *Journal of Biological Chemistry*, *269*(26), 17697–17704. [https://doi.org/10.1016/S0021-9258\(17\)32497-3](https://doi.org/10.1016/S0021-9258(17)32497-3)
- Bokar, J. A., Shambaugh, M. E., Polayes, D., Matera, A. G., & Rottman, F. M. (1997). Purification and cDNA cloning of the AdoMet-binding subunit of the human mRNA (N6-adenosine)-methyltransferase. *RNA (New York, N.Y.)*, *3*(11), 1233–1247. <http://europepmc.org/abstract/MED/9409616>

8. References

- Boulias, K., Toczyłowska-Socha, D., Hawley, B. R., Liberman, N., Takashima, K., Zaccara, S., Guez, T., Vasseur, J. J., Debart, F., Aravind, L., Jaffrey, S. R., & Greer, E. L. (2019). Identification of the m6Am Methyltransferase PCIF1 Reveals the Location and Functions of m6Am in the Transcriptome. *Molecular Cell*, *75*(3), 631–643.e8. <https://doi.org/10.1016/J.MOLCEL.2019.06.006>
- Broadie, K., & Bate, M. (1995). The Drosophila NMJ: a genetic model system for synapse formation and function. *Seminars in Developmental Biology*, *6*(3), 221–231. [https://doi.org/10.1016/S1044-5781\(06\)80031-9](https://doi.org/10.1016/S1044-5781(06)80031-9)
- Brockdorff, N., Bowness, J. S., & Wei, G. (2020). Progress toward understanding chromosome silencing by Xist RNA. *Genes & Development*, *34*(11–12), 733–744. <https://doi.org/10.1101/gad.337196.120>
- Brown, C. J., Ballabio, A., Rupert, J. L., Lafreniere, R. G., Grompe, M., Tonlorenzi, R., & Willard, H. F. (1991). A gene from the region of the human X inactivation centre is expressed exclusively from the inactive X chromosome. *Nature*, *349*(6304), 38–44. <https://doi.org/10.1038/349038a0>
- Brown, J. A., Kinzig, C. G., DeGregorio, S. J., & Steitz, J. A. (2016). Methyltransferase-like protein 16 binds the 3'-terminal triple helix of MALAT1 long noncoding RNA. *Proceedings of the National Academy of Sciences*, *113*(49), 14013–14018. <https://doi.org/10.1073/pnas.1614759113>
- Busch, H. (1976). The function of the 5' cap of mRNA and nuclear RNA species. *Perspectives in Biology and Medicine*, *19*(4), 549–567. <https://doi.org/10.1353/pbm.1976.0064>
- Byrne, R. T., Konevega, A. L., Rodnina, M. v., & Antson, A. A. (2010). The crystal structure of unmodified tRNA Phe from Escherichia coli. *Nucleic Acids Research*, *38*(12), 4154–4162. <https://doi.org/10.1093/nar/gkq133>
- Cai, X., Wang, X., Cao, C., Gao, Y., Zhang, S., Yang, Z., Liu, Y., Zhang, X., Zhang, W., & Ye, L. (2018). HBXIP-elevated methyltransferase METTL3 promotes the progression of breast cancer via inhibiting tumor suppressor let-7g. *Cancer Letters*, *415*, 11–19. <https://doi.org/https://doi.org/10.1016/j.canlet.2017.11.018>
- Camper, S. A., Albers, R. J., Coward, J. K., & Rottman, F. M. (1984). Effect of undermethylation on mRNA cytoplasmic appearance and half-life. *Molecular and Cellular Biology*, *4*(3), 538–543. <https://doi.org/10.1128/mcb.4.3.538-543.1984>
- Carlile, T. M., Martinez, N. M., Schaening, C., Su, A., Bell, T. A., Zinshteyn, B., & Gilbert, W. V. (2019). mRNA structure determines modification by pseudouridine synthase 1. *Nature Chemical Biology*, *15*(10), 966–974. <https://doi.org/10.1038/s41589-019-0353-z>
- Carlile, T. M., Rojas-Duran, M. F., Zinshteyn, B., Shin, H., Bartoli, K. M., & Gilbert, W. v. (2014). Pseudouridine profiling reveals regulated mRNA pseudouridylation in yeast and human cells. *Nature*, *515*(7525), 143–146. <https://doi.org/10.1038/nature13802>
- Carré, C., Jacquier, C., Bougé, A.-L., de Chaumont, F., Besnard-Guerin, C., Thomassin, H., Pidoux, J., Da Silva, B., Chalatsi, E., Zahra, S., Olivo-Marin, J.-C., Munier-Lehmann, H., & Antoniewski, C. (2013). AutomiG, a Biosensor to Detect Alterations in miRNA Biogenesis and in Small RNA Silencing Guided by Perfect Target Complementarity. *PLOS ONE*, *8*(9), e74296-. <https://doi.org/10.1371/journal.pone.0074296>
- Carroll, S. M., Narayan, P., & Rottman, F. (1990). N6-methyladenosine residues in an intron-specific region of prolactin pre-mRNA. *Molecular and Cellular Biology*, *10*, 4456–4465.
- Casas-Vila, N., Bluhm, A., Sayols, S., Dinges, N., Dejung, M., Altenhein, T., Kappei, D., Altenhein, B., Roignant, J.-Y., & Butter, F. (2017). The developmental proteome of Drosophila melanogaster. *Genome Research*, *27*(7), 1273–1285. <https://doi.org/10.1101/gr.213694.116>
- Cavallin, I., Bartosovic, M., Skalicky, T., Rengaraj, P., Demko, M., Schmidt-Dengler, M. C., Drino, A., Helm, M., & Vanacova, S. (2022). HITS-CLIP analysis of human ALKBH8 reveals interactions with fully processed substrate tRNAs and with specific noncoding RNAs. *RNA*, *28*(12), 1568–1581. <https://doi.org/10.1261/rna.079421.122>
- Chang, M., Lv, H., Zhang, W., Ma, C., He, X., Zhao, S., Zhang, Z.-W., Zeng, Y.-X., Song, S., Niu, Y., & Tong, W.-M. (2017). Region-specific RNA m6A methylation represents a new layer of control in the gene regulatory network in the mouse brain. *Open Biology*, *7*(9), 170166. <https://doi.org/10.1098/rsob.170166>
- Chang, Y. Z., Chai, R. C., Pang, B., Chang, X., An, S. Y., Zhang, K. N., Jiang, T., & Wang, Y. Z. (2021). METTL3 enhances the stability of MALAT1 with the assistance of HuR via m6A modification and activates NF-κB to promote the malignant progression of IDH-wildtype glioma. *Cancer Letters*, *511*, 36–46. <https://doi.org/10.1016/J.CANLET.2021.04.020>
- Chelmicki, T., Roger, E., Teissandier, A., Dura, M., Bonneville, L., Rucli, S., Dossin, F., Fouassier, C., Lameiras, S., & Bourc'his, D. (2021). m6A RNA methylation regulates the fate of endogenous retroviruses. *Nature*, *591*(7849), 312–316. <https://doi.org/10.1038/s41586-020-03135-1>
- Chen, K., Lu, Z., Wang, X., Fu, Y., Luo, G.-Z., Liu, N., Han, D., Dominissini, D., Dai, Q., Pan, T., & He, C. (2015). High-Resolution N6-Methyladenosine (m6A) Map Using Photo-Crosslinking-Assisted m6A Sequencing. *Angewandte Chemie International Edition*, *54*(5), 1587–1590. <https://doi.org/https://doi.org/10.1002/anie.201410647>
- Chen, T., Hao, Y. J., Zhang, Y., Li, M. M., Wang, M., Han, W., Wu, Y., Lv, Y., Hao, J., Wang, L., Li, A., Yang, Y., Jin, K. X., Zhao, X., Li, Y., Ping, X. L., Lai, W. Y., Wu, L. G., Jiang, G., ... Zhou, Q. (2015). m6A RNA Methylation Is Regulated by MicroRNAs and Promotes Reprogramming to Pluripotency. *Cell Stem Cell*, *16*(3), 289–301. <https://doi.org/10.1016/J.STEM.2015.01.016>
- Cheng, Y., Xie, W., Pickering, B. F., Chu, K. L., Savino, A. M., Yang, X., Luo, H., Nguyen, D. T., Mo, S., Barin, E., Velleca, A., Rohwetter, T. M., Patel, D. J., Jaffrey, S. R., & Kharras, M. G. (2021). N6-Methyladenosine on mRNA facilitates a phase-separated nuclear body that suppresses myeloid leukemic differentiation. *Cancer Cell*, *39*(7), 958–972.e8. <https://doi.org/10.1016/J.CCELL.2021.04.017>
- Choe, J., Lin, S., Zhang, W., Liu, Q., Wang, L., Ramirez-Moya, J., Du, P., Kim, W., Tang, S., Sliz, P., Santisteban, P., George, R. E., Richards, W. G., Wong, K.-K., Locker, N., Slack, F. J., & Gregory, R. I. (2018). mRNA circularization by METTL3–eIF3h enhances translation and promotes oncogenesis. *Nature*, *561*(7724), 556–560. <https://doi.org/10.1038/s41586-018-0538-8>

8. References

- Choi, J., Jeong, K.-W., Demirci, H., Chen, J., Petrov, A., Prabhakar, A., O'Leary, S. E., Dominissini, D., Rechavi, G., Soltis, S. M., Ehrenberg, M., & Puglisi, J. D. (2016). N6-methyladenosine in mRNA disrupts tRNA selection and translation-elongation dynamics. *Nature Structural & Molecular Biology*, 23(2), 110–115. <https://doi.org/10.1038/nsmb.3148>
- Chu, J.-M., Ye, T.-T., Ma, C.-J., Lan, M.-D., Liu, T., Yuan, B.-F., & Feng, Y.-Q. (2018). Existence of Internal N7-Methylguanosine Modification in mRNA Determined by Differential Enzyme Treatment Coupled with Mass Spectrometry Analysis. *ACS Chemical Biology*, 13(12), 3243–3250. <https://doi.org/10.1021/acscchembio.7b00906>
- Coffee Jr, R. L., Tessier, C. R., Woodruff III, E. A., & Broadie, K. (2010). Fragile X mental retardation protein has a unique, evolutionarily conserved neuronal function not shared with FXR1P or FXR2P. *Disease Models & Mechanisms*, 3(7–8), 471–485. <https://doi.org/10.1242/dmm.004598>
- Cohn, W. E. (1959). 5-Ribosyl uracil, a carbon-carbon ribofuranosyl nucleoside in ribonucleic acids. *Biochimica et Biophysica Acta*, 32(C), 569–571. [https://doi.org/10.1016/0006-3002\(59\)90644-4](https://doi.org/10.1016/0006-3002(59)90644-4)
- Cohn, W. E., & Volkin, E. (1951). Nucleoside-5'-Phosphates from Ribonucleic Acid. *Nature*, 167(4247), 483–484. <https://doi.org/10.1038/167483a0>
- Coots, R. A., Liu, X. M., Mao, Y., Dong, L., Zhou, J., Wan, J., Zhang, X., & Qian, S. B. (2017). m6A Facilitates eIF4F-Independent mRNA Translation. *Molecular Cell*, 68(3), 504–514.e7. <https://doi.org/10.1016/j.molcel.2017.10.002>
- Cui, J., Liu, Q., Sendinc, E., Shi, Y., & Gregory, R. I. (2021). Nucleotide resolution profiling of m3C RNA modification by HAC-seq. *Nucleic Acids Research*, 49(5), e27–e27. <https://doi.org/10.1093/nar/gkaa1186>
- Cui, Q., Shi, H., Ye, P., Li, L., Qu, Q., Sun, G., Sun, G., Lu, Z., Huang, Y., Yang, C. G., Riggs, A. D., He, C., & Shi, Y. (2017). m6A RNA Methylation Regulates the Self-Renewal and Tumorigenesis of Glioblastoma Stem Cells. *Cell Reports*, 18(11), 2622–2634. <https://doi.org/10.1016/j.celrep.2017.02.059>
- Czech, B., Zhou, R., Erlich, Y., Brennecke, J., Binari, R., Villalta, C., Gordon, A., Perrimon, N., & Hannon, G. J. (2009). Hierarchical Rules for Argonaute Loading in Drosophila. *Molecular Cell*, 36(3), 445–456. <https://doi.org/10.1016/j.molcel.2009.09.028>
- Dai, Q., Moshitch-Moshkovitz, S., Han, D., Kol, N., Amariglio, N., Rechavi, G., Dominissini, D., & He, C. (2017). Nm-seq maps 2'-O-methylation sites in human mRNA with base precision. *Nature Methods*, 14(7), 695–698. <https://doi.org/10.1038/nmeth.4294>
- Dai, Q., Zhang, L.-S., Sun, H.-L., Pajdzik, K., Yang, L., Ye, C., Ju, C.-W., Liu, S., Wang, Y., Zheng, Z., Zhang, L., Harada, B. T., Dou, X., Irklyenko, I., Feng, X., Zhang, W., Pan, T., & He, C. (2023). Quantitative sequencing using BID-seq uncovers abundant pseudouridines in mammalian mRNA at base resolution. *Nature Biotechnology*, 41(3), 344–354. <https://doi.org/10.1038/s41587-022-01505-w>
- Davis, F. F., & Allen, F. W. (1957). RIBONUCLEIC ACIDS FROM YEAST WHICH CONTAIN A FIFTH NUCLEOTIDE. *Journal of Biological Chemistry*, 227(2), 907–915. [https://doi.org/10.1016/S0021-9258\(18\)70770-9](https://doi.org/10.1016/S0021-9258(18)70770-9)
- Delatte, B., Wang, F., Ngoc, L. V., Collignon, E., Bonvin, E., Depluis, R., Calonne, E., Hassabi, B., Putmans, P., Awe, S., Wetzels, C., Kreher, J., Soin, R., Creppe, C., Limbach, P. A., Gueydan, C., Kruys, V., Brehm, A., Minakhina, S., ... Fuks, F. (2016). Transcriptome-wide distribution and function of RNA hydroxymethylcytosine. *Science*, 351(6270), 282–285. <https://doi.org/10.1126/science.aac5253>
- Desrosiers, R., Friderici, K., & Rottman, F. (1974). Identification of Methylated Nucleosides in Messenger RNA from Novikoff Hepatoma Cells. *Proceedings of the National Academy of Sciences*, 71(10), 3971–3975. <https://doi.org/10.1073/pnas.71.10.3971>
- Devarkar, S. C., Wang, C., Miller, M. T., Ramanathan, A., Jiang, F., Khan, A. G., Patel, S. S., & Marcotrigiano, J. (2016). Structural basis for m7G recognition and 2'-O-methyl discrimination in capped RNAs by the innate immune receptor RIG-I. *Proceedings of the National Academy of Sciences*, 113(3), 596–601. <https://doi.org/10.1073/pnas.1515152113>
- Díaz-Díaz, A., Roca-Lema, D., Casas-Pais, A., Romay, G., Colombo, G., Concha, Á., Graña, B., & Figueroa, A. (2020). Heat Shock Protein 90 Chaperone Regulates the E3 Ubiquitin-Ligase Hakai Protein Stability. *Cancers*, 12(1). <https://doi.org/10.3390/cancers12010215>
- Dierks, D., Garcia-Campos, M. A., Uzonyi, A., Safera, M., Edelheit, S., Rossi, A., Sideri, T., Varier, R. A., Brandis, A., Stelzer, Y., van Werven, F., Scherz-Shouval, R., & Schwartz, S. (2021). Multiplexed profiling facilitates robust m6A quantification at site, gene and sample resolution. *Nature Methods*, 18(9), 1060–1067. <https://doi.org/10.1038/s41592-021-01242-z>
- Dominissini, D., Moshitch-Moshkovitz, S., Schwartz, S., Salmon-Divon, M., Ungar, L., Osenberg, S., Cesarkas, K., Jacob-Hirsch, J., Amariglio, N., Kupiec, M., Sorek, R., & Rechavi, G. (2012). Topology of the human and mouse m6A RNA methylomes revealed by m6A-seq. *Nature*, 485(7397), 201–206. <https://doi.org/10.1038/nature11112>
- Doxtader, K. A., Wang, P., Scarborough, A. M., Seo, D., Conrad, N. K., & Nam, Y. (2018). Structural Basis for Regulation of METTL16, an S-Adenosylmethionine Homeostasis Factor. *Molecular Cell*, 71(6), 1001–1011.e4.
- Draycott, A. S., Schaening-Burgos, C., Rojas-Duran, M. F., Wilson, L., Schärffen, L., Neugebauer, K. M., Nachtergaele, S., & Gilbert, W. v. (2022). Transcriptome-wide mapping reveals a diverse dihydrouridine landscape including mRNA. *PLoS Biology*, 20.
- Du, H., Zhao, Y., He, J., Zhang, Y., Xi, H., Liu, M., Ma, J., & Wu, L. (2016). YTHDF2 destabilizes m6A-containing RNA through direct recruitment of the CCR4–NOT deadenylase complex. *Nature Communications*, 7(1), 12626. <https://doi.org/10.1038/ncomms12626>
- Du, Y., Hou, G., Zhang, H., Dou, J., He, J., Guo, Y., Li, L., Chen, R., Wang, Y., Deng, R., Huang, J., Jiang, B., Xu, M., Cheng, J., Chen, G.-Q., Zhao, X., & Yu, J. (2018). SUMOylation of the m6A-RNA methyltransferase METTL3 modulates its function. *Nucleic Acids Research*, 46(10), 5195–5208. <https://doi.org/10.1093/nar/gky156>
- Duda, K. J., Ching, R. W., Jerabek, L., Shukeir, N., Erikson, G., Engist, B., Onishi-Seebacher, M., Perrera, V., Richter, F., Mittler, G., Fritz, K., Helm, M., Knuckles, P., Bühler, M., & Jenuwein, T. (2021). m6A RNA methylation of major satellite repeat transcripts facilitates chromatin

8. References

- association and RNA:DNA hybrid formation in mouse heterochromatin. *Nucleic Acids Research*, 49(10), 5568–5587. <https://doi.org/10.1093/nar/gkab364>
- Duncan, T., Trewick, S. C., Koivisto, P., Bates, P. A., Lindahl, T., & Sedgwick, B. (2002). Reversal of DNA alkylation damage by two human dioxygenases. *Proceedings of the National Academy of Sciences*, 99(26), 16660–16665. <https://doi.org/10.1073/pnas.262589799>
- Eberhart, D. E., Malter, H. E., Feng, Y., & Warren, S. T. (1996). The Fragile X Mental Retardation Protein is a Ribonucleoprotein Containing Both Nuclear Localization and Nuclear Export Signals. *Human Molecular Genetics*, 5(8), 1083–1091. <https://doi.org/10.1093/hmg/5.8.1083>
- Edens, B. M., Vissers, C., Su, J., Arumugam, S., Xu, Z., Shi, H., Miller, N., Rojas Ringeling, F., Ming, G. li, He, C., Song, H., & Ma, Y. C. (2019). FMRP Modulates Neural Differentiation through m6A-Dependent mRNA Nuclear Export. *Cell Reports*, 28(4), 845–854.e5. <https://doi.org/10.1016/j.celrep.2019.06.072>
- Edupuganti, R. R., Geiger, S., Lindeboom, R. G. H., Shi, H., Hsu, P. J., Lu, Z., Wang, S.-Y., Baltissen, M. P. A., Jansen, P. W. T. C., Rossa, M., Müller, M., Stunnenberg, H. G., He, C., Carell, T., & Vermeulen, M. (2017). N6-methyladenosine (m6A) recruits and repels proteins to regulate mRNA homeostasis. *Nature Structural & Molecular Biology*, 24(10), 870–878. <https://doi.org/10.1038/nsmb.3462>
- Engel, M., Eggert, C., Kaplick, P. M., Eder, M., Röh, S., Tietze, L., Namendorf, C., Arloth, J., Weber, P., Rex-Haffner, M., Geula, S., Jakovcevski, M., Hanna, J. H., Leshkowitz, D., Uhr, M., Wotjak, C. T., Schmidt, M. v., Deussing, J. M., Binder, E. B., & Chen, A. (2018). The Role of m6A/mRNA Methylation in Stress Response Regulation. *Neuron*, 99(2), 389–403.e9. <https://doi.org/10.1016/j.neuron.2018.07.009>
- Enroth, C., Poulsen, L. D., Iversen, S., Kirpekar, F., Albrechtsen, A., & Vinther, J. (2019). Detection of internal N7-methylguanosine (m7G) RNA modifications by mutational profiling sequencing. *Nucleic Acids Research*, 47(20), e126–e126. <https://doi.org/10.1093/nar/gkz736>
- Epstein, P., Reddy, R., Henning, D., & Busch, H. (1980). The nucleotide sequence of nuclear U6 (4.7 S) RNA. *Journal of Biological Chemistry*, 255(18), 8901–8906. [https://doi.org/10.1016/S0021-9258\(18\)43587-9](https://doi.org/10.1016/S0021-9258(18)43587-9)
- Featherstone, D. E., Davis, W. S., Dubreuil, R. R., & Broadie, K. (2001). α - and β -Spectrin Mutations Disrupt Presynaptic Neurotransmitter Release. *The Journal of Neuroscience*, 21(12), 4215. <https://doi.org/10.1523/JNEUROSCI.21-12-04215.2001>
- Fedeles, B. I., Singh, V., Delaney, J. C., Li, D., & Essigmann, J. M. (2015). The AlkB Family of Fe(II)/ α -Ketoglutarate-dependent Dioxygenases: Repairing Nucleic Acid Alkylation Damage and Beyond. *Journal of Biological Chemistry*, 290(34), 20734–20742. <https://doi.org/10.1074/JBC.R115.656462>
- Feng, C., Liu, Y., Wang, G., Deng, Z., Zhang, Q., Wu, W., Tong, Y., Cheng, C., & Chen, Z. (2014). Crystal Structures of the Human RNA Demethylase Alkbh5 Reveal Basis for Substrate Recognition. *Journal of Biological Chemistry*, 289(17), 11571–11583. <https://doi.org/10.1074/JBC.M113.546168>
- Figueroa, A., Kotani, H., Toda, Y., Mazan-Mamczarz, K., Mueller, E.-C., Otto, A., Disch, L., Norman, M., Ramdasi, R. M., Keshtgar, M., Gorospe, M., & Fujita, Y. (2009). Novel Roles of Hakai in Cell Proliferation and Oncogenesis. *Molecular Biology of the Cell*, 20(15), 3533–3542. <https://doi.org/10.1091/mbc.e08-08-0845>
- Finet, O., Yague-Sanz, C., Krüger, L. K., Tran, P., Migeot, V., Louski, M., Nevers, A., Rougemaille, M., Sun, J., Ernst, F. G. M., Wacheul, L., Wery, M., Morillon, A., Dedon, P., Lafontaine, D. L. J., & Hermand, D. (2022). Transcription-wide mapping of dihydrouridine reveals that mRNA dihydrouridylation is required for meiotic chromosome segregation. *Molecular Cell*, 82(2), 404–419.e9. <https://doi.org/10.1016/j.molcel.2021.11.003>
- Fish, L., Navickas, A., Culbertson, B., Xu, Y., Nguyen, H. C. B., Zhang, S., Hochman, M., Okimoto, R., Dill, B. D., Molina, H., Najafabadi, H. S., Alarcón, C., Ruggero, D., & Goodarzi, H. (2019). Nuclear TARBP2 Drives Oncogenic Dysregulation of RNA Splicing and Decay. *Molecular Cell*, 75(5), 967–981.e9. <https://doi.org/10.1016/j.molcel.2019.06.001>
- Fleming, A. M., Nguyen, N.-L., & Burrows, C. J. (2019). Colocalization of m6A and G-Quadruplex-Forming Sequences in Viral RNA (HIV, Zika, Hepatitis B, and SV40) Suggests Topological Control of Adenosine N6-Methylation. *ACS Central Science*, 5, 218–228.
- Fridell, R. A., Benson, R. E., Hua, J., Bogerd, H. P., & Cullen, B. R. (1996). A nuclear role for the Fragile X mental retardation protein. *The EMBO Journal*, 15(19), 5408–5414. <https://doi.org/https://doi.org/10.1002/j.1460-2075.1996.tb00924.x>
- Fu, D., Calvo, J. A., & Samson, L. D. (2012). Balancing repair and tolerance of DNA damage caused by alkylating agents. *Nature Reviews Cancer*, 12(2), 104–120. <https://doi.org/10.1038/nrc3185>
- Fu, D., Jordan, J. J., & Samson, L. D. (2013). Human ALKBH7 is required for alkylation and oxidation-induced programmed necrosis. *Genes & Development*, 27(10), 1089–1100. <https://doi.org/10.1101/gad.215533.113>
- Fu, L., Amato, N. J., Wang, P., McGowan, S. J., Niedernhofer, L. J., & Wang, Y. (2015). Simultaneous Quantification of Methylated Cytidine and Adenosine in Cellular and Tissue RNA by Nano-Flow Liquid Chromatography–Tandem Mass Spectrometry Coupled with the Stable Isotope-Dilution Method. *Analytical Chemistry*, 87(15), 7653–7659. <https://doi.org/10.1021/acs.analchem.5b00951>
- Fu, L., Guerrero, C. R., Zhong, N., Amato, N. J., Liu, Y., Liu, S., Cai, Q., Ji, D., Jin, S.-G., Niedernhofer, L. J., Pfeifer, G. P., Xu, G.-L., & Wang, Y. (2014). Tet-Mediated Formation of 5-Hydroxymethylcytosine in RNA. *Journal of the American Chemical Society*, 136(33), 11582–11585. <https://doi.org/10.1021/ja505305z>
- Fu, Y., Dai, Q., Zhang, W., Ren, J., Pan, T., & He, C. (2010). The AlkB Domain of Mammalian ABH8 Catalyzes Hydroxylation of 5-Methoxycarbonylmethyluridine at the Wobble Position of tRNA. *Angewandte Chemie International Edition*, 49(47), 8885–8888. <https://doi.org/https://doi.org/10.1002/anie.201001242>
- Fu, Y., Jia, G., Pang, X., Wang, R. N., Wang, X., Li, C. J., Smemo, S., Dai, Q., Bailey, K. A., Nobrega, M. A., Han, K.-L., Cui, Q., & He, C. (2013). FTO-mediated formation of N6-hydroxymethyladenosine and N6-formyladenosine in mammalian RNA. *Nature Communications*, 4(1), 1798. <https://doi.org/10.1038/ncomms2822>

8. References

- Fu, Y., & Zhuang, X. (2020). m6A-binding YTHDF proteins promote stress granule formation. *Nature Chemical Biology*, *16*(9), 955–963. <https://doi.org/10.1038/s41589-020-0524-y>
- Fujita, Y., Krause, G., Scheffner, M., Zechner, D., Leddy, H. E. M., Behrens, J., Sommer, T., & Birchmeier, W. (2002). Hakai, a c-Cbl-like protein, ubiquitinates and induces endocytosis of the E-cadherin complex. *Nature Cell Biology*, *4*(3), 222–231. <https://doi.org/10.1038/ncb758>
- Fukumami, Y., Naruse, C., & Asano, M. (2008). Wtap is required for differentiation of endoderm and mesoderm in the mouse embryo. *Developmental Dynamics*, *237*.
- Fustin, J. M., Doi, M., Yamaguchi, Y., Hida, H., Nishimura, S., Yoshida, M., Isagawa, T., Morioka, M. S., Kakeya, H., Manabe, I., & Okamura, H. (2013). RNA-Methylation-Dependent RNA Processing Controls the Speed of the Circadian Clock. *Cell*, *155*(4), 793–806. <https://doi.org/10.1016/j.cell.2013.10.026>
- Galloway, A., & Cowling, V. H. (2019). mRNA cap regulation in mammalian cell function and fate. *Biochimica et Biophysica Acta (BBA) - Gene Regulatory Mechanisms*, *1862*(3), 270–279. <https://doi.org/10.1016/j.bbagr.2018.09.011>
- Gao, Y., Liu, X., Wu, B., Wang, H., Xi, F., Kohnen, M. v., Reddy, A. S. N., & Gu, L. (2021). Quantitative profiling of N⁶-methyladenosine at single-base resolution in stem-differentiating xylem of *Populus trichocarpa* using Nanopore direct RNA sequencing. *Genome Biology*, *22*(1), 22. <https://doi.org/10.1186/s13059-020-02241-7>
- Gao, Y., Pei, G., Li, D., Li, R., Shao, Y., Zhang, Q. C., & Li, P. (2019). Multivalent m6A motifs promote phase separation of YTHDF proteins. *Cell Research*, *29*(9), 767–769. <https://doi.org/10.1038/s41422-019-0210-3>
- Garalde, D. R., Snell, E. A., Jachimowicz, D., Sipos, B., Lloyd, J. H., Bruce, M., Pantic, N., Admassu, T., James, P., Warland, A., Jordan, M., Ciccone, J., Serra, S., Keenan, J., Martin, S., McNeill, L., Wallace, E. J., Jayasinghe, L., Wright, C., ... Turner, D. J. (2018). Highly parallel direct RNA sequencing on an array of nanopores. *Nature Methods*, *15*(3), 201–206. <https://doi.org/10.1038/nmeth.4577>
- Garcia-Campos, M. A., Edelheit, S., Toth, U., Safra, M., Shachar, R., Viukov, S., Winkler, R., Nir, R., Lasman, L., Brandis, A., Hanna, J. H., Rossmanith, W., & Schwartz, S. (2019). Deciphering the “m6A Code” via Antibody-Independent Quantitative Profiling. *Cell*, *178*(3), 731–747. <https://doi.org/10.1016/j.cell.2019.06.013>
- Gay, D. M., Lund, A. H., & Jansson, M. D. (2022). Translational control through ribosome heterogeneity and functional specialization. *Trends in Biochemical Sciences*, *47*(1), 66–81. <https://doi.org/10.1016/j.tibs.2021.07.001>
- Geon-Woo, K., Hasan, I., & Aleem, S. (2021). The RNA Binding Proteins YTHDC1 and FMRP Regulate the Nuclear Export of N⁶-Methyladenosine-Modified Hepatitis B Virus Transcripts and Affect the Viral Life Cycle. *Journal of Virology*, *95*(13), e00097-21. <https://doi.org/10.1128/JVI.00097-21>
- Gerken, T., Girard, C. A., Tung, Y.-C. L., Webby, C. J., Saudek, V., Hewitson, K. S., Yeo, G. S. H., McDonough, M. A., Cunliffe, S., McNeill, L. A., Galvanovskis, J., Rorsman, P., Robins, P., Prieur, X., Coll, A. P., Ma, M., Jovanovic, Z., Farooqi, I. S., Sedgwick, B., ... Schofield, C. J. (2007). The Obesity-Associated FTO Gene Encodes a 2-Oxoglutarate-Dependent Nucleic Acid Demethylase. *Science*, *318*(5855), 1469–1472. <https://doi.org/10.1126/science.1151710>
- Geula, S., Moshitch-Moshkovitz, S., Dominissini, D., Mansour, A. A., Kol, N., Salmon-Divon, M., Hershkovitz, V., Peer, E., Mor, N., Manor, Y. S., Ben-Haim, M. S., Eyal, E., Yunger, S., Pinto, Y., Jaitin, D. A., Viukov, S., Rais, Y., Krupalnik, V., Chomsky, E., ... Hanna, J. H. (2015). m6A mRNA methylation facilitates resolution of naïve pluripotency toward differentiation. *Science*, *347*(6225), 1002–1006. <https://doi.org/10.1126/science.1261417>
- Ghildiyal, M., Xu, J., Seitz, H., Weng, Z., & Zamore, P. D. (2010). Sorting of *Drosophila* small silencing RNAs partitions microRNA* strands into the RNA interference pathway. *RNA*, *16*(1), 43–56. <https://doi.org/10.1261/rna.1972910>
- Granadino, B., Campuzano, S., & Sánchez, L. (1990). The *Drosophila melanogaster* fl(2)d gene is needed for the female-specific splicing of Sex-lethal RNA. *The EMBO Journal*, *9*(8), 2597–2602. <https://doi.org/https://doi.org/10.1002/j.1460-2075.1990.tb07441.x>
- Gromadzka, A. M., Steckelberg, A.-L., Singh, K. K., Hofmann, K., & Gehring, N. H. (2016). A short conserved motif in ALYREF directs cap- and EJC-dependent assembly of export complexes on spliced mRNAs. *Nucleic Acids Research*, *44*(5), 2348–2361. <https://doi.org/10.1093/nar/gkw009>
- Grozhih, A. v., & Jaffrey, S. R. (2018). Distinguishing RNA modifications from noise in epitranscriptome maps. *Nature Chemical Biology*, *14*(3), 215–225. <https://doi.org/10.1038/nchembio.2546>
- Gu, J., Patton, J. R., Shimba, S., & Reddy, R. (1996). Localization of modified nucleotides in *Schizosaccharomyces pombe* spliceosomal small nuclear RNAs: modified nucleotides are clustered in functionally important regions. *RNA*, *2* 9, 909–918.
- Guo, J., Tang, H.-W., Li, J., Perrimon, N., & Yan, D. (2018). Xio is a component of the *Drosophila* sex determination pathway and RNA N⁶-methyladenosine methyltransferase complex. *Proceedings of the National Academy of Sciences*, *115*(14), 3674–3679. <https://doi.org/10.1073/pnas.1720945115>
- Haag, S., Sloan, K. E., Ranjan, N., Warda, A. S., Kretschmer, J., Blessing, C., Hübner, B., Seikowski, J., Dennerlein, S., Rehling, P., Rodnina, M. v., Höbartner, C., & Bohnsack, M. T. (2016). NSUN3 and ABH1 modify the wobble position of mt-tRNA^{Met} to expand codon recognition in mitochondrial translation. *The EMBO Journal*, *35*(19), 2104–2119. <https://doi.org/https://doi.org/10.15252/embj.201694885>
- Hafner, M., Landthaler, M., Burger, L., Khorshid, M., Hausser, J., Berninger, P., Rothballer, A., Ascano, M., Jungkamp, A. C., Munschauer, M., Ulrich, A., Wardle, G. S., Dewell, S., Zavolan, M., & Tuschl, T. (2010). Transcriptome-wide Identification of RNA-Binding Protein and MicroRNA Target Sites by PAR-CLIP. *Cell*, *141*(1), 129–141. <https://doi.org/10.1016/j.cell.2010.03.009>

8. References

- Haline-Vaz, T., Lima Silva, T. C., & Zanchin, N. I. T. (2008). The human interferon-regulated ISG95 protein interacts with RNA polymerase II and shows methyltransferase activity. *Biochemical and Biophysical Research Communications*, 372(4), 719–724. <https://doi.org/10.1016/J.BBRC.2008.05.137>
- Han, D., Longhini, A. P., Zhang, X., Hoang, V., Wilson, M. Z., & Kosik, K. S. (2022). Dynamic assembly of the mRNA m6A methyltransferase complex is regulated by METTL3 phase separation. *PLoS Biology*, 20(2), e3001535-. <https://doi.org/10.1371/journal.pbio.3001535>
- Han, Z., Niu, T., Chang, J., Lei, X., Zhao, M., Wang, Q., Cheng, W., Wang, J., Feng, Y., & Chai, J. (2010). Crystal structure of the FTO protein reveals basis for its substrate specificity. *Nature*, 464(7292), 1205–1209. <https://doi.org/10.1038/nature08921>
- Harada, F., Kato, N., & Nishimura, S. (1980). The nucleotide sequence of nuclear 4.8S RNA of mouse cells. *Biochemical and Biophysical Research Communications*, 95(3), 1332–1340. [https://doi.org/10.1016/0006-291X\(80\)91620-4](https://doi.org/10.1016/0006-291X(80)91620-4)
- Hartmann, A. M., Naylor, O., Schwaiger, F., Obermeier, A., & Stamm, S. (1999). The interaction and colocalization of Sam68 with the splicing-associated factor YT521-B in nuclear dots is regulated by the Src family kinase p59(fyn). *Molecular Biology of the Cell*, 10 11, 3909–3926.
- Hausmann, I. U., Bodi, Z., Sanchez-Moran, E., Mongan, N. P., Archer, N., Fray, R. G., & Soller, M. (2016). m6A potentiates Sxl alternative pre-mRNA splicing for robust Drosophila sex determination. *Nature*, 540(7632), 301–304. <https://doi.org/10.1038/nature20577>
- He, P. C., Wei, J., Dou, X., Harada, B. T., Zhang, Z., Ge, R., Liu, C., Zhang, L.-S., Yu, X., Wang, S., Lyu, R., Zou, Z., Chen, M., & He, C. (2023). Exon architecture controls mRNA m6A suppression and gene expression. *Science*, 0(0), eabj9090. <https://doi.org/10.1126/science.abj9090>
- Heck, A. M., Russo, J., Wilusz, J., Nishimura, E. O., & Wilusz, C. J. (2020). YTHDF2 destabilizes m6A-modified neural-specific RNAs to restrain differentiation in induced pluripotent stem cells. *RNA*, 26(6), 739–755. <https://doi.org/10.1261/rna.073502.119>
- Hendra, C., Pratanwanich, P. N., Wan, Y. K., Goh, W. S. S., Thiery, A., & Göke, J. (2022). Detection of m6A from direct RNA sequencing using a multiple instance learning framework. *Nature Methods*, 19(12), 1590–1598. <https://doi.org/10.1038/s41592-022-01666-1>
- Hess, M. E., Hess, S., Meyer, K. D., Verhagen, L. A. W., Koch, L., Brönneke, H. S., Dietrich, M. O., Jordan, S. D., Saletore, Y., Elemento, O., Belgardt, B. F., Franz, T., Horvath, T. L., Rütger, U., Jaffrey, S. R., Kloppenburg, P., & Brüning, J. C. (2013). The fat mass and obesity associated gene (Fto) regulates activity of the dopaminergic midbrain circuitry. *Nature Neuroscience*, 16(8), 1042–1048. <https://doi.org/10.1038/nn.3449>
- Hilfiker, A., Amrein, H., Dubendorfer, A., Schneiter, R., & Nothiger, R. (1995). The gene virilizer is required for female-specific splicing controlled by Sxl, the master gene for sexual development in Drosophila. *Development*, 121(12), 4017–4026. <https://doi.org/10.1242/dev.121.12.4017>
- Horiuchi, K., Kawamura, T., Iwanari, H., Ohashi, R., Naito, M., Kodama, T., & Hamakubo, T. (2013). Identification of Wilms' Tumor 1-associating Protein Complex and Its Role in Alternative Splicing and the Cell Cycle. *Journal of Biological Chemistry*, 288(46), 33292–33302. <https://doi.org/10.1074/JBC.M113.500397>
- Horowitz, S., Horowitz, A. T., Nilsen, T. W., Munns, T. W., & Rottman, F. (1984). Mapping of N6-methyladenosine residues in bovine prolactin mRNA. *Proceedings of the National Academy of Sciences of the United States of America*, 81 18, 5667–5671.
- Hosamani, R., & Muralidhara. (2013). ACUTE EXPOSURE OF Drosophila melanogaster TO PARAQUAT CAUSES OXIDATIVE STRESS AND MITOCHONDRIAL DYSFUNCTION. *Archives of Insect Biochemistry and Physiology*, 83(1), 25–40. <https://doi.org/https://doi.org/10.1002/arch.21094>
- Hsu, P. J., Fei, Q., Dai, Q., Shi, H., Dominissini, D., Ma, L., & He, C. (2019). Single base resolution mapping of 2'-O-methylation sites in human mRNA and in 3' terminal ends of small RNAs. *Methods*, 156, 85–90. <https://doi.org/10.1016/J.YMETH.2018.11.007>
- Hsu, P. J., Shi, H., Zhu, A. C., Lu, Z., Miller, N., Edens, B. M., Ma, Y. C., & He, C. (2019). The RNA-binding protein FMRP facilitates the nuclear export of N6-methyladenosine-containing mRNAs. *Journal of Biological Chemistry*, 294(52), 19889–19895. <https://doi.org/10.1074/JBC.AC119.010078>
- Hsu, P. J., Zhu, Y., Ma, H., Guo, Y., Shi, X., Liu, Y., Qi, M., Lu, Z., Shi, H., Wang, J., Cheng, Y., Luo, G., Dai, Q., Liu, M., Guo, X., Sha, J., Shen, B., & He, C. (2017). Ythdc2 is an N6-methyladenosine binding protein that regulates mammalian spermatogenesis. *Cell Research*, 27(9), 1115–1127. <https://doi.org/10.1038/cr.2017.99>
- Hu, L., Liu, S., Peng, Y., Ge, R., Su, R., Senevirathne, C., Harada, B. T., Dai, Q., Wei, J., Zhang, L., Hao, Z., Luo, L., Wang, H., Wang, Y., Luo, M., Chen, M., Chen, J., & He, C. (2022). m6A RNA modifications are measured at single-base resolution across the mammalian transcriptome. *Nature Biotechnology*, 40(8), 1210–1219. <https://doi.org/10.1038/s41587-022-01243-z>
- Huang, H., Weng, H., Sun, W., Qin, X., Shi, H., Wu, H., Zhao, B. S., Mesquita, A., Liu, C., Yuan, C. L., Hu, Y.-C., Hüttelmaier, S., Skibbe, J. R., Su, R., Deng, X., Dong, L., Sun, M., Li, C., Nachtergaele, S., ... Chen, J. (2018). Recognition of RNA N6-methyladenosine by IGF2BP proteins enhances mRNA stability and translation. *Nature Cell Biology*, 20(3), 285–295. <https://doi.org/10.1038/s41556-018-0045-z>
- Huang, H., Weng, H., Zhou, K., Wu, T., Zhao, B. S., Sun, M., Chen, Z., Deng, X., Xiao, G., Auer, F., Klemm, L., Wu, H., Zuo, Z., Qin, X., Dong, Y., Zhou, Y., Qin, H., Tao, S., Du, J., ... Chen, J. (2019). Histone H3 trimethylation at lysine 36 guides m6A RNA modification co-transcriptionally. *Nature*, 567(7748), 414–419. <https://doi.org/10.1038/s41586-019-1016-7>
- Huang, T., Chen, W., Liu, J., Gu, N., & Zhang, R. (2019). Genome-wide identification of mRNA 5-methylcytosine in mammals. *Nature Structural & Molecular Biology*, 26(5), 380–388. <https://doi.org/10.1038/s41594-019-0218-x>
- Huang, W., Lan, M.-D., Qi, C.-B., Zheng, S.-J., Wei, S.-Z., Yuan, B.-F., & Feng, Y.-Q. (2016). Formation and determination of the oxidation products of 5-methylcytosine in RNA. *Chemical Science*, 7(8), 5495–5502. <https://doi.org/10.1039/C6SC01589A>
- Huber, S. M., van Delft, P., Mendil, L., Bachman, M., Smollett, K., Werner, F., Miska, E. A., & Balasubramanian, S. (2015). Formation and Abundance of 5-Hydroxymethylcytosine in RNA. *ChemBioChem*, 16(5), 752–755. <https://doi.org/https://doi.org/10.1002/cbic.201500013>

8. References

- Huong, T. T., Ngoc, L. N. T., & Kang, H. (2020). Functional Characterization of a Putative RNA Demethylase ALKBH6 in Arabidopsis Growth and Abiotic Stress Responses. *International Journal of Molecular Sciences*, 21(18). <https://doi.org/10.3390/ijms21186707>
- Hussain, S., Sajini, A. A., Blanco, S., Dietmann, S., Lombard, P., Sugimoto, Y., Paramor, M., Gleeson, J. G., Odom, D. T., Ule, J., & Frye, M. (2013). NSun2-Mediated Cytosine-5 Methylation of Vault Noncoding RNA Determines Its Processing into Regulatory Small RNAs. *Cell Reports*, 4(2), 255–261. <https://doi.org/10.1016/J.CELREP.2013.06.029>
- Ignatova, V. v, Stolz, P., Kaiser, S., Gustafsson, T. H., Lastres, P. R., Sanz-Moreno, A., Cho, Y.-L., Amarie, O. v, Aguilar-Pimentel, A., Klein-Rodewald, T., Calzada-Wack, J., Becker, L., Marschall, S., Kraiger, M., Garrett, L., Seisenberger, C., Hölter, S. M., Borland, K., van de Logt, E., ... Schneider, R. (2020). The rRNA m6A methyltransferase METTL5 is involved in pluripotency and developmental programs. *Genes & Development*, 34(9–10), 715–729. <https://doi.org/10.1101/gad.333369.119>
- Imai, Y., Matsuo, N., Ogawa, S., Tohyama, M., & Takagi, T. (1998). Cloning of a gene, YT521, for a novel RNA splicing-related protein induced by hypoxia/reoxygenation. *Molecular Brain Research*, 53(1–2), 33–40. [https://doi.org/10.1016/S0169-328X\(97\)00262-3](https://doi.org/10.1016/S0169-328X(97)00262-3)
- Incarinato, D., Anselmi, F., Morandi, E., Neri, F., Maldotti, M., Rapelli, S., Parlato, C., Basile, G., & Oliviero, S. (2017). High-throughput single-base resolution mapping of RNA 2'-O-methylated residues. *Nucleic Acids Research*, 45(3), 1433–1441. <https://doi.org/10.1093/nar/gkw810>
- Inuzuka, H., Gao, D., Finley, L. W. S., Yang, W., Wan, L., Fukushima, H., Chin, Y. R., Zhai, B., Shaik, S., Lau, A. W., Wang, Z., Gygi, S. P., Nakayama, K., Teruya-Feldstein, J., Tokar, A., Haigis, M. C., Pandolfi, P. P., & Wei, W. (2012). Acetylation-Dependent Regulation of Skp2 Function. *Cell*, 150(1), 179–193. <https://doi.org/10.1016/J.CELL.2012.05.038>
- Irwin, S. A., Patel, B., Idupulapati, M., Harris, J. B., Crisostomo, R. A., Larsen, B. P., Kooy, F., Willems, P. J., Cras, P., Kozlowski, P. B., Swain, R. A., Weiler, I. J., & Greenough, W. T. (2001). Abnormal dendritic spine characteristics in the temporal and visual cortices of patients with fragile-X syndrome: A quantitative examination. *American Journal of Medical Genetics*, 98(2), 161–167. [https://doi.org/https://doi.org/10.1002/1096-8628\(20010115\)98:2<161::AID-AJMG1025>3.0.CO;2-B](https://doi.org/https://doi.org/10.1002/1096-8628(20010115)98:2<161::AID-AJMG1025>3.0.CO;2-B)
- Ivanova, I., Much, C., di Giacomo, M., Azzi, C., Morgan, M., Moreira, P. N., Monahan, J., Carrieri, C., Enright, A. J., & O'Carroll, D. (2017). The RNA m6A Reader YTHDF2 Is Essential for the Post-transcriptional Regulation of the Maternal Transcriptome and Oocyte Competence. *Molecular Cell*, 67(6), 1059-1067.e4. <https://doi.org/10.1016/J.MOLCEL.2017.08.003>
- Iyer, L. M., Zhang, D., & Aravind, L. (2016). Adenine methylation in eukaryotes: Apprehending the complex evolutionary history and functional potential of an epigenetic modification. *BioEssays*, 38(1), 27–40. <https://doi.org/https://doi.org/10.1002/bies.201500104>
- Jacob, N., Jan, C., Jens, L.-A., H, J. A., M, W. U., & C, N. F. (1999). A Family of Insulin-Like Growth Factor II mRNA-Binding Proteins Represses Translation in Late Development. *Molecular and Cellular Biology*, 19(2), 1262–1270. <https://doi.org/10.1128/MCB.19.2.1262>
- Jain, D., Puno, M. R., Meydan, C., Lailier, N., Mason, C. E., Lima, C. D., Anderson, K. v, & Keeney, S. (2018). ketu mutant mice uncover an essential meiotic function for the ancient RNA helicase YTHDC2. *ELife*, 7, e30919. <https://doi.org/10.7554/eLife.30919>
- Jia, G., Fu, Y., Zhao, X., Dai, Q., Zheng, G., Yang, Y., Yi, C., Lindahl, T., Pan, T., Yang, Y.-G., & He, C. (2011). N6-Methyladenosine in nuclear RNA is a major substrate of the obesity-associated FTO. *Nature Chemical Biology*, 7(12), 885–887. <https://doi.org/10.1038/nchembio.687>
- Jia, G., Yang, C. G., Yang, S., Jian, X., Yi, C., Zhou, Z., & He, C. (2008). Oxidative demethylation of 3-methylthymine and 3-methyluracil in single-stranded DNA and RNA by mouse and human FTO. *FEBS Letters*, 582(23–24), 3313–3319. <https://doi.org/10.1016/J.FEBSLET.2008.08.019>
- Jiang, X., Liu, B., Nie, Z., Duan, L., Xiong, Q., Jin, Z., Yang, C., & Chen, Y. (2021). The role of m6A modification in the biological functions and diseases. *Signal Transduction and Targeted Therapy*, 6(1), 74. <https://doi.org/10.1038/s41392-020-00450-x>
- Jin, D., Guo, J., Wu, Y., Du, J., Yang, L., Wang, X., Di, W., Hu, B., An, J., Kong, L., Pan, L., & Su, G. (2019). m6A mRNA methylation initiated by METTL3 directly promotes YAP translation and increases YAP activity by regulating the MALAT1-miR-1914-3p-YAP axis to induce NSCLC drug resistance and metastasis. *Journal of Hematology & Oncology*, 12(1), 135. <https://doi.org/10.1186/s13045-019-0830-6>
- Jin, S., Pan, L., Liu, Z., Wang, Q., Xu, Z., & Zhang, Y. Q. (2009). Drosophila Tubulin-specific chaperone E functions at neuromuscular synapses and is required for microtubule network formation. *Development*, 136(9), 1571–1581. <https://doi.org/10.1242/dev.029983>
- Kaido, M., Wada, H., Shindo, M., & Hayashi, S. (2009). Essential requirement for RING finger E3 ubiquitin ligase Hakai in early embryonic development of Drosophila. *Genes to Cells*, 14(9), 1067–1077. <https://doi.org/https://doi.org/10.1111/j.1365-2443.2009.01335.x>
- Kan, L., Grozhik, A. v, Vedanayagam, J., Patil, D. P., Pang, N., Lim, K.-S., Huang, Y.-C., Joseph, B., Lin, C.-J., Despic, V., Guo, J., Yan, D., Kondo, S., Deng, W.-M., Dedon, P. C., Jaffrey, S. R., & Lai, E. C. (2017). The m6A pathway facilitates sex determination in Drosophila. *Nature Communications*, 8(1), 15737. <https://doi.org/10.1038/ncomms15737>
- Kan, L., Ott, S., Joseph, B., Park, E. S., Dai, W., Kleiner, R. E., Claridge-Chang, A., & Lai, E. C. (2021). A neural m6A/Ythdf pathway is required for learning and memory in Drosophila. *Nature Communications*, 12(1), 1458. <https://doi.org/10.1038/s41467-021-21537-1>
- Kane, S. E., & Beemon, K. (1985). Precise localization of m6A in Rous sarcoma virus RNA reveals clustering of methylation sites: implications for RNA processing. *Molecular and Cellular Biology*, 5(9), 2298–2306. <https://doi.org/10.1128/mcb.5.9.2298-2306.1985>
- Kang, H. J., Cheon, N. Y., Park, H., Jeong, G. W., Ye, B. J., Yoo, E. J., Lee, J. H., Hur, J.-H., Lee, E.-A., Kim, H., Lee, K., Choi, S. Y., Lee-Kwon, W., Myung, K., Lee, J. Y., & Kwon, H. M. (2021). TonEBP recognizes R-loops and initiates m6A RNA methylation for R-loop resolution. *Nucleic Acids Research*, 49(1), 269–284. <https://doi.org/10.1093/nar/gkaa1162>
- Kasowitz, S. D., Ma, J., Anderson, S. J., Leu, N. A., Xu, Y., Gregory, B. D., Schultz, R. M., & Wang, P. J. (2018). Nuclear m6A reader YTHDC1 regulates alternative polyadenylation and splicing during mouse oocyte development. *PLOS Genetics*, 14(5), e1007412. <https://doi.org/10.1371/journal.pgen.1007412>
- Kawarada, L., Suzuki, T., Ohira, T., Hirata, S., Miyauchi, K., & Suzuki, T. (2017). ALKBH1 is an RNA dioxygenase responsible for cytoplasmic and mitochondrial tRNA modifications. *Nucleic Acids Research*, 45(12), 7401–7415. <https://doi.org/10.1093/nar/gkx354>

8. References

- Ke, S., Alemu, E. A., Mertens, C., Gantman, E. C., Fak, J. J., Mele, A., Haripal, B., Zucker-Scharff, I., Moore, M. J., Park, C. Y., Vågbø, C. B., Kusznierczyk, A., Klungland, A., Darnell, J. E., & Darnell, R. B. (2015a). A majority of m6A residues are in the last exons, allowing the potential for 3' UTR regulation. *Genes & Development*, *29*(19), 2037–2053. <https://doi.org/10.1101/gad.269415.115>
- Ke, S., Alemu, E. A., Mertens, C., Gantman, E. C., Fak, J. J., Mele, A., Haripal, B., Zucker-Scharff, I., Moore, M. J., Park, C. Y., Vågbø, C. B., Kusznierczyk, A., Klungland, A., Darnell, J. E., & Darnell, R. B. (2015b). A majority of m6A residues are in the last exons, allowing the potential for 3' UTR regulation. *Genes & Development*, *29*(19), 2037–2053. <https://doi.org/10.1101/gad.269415.115>
- Ke, S., Pandya-Jones, A., Saito, Y., Fak, J. J., Vågbø, C. B., Geula, S., Hanna, J. H., Black, D. L., Darnell, J. E., & Darnell, R. B. (2017). m6A mRNA modifications are deposited in nascent pre-mRNA and are not required for splicing but do specify cytoplasmic turnover. *Genes & Development*, *31*(10), 990–1006. <https://doi.org/10.1101/gad.301036.117>
- Khan, M., Hou, S., Chen, M., & Lei, H. (2022). Mechanisms of RNA export and nuclear retention. *WIREs RNA*, *n/a*(n/a), e1755. <https://doi.org/https://doi.org/10.1002/wrna.1755>
- Kim, M., Bellini, M., & Ceman, S. (2009). Fragile X mental retardation protein FMRP binds mRNAs in the nucleus. *Molecular and Cellular Biology*, *29*(1), 214–228. <https://doi.org/10.1128/mcb.01377-08>
- Kleiber, N., Lemus-Diaz, N., Stiller, C., Heinrichs, M., Mai, M. M.-Q., Hackert, P., Richter-Dennerlein, R., Höbartner, C., Bohnsack, K. E., & Bohnsack, M. T. (2022). The RNA methyltransferase METTL8 installs m3C32 in mitochondrial tRNAs^{Thr/Ser}(UCN) to optimise tRNA structure and mitochondrial translation. *Nature Communications*, *13*(1), 209. <https://doi.org/10.1038/s41467-021-27905-1>
- Knuckles, P., Carl, S. H., Musheev, M., Niehrs, C., Wenger, A., & Bühler, M. (2017). RNA fate determination through cotranscriptional adenosine methylation and microprocessor binding. *Nature Structural & Molecular Biology*, *24*(7), 561–569. <https://doi.org/10.1038/nsmb.3419>
- Knuckles, P., Lence, T., Haussmann, I. U., Jacob, D., Kreim, N., Carl, S. H., Masiello, I., Hares, T., Villaseñor, R., Hess, D., Andrade-Navarro, M. A., Biggiogera, M., Helm, M., Soller, M., Bühler, M., & Roignant, J.-Y. (2018). Zc3h13/Flacc is required for adenosine methylation by bridging the mRNA-binding factor Rbm15/Spenito to the m6A machinery component Wtap/Fl(2)d. *Genes & Development*. <https://doi.org/10.1101/gad.309146.117>
- Kobayashi, M., Ohsugi, M., Sasako, T., Awazawa, M., Umehara, T., Iwane, A., Kobayashi, N., Okazaki, Y., Kubota, N., Suzuki, R., Waki, H., Horiuchi, K., Hamakubo, T., Kodama, T., Aoe, S., Tobe, K., Kadowaki, T., & Ueki, K. (2018). The RNA Methyltransferase Complex of WTAP, METTL3, and METTL14 Regulates Mitotic Clonal Expansion in Adipogenesis. *Molecular and Cellular Biology*, *38*(16), e00116-18. <https://doi.org/10.1128/mcb.00116-18>
- Koh, C. W. Q., Goh, Y. T., & Goh, W. S. S. (2019). Atlas of quantitative single-base-resolution N6-methyl-adenine methylomes. *Nature Communications*, *10*(1), 5636. <https://doi.org/10.1038/s41467-019-13561-z>
- Kondo, S., & Ueda, R. (2013). Highly Improved Gene Targeting by Germline-Specific Cas9 Expression in Drosophila. *Genetics*, *195*(3), 715–721. <https://doi.org/10.1534/genetics.113.156737>
- König, J., Zarnack, K., Rot, G., Curk, T., Kayikci, M., Zupan, B., Turner, D. J., Luscombe, N. M., & Ule, J. (2010). iCLIP reveals the function of hnRNP particles in splicing at individual nucleotide resolution. *Nature Structural & Molecular Biology*, *17*(7), 909–915. <https://doi.org/10.1038/nsmb.1838>
- Kontur, C., Jeong, M., Cifuentes, D., & Giraldez, A. J. (2020). Ythdf m6A Readers Function Redundantly during Zebrafish Development. *Cell Reports*, *33*(13), 108598. <https://doi.org/10.1016/j.celrep.2020.108598>
- Körtel, N., Rücklé, C., Zhou, Y., Busch, A., Hoch-Kraft, P., Sutandy, F. X. R., Haase, J., Pradhan, M., Musheev, M., Ostareck, D., Ostareck-Lederer, A., Dieterich, C., Hüttelmaier, S., Niehrs, C., Rausch, O., Dominissini, D., König, J., & Zarnack, K. (2021). Deep and accurate detection of m6A RNA modifications using miCLIP2 and m6Aboost machine learning. *Nucleic Acids Research*, *49*(16), e92–e92. <https://doi.org/10.1093/nar/gkab485>
- Kretschmer, J., Rao, H., Hackert, P., Sloan, K. E., Höbartner, C., & Bohnsack, M. T. (2018). The m6A reader protein YTHDC2 interacts with the small ribosomal subunit and the 5'–3' exoribonuclease XRN1. *RNA*, *24*(10), 1339–1350. <https://doi.org/10.1261/rna.064238.117>
- Krogh, N., Jansson, M. D., Häfner, S. J., Tehler, D., Birkedal, U., Christensen-Dalsgaard, M., Lund, A. H., & Nielsen, H. (2016). Profiling of 2'-O-Me in human rRNA reveals a subset of fractionally modified positions and provides evidence for ribosome heterogeneity. *Nucleic Acids Research*, *44*(16), 7884–7895. <https://doi.org/10.1093/nar/gkw482>
- Kurowski, M. A., Bhagwat, A. S., Papaj, G., & Bujnicki, J. M. (2003). Phylogenomic identification of five new human homologs of the DNA repair enzyme AlkB. *BMC Genomics*, *4*(1), 48. <https://doi.org/10.1186/1471-2164-4-48>
- Kweon, S. M., Chen, Y., Moon, E., Kvederaviciute, K., Klimasauskas, S., & Feldman, D. E. (2019). An Adversarial DNA N6-Methyladenine-Sensor Network Preserves Polycomb Silencing. *Molecular Cell*, *74*(6), 1138–1147.e6. <https://doi.org/10.1016/j.molcel.2019.03.018>
- Lasman, L., Krupalnik, V., Viukov, S., Mor, N., Aguilera-Castrejon, A., Schneider, D., Bayerl, J., Mizrahi, O., Peles, S., Tawil, S., Sathe, S., Nachshon, A., Shani, T., Zerbib, M., Kilimnik, I., Aigner, S., Shankar, A., Mueller, J. R., Schwartz, S., ... Hanna, J. H. (2020). Context-dependent functional compensation between Ythdf m6A reader proteins. *Genes & Development*, *34*(19–20), 1373–1391. <https://doi.org/10.1101/gad.340695.120>
- Lee, J. H., Wang, R., Xiong, F., Krakowiak, J., Liao, Z., Nguyen, P. T., Moroz-Omori, E. v., Shao, J., Zhu, X., Bolt, M. J., Wu, H., Singh, P. K., Bi, M., Shi, C. J., Jamal, N., Li, G., Mistry, R., Jung, S. Y., Tsai, K. L., ... Li, W. (2021). Enhancer RNA m6A methylation facilitates transcriptional condensate formation and gene activation. *Molecular Cell*, *81*(16), 3368–3385.e9. <https://doi.org/10.1016/j.molcel.2021.07.024>
- Lee, J. M., Hammarén, H. M., Savitski, M. M., & Baek, S. H. (2023). Control of protein stability by post-translational modifications. *Nature Communications*, *14*(1), 201. <https://doi.org/10.1038/s41467-023-35795-8>

8. References

- Lee, M., Paik, S. K., Lee, M. J., Kim, Y. J., Kim, S., Nahm, M., Oh, S. J., Kim, H. M., Yim, J., Lee, C. J., Bae, Y. C., & Lee, S. (2009). Drosophila Atlastin regulates the stability of muscle microtubules and is required for synapse development. *Developmental Biology*, *330*(2), 250–262. <https://doi.org/10.1016/J.YDBIO.2009.03.019>
- Leger, A., Amaral, P. P., Pandolfini, L., Capitanich, C., Capraro, F., Miano, V., Migliori, V., Toolan-Kerr, P., Sideri, T., Enright, A. J., Tzelepis, K., van Werven, F. J., Luscombe, N. M., Barbieri, I., Ule, J., Fitzgerald, T., Birney, E., Leonardi, T., & Kouzarides, T. (2021). RNA modifications detection by comparative Nanopore direct RNA sequencing. *Nature Communications*, *12*(1), 7198. <https://doi.org/10.1038/s41467-021-27393-3>
- Leismann, J., Spagnuolo, M., Pradhan, M., Wacheul, L., Vu, M. A., Musheev, M., Mier, P., Andrade-Navarro, M. A., Graille, M., Niehrs, C., Lafontaine, D. L. J., & Roignant, J.-Y. (2020). The 18S ribosomal RNA m6A methyltransferase Mettl5 is required for normal walking behavior in Drosophila. *EMBO Reports*, *21*(7), e49443. <https://doi.org/10.15252/embr.201949443>
- Lence, T., Akhtar, J., Bayer, M., Schmid, K., Spindler, L., Ho, C. H., Kreim, N., Andrade-Navarro, M. A., Poeck, B., Helm, M., & Roignant, J.-Y. (2016). m6A modulates neuronal functions and sex determination in Drosophila. *Nature*, *540*(7632), 242–247. <https://doi.org/10.1038/nature20568>
- Lesbirel, S., Viphakone, N., Parker, M., Parker, J., Heath, C., Sudbery, I., & Wilson, S. A. (2018). The m6A-methylase complex recruits TREX and regulates mRNA export. *Scientific Reports*, *8*(1), 13827. <https://doi.org/10.1038/s41598-018-32310-8>
- Li, A., Chen, Y.-S., Ping, X.-L., Yang, X., Xiao, W., Yang, Y., Sun, H.-Y., Zhu, Q., Baidya, P., Wang, X., Bhattarai, D. P., Zhao, Y.-L., Sun, B.-F., & Yang, Y.-G. (2017a). Cytoplasmic m6A reader YTHDF3 promotes mRNA translation. *Cell Research*, *27*(3), 444–447. <https://doi.org/10.1038/cr.2017.10>
- Li, A., Chen, Y.-S., Ping, X.-L., Yang, X., Xiao, W., Yang, Y., Sun, H.-Y., Zhu, Q., Baidya, P., Wang, X., Bhattarai, D. P., Zhao, Y.-L., Sun, B.-F., & Yang, Y.-G. (2017b). Cytoplasmic m6A reader YTHDF3 promotes mRNA translation. *Cell Research*, *27*(3), 444–447. <https://doi.org/10.1038/cr.2017.10>
- Li, D., Zhang, H., Hong, Y., Huang, L., Li, X., Zhang, Y., Ouyang, Z., & Song, F. (2014). Genome-Wide Identification, Biochemical Characterization, and Expression Analyses of the YTH Domain-Containing RNA-Binding Protein Family in Arabidopsis and Rice. *Plant Molecular Biology Reporter*, *32*(6), 1169–1186. <https://doi.org/10.1007/s11105-014-0724-2>
- Li, F., Zhao, D., Wu, J., & Shi, Y. (2014). Structure of the YTH domain of human YTHDF2 in complex with an m6A mononucleotide reveals an aromatic cage for m6A recognition. *Cell Research*, *24*(12), 1490–1492. <https://doi.org/10.1038/cr.2014.153>
- Li, L., Krasnykov, K., Homolka, D., Gos, P., Mendel, M., Fish, R. J., Pandey, R. R., & Pillai, R. S. (2022). The XRN1-regulated RNA helicase activity of YTHDC2 ensures mouse fertility independently of m6A recognition. *Molecular Cell*, *82*(9), 1678-1690.e12. <https://doi.org/10.1016/J.MOLCEL.2022.02.034>
- Li, M., Zhao, X., Wang, W., Shi, H., Pan, Q., Lu, Z., Perez, S. P., Suganthan, R., He, C., Bjørås, M., & Klungland, A. (2018). Ythdf2-mediated m6A mRNA clearance modulates neural development in mice. *Genome Biology*, *19*(1), 69. <https://doi.org/10.1186/s13059-018-1436-y>
- Li, M.-M., Nilsen, A., Shi, Y., Fusser, M., Ding, Y.-H., Fu, Y., Liu, B., Niu, Y., Wu, Y.-S., Huang, C.-M., Olofsson, M., Jin, K.-X., Lv, Y., Xu, X.-Z., He, C., Dong, M.-Q., Rendtlew Danielsen, J. M., Klungland, A., & Yang, Y.-G. (2013). ALKBH4-dependent demethylation of actin regulates actomyosin dynamics. *Nature Communications*, *4*(1), 1832. <https://doi.org/10.1038/ncomms2863>
- Li, X., Zhu, P., Ma, S., Song, J., Bai, J., Sun, F., & Yi, C. (2015). Chemical pulldown reveals dynamic pseudouridylation of the mammalian transcriptome. *Nature Chemical Biology*, *11*(8), 592–597. <https://doi.org/10.1038/nchembio.1836>
- Li, Y., Su, R., Deng, X., Chen, Y., & Chen, J. (2022). FTO in cancer: functions, molecular mechanisms, and therapeutic implications. *Trends in Cancer*, *8*(7), 598–614. <https://doi.org/10.1016/J.TRECAN.2022.02.010>
- Li, Y., Xia, L., Tan, K., Ye, X., Zuo, Z., Li, M., Xiao, R., Wang, Z., Liu, X., Deng, M., Cui, J., Yang, M., Luo, Q., Liu, S., Cao, X., Zhu, H., Liu, T., Hu, J., Shi, J., ... Xia, L. (2020). N6-Methyladenosine co-transcriptionally directs the demethylation of histone H3K9me2. *Nature Genetics*, *52*(9), 870–877. <https://doi.org/10.1038/s41588-020-0677-3>
- Li, Z., Weng, H., Su, R., Weng, X., Zuo, Z., Li, C., Huang, H., Nachtergaele, S., Dong, L., Hu, C., Qin, X., Tang, L., Wang, Y., Hong, G. M., Huang, H., Wang, X., Chen, P., Gurbuxani, S., Arnovitz, S., ... Chen, J. (2017). FTO Plays an Oncogenic Role in Acute Myeloid Leukemia as a N6-Methyladenosine RNA Demethylase. *Cancer Cell*, *31*(1), 127–141. <https://doi.org/10.1016/J.CCELL.2016.11.017>
- Lin, S., Choe, J., Du, P., Triboulet, R., & Gregory, R. I. (2016). The m6A Methyltransferase METTL3 Promotes Translation in Human Cancer Cells. *Molecular Cell*, *62*(3), 335–345. <https://doi.org/10.1016/J.MOLCEL.2016.03.021>
- Lin, X., Chai, G., Wu, Y., Li, J., Chen, F., Liu, J., Luo, G., Tauler, J., Du, J., Lin, S., He, C., & Wang, H. (2019). RNA m6A methylation regulates the epithelial mesenchymal transition of cancer cells and translation of Snail. *Nature Communications*, *10*(1), 2065. <https://doi.org/10.1038/s41467-019-09865-9>
- Lin, Z., Hsu, P. J., Xing, X., Fang, J., Lu, Z., Zou, Q., Zhang, K. J., Zhang, X., Zhou, Y., & Zhang, T. (2017). Mettl3/Mettl14-mediated mRNA N(6)-methyladenosine modulates murine spermatogenesis. *Cell Research*, *27*, 1216–1230.
- Linder, B., Grozhik, A. v, Olarerin-George, A. O., Meydan, C., Mason, C. E., & Jaffrey, S. R. (2015). Single-nucleotide-resolution mapping of m6A and m6Am throughout the transcriptome. *Nature Methods*, *12*(8), 767–772. <https://doi.org/10.1038/nmeth.3453>
- Little, N. A., Hastie, N. D., & Davies, R. C. (2000). Identification of WTAP, a novel Wilms' tumour 1-associating protein. *Human Molecular Genetics*, *9*(15), 2231–2239. <https://doi.org/10.1093/oxfordjournals.hmg.a018914>

8. References

- Liu, C., Sun, H., Yi, Y., Shen, W., Li, K., Xiao, Y., Li, F., Li, Y., Hou, Y., Lu, B., Liu, W., Meng, H., Peng, J., Yi, C., & Wang, J. (2022). Absolute quantification of single-base m6A methylation in the mammalian transcriptome using GLORI. *Nature Biotechnology*. <https://doi.org/10.1038/s41587-022-01487-9>
- Liu, F., Clark, W., Luo, G., Wang, X., Fu, Y., Wei, J., Wang, X., Hao, Z., Dai, Q., Zheng, G., Ma, H., Han, D., Evans, M., Klungland, A., Pan, T., & He, C. (2016). ALKBH1-Mediated tRNA Demethylation Regulates Translation. *Cell*, *167*(3), 816–828.e16. <https://doi.org/10.1016/j.cell.2016.09.038>
- Liu, H., Begik, O., Lucas, M. C., Ramirez, J. M., Mason, C. E., Wiener, D., Schwartz, S., Mattick, J. S., Smith, M. A., & Novoa, E. M. (2019). Accurate detection of m6A RNA modifications in native RNA sequences. *Nature Communications*, *10*(1), 4079. <https://doi.org/10.1038/s41467-019-11713-9>
- Liu, J., Dou, X., Chen, C., Chen, C., Liu, C., Xu, M. M., Zhao, S., Shen, B., Gao, Y., Han, D., & He, C. (2020). N6-methyladenosine of chromosome-associated regulatory RNA regulates chromatin state and transcription. *Science*, *367*(6477), 580–586. <https://doi.org/10.1126/science.aay6018>
- Liu, J., Eckert, M. A., Harada, B. T., Liu, S.-M., Lu, Z., Yu, K., Tienda, S. M., Chryplewicz, A., Zhu, A. C., Yang, Y., Huang, J.-T., Chen, S.-M., Xu, Z.-G., Leng, X.-H., Yu, X.-C., Cao, J., Zhang, Z., Liu, J., Lengyel, E., & He, C. (2018). m6A mRNA methylation regulates AKT activity to promote the proliferation and tumorigenicity of endometrial cancer. *Nature Cell Biology*, *20*(9), 1074–1083. <https://doi.org/10.1038/s41556-018-0174-4>
- Liu, J., Gao, M., He, J., Wu, K., Lin, S., Jin, L., Chen, Y., Liu, H., Shi, J., Wang, X., Chang, L., Lin, Y., Zhao, Y.-L., Zhang, X., Zhang, M., Luo, G.-Z., Wu, G., Pei, D., Wang, J., ... Chen, J. (2021). The RNA m6A reader YTHDC1 silences retrotransposons and guards ES cell identity. *Nature*, *591*(7849), 322–326. <https://doi.org/10.1038/s41586-021-03313-9>
- Liu, J., Harada, B. T., & He, C. (2019). Regulation of Gene Expression by N6-methyladenosine in Cancer. *Trends in Cell Biology*, *29*(6), 487–499. <https://doi.org/https://doi.org/10.1016/j.tcb.2019.02.008>
- Liu, J., Ren, D., Du, Z., Wang, H., Zhang, H., & Jin, Y. (2018). m6A demethylase FTO facilitates tumor progression in lung squamous cell carcinoma by regulating MZF1 expression. *Biochemical and Biophysical Research Communications*, *502*(4), 456–464. <https://doi.org/10.1016/j.bbrc.2018.05.175>
- Liu, J., Yue, Y., Han, D., Wang, X., Fu, Y., Zhang, L., Jia, G., Yu, M., Lu, Z., Deng, X., Dai, Q., Chen, W., & He, C. (2014a). A METTL3–METTL14 complex mediates mammalian nuclear RNA N6-adenosine methylation. *Nature Chemical Biology*, *10*(2), 93–95. <https://doi.org/10.1038/nchembio.1432>
- Liu, J., Yue, Y., Han, D., Wang, X., Fu, Y., Zhang, L., Jia, G., Yu, M., Lu, Z., Deng, X., Dai, Q., Chen, W., & He, C. (2014b). A METTL3–METTL14 complex mediates mammalian nuclear RNA N6-adenosine methylation. *Nature Chemical Biology*, *10*(2), 93–95. <https://doi.org/10.1038/nchembio.1432>
- Liu, M., Jiang, K., Lin, G., Liu, P., Yan, Y., Ye, T., Yao, G., Barr, M. P., Liang, D., Wang, Y., Gong, P., Meng, S., & Piao, H. (2018). Ajuba inhibits hepatocellular carcinoma cell growth via targeting of β -catenin and YAP signaling and is regulated by E3 ligase Hakai through neddylation. *Journal of Experimental & Clinical Cancer Research*, *37*(1), 165. <https://doi.org/10.1186/s13046-018-0806-3>
- Liu, N., Dai, Q., Zheng, G., He, C., Parisien, M., & Pan, T. (2015). N6-methyladenosine-dependent RNA structural switches regulate RNA–protein interactions. *Nature*, *518*(7540), 560–564. <https://doi.org/10.1038/nature14234>
- Liu, N., Parisien, M., Dai, Q., Zheng, G., He, C., & Pan, T. (2013). Probing N6-methyladenosine RNA modification status at single nucleotide resolution in mRNA and long noncoding RNA. *RNA*, *19*(12), 1848–1856. <https://doi.org/10.1261/rna.041178.113>
- Liu, N., Zhou, K. I., Parisien, M., Dai, Q., Diatchenko, L., & Pan, T. (2017). N6-methyladenosine alters RNA structure to regulate binding of a low-complexity protein. *Nucleic Acids Research*, *45*(10), 6051–6063. <https://doi.org/10.1093/nar/gkx141>
- Liu, R., Kasowitz, S. D., Homolka, D., Leu, N. A., Shaked, J. T., Ruthel, G., Jain, D., Lin, H., Keeney, S., Luo, M., Pillai, R. S., & Wang, P. J. (2021a). YTHDC2 is essential for pachytene progression and prevents aberrant microtubule-driven telomere clustering in male meiosis. *Cell Reports*, *37*(11), 110110. <https://doi.org/10.1016/j.celrep.2021.110110>
- Liu, R., Kasowitz, S. D., Homolka, D., Leu, N. A., Shaked, J. T., Ruthel, G., Jain, D., Lin, H., Keeney, S., Luo, M., Pillai, R. S., & Wang, P. J. (2021b). YTHDC2 is essential for pachytene progression and prevents aberrant microtubule-driven telomere clustering in male meiosis. *Cell Reports*, *37*(11), 110110. <https://doi.org/10.1016/j.celrep.2021.110110>
- Lorenz, D. A., Sathe, S., Einstein, J. M., & Yeo, G. W. (2020). Direct RNA sequencing enables m6A detection in endogenous transcript isoforms at base-specific resolution. *RNA*, *26*(1), 19–28. <https://doi.org/10.1261/rna.072785.119>
- Louloupi, A., Ntini, E., Conrad, T., & Ørom, U. A. V. (2018). Transient N6-Methyladenosine Transcriptome Sequencing Reveals a Regulatory Role of m6A in Splicing Efficiency. *Cell Reports*, *23*(12), 3429–3437. <https://doi.org/10.1016/j.celrep.2018.05.077>
- Lovejoy, A. F., Riordan, D. P., & Brown, P. O. (2014). Transcriptome-Wide Mapping of Pseudouridines: Pseudouridine Synthases Modify Specific mRNAs in *S. cerevisiae*. *PLOS ONE*, *9*(10), e110799. <https://doi.org/10.1371/journal.pone.0110799>
- Lu, R., Wang, H., Liang, Z., Ku, L., O'Donnell, W. T., Li, W., Warren, S. T., & Feng, Y. (2004). The fragile X protein controls microtubule-associated protein 1B translation and microtubule stability in brain neuron development. *Proceedings of the National Academy of Sciences*, *101*(42), 15201–15206. <https://doi.org/10.1073/pnas.0404995101>
- Luo, S., & Tong, L. (2014). Molecular basis for the recognition of methylated adenines in RNA by the eukaryotic YTH domain. *Proceedings of the National Academy of Sciences*, *111*(38), 13834–13839. <https://doi.org/10.1073/pnas.1412742111>

8. References

- Ly, C. V, Yao, C.-K., Verstreken, P., Ohyama, T., & Bellen, H. J. (2008). straightjacket is required for the synaptic stabilization of cacophony, a voltage-gated calcium channel $\alpha 1$ subunit. *Journal of Cell Biology*, *181*(1), 157–170. <https://doi.org/10.1083/jcb.200712152>
- Ma, C., Chang, M., Lv, H., Zhang, Z.-W., Zhang, W., He, X., Wu, G., Zhao, S., Zhang, Y., Wang, D., Teng, X., Liu, C., Li, Q., Klungland, A., Niu, Y., Song, S., & Tong, W.-M. (2018). RNA m6A methylation participates in regulation of postnatal development of the mouse cerebellum. *Genome Biology*, *19*(1), 68. <https://doi.org/10.1186/s13059-018-1435-z>
- Ma, C., Liao, S., & Zhu, Z. (2019). Crystal structure of human YTHDC2 YTH domain. *Biochemical and Biophysical Research Communications*, *518*(4), 678–684. <https://doi.org/10.1016/J.BBRC.2019.08.107>
- Ma, C.-J., Ding, J.-H., Ye, T.-T., Yuan, B.-F., & Feng, Y.-Q. (2019). AlkB Homologue 1 Demethylates N^6 -Methylcytidine in mRNA of Mammals. *ACS Chemical Biology*, *14*(7), 1418–1425. <https://doi.org/10.1021/acschembio.8b01001>
- Ma, H., Wang, X., Cai, J., Dai, Q., Natchiar, S. K., Lv, R., Chen, K., Lu, Z., Chen, H., Shi, Y. G., Lan, F., Fan, J., Klaholz, B. P., Pan, T., Shi, Y., & He, C. (2019). N^6 -Methyladenosine methyltransferase ZCCHC4 mediates ribosomal RNA methylation. *Nature Chemical Biology*, *15*(1), 88–94. <https://doi.org/10.1038/s41589-018-0184-3>
- Ma, J., Yang, F., Zhou, C., Liu, F., Yuan, J., Wang, F., Wang, T., Xu, Q., Zhou, W., & Sun, S. (2017). METTL14 suppresses the metastatic potential of hepatocellular carcinoma by modulating N^6 -methyladenosine-dependent primary MicroRNA processing. *Hepatology*, *65*(2). https://journals.lww.com/hep/Fulltext/2017/02000/METTL14_suppresses_the_metastatic_potential_of.15.aspx
- Ma, L., Lu, H., Tian, Z., Yang, M., Ma, J., Shang, G., Liu, Y., Xie, M., Wang, G., Wu, W., Zhang, Z., Dai, S., & Chen, Z. (2022). Structural insights into the interactions and epigenetic functions of human nucleic acid repair protein ALKBH6. *Journal of Biological Chemistry*, *298*(3), 101671. <https://doi.org/10.1016/J.JBC.2022.101671>
- Machnicka, M. A., Olchowik, A., Grosjean, H., & Bujnicki, J. M. (2014). Distribution and frequencies of post-transcriptional modifications in tRNAs. *RNA Biology*, *11*(12), 1619–1629. <https://doi.org/10.4161/15476286.2014.992273>
- Malbec, L., Zhang, T., Chen, Y.-S., Zhang, Y., Sun, B.-F., Shi, B.-Y., Zhao, Y.-L., Yang, Y., & Yang, Y.-G. (2019). Dynamic methylome of internal mRNA N^7 -methylguanosine and its regulatory role in translation. *Cell Research*, *29*(11), 927–941. <https://doi.org/10.1038/s41422-019-0230-z>
- Malka, Y., Alkan, F., Ju, S., Körner, P. R., Pataskar, A., Shulman, E., Loayza-Puch, F., Champagne, J., Wenzel, C., Faller, W. J., Elkon, R., Lee, C., & Agami, R. (2022). Alternative cleavage and polyadenylation generates downstream uncapped RNA isoforms with translation potential. *Molecular Cell*, *82*(20), 3840–3855.e8. <https://doi.org/10.1016/J.MOLCEL.2022.09.036>
- Mao, Y., Dong, L., Liu, X.-M., Guo, J., Ma, H., Shen, B., & Qian, S.-B. (2019). m6A in mRNA coding regions promotes translation via the RNA helicase-containing YTHDC2. *Nature Communications*, *10*(1), 5332. <https://doi.org/10.1038/s41467-019-13317-9>
- Marchand, V., Ayadi, L., Ernst, F. G. M., Hertler, J., Bourguignon-Igel, V., Galvanin, A., Kotter, A., Helm, M., Lafontaine, D. L. J., & Motorin, Y. (2018). AlkAniline-Seq: Profiling of m7G and m3C RNA Modifications at Single Nucleotide Resolution. *Angewandte Chemie International Edition*, *57*(51), 16785–16790. <https://doi.org/https://doi.org/10.1002/anie.201810946>
- Marchand, V., Blanloeil-Oillo, F., Helm, M., & Motorin, Y. (2016). Illumina-based RiboMethSeq approach for mapping of 2'-O-Me residues in RNA. *Nucleic Acids Research*, *44*(16), e135–e135. <https://doi.org/10.1093/nar/gkw547>
- Markaki, Y., Gan Chong, J., Wang, Y., Jacobson, E. C., Luong, C., Tan, S. Y. X., Jachowicz, J. W., Strehle, M., Maestrini, D., Banerjee, A. K., Mistry, B. A., Dror, I., Dossin, F., Schöneberg, J., Heard, E., Guttman, M., Chou, T., & Plath, K. (2021). Xist nucleates local protein gradients to propagate silencing across the X chromosome. *Cell*, *184*(25), 6174–6192.e32. <https://doi.org/10.1016/J.CELL.2021.10.022>
- Markmiller, S., Soltanieh, S., Server, K. L., Mak, R., Jin, W., Fang, M. Y., Luo, E. C., Krach, F., Yang, D., Sen, A., Fulzele, A., Wozniak, J. M., Gonzalez, D. J., Kankel, M. W., Gao, F. B., Bennett, E. J., Lécuycer, E., & Yeo, G. W. (2018). Context-Dependent and Disease-Specific Diversity in Protein Interactions within Stress Granules. *Cell*, *172*(3), 590–604.e13. <https://doi.org/10.1016/J.CELL.2017.12.032>
- Martinez, N. M., Su, A., Burns, M. C., Nussbacher, J. K., Schaening, C., Sathe, S., Yeo, G. W., & Gilbert, W. v. (2022). Pseudouridine synthases modify human pre-mRNA co-transcriptionally and affect pre-mRNA processing. *Molecular Cell*, *82*(3), 645–659.e9. <https://doi.org/10.1016/J.MOLCEL.2021.12.023>
- Mauer, J., Luo, X., Blanjoie, A., Jiao, X., Grozhik, A. V., Patil, D. P., Linder, B., Pickering, B. F., Vasseur, J.-J., Chen, Q., Gross, S. S., Elemento, O., Debart, F., Kiledjian, M., & Jaffrey, S. R. (2017). Reversible methylation of m6Am in the 5' cap controls mRNA stability. *Nature*, *541*(7637), 371–375. <https://doi.org/10.1038/nature21022>
- Mauer, J., Sindelar, M., Despici, V., Guez, T., Hawley, B. R., Vasseur, J.-J., Rentmeister, A., Gross, S. S., Pellizzoni, L., Debart, F., Goodarzi, H., & Jaffrey, S. R. (2019). FTO controls reversible m6Am RNA methylation during snRNA biogenesis. *Nature Chemical Biology*, *15*(4), 340–347. <https://doi.org/10.1038/s41589-019-0231-8>
- McMahon, A. C., Rahman, R., Jin, H., Shen, J. L., Fieldsend, A., Luo, W., & Rosbash, M. (2016). TRIBE: Hijacking an RNA-Editing Enzyme to Identify Cell-Specific Targets of RNA-Binding Proteins. *Cell*, *165*(3), 742–753. <https://doi.org/10.1016/J.CELL.2016.03.007>
- Meng, T.-G., Lu, X., Guo, L., Hou, G.-M., Ma, X.-S., Li, Q.-N., Huang, L., Fan, L.-H., Zhao, Z.-H., Ou, X.-H., Yang, Y.-C. O., Schatten, H., Li, L., Wang, Z.-B., & Sun, Q.-Y. (2019). Mettl14 is required for mouse postimplantation development by facilitating epiblast maturation. *The FASEB Journal*, *33*(1), 1179–1187. <https://doi.org/https://doi.org/10.1096/fj.201800719R>
- Menon, K. P., Carrillo, R. A., & Zinn, K. (2013). Development and plasticity of the Drosophila larval neuromuscular junction. *Wiley Interdisciplinary Reviews. Developmental Biology*, *2*(5), 647–670. <https://doi.org/10.1002/wdev.108>
- Merkurjev, D., Hong, W.-T., Iida, K., Oomoto, I., Goldie, B. J., Yamaguti, H., Ohara, T., Kawaguchi, S., Hirano, T., Martin, K. C., Pellegrini, M., & Wang, D. O. (2018). Synaptic N^6 -methyladenosine (m6A) epitranscriptome reveals functional partitioning of localized transcripts. *Nature Neuroscience*, *21*(7), 1004–1014. <https://doi.org/10.1038/s41593-018-0173-6>

8. References

- Meyer, K. D. (2019). DART-seq: an antibody-free method for global m6A detection. *Nature Methods*, 16(12), 1275–1280. <https://doi.org/10.1038/s41592-019-0570-0>
- Meyer, K. D., Patil, D. P., Zhou, J., Zinoviev, A., Skabkin, M. A., Elemento, O., Pestova, T. v., Qian, S. B., & Jaffrey, S. R. (2015). 5' UTR m6A Promotes Cap-Independent Translation. *Cell*, 163(4), 999–1010. <https://doi.org/10.1016/J.CELL.2015.10.012>
- Meyer, K. D., Saletore, Y., Zumbo, P., Elemento, O., Mason, C. E., & Jaffrey, S. R. (2012). Comprehensive Analysis of mRNA Methylation Reveals Enrichment in 3' UTRs and near Stop Codons. *Cell*, 149(7), 1635–1646. <https://doi.org/10.1016/J.CELL.2012.05.003>
- Molinie, B., Wang, J., Lim, K. S., Hillebrand, R., Lu, Z., van Wittenberghe, N., Howard, B. D., Daneshvar, K., Mullen, A. C., Dedon, P., Xing, Y., & Giallourakis, C. C. (2016). m6A-LAIC-seq reveals the census and complexity of the m6A epitranscriptome. *Nature Methods*, 13(8), 692–698. <https://doi.org/10.1038/nmeth.3898>
- Motorin, Y., & Helm, M. (2010). tRNA stabilization by modified nucleotides. *Biochemistry*, 49 24, 4934–4944.
- Mu, H. Y., Zhang, T., Yang, Y., Zhang, D. R., Gao, J., Li, J. H., Yue, L., Gao, D. F., Shi, B. B., & Han, Y. (2021). METTL3-mediated mRNA N6-methyladenosine is required for oocyte and follicle development in mice. *Cell Death and Disease*, 12, 989.
- Mukherjee, M., Chow, S. Y., Yusoff, P., Seetharaman, J., Ng, C., Sinniah, S., Koh, X. W., Asgar, N. F. M., Li, D., Yim, D., Jackson, R. A., Yew, J., Qian, J., Iyu, A., Lim, Y. P., Zhou, X., Sze, S. K., Guy, G. R., & Sivaraman, J. (2012). Structure of a novel phosphotyrosine-binding domain in Hakai that targets E-cadherin. *The EMBO Journal*, 31(5), 1308–1319. <https://doi.org/https://doi.org/10.1038/emboj.2011.496>
- Murat, P., Marsico, G., Herdy, B., Ghanbarian, A., Portella, G., & Balasubramanian, S. (2018). RNA G-quadruplexes at upstream open reading frames cause DHX36- and DHX9-dependent translation of human mRNAs. *Genome Biology*, 19(1), 229. <https://doi.org/10.1186/s13059-018-1602-2>
- Narayan, P., & Rottman, F. M. (1988). An In Vitro System for Accurate Methylation of Internal Adenosine Residues in Messenger RNA. *Science*, 242(4882), 1159–1162. <https://doi.org/10.1126/science.3187541>
- Nayler, O., Hartmann, A. M., & Stamm, S. (2000). The ER repeat protein YT521-B localizes to a novel subnuclear compartment. *The Journal of Cell Biology*, 150(5), 949–962. <https://doi.org/10.1083/jcb.150.5.949>
- Nimchinsky, E. A., Oberlander, A. M., & Svoboda, K. (2001). Abnormal Development of Dendritic Spines in FMR1 Knock-Out Mice. *The Journal of Neuroscience*, 21(14), 5139. <https://doi.org/10.1523/JNEUROSCI.21-14-05139.2001>
- Nishikura, K. (2016). A-to-I editing of coding and non-coding RNAs by ADARs. *Nature Reviews Molecular Cell Biology*, 17(2), 83–96. <https://doi.org/10.1038/nrm.2015.4>
- Ontiveros, R. J., Stoute, J., & Liu, K. F. (2019). The chemical diversity of RNA modifications. *The Biochemical Journal*, 476 8, 1227–1245.
- Ortega, A., Niksic, M., Bachi, A., Wilm, M., Sánchez, L., Hastie, N., & Valcárcel, J. (2003). Biochemical Function of Female-Lethal (2)D/Wilms' Tumor Suppressor-1-associated Proteins in Alternative Pre-mRNA Splicing. *Journal of Biological Chemistry*, 278(5), 3040–3047. <https://doi.org/10.1074/JBC.M210737200>
- Ougland, R., Lando, D., Jonson, I., Dahl, J. A., Moen, M. N., Nordstrand, L. M., Rognes, T., Lee, J. T., Klungland, A., Kouzarides, T., & Larsen, E. (2012). ALKBH1 is a Histone H2A Dioxygenase Involved in Neural Differentiation. *Stem Cells*, 30(12), 2672–2682. <https://doi.org/10.1002/stem.1228>
- Pandey, R. R., Delfino, E., Homolka, D., Roithova, A., Chen, K. M., Li, L., Franco, G., Vågbo, C. B., Taillebourg, E., Fauvarque, M. O., & Pillai, R. S. (2020). The Mammalian Cap-Specific m6Am RNA Methyltransferase PCIF1 Regulates Transcript Levels in Mouse Tissues. *Cell reports*, 32(7), 108038. <https://doi.org/10.1016/j.celrep.2020.108038>
- Park, O. H., Ha, H., Lee, Y., Boo, S. H., Kwon, D. H., Song, H. K., & Kim, Y. K. (2019). Endoribonucleolytic Cleavage of m6A-Containing RNAs by RNase P/MRP Complex. *Molecular Cell*, 74(3), 494–507.e8. <https://doi.org/10.1016/J.MOLCEL.2019.02.034>
- Parker, M. T., Knop, K., Sherwood, A. v, Schurch, N. J., Mackinnon, K., Gould, P. D., Hall, A. J. W., Barton, G. J., & Simpson, G. G. (2020). Nanopore direct RNA sequencing maps the complexity of Arabidopsis mRNA processing and m6A modification. *ELife*, 9, e49658. <https://doi.org/10.7554/eLife.49658>
- Patil, D. P., Chen, C.-K., Pickering, B. F., Chow, A., Jackson, C., Guttman, M., & Jaffrey, S. R. (2016). m6A RNA methylation promotes XIST-mediated transcriptional repression. *Nature*, 537(7620), 369–373. <https://doi.org/10.1038/nature19342>
- Patil, D. P., Pickering, B. F., & Jaffrey, S. R. (2018). Reading m6A in the Transcriptome: m6A-Binding Proteins. *Trends in Cell Biology*, 28(2), 113–127. <https://doi.org/10.1016/J.TCB.2017.10.001>
- Pendleton, K. E., Chen, B., Liu, K., Hunter, O. v., Xie, Y., Tu, B. P., & Conrad, N. K. (2017). The U6 snRNA m6A Methyltransferase METTL16 Regulates SAM Synthetase Intron Retention. *Cell*, 169(5), 824–835.e14. <https://doi.org/10.1016/J.CELL.2017.05.003>
- Perry, R. P., & Kelley, D. E. (1974). Existence of methylated messenger RNA in mouse L cells. *Cell*, 1(1), 37–42. [https://doi.org/10.1016/0092-8674\(74\)90153-6](https://doi.org/10.1016/0092-8674(74)90153-6)
- Ping, X.-L., Sun, B.-F., Wang, L., Xiao, W., Yang, X., Wang, W.-J., Adhikari, S., Shi, Y., Lv, Y., Chen, Y.-S., Zhao, X., Li, A., Yang, Y., Dahal, U., Lou, X.-M., Liu, X., Huang, J., Yuan, W.-P., Zhu, X.-F., ... Yang, Y.-G. (2014). Mammalian WTAP is a regulatory subunit of the RNA N6-methyladenosine methyltransferase. *Cell Research*, 24(2), 177–189. <https://doi.org/10.1038/cr.2014.3>
- Pinto, R., Vågbo, C. B., Jakobsson, M. E., Kim, Y., Baltissen, M. P., O'Donohue, M.-F., Guzmán, U. H., Małecki, J. M., Wu, J., Kirpekar, F., Olsen, J. v, Gleizes, P.-E., Vermeulen, M., Leidel, S. A., Slupphaug, G., & Falnes, P. Ø. (2020). The human methyltransferase ZCCHC4 catalyses N6-methyladenosine modification of 28S ribosomal RNA. *Nucleic Acids Research*, 48(2), 830–846. <https://doi.org/10.1093/nar/gkz1147>

8. References

- Pratanwanich, P. N., Yao, F., Chen, Y., Koh, C. W. Q., Wan, Y. K., Hendra, C., Poon, P., Goh, Y. T., Yap, P. M. L., Chooi, J. Y., Chng, W. J., Ng, S. B., Thiery, A., Goh, W. S. S., & Göke, J. (2021). Identification of differential RNA modifications from nanopore direct RNA sequencing with xPore. *Nature Biotechnology*, *39*(11), 1394–1402. <https://doi.org/10.1038/s41587-021-00949-w>
- Qi, M., Sun, H., Guo, Y., Zhou, Y., Gu, X., Jin, J., Chen, X., Wang, F., Ma, H., & Guo, X. (2022). m(6)A reader protein YTHDF2 regulates spermatogenesis by timely clearance of phase-specific transcripts. *Cell Proliferation*, *55*.
- Qu, J., Yan, H., Hou, Y., Cao, W., Liu, Y., Zhang, E., He, J., & Cai, Z. (2022). RNA demethylase ALKBH5 in cancer: from mechanisms to therapeutic potential. *Journal of Hematology & Oncology*, *15*(1), 8. <https://doi.org/10.1186/s13045-022-01224-4>
- Ranji, A., & Boris-Lawrie, K. (2010). RNA helicases. *RNA Biology*, *7*(6), 775–787. <https://doi.org/10.4161/rna.7.6.14249>
- Ren, W., Lu, J., Huang, M., Gao, L., Li, D., Wang, G. G., & Song, J. (2019). Structure and regulation of ZCCHC4 in m6A-methylation of 28S rRNA. *Nature Communications*, *10*(1), 5042. <https://doi.org/10.1038/s41467-019-12923-x>
- Richard, E. M., Polla, D. L., Assir, M. Z., Contreras, M., Shahzad, M., Khan, A. A., Razzaq, A., Akram, J., Tarar, M. N., Blanpied, T. A., Ahmed, Z. M., Abou Jamra, R., Wiczorek, D., van Bokhoven, H., Riazuddin, S., & Riazuddin, S. (2019). Bi-allelic Variants in METTL5 Cause Autosomal-Recessive Intellectual Disability and Microcephaly. *The American Journal of Human Genetics*, *105*(4), 869–878. <https://doi.org/10.1016/J.AJHG.2019.09.007>
- Ries, R. J., Zaccara, S., Klein, P., Olarerin-George, A., Namkoong, S., Pickering, B. F., Patil, D. P., Kwak, H., Lee, J. H., & Jaffrey, S. R. (2019). m6A enhances the phase separation potential of mRNA. *Nature*, *571*(7765), 424–428. <https://doi.org/10.1038/s41586-019-1374-1>
- Ringvoll, J., Moen, M. N., Nordstrand, L. M., Meira, L. B., Pang, B., Bekkelund, A., Dedon, P. C., Bjelland, S., Samson, L. D., Falnes, P. Ø., & Klungland, A. (2008). AlkB homologue 2-mediated repair of ethenoadenine lesions in mammalian DNA. *Cancer Research*, *68*(11), 4142–4149. <https://doi.org/10.1158/0008-5472.can-08-0796>
- Ringvoll, J., Nordstrand, L. M., Vågbo, C. B., Talstad, V., Reite, K., Aas, P. A., Lauritzen, K. H., Liabakk, N. B., Bjørk, A., Doughty, R. W., Falnes, P. Ø., Krokan, H. E., & Klungland, A. (2006). Repair deficient mice reveal mABH2 as the primary oxidative demethylase for repairing 1meA and 3meC lesions in DNA. *The EMBO Journal*, *25*(10), 2189–2198. <https://doi.org/https://doi.org/10.1038/sj.emboj.7601109>
- Rong, B., Zhang, Q., Wan, J., Xing, S., Dai, R., Li, Y., Cai, J., Xie, J., Song, Y., Chen, J., Zhang, L., Yan, G., Zhang, W., Gao, H., Han, J. D. J., Qu, Q., Ma, H., Tian, Y., & Lan, F. (2020). Ribosome 18S m6A Methyltransferase METTL5 Promotes Translation Initiation and Breast Cancer Cell Growth. *Cell Reports*, *33*(12), 108544. <https://doi.org/10.1016/J.CELREP.2020.108544>
- Roost, C., Lynch, S. R., Batista, P. J., Qu, K., Chang, H. Y., & Kool, E. T. (2015). Structure and Thermodynamics of N6-Methyladenosine in RNA: A Spring-Loaded Base Modification. *Journal of the American Chemical Society*, *137*(5), 2107–2115. <https://doi.org/10.1021/ja513080v>
- Roundtree, I. A., Luo, G.-Z., Zhang, Z., Wang, X., Zhou, T., Cui, Y., Sha, J., Huang, X., Guerrero, L., Xie, P., He, E., Shen, B., & He, C. (2017). YTHDC1 mediates nuclear export of N6-methyladenosine methylated mRNAs. *ELife*, *6*, e31311. <https://doi.org/10.7554/eLife.31311>
- Rousseau, F., Labelle, Y., Bussi eres, J., & Lindsay, C. (2011). The fragile x mental retardation syndrome 20 years after the FMR1 gene discovery: an expanding universe of knowledge. *The Clinical Biochemist. Reviews*, *32*(3), 135–162. <http://europepmc.org/abstract/MED/21912443>
- Ruszkowska, A., Ruszkowski, M., Dauter, Z., & Brown, J. A. (2018). Structural insights into the RNA methyltransferase domain of METTL16. *Scientific Reports*, *8*(1), 5311. <https://doi.org/10.1038/s41598-018-23608-8>
- Ru i cka, K., Zhang, M., Campilho, A., Bodi, Z., Kashif, M., Saleh, M., Eeckhout, D., El-Showk, S., Li, H., Zhong, S., De Jaeger, G., Mongan, N. P., Hej atko, J., Helariutta, Y., & Fray, R. G. (2017). Identification of factors required for m6A mRNA methylation in Arabidopsis reveals a role for the conserved E3 ubiquitin ligase HAKAI. *New Phytologist*, *215*(1), 157–172. <https://doi.org/https://doi.org/10.1111/nph.14586>
- Safra, M., Nir, R., Farouq, D., Vainberg Slutskin, I., & Schwartz, S. (2017). TRUB1 is the predominant pseudouridine synthase acting on mammalian mRNA via a predictable and conserved code. *Genome Research*, *27*(3), 393–406. <https://doi.org/10.1101/gr.207613.116>
- Safra, M., Sas-Chen, A., Nir, R., Winkler, R., Nachshon, A., Bar-Yaacov, D., Erlacher, M., Rossmanith, W., Stern-Ginossar, N., & Schwartz, S. (2017). The m1A landscape on cytosolic and mitochondrial mRNA at single-base resolution. *Nature*, *551*(7679), 251–255. <https://doi.org/10.1038/nature24456>
- Saito, Y., Hawley, B. R., Puno, M. R., Sarathy, S. N., Lima, C. D., Jaffrey, S. R., Darnell, R. B., Keeney, S., & Jain, D. (2022). YTHDC2 control of gametogenesis requires helicase activity but not m6A binding. *Genes & Development*, *36*(3–4), 180–194. <https://doi.org/10.1101/gad.349190.121>
- Sas-Chen, A., Thomas, J. M., Matzov, D., Taoka, M., Nance, K. D., Nir, R., Bryson, K. M., Shachar, R., Liman, G. L. S., Burkhart, B. W., Gamage, S. T., Nobe, Y., Briney, C. A., Levy, M. J., Fuchs, R. T., Robb, G. B., Hartmann, J., Sharma, S., Lin, Q., ... Schwartz, S. (2020). Dynamic RNA acetylation revealed by quantitative cross-evolutionary mapping. *Nature*, *583*(7817), 638–643. <https://doi.org/10.1038/s41586-020-2418-2>
- Schneider, J., & Imler, J. L. (2021). Sensing and signalling viral infection in drosophila. *Developmental & Comparative Immunology*, *117*, 103985. <https://doi.org/10.1016/J.DCI.2020.103985>
- Sch oller, E., Marks, J., Marchand, V., Bruckmann, A., Powell, C. A., Reichold, M., Mutti, C. D., Dettmer, K., Feederle, R., H uttelmaier, S., Helm, M., Oefner, P., Minczuk, M., Motorin, Y., Hafner, M., & Meister, G. (2021). Balancing of mitochondrial translation through METTL8-mediated m3C modification of mitochondrial tRNAs. *Molecular Cell*, *81*(23), 4810–4825.e12. <https://doi.org/10.1016/J.MOLCEL.2021.10.018>
- Sch oller, E., Weichmann, F., Treiber, T., Ringle, S., Treiber, N., Flatley, A., Feederle, R., Bruckmann, A., & Meister, G. (2018). Interactions, localization, and phosphorylation of the m6A generating METTL3-METTL14-WTAP complex. *RNA (New York, N.Y.)*, *24*(4), 499–512. <https://doi.org/10.1261/rna.064063.117>

8. References

- Schuberth-Wagner, C., Ludwig, J., Bruder, A. K., Herzner, A. M., Zillinger, T., Goldeck, M., Schmidt, T., Schmid-Burgk, J. L., Kerber, R., Wolter, S., Stümpel, J. P., Roth, A., Bartok, E., Drosten, C., Coch, C., Hornung, V., Barchet, W., Kümmerer, B. M., Hartmann, G., & Schlee, M. (2015). A Conserved Histidine in the RNA Sensor RIG-I Controls Immune Tolerance to N1-2'O-Methylated Self RNA. *Immunity*, *43*(1), 41–51. <https://doi.org/10.1016/J.IMMUNI.2015.06.015>
- Schumann, U., Zhang, H.-N., Sibbritt, T., Pan, A., Horvath, A., Gross, S., Clark, S. J., Yang, L., & Preiss, T. (2020). Multiple links between 5-methylcytosine content of mRNA and translation. *BMC Biology*, *18*(1), 40. <https://doi.org/10.1186/s12915-020-00769-5>
- Schwartz, S. (2018). m1A within cytoplasmic mRNAs at single nucleotide resolution: a reconciled transcriptome-wide map. *RNA*, *24*, 1427–1436.
- Schwartz, S., Agarwala, S. D., Mumbach, M. R., Jovanovic, M., Mertins, P., Shishkin, A., Tabach, Y., Mikkelsen, T. S., Satija, R., Ruvkun, G., Carr, S. A., Lander, E. S., Fink, G. R., & Regev, A. (2013). High-Resolution Mapping Reveals a Conserved, Widespread, Dynamic mRNA Methylation Program in Yeast Meiosis. *Cell*, *155*(6), 1409–1421. <https://doi.org/10.1016/J.CELL.2013.10.047>
- Schwartz, S., Bernstein, D. A., Mumbach, M. R., Jovanovic, M., Herbst, R. H., León-Ricardo, B. X., Engreitz, J. M., Guttman, M., Satija, R., Lander, E. S., Fink, G., & Regev, A. (2014). Transcriptome-wide Mapping Reveals Widespread Dynamic-Regulated Pseudouridylation of ncRNA and mRNA. *Cell*, *159*(1), 148–162. <https://doi.org/10.1016/J.CELL.2014.08.028>
- Schwartz, S., Mumbach, M. R., Jovanovic, M., Wang, T., Maciag, K., Bushkin, G. G., Mertins, P., Ter-Ovanesyan, D., Habib, N., Cacchiarelli, D., Sanjana, N. E., Freinkman, E., Pacold, M. E., Satija, R., Mikkelsen, T. S., Hacohen, N., Zhang, F., Carr, S. A., Lander, E. S., & Regev, A. (2014). Perturbation of m6A Writers Reveals Two Distinct Classes of mRNA Methylation at Internal and 5' Sites. *Cell Reports*, *8*(1), 284–296. <https://doi.org/10.1016/J.CELREP.2014.05.048>
- Selmi, T., Hussain, S., Dietmann, S., Heiß, M., Borland, K., Flad, S., Carter, J.-M., Dennison, R., Huang, Y.-L., Kellner, S., Bornelöv, S., & Frye, M. (2021). Sequence- and structure-specific cytosine-5 mRNA methylation by NSUN6. *Nucleic Acids Research*, *49*(2), 1006–1022. <https://doi.org/10.1093/nar/gkaa1193>
- Sendinc, E., Valle-Garcia, D., Dhall, A., Chen, H., Henriques, T., Navarrete-Perea, J., Sheng, W., Gygi, S. P., Adelman, K., & Shi, Y. (2019). PCIF1 Catalyzes m6Am mRNA Methylation to Regulate Gene Expression. *Molecular Cell*, *75*(3), 620-630.e9. <https://doi.org/10.1016/J.MOLCEL.2019.05.030>
- Sepich-Poore, C., Zheng, Z., Schmitt, E., Wen, K., Zhang, Z. S., Cui, X. L., Dai, Q., hu, A. C., Zhang, L., Castillo, A. S., Tan, H., Peng, J., Zhuang, X., He, C., & Nachtergaele, S. (2022). The METTL5-TRMT112 N6-methyladenosine methyltransferase complex regulates mRNA translation via 18S rRNA methylation. *Journal of Biological Chemistry*, *298*(3), 101590. <https://doi.org/10.1016/J.JBC.2022.101590>
- Shi, H., Wang, X., Lu, Z., Zhao, B. S., Ma, H., Hsu, P. J., Liu, C., & He, C. (2017). YTHDF3 facilitates translation and decay of N6-methyladenosine-modified RNA. *Cell Research*, *27*(3), 315–328. <https://doi.org/10.1038/cr.2017.15>
- Shi, H., Zhang, X., Weng, Y.-L., Lu, Z., Liu, Y., Lu, Z., Li, J., Hao, P., Zhang, Y., Zhang, F., Wu, Y., Delgado, J. Y., Su, Y., Patel, M. J., Cao, X., Shen, B., Huang, X., Ming, G., Zhuang, X., ... Zhou, T. (2018). m6A facilitates hippocampus-dependent learning and memory through YTHDF1. *Nature*, *563*(7730), 249–253. <https://doi.org/10.1038/s41586-018-0666-1>
- Shima, H., Matsumoto, M., Ishigami, Y., Ebina, M., Muto, A., Sato, Y., Kumagai, S., Ochiai, K., Suzuki, T., & Igarashi, K. (2017). S-Adenosylmethionine Synthesis Is Regulated by Selective N6-Adenosine Methylation and mRNA Degradation Involving METTL16 and YTHDC1. *Cell Reports*, *21*(12), 3354–3363. <https://doi.org/10.1016/J.CELREP.2017.11.092>
- Shu, X., Cao, J., Cheng, M., Xiang, S., Gao, M., Li, T., Ying, X., Wang, F., Yue, Y., Lu, Z., Dai, Q., Cui, X., Ma, L., Wang, Y., He, C., Feng, X., & Liu, J. (2020). A metabolic labeling method detects m6A transcriptome-wide at single base resolution. *Nature Chemical Biology*, *16*(8), 887–895. <https://doi.org/10.1038/s41589-020-0526-9>
- Sigrist, S. J., Reiff, D. F., Thiel, P. R., Steinert, J. R., & Schuster, C. M. (2003). Experience-Dependent Strengthening of &emph;Drosophila&emph; Neuromuscular Junctions. *The Journal of Neuroscience*, *23*(16), 6546. <https://doi.org/10.1523/JNEUROSCI.23-16-06546.2003>
- Sigrist, S. J., Thiel, P. R., Reiff, D. F., Lachance, P. E. D., Lasko, P., & Schuster, C. M. (2000). Postsynaptic translation affects the efficacy and morphology of neuromuscular junctions. *Nature*, *405*(6790), 1062–1065. <https://doi.org/10.1038/35016598>
- Sittler, A., Devys, D., Weber, C., & Mandel, J.-L. (1996). Alternative Splicing of Exon 14 Determines Nuclear or Cytoplasmic Localisation of FMR1 Protein Isoforms. *Human Molecular Genetics*, *5*(1), 95–102. <https://doi.org/10.1093/hmg/5.1.95>
- Ślédź, P., & Jinek, M. (2016). Structural insights into the molecular mechanism of the m6A writer complex. *ELife*, *5*, e18434. <https://doi.org/10.7554/eLife.18434>
- Sloan, K. E., Warda, A. S., Sharma, S., Entian, K.-D., Lafontaine, D. L. J., & Bohnsack, M. T. (2017). Tuning the ribosome: The influence of rRNA modification on eukaryotic ribosome biogenesis and function. *RNA Biology*, *14*(9), 1138–1152. <https://doi.org/10.1080/15476286.2016.1259781>
- Slobodin, B., Han, R., Calderone, V., Vrieland, J. A. F. O., Loayza-Puch, F., Elkon, R., & Agami, R. (2017). Transcription Impacts the Efficiency of mRNA Translation via Co-transcriptional N6-adenosine Methylation. *Cell*, *169*(2), 326-337.e12. <https://doi.org/10.1016/J.CELL.2017.03.031>
- Smemo, S., Tena, J. J., Kim, K.-H., Gamazon, E. R., Sakabe, N. J., Gómez-Marín, C., Aneas, I., Credidio, F. L., Sobreira, D. R., Wasserman, N. F., Lee, J. H., Puvindran, V., Tam, D., Shen, M., Son, J. E., Vakili, N. A., Sung, H.-K., Naranjo, S., Acemel, R. D., ... Nóbrega, M. A. (2014). Obesity-associated variants within FTO form long-range functional connections with IRX3. *Nature*, *507*(7492), 371–375. <https://doi.org/10.1038/nature13138>

8. References

- Songe-Møller, L., van den Born, E., Leihne, V., Vågbø, C. B., Kristoffersen, T., Krokan, H. E., Kirpekar, F., Falnes, P. Ø., & Klungland, A. (2010). Mammalian ALKBH8 Possesses tRNA Methyltransferase Activity Required for the Biogenesis of Multiple Wobble Uridine Modifications Implicated in Translational Decoding. *Molecular and Cellular Biology*, *30*, 1814–1827.
- Spitale, R. C., Flynn, R. A., Zhang, Q. C., Crisalli, P., Lee, B., Jung, J.-W., Kuchelmeister, H. Y., Batista, P. J., Torre, E. A., Kool, E. T., & Chang, H. Y. (2015). Structural imprints in vivo decode RNA regulatory mechanisms. *Nature*, *519*(7544), 486–490. <https://doi.org/10.1038/nature14263>
- Stoilov, P., Rafalska, I., & Stamm, S. (2002). YTH: a new domain in nuclear proteins. *Trends in Biochemical Sciences*, *27*(10), 495–497. [https://doi.org/10.1016/S0968-0004\(02\)02189-8](https://doi.org/10.1016/S0968-0004(02)02189-8)
- Stoltzfus, C. M., & Dane, R. W. (1982). Accumulation of Spliced Avian Retrovirus mRNA Is Inhibited in S-Adenosylmethionine-Depleted Chicken Embryo Fibroblasts. *Journal of Virology*, *42*(3), 918–931. <https://doi.org/10.1128/jvi.42.3.918-931.1982>
- Stratigopoulos, G., Martin Carli, J. F., O'Day, D. R., Wang, L., Leduc, C. A., Lanzano, P., Chung, W. K., Rosenbaum, M., Egli, D., Doherty, D. A., & Leibel, R. L. (2014). Hypomorphism for RRGRI1L, a ciliary gene vicinal to the FTO locus, causes increased adiposity in mice. *Cell Metabolism*, *19*(5), 767–779. <https://doi.org/10.1016/j.cmet.2014.04.009>
- Su, S., Li, S., Deng, T., Gao, M., Yin, Y., Wu, B., Peng, C., Liu, J., Ma, J., & Zhang, K. (2022). Cryo-EM structures of human m6A writer complexes. *Cell Research*, *32*(11), 982–994. <https://doi.org/10.1038/s41422-022-00725-8>
- Sui, X., Hu, Y., Ren, C., Cao, Q., Zhou, S., Cao, Y., Li, M., Shu, W., & Huo, R. (2020). METTL3-mediated m6A is required for murine oocyte maturation and maternal-to-zygotic transition. *Cell Cycle*, *19*(4), 391–404. <https://doi.org/10.1080/15384101.2019.1711324>
- Sui, X. S., Hu, Y., Ren, C., Cao, Q. Q., Zhou, S., Cao, Y. M., Li, M. R., Shu, W. J., & Huo, R. (2020). METTL3-mediated m(6)A is required for murine oocyte maturation and maternal-to-zygotic transition. *Cell Cycle*, *19*, 391–404.
- Sun, H. L., Zhu, A. C., Gao, Y., Terajima, H., Fei, Q., Liu, S., Zhang, L., Zhang, Z., Harada, B. T., He, Y. Y., Bissonnette, M. B., Hung, M. C., & He, C. (2020). Stabilization of ERK-Phosphorylated METTL3 by USP5 Increases m6A Methylation. *Molecular Cell*, *80*(4), 633–647.e7. <https://doi.org/10.1016/J.MOLCEL.2020.10.026>
- Sun, H., Zhang, M., Li, K., Bai, D., & Yi, C. (2019). Cap-specific, terminal N6-methylation by a mammalian m6Am methyltransferase. *Cell Research*, *29*(1), 80–82. <https://doi.org/10.1038/s41422-018-0117-4>
- Sundheim, O., Talstad, V. A., Vågbø, C. B., Slupphaug, G., & Krokan, H. E. (2008). AlkB demethylases flip out in different ways. *DNA Repair*, *7*(11), 1916–1923. <https://doi.org/10.1016/J.DNAREP.2008.07.015>
- Suthar, M. K., Purva, M., Maherchandani, S., & Kashyap, S. K. (2016). Identification and in silico analysis of cattle DEXH/D box RNA helicases. *SpringerPlus*, *5*(1), 25. <https://doi.org/10.1186/s40064-015-1640-0>
- Suzuki, T. (2021). The expanding world of tRNA modifications and their disease relevance. *Nature Reviews Molecular Cell Biology*, *22*(6), 375–392. <https://doi.org/10.1038/s41580-021-00342-0>
- Tafesh-Edwards, G., & Eleftherianos, I. (2020). Drosophila immunity against natural and nonnatural viral pathogens. *Virology*, *540*, 165–171. <https://doi.org/10.1016/J.VIROL.2019.12.001>
- Tanabe, A., Tanikawa, K., Tsunetomi, M., Takai, K., Ikeda, H., Konno, J., Torigoe, T., Maeda, H., Kutomi, G., Okita, K., Mori, M., & Sahara, H. (2016). RNA helicase YTHDC2 promotes cancer metastasis via the enhancement of the efficiency by which HIF-1 α mRNA is translated. *Cancer Letters*, *376*(1), 34–42. <https://doi.org/10.1016/J.CANLET.2016.02.022>
- Tang, C., Klukovich, R., Peng, H., Wang, Z., Yu, T., Zhang, Y., Zheng, H., Klungland, A., & Yan, W. (2018). ALKBH5-dependent m6A demethylation controls splicing and stability of long 3'-UTR mRNAs in male germ cells. *Proceedings of the National Academy of Sciences*, *115*(2), E325–E333. <https://doi.org/10.1073/pnas.1717794115>
- Tardu, M., Jones, J. D., Kennedy, R. T., Lin, Q., & Koutmou, K. S. (2019). Identification and Quantification of Modified Nucleosides in *Saccharomyces cerevisiae* mRNAs. *ACS Chemical Biology*, *14*(7), 1403–1409. <https://doi.org/10.1021/acschembio.9b00369>
- Tegowski, M., Flamand, M. N., & Meyer, K. D. (2022). scDART-seq reveals distinct m6A signatures and mRNA methylation heterogeneity in single cells. *Molecular Cell*, *82*(4), 868–878.e10. <https://doi.org/10.1016/J.MOLCEL.2021.12.038>
- Theler, D., Dominguez, C., Blatter, M., Boudet, J., & Allain, F. H.-T. (2014). Solution structure of the YTH domain in complex with N6-methyladenosine RNA: a reader of methylated RNA. *Nucleic Acids Research*, *42*(22), 13911–13919. <https://doi.org/10.1093/nar/gku1116>
- Tomari, Y., Du, T., & Zamore, P. D. (2007). Sorting of *Drosophila* Small Silencing RNAs. *Cell*, *130*(2), 299–308. <https://doi.org/10.1016/J.CELL.2007.05.057>
- Trajković, J., Makevic, V., Pesic, M., Pavković-Lučić, S., Milojević, S., Cvjetković, S., Hagerman, R., Budimirović, D. B., & Protic, D. (2023). *Drosophila melanogaster* as a Model to Study Fragile X-Associated Disorders. *Genes*, *14*(1). <https://doi.org/10.3390/genes14010087>
- Tsujikawa, K., Koike, K., Kitae, K., Shinkawa, A., Arima, H., Suzuki, T., Tsuchiya, M., Makino, Y., Furukawa, T., Konishi, N., & Yamamoto, H. (2007). Expression and sub-cellular localization of human ABH family molecules. *Journal of Cellular and Molecular Medicine*, *11*(5), 1105–1116. <https://doi.org/https://doi.org/10.1111/j.1582-4934.2007.00094.x>
- Tuck, M. T. (1992). The formation of internal 6-methyladenine residues in eucaryotic messenger rna. *International Journal of Biochemistry*, *24*(3), 379–386. [https://doi.org/10.1016/0020-711X\(92\)90028-Y](https://doi.org/10.1016/0020-711X(92)90028-Y)
- Ueda, Y., Ooshio, I., Fusamae, Y., Kitae, K., Kawaguchi, M., Jingushi, K., Hase, H., Harada, K., Hirata, K., & Tsujikawa, K. (2017). AlkB homolog 3-mediated tRNA demethylation promotes protein synthesis in cancer cells. *Scientific Reports*, *7*(1), 42271. <https://doi.org/10.1038/srep42271>

8. References

- Ule, J., Jensen, K. B., Ruggiu, M., Mele, A., Ule, A., & Darnell, R. B. (2003). CLIP Identifies Nova-Regulated RNA Networks in the Brain. *Science*, 302(5648), 1212–1215. <https://doi.org/10.1126/science.1090095>
- Uzonyi, A., Dierks, D., Nir, R., Kwon, O. S., Toth, U., Barbosa, I., Burel, C., Brandis, A., Rossmannith, W., le Hir, H., Slobodin, B., & Schwartz, S. (2023). Exclusion of m6A from splice-site proximal regions by the exon junction complex dictates m6A topologies and mRNA stability. *Molecular Cell*, 83(2), 237–251.e7. <https://doi.org/10.1016/j.MOLCEL.2022.12.026>
- van den Born, E., Vågbo, C. B., Songe-Møller, L., Leihne, V., Lien, G. F., Leszczynska, G., Malkiewicz, A., Krokan, H. E., Kirpekar, F., Klungland, A., & Falnes, P. Ø. (2011). ALKBH8-mediated formation of a novel diastereomeric pair of wobble nucleosides in mammalian tRNA. *Nature Communications*, 2(1), 172. <https://doi.org/10.1038/ncomms1173>
- van Tran, N., Ernst, F. G. M., Hawley, B. R., Zorbas, C., Ulryck, N., Hackert, P., Bohnsack, K. E., Bohnsack, M. T., Jaffrey, S. R., Graille, M., & Lafontaine, D. L. J. (2019). The human 18S rRNA m6A methyltransferase METTL5 is stabilized by TRMT112. *Nucleic Acids Research*, 47(15), 7719–7733. <https://doi.org/10.1093/nar/gkz619>
- Vespa, L., Vachon, G., Berger, F., Perazza, D., Faure, J.-D., & Herzog, M. (2004). The Immunophilin-Interacting Protein AtFIP37 from Arabidopsis Is Essential for Plant Development and Is Involved in Trichome Endoreduplication. *Plant Physiology*, 134(4), 1283–1292. <https://doi.org/10.1104/pp.103.028050>
- Vu, L. P., Pickering, B. F., Cheng, Y., Zaccara, S., Nguyen, D., Minuesa, G., Chou, T., Chow, A., Saletore, Y., MacKay, M., Schulman, J., Famulare, C., Patel, M., Klimek, V. M., Garrett-Bakelman, F. E., Melnick, A., Carroll, M., Mason, C. E., Jaffrey, S. R., & Kharas, M. G. (2017). The N6-methyladenosine (m6A)-forming enzyme METTL3 controls myeloid differentiation of normal hematopoietic and leukemia cells. *Nature Medicine*, 23(11), 1369–1376. <https://doi.org/10.1038/nm.4416>
- Walters, B. J., Mercaldo, V., Gillon, C. J., Yip, M., Neve, R. L., Boyce, F. M., Frankland, P. W., & Josselyn, S. A. (2017). The Role of The RNA Demethylase FTO (Fat Mass and Obesity-Associated) and mRNA Methylation in Hippocampal Memory Formation. *Neuropsychopharmacology*, 42(7), 1502–1510. <https://doi.org/10.1038/npp.2017.31>
- Wan, C., Borgeson, B., Phanse, S., Tu, F., Drew, K., Clark, G., Xiong, X., Kagan, O., Kwan, J., Bezginov, A., Chessman, K., Pal, S., Cromar, G., Papoulas, O., Ni, Z., Boutz, D. R., Stoilova, S., Havugimana, P. C., Guo, X., ... Emili, A. (2015). Panorama of ancient metazoan macromolecular complexes. *Nature*, 525(7569), 339–344. <https://doi.org/10.1038/nature14877>
- Wang, C., Zhu, Y., Bao, H., Jiang, Y., Xu, C., Wu, J., & Shi, Y. (2016). A novel RNA-binding mode of the YTH domain reveals the mechanism for recognition of determinant of selective removal by Mmi1. *Nucleic Acids Research*, 44(2), 969–982. <https://doi.org/10.1093/nar/gkv1382>
- Wang, C.-X., Cui, G.-S., Liu, X., Xu, K., Wang, M., Zhang, X.-X., Jiang, L.-Y., Li, A., Yang, Y., Lai, W.-Y., Sun, B.-F., Jiang, G.-B., Wang, H.-L., Tong, W.-M., Li, W., Wang, X.-J., Yang, Y.-G., & Zhou, Q. (2018). METTL3-mediated m6A modification is required for cerebellar development. *PLOS Biology*, 16(6), e2004880. <https://doi.org/10.1371/journal.pbio.2004880>
- Wang, P., Doxtader, K. A., & Nam, Y. (2016). Structural Basis for Cooperative Function of Mettl3 and Mettl14 Methyltransferases. *Molecular Cell*, 63(2), 306–317. <https://doi.org/10.1016/j.MOLCEL.2016.05.041>
- Wang, X., Feng, J., Xue, Y., Guan, Z., Zhang, D., Liu, Z., Gong, Z., Wang, Q., Huang, J., Tang, C., Zou, T., & Yin, P. (2016). Structural basis of N(6)-adenosine methylation by the METTL3-METTL14 complex. *Nature*, 534(7608), 575–578. <https://doi.org/10.1038/nature18298>
- Wang, X., Lu, Z., Gomez, A., Hon, G. C., Yue, Y., Han, D., Fu, Y., Parisien, M., Dai, Q., Jia, G., Ren, B., Pan, T., & He, C. (2014a). N6-methyladenosine-dependent regulation of messenger RNA stability. *Nature*, 505(7481), 117–120. <https://doi.org/10.1038/nature12730>
- Wang, X., Lu, Z., Gomez, A., Hon, G. C., Yue, Y., Han, D., Fu, Y., Parisien, M., Dai, Q., Jia, G., Ren, B., Pan, T., & He, C. (2014b). N6-methyladenosine-dependent regulation of messenger RNA stability. *Nature*, 505(7481), 117–120. <https://doi.org/10.1038/nature12730>
- Wang, X., Zhao, B. S., Roundtree, I. A., Lu, Z., Han, D., Ma, H., Weng, X., Chen, K., Shi, H., & He, C. (2015). N(6)-methyladenosine Modulates Messenger RNA Translation Efficiency. *Cell*, 161(6), 1388–1399. <https://doi.org/10.1016/j.cell.2015.05.014>
- Wang, Y., Li, Y., Toth, J. I., Petroski, M. D., Zhang, Z., & Zhao, J. C. (2014). N6-methyladenosine modification destabilizes developmental regulators in embryonic stem cells. *Nature Cell Biology*, 16(2), 191–198. <https://doi.org/10.1038/ncb2902>
- Wang, Y., Li, Y., Yue, M., Wang, J., Kumar, S., Wechsler-Reya, R. J., Zhang, Z., Ogawa, Y., Kellis, M., Duester, G., & Zhao, J. C. (2018). N6-methyladenosine RNA modification regulates embryonic neural stem cell self-renewal through histone modifications. *Nature Neuroscience*, 21(2), 195–206. <https://doi.org/10.1038/s41593-017-0057-1>
- Wang, Y., Xiao, Y., Dong, S., Yu, Q., & Jia, G. (2020). Antibody-free enzyme-assisted chemical approach for detection of N6-methyladenosine. *Nature Chemical Biology*, 16(8), 896–903. <https://doi.org/10.1038/s41589-020-0525-x>
- Wang, Y., Zhang, L., Ren, H., Ma, L., Guo, J., Mao, D., Lu, Z., Lu, L., & Yan, D. (2021). Role of Hakai in m6A modification pathway in Drosophila. *Nature Communications*, 12(1), 2159. <https://doi.org/10.1038/s41467-021-22424-5>
- Warda, A. S., Kretschmer, J., Hackert, P., Lenz, C., Urlaub, H., Höbartner, C., Sloan, K. E., & Bohnsack, M. T. (2017). Human METTL16 is a N6-methyladenosine (m6A) methyltransferase that targets pre-mRNAs and various non-coding RNAs. *EMBO Reports*, 18(11), 2004–2014. <https://doi.org/https://doi.org/10.15252/embr.201744940>
- Watkins, N. J., & Bohnsack, M. T. (2012). The box C/D and H/ACA snoRNPs: key players in the modification, processing and the dynamic folding of ribosomal RNA. *Wiley Interdisciplinary Reviews: RNA*, 3.
- Wei, C. M., Gershowitz, A., & Moss, B. (1975). Methylated nucleotides block 5' terminus of HeLa cell messenger RNA. *Cell*, 4(4), 379–386. [https://doi.org/10.1016/0092-8674\(75\)90158-0](https://doi.org/10.1016/0092-8674(75)90158-0)
- Wei, C. M., Gershowitz, A., & Moss, B. (1976). 5'-Terminal and internal methylated nucleotide sequences in HeLa cell mRNA. *Biochemistry*, 15 2, 397–401.

8. References

- Wei, G., Almeida, M., Pintacuda, G., Coker, H., Bowness, J. S., Ule, J., & Brockdorff, N. (2021). Acute depletion of METTL3 implicates N6-methyladenosine in alternative intron/exon inclusion in the nascent transcriptome. *Genome Research*, 31(8), 1395–1408. <https://doi.org/10.1101/gr.271635.120>
- Wei, J., Liu, F., Lu, Z., Fei, Q., Ai, Y., He, P. C., Shi, H., Cui, X., Su, R., Klungland, A., Jia, G., Chen, J., & He, C. (2018). Differential m6A, m6Am, and m1A Demethylation Mediated by FTO in the Cell Nucleus and Cytoplasm. *Molecular Cell*, 71(6), 973-985.e5. <https://doi.org/10.1016/J.MOLCEL.2018.08.011>
- Wei, J., Yu, X., Yang, L., Liu, X., Gao, B., Huang, B., Dou, X., Liu, J., Zou, Z., Cui, X.-L., Zhang, L.-S., Zhao, X., Liu, Q., He, P. C., Sepich-Poore, C., Zhong, N., Liu, W., Li, Y., Kou, X., ... He, C. (2022). FTO mediates LINE1 m6A demethylation and chromatin regulation in mESCs and mouse development. *Science*, 376(6596), 968–973. <https://doi.org/10.1126/science.abe9582>
- Wen, J., Lv, R., Ma, H., Shen, H., He, C., Wang, J., Jiao, F., Liu, H., Yang, P., Tan, L., Lan, F., Shi, Y. G., He, C., Shi, Y., & Diao, J. (2018). Zc3h13 Regulates Nuclear RNA m6A Methylation and Mouse Embryonic Stem Cell Self-Renewal. *Molecular Cell*, 69(6), 1028-1038.e6. <https://doi.org/10.1016/J.MOLCEL.2018.02.015>
- Weng, H., Huang, H., Wu, H., Qin, X., Zhao, B. S., Dong, L., Shi, H., Skibbe, J., Shen, C., Hu, C., Sheng, Y., Wang, Y., Wunderlich, M., Zhang, B., Dore, L. C., Su, R., Deng, X., Ferchen, K., Li, C., ... Chen, J. (2018). METTL14 Inhibits Hematopoietic Stem/Progenitor Differentiation and Promotes Leukemogenesis via mRNA m6A Modification. *Cell Stem Cell*, 22(2), 191-205.e9. <https://doi.org/https://doi.org/10.1016/j.stem.2017.11.016>
- Weng, Y. L., Wang, X., An, R., Cassin, J., Vissers, C., Liu, Y., Liu, Y., Xu, T., Wang, X., Wong, S. Z. H., Joseph, J., Dore, L. C., Dong, Q., Zheng, W., Jin, P., Wu, H., Shen, B., Zhuang, X., He, C., ... Ming, G. li. (2018). Epitranscriptomic m6A Regulation of Axon Regeneration in the Adult Mammalian Nervous System. *Neuron*, 97(2), 313-325.e6. <https://doi.org/10.1016/J.NEURON.2017.12.036>
- Werner, M., Purta, E., Kaminska, K. H., Cymerman, I. A., Campbell, D. A., Mittra, B., Zamudio, J. R., Sturm, N. R., Jaworski, J., & Bujnicki, J. M. (2011). 2'-O-ribose methylation of cap2 in human: function and evolution in a horizontally mobile family. *Nucleic Acids Research*, 39(11), 4756–4768. <https://doi.org/10.1093/nar/gkr038>
- Westbye, M. P., Feyzi, E., Aas, P. A., Vågbo, C. B., Talstad, V., Kavli, B., Hagen, L., Sundheim, O., Akbari, M., Liabakk, N. B., Slupphaug, G., Otterlei, M., & Krokan, H. E. (2008). Human AlkB Homolog 1 is a Mitochondrial Protein That Demethylates 3-Methylcytosine in DNA and RNA*. *Journal of Biological Chemistry*, 283, 25046–25056.
- Westmark, C. J., Maloney, B., Alisch, R. S., Sokol, D. K., & Lahiri, D. K. (2020). FMRP Regulates the Nuclear Export of Adam9 and Psen1 mRNAs: Secondary Analysis of an N6-Methyladenosine Dataset. *Scientific Reports*, 10(1), 10781. <https://doi.org/10.1038/s41598-020-66394-y>
- Widagdo, J., Zhao, Q.-Y., Kempen, M.-J., Tan, M. C., Ratnu, V. S., Wei, W., Leighton, L., Spadaro, P. A., Edson, J., Anggono, V., & Bredy, T. W. (2016). Experience-Dependent Accumulation of m-Methyladenosine in the Prefrontal Cortex Is Associated with Memory Processes in Mice. *The Journal of Neuroscience*, 36(25), 6771. <https://doi.org/10.1523/JNEUROSCI.4053-15.2016>
- Wiener, D., & Schwartz, S. (2021). The epitranscriptome beyond m6A. *Nature Reviews Genetics*, 22(2), 119–131. <https://doi.org/10.1038/s41576-020-00295-8>
- Wojtas, M. N., Pandey, R. R., Mendel, M., Homolka, D., Sachidanandam, R., & Pillai, R. S. (2017). Regulation of m6A Transcripts by the 3'→5' RNA Helicase YTHDC2 Is Essential for a Successful Meiotic Program in the Mammalian Germline. *Molecular Cell*, 68(2), 374-387.e12. <https://doi.org/10.1016/J.MOLCEL.2017.09.021>
- Worpenberg, L., Jakobi, T., Dieterich, C., & Roignant, J.-Y. (2019). Identification of Methylated Transcripts Using the TRIBE Approach. In N. Wajapeyee & R. Gupta (Eds.), *Epitranscriptomics: Methods and Protocols* (pp. 89–106). Springer New York. https://doi.org/10.1007/978-1-4939-8808-2_7
- Worpenberg, L., Paolantoni, C., Longhi, S., Mulorz, M. M., Lence, T., Wessels, H.-H., Dassi, E., Aiello, G., Sutandy, F. X. R., Scheibe, M., Edupuganti, R. R., Busch, A., Möckel, M. M., Vermeulen, M., Butter, F., König, J., Notarangelo, M., Ohler, U., Dieterich, C., ... Roignant, J.-Y. (2021). Ythdf is a N6-methyladenosine reader that modulates Fmr1 target mRNA selection and restricts axonal growth in Drosophila. *The EMBO Journal*, 40(4), e104975. <https://doi.org/https://doi.org/10.15252/embj.2020104975>
- Wright, A., & Vissel, B. (2012). The essential role of AMPA receptor GluR2 subunit RNA editing in the normal and diseased brain. *Frontiers in Molecular Neuroscience*, 5. <https://doi.org/10.3389/fnmol.2012.00034>
- Wu, B., Su, S., Patil, D. P., Liu, H., Gan, J., Jaffrey, S. R., & Ma, J. (2018). Molecular basis for the specific and multivalent recognitions of RNA substrates by human hnRNP A2/B1. *Nature Communications*, 9(1), 420. <https://doi.org/10.1038/s41467-017-02770-z>
- Wu, Q., Schapira, M., Arrowsmith, C. H., & Barsyte-Lovejoy, D. (2021). Protein arginine methylation: from enigmatic functions to therapeutic targeting. *Nature Reviews Drug Discovery*, 20(7), 509–530. <https://doi.org/10.1038/s41573-021-00159-8>
- Wu, R., Chen, Y., Liu, Y., Zhuang, L., Chen, W., Zeng, B., Liao, X., Guo, G., Wang, Y., & Wang, X. (2021). m6A methylation promotes white-to-beige fat transition by facilitating Hif1a translation. *EMBO Reports*, 22(11), e52348. <https://doi.org/https://doi.org/10.15252/embr.202052348>
- Wu, R., Li, A., Sun, B., Sun, J.-G., Zhang, J., Zhang, T., Chen, Y., Xiao, Y., Gao, Y., Zhang, Q., Ma, J., Yang, X., Liao, Y., Lai, W.-Y., Qi, X., Wang, S., Shu, Y., Wang, H.-L., Wang, F., ... Yuan, Z. (2019). A novel m6A reader Prrc2a controls oligodendroglial specification and myelination. *Cell Research*, 29(1), 23–41. <https://doi.org/10.1038/s41422-018-0113-8>
- Wu, T. P., Wang, T., Seetin, M. G., Lai, Y., Zhu, S., Lin, K., Liu, Y., Byrum, S. D., Mackintosh, S. G., Zhong, M., Tackett, A., Wang, G., Hon, L. S., Fang, G., Swenberg, J. A., & Xiao, A. Z. (2016). DNA methylation on N(6)-adenine in mammalian embryonic stem cells. *Nature*, 532(7599), 329–333. <https://doi.org/10.1038/nature17640>

8. References

- Wu, Y., Xu, X., Qi, M., Chen, C., Li, M., Yan, R., Kou, X., Zhao, Y., Liu, W., Li, Y., Liu, X., Zhang, M., Yi, C., Liu, H., Xiang, J., Wang, H., Shen, B., Gao, Y., & Gao, S. (2022). N6-methyladenosine regulates maternal RNA maintenance in oocytes and timely RNA decay during mouse maternal-to-zygotic transition. *Nature Cell Biology*, *24*(6), 917–927. <https://doi.org/10.1038/s41556-022-00915-x>
- Xiang, Y., Laurent, B., Hsu, C.-H., Nachtergaele, S., Lu, Z., Sheng, W., Xu, C., Chen, H., Ouyang, J., Wang, S., Ling, D., Hsu, P.-H., Zou, L., Jambhekar, A., He, C., & Shi, Y. (2017). RNA m6A methylation regulates the ultraviolet-induced DNA damage response. *Nature*, *543*(7646), 573–576. <https://doi.org/10.1038/nature21671>
- Xiao, W., Adhikari, S., Dahal, U., Chen, Y. S., Hao, Y. J., Sun, B. F., Sun, H. Y., Li, A., Ping, X. L., Lai, W. Y., Wang, X., Ma, H. L., Huang, C. M., Yang, Y., Huang, N., Jiang, G. bin, Wang, H. L., Zhou, Q., Wang, X. J., ... Yang, Y. G. (2016). Nuclear m6A Reader YTHDC1 Regulates mRNA Splicing. *Molecular Cell*, *61*(4), 507–519. <https://doi.org/10.1016/J.MOLCEL.2016.01.012>
- Xiao, Y., Wang, Y., Tang, Q., Wei, L., Zhang, X., & Jia, G. (2018). An Elongation- and Ligation-Based qPCR Amplification Method for the Radiolabeling-Free Detection of Locus-Specific N6-Methyladenosine Modification. *Angewandte Chemie International Edition*, *57*(49), 15995–16000. <https://doi.org/https://doi.org/10.1002/anie.201807942>
- Xiao, Y.-L., Liu, S., Ge, R., Wu, Y., He, C., Chen, M., & Tang, W. (2023). Transcriptome-wide profiling and quantification of N6-methyladenosine by enzyme-assisted adenosine deamination. *Nature Biotechnology*. <https://doi.org/10.1038/s41587-022-01587-6>
- Xiong, F., Wang, R., Lee, J.-H., Li, S., Chen, S.-F., Liao, Z., Hasani, L. al, Nguyen, P. T., Zhu, X., Krakowiak, J., Lee, D.-F., Han, L., Tsai, K.-L., Liu, Y., & Li, W. (2021). RNA m6A modification orchestrates a LINE-1–host interaction that facilitates retrotransposition and contributes to long gene vulnerability. *Cell Research*, *31*(8), 861–885. <https://doi.org/10.1038/s41422-021-00515-8>
- Xu, C., Liu, K., Ahmed, H., Loppnau, P., Schapira, M., & Min, J. (2015). Structural Basis for the Discriminative Recognition of N6-Methyladenosine RNA by the Human YT521-B Homology Domain Family of Proteins. *Journal of Biological Chemistry*, *290*(41), 24902–24913. <https://doi.org/10.1074/JBC.M115.680389>
- Xu, C., Liu, K., Tempel, W., Demetriades, M., Aik, W. S., Schofield, C. J., & Min, J. (2014). Structures of Human ALKBH5 Demethylase Reveal a Unique Binding Mode for Specific Single-stranded N6-Methyladenosine RNA Demethylation. *Journal of Biological Chemistry*, *289*(25), 17299–17311. <https://doi.org/10.1074/JBC.M114.550350>
- Xu, C., Wang, X., Liu, K., Roundtree, I. A., Tempel, W., Li, Y., Lu, Z., He, C., & Min, J. (2014). Structural basis for selective binding of m6A RNA by the YTHDC1 YTH domain. *Nature Chemical Biology*, *10*(11), 927–929. <https://doi.org/10.1038/nchembio.1654>
- Xu, K., Yang, Y., Feng, G. H., Sun, B. F., Chen, J. Q., Li, Y. F., Chen, Y. S., Zhang, X. X., Wang, C. X., & Jiang, L. Y. (2017). Mettl3-mediated m(6)A regulates spermatogonial differentiation and meiosis initiation. *Cell Research*, *27*, 1100–1114.
- Xu, L., Liu, X., Sheng, N., Oo, K. S., Liang, J., Chionh, Y. H., Xu, J., Ye, F., Gao, Y. G., Dedon, P. C., & Fu, X. Y. (2017). Three distinct 3-methylcytidine (m3C) methyltransferases modify tRNA and mRNA in mice and humans. *Journal of Biological Chemistry*, *292*(35), 14695–14703. <https://doi.org/10.1074/JBC.M117.798298>
- Xu, W., He, C., Kaye, E. G., Li, J., Mu, M., Nelson, G. M., Dong, L., Wang, J., Wu, F., Shi, Y. G., Adelman, K., Lan, F., Shi, Y., & Shen, H. (2022). Dynamic control of chromatin-associated m6A methylation regulates nascent RNA synthesis. *Molecular Cell*, *82*(6), 1156-1168.e7. <https://doi.org/10.1016/J.MOLCEL.2022.02.006>
- Xu, W., Li, J., He, C., Wen, J., Ma, H., Rong, B., Diao, J., Wang, L., Wang, J., Wu, F., Tan, L., Shi, Y. G., Shi, Y., & Shen, H. (2021). METTL3 regulates heterochromatin in mouse embryonic stem cells. *Nature*, *591*(7849), 317–321. <https://doi.org/10.1038/s41586-021-03210-1>
- Xu, W., Rahman, R., & Rosbash, M. (2018). Mechanistic implications of enhanced editing by a HyperTRIBE RNA-binding protein. *RNA*, *24*(2), 173–182. <https://doi.org/10.1261/rna.064691.117>
- Yang, F., Jin, H., Que, B., Chao, Y., Zhang, H., Ying, X., Zhou, Z., Yuan, Z., Su, J., Wu, B., Zhang, W., Qi, D., Chen, D., Min, W., Lin, S., & Ji, W. (2019). Dynamic m6A mRNA methylation reveals the role of METTL3-m6A-CDP1 signaling axis in chemical carcinogenesis. *Oncogene*, *38*(24), 4755–4772. <https://doi.org/10.1038/s41388-019-0755-0>
- Yang, J.-Y., Zong, C. S., Xia, W., Wei, Y., Ali-Seyed, M., Li, Z., Broglio, K., Berry, D. A., & Hung, M.-C. (2006). MDM2 Promotes Cell Motility and Invasiveness by Regulating E-Cadherin Degradation. *Molecular and Cellular Biology*, *26*(19), 7269–7282. <https://doi.org/10.1128/MCB.00172-06>
- Yang, X., Liu, Q.-L., Xu, W., Zhang, Y.-C., Yang, Y., Ju, L.-F., Chen, J., Chen, Y.-S., Li, K., Ren, J., Sun, Q., & Yang, Y.-G. (2019). m6A promotes R-loop formation to facilitate transcription termination. *Cell Research*, *29*(12), 1035–1038. <https://doi.org/10.1038/s41422-019-0235-7>
- Yang, X., Triboulet, R., Liu, Q., Sendinc, E., & Gregory, R. I. (2022). Exon junction complex shapes the m6A epitranscriptome. *Nature Communications*, *13*(1), 7904. <https://doi.org/10.1038/s41467-022-35643-1>
- Yang, X., Yang, Y., Sun, B.-F., Chen, Y.-S., Xu, J.-W., Lai, W.-Y., Li, A., Wang, X., Bhattarai, D. P., Xiao, W., Sun, H.-Y., Zhu, Q., Ma, H.-L., Adhikari, S., Sun, M., Hao, Y.-J., Zhang, B., Huang, C.-M., Huang, N., ... Yang, Y.-G. (2017). 5-methylcytosine promotes mRNA export — NSUN2 as the methyltransferase and ALYREF as an m5C reader. *Cell Research*, *27*(5), 606–625. <https://doi.org/10.1038/cr.2017.55>
- Yang, Y., Fan, X., Mao, M., Song, X., Wu, P., Zhang, Y., Jin, Y., Yang, Y., Chen, L.-L., Wang, Y., Wong, C. C. L., Xiao, X., & Wang, Z. (2017). Extensive translation of circular RNAs driven by N6-methyladenosine. *Cell Research*, *27*(5), 626–641. <https://doi.org/10.1038/cr.2017.31>
- Yang, Y., Wang, L., Han, X., Yang, W. L., Zhang, M., Ma, H. L., Sun, B. F., Li, A., Xia, J., Chen, J., Heng, J., Wu, B., Chen, Y. S., Xu, J. W., Yang, X., Yao, H., Sun, J., Lyu, C., Wang, H. L., ... Yang, Y. G. (2019). RNA 5-Methylcytosine Facilitates the Maternal-to-Zygotic Transition by Preventing Maternal mRNA Decay. *Molecular Cell*, *75*(6), 1188-1202.e11. <https://doi.org/10.1016/J.MOLCEL.2019.06.033>

8. References

- Yoon, K. J., Ringeling, F. R., Vissers, C., Jacob, F., Pokrass, M., Jimenez-Cyrus, D., Su, Y., Kim, N. S., Zhu, Y., Zheng, L., Kim, S., Wang, X., Doré, L. C., Jin, P., Regot, S., Zhuang, X., Canzar, S., He, C., Ming, G. I., & Song, H. (2017). Temporal Control of Mammalian Cortical Neurogenesis by m6A Methylation. *Cell*, *171*(4), 877–889.e17. <https://doi.org/10.1016/J.CELL.2017.09.003>
- Youn, J. Y., Dunham, W. H., Hong, S. J., Knight, J. D. R., Bashkurov, M., Chen, G. I., Bagci, H., Rathod, B., MacLeod, G., Eng, S. W. M., Angers, S., Morris, Q., Fabian, M., Côté, J. F., & Gingras, A. C. (2018). High-Density Proximity Mapping Reveals the Subcellular Organization of mRNA-Associated Granules and Bodies. *Molecular Cell*, *69*(3), 517–532.e11. <https://doi.org/10.1016/J.MOLCEL.2017.12.020>
- Yu, & Allen. (1959). Studies of an isomer of uridine isolated from ribonucleic acids. *Biochimica et Biophysica Acta*, *32*(C), 393–406. [https://doi.org/10.1016/0006-3002\(59\)90612-2](https://doi.org/10.1016/0006-3002(59)90612-2)
- Yu, F., Wei, J., Cui, X., Yu, C., Ni, W., Bungert, J., Wu, L., He, C., & Qian, Z. (2021). Post-translational modification of RNA m6A demethylase ALKBH5 regulates ROS-induced DNA damage response. *Nucleic Acids Research*, *49*(10), 5779–5797. <https://doi.org/10.1093/nar/gkab415>
- Yu, J., Chen, M., Huang, H., Zhu, J., Song, H., Zhu, J., Park, J., & Ji, S.-J. (2018). Dynamic m6A modification regulates local translation of mRNA in axons. *Nucleic Acids Research*, *46*(3), 1412–1423. <https://doi.org/10.1093/nar/gkx1182>
- Yue, Y., Liu, J., Cui, X., Cao, J., Luo, G., Zhang, Z., Cheng, T., Gao, M., Shu, X., Ma, H., Wang, F., Wang, X., Shen, B., Wang, Y., Feng, X., He, C., & Liu, J. (2018). VIRMA mediates preferential m6A mRNA methylation in 3'UTR and near stop codon and associates with alternative polyadenylation. *Cell Discovery*, *4*(1), 10. <https://doi.org/10.1038/s41421-018-0019-0>
- Zaccara, S., & Jaffrey, S. R. (2020). A Unified Model for the Function of YTHDF Proteins in Regulating m6A-Modified mRNA. *Cell*, *181*(7), 1582–1595.e18. <https://doi.org/10.1016/J.CELL.2020.05.012>
- Zdzalik, D., Domańska, A., Prorok, P., Kosicki, K., van den Born, E., Farnes, P. T., Rizzo, C. J., Guengerich, F. P., & Tudek, B. (2015). Differential repair of etheno-DNA adducts by bacterial and human AlkB proteins. *DNA Repair*, *30*, 1–10. <https://doi.org/10.1016/J.DNAREP.2015.02.021>
- Zhang, C., Chen, L., Peng, D., Jiang, A., He, Y., Zeng, Y., Xie, C., Zhou, H., Luo, X., Liu, H., Chen, L., Ren, J., Wang, W., & Zhao, Y. (2020). METTL3 and N6-Methyladenosine Promote Homologous Recombination-Mediated Repair of DSBs by Modulating DNA-RNA Hybrid Accumulation. *Molecular Cell*, *79*(3), 425–442.e7. <https://doi.org/10.1016/J.MOLCEL.2020.06.017>
- Zhang, C., Samanta, D., Lu, H., Bullen, J. W., Zhang, H., Chen, L., He, X., & Semenza, G. L. (2016). Hypoxia induces the breast cancer stem cell phenotype by HIF-dependent and ALKBH5-mediated m6A-demethylation of NANOG mRNA. *Proceedings of the National Academy of Sciences*, *113*(14), E2047–E2056. <https://doi.org/10.1073/pnas.1602883113>
- Zhang, F., Kang, Y., Wang, M., Li, Y., Xu, T., Yang, W., Song, H., Wu, H., Shu, Q., & Jin, P. (2018). Fragile X mental retardation protein modulates the stability of its m6A-marked messenger RNA targets. *Human Molecular Genetics*, *27*(22), 3936–3950. <https://doi.org/10.1093/hmg/ddy292>
- Zhang, G., Xu, Y., Wang, X., Zhu, Y., Wang, L., Zhang, W., Wang, Y., Gao, Y., Wu, X., Cheng, Y., Sun, Q., & Chen, D. (2022). Dynamic FMR1 granule phase switch instructed by m6A modification contributes to maternal RNA decay. *Nature Communications*, *13*(1), 859. <https://doi.org/10.1038/s41467-022-28547-7>
- Zhang, L. S., Liu, C., Ma, H., Dai, Q., Sun, H. L., Luo, G., Zhang, Z., Zhang, L., Hu, L., Dong, X., & He, C. (2019). Transcriptome-wide Mapping of Internal N7-Methylguanosine Methylome in Mammalian mRNA. *Molecular Cell*, *74*(6), 1304–1316.e8. <https://doi.org/10.1016/J.MOLCEL.2019.03.036>
- Zhang, L.-S., Xiong, Q.-P., Peña Perez, S., Liu, C., Wei, J., Le, C., Zhang, L., Harada, B. T., Dai, Q., Feng, X., Hao, Z., Wang, Y., Dong, X., Hu, L., Wang, E.-D., Pan, T., Klungland, A., Liu, R.-J., & He, C. (2021). ALKBH7-mediated demethylation regulates mitochondrial polycistronic RNA processing. *Nature Cell Biology*, *23*(7), 684–691. <https://doi.org/10.1038/s41556-021-00709-7>
- Zhang, M., Jiang, Z., Ma, Y., Liu, W., Zhuang, Y., Lu, B., Li, K., Peng, J., & Yi, C. (2023). Quantitative profiling of pseudouridylation landscape in the human transcriptome. *Nature Chemical Biology*. <https://doi.org/10.1038/s41589-023-01304-7>
- Zhang, M., Yang, S., Nelakanti, R., Zhao, W., Liu, G., Li, Z., Liu, X., Wu, T., Xiao, A., & Li, H. (2020). Mammalian ALKBH1 serves as an N6-mA demethylase of unpairing DNA. *Cell Research*, *30*(3), 197–210. <https://doi.org/10.1038/s41422-019-0237-5>
- Zhang, S., Zhao, B. S., Zhou, A., Lin, K., Zheng, S., Lu, Z., Chen, Y., Sulman, E. P., Xie, K., Bögl, O., Majumder, S., He, C., & Huang, S. (2017). m6A Demethylase ALKBH5 Maintains Tumorigenicity of Glioblastoma Stem-like Cells by Sustaining FOXM1 Expression and Cell Proliferation Program. *Cancer Cell*, *31*(4), 591–606.e6. <https://doi.org/10.1016/J.CCELL.2017.02.013>
- Zhang, Y. Q., Bailey, A. M., Matthies, H. J. G., Renden, R. B., Smith, M. A., Speese, S. D., Rubin, G. M., & Broadie, K. (2001). Drosophila Fragile X-Related Gene Regulates the MAP1B Homolog Futsch to Control Synaptic Structure and Function. *Cell*, *107*(5), 591–603. [https://doi.org/10.1016/S0092-8674\(01\)00589-X](https://doi.org/10.1016/S0092-8674(01)00589-X)
- Zhang, Y., Sun, L., Gao, X., Guo, A., Diao, Y., & Zhao, Y. (2019). RNF43 ubiquitinates and degrades phosphorylated E-cadherin by c-Src to facilitate epithelial-mesenchymal transition in lung adenocarcinoma. *BMC Cancer*, *19*(1), 670. <https://doi.org/10.1186/s12885-019-5880-1>
- Zhang, Z., Chen, L.-Q., Zhao, Y.-L., Yang, C.-G., Roundtree, I. A., Zhang, Z., Ren, J., Xie, W., He, C., & Luo, G.-Z. (2019). Single-base mapping of m6A by an antibody-independent method. *Science Advances*, *5*(7), eaax0250. <https://doi.org/10.1126/sciadv.aax0250>
- Zhang, Z., Luo, K., Zou, Z., Qiu, M., Tian, J., Sieh, L., Shi, H., Zou, Y., Wang, G., Morrison, J., Zhu, A. C., Qiao, M., Li, Z., Stephens, M., He, X., & He, C. (2020). Genetic analyses support the contribution of mRNA N6-methyladenosine (m6A) modification to human disease heritability. *Nature Genetics*, *52*(9), 939–949. <https://doi.org/10.1038/s41588-020-0644-z>
- Zhang, Z., Wang, M., Xie, D., Huang, Z., Zhang, L., Yang, Y., Ma, D., Li, W., Zhou, Q., Yang, Y.-G., & Wang, X.-J. (2018). METTL3-mediated N6-methyladenosine mRNA modification enhances long-term memory consolidation. *Cell Research*, *28*(11), 1050–1061. <https://doi.org/10.1038/s41422-018-0092-9>

8. References

- Zhao, B. S., Wang, X., Beadell, A. v, Lu, Z., Shi, H., Kuuspalu, A., Ho, R. K., & He, C. (2017). m6A-dependent maternal mRNA clearance facilitates zebrafish maternal-to-zygotic transition. *Nature*, *542*(7642), 475–478. <https://doi.org/10.1038/nature21355>
- Zhao, S., Devega, R., Francois, A., & Kidane, D. (2021). Human ALKBH6 Is Required for Maintenance of Genomic Stability and Promoting Cell Survival During Exposure of Alkylating Agents in Pancreatic Cancer. *Frontiers in Genetics*, *12*. <https://www.frontiersin.org/articles/10.3389/fgene.2021.635808>
- Zhao, X., Yang, Y., Sun, B.-F., Shi, Y., Yang, X., Xiao, W., Hao, Y.-J., Ping, X.-L., Chen, Y.-S., Wang, W.-J., Jin, K.-X., Wang, X., Huang, C.-M., Fu, Y., Ge, X.-M., Song, S.-H., Jeong, H. S., Yanagisawa, H., Niu, Y., ... Yang, Y.-G. (2014). FTO-dependent demethylation of N6-methyladenosine regulates mRNA splicing and is required for adipogenesis. *Cell Research*, *24*(12), 1403–1419. <https://doi.org/10.1038/cr.2014.151>
- Zheng, G., Dahl, J. A., Niu, Y., Fedorcsak, P., Huang, C. M., Li, C. J., Vågbo, C. B., Shi, Y., Wang, W. L., Song, S. H., Lu, Z., Bosmans, R. P. G., Dai, Q., Hao, Y. J., Yang, X., Zhao, W. M., Tong, W. M., Wang, X. J., Bogdan, F., ... He, C. (2013). ALKBH5 Is a Mammalian RNA Demethylase that Impacts RNA Metabolism and Mouse Fertility. *Molecular Cell*, *49*(1), 18–29. <https://doi.org/10.1016/J.MOLCEL.2012.10.015>
- Zhong, S., Li, H., Bodi, Z., Button, J., Vespa, L., Herzog, M., & Fray, R. G. (2008). MTA Is an Arabidopsis Messenger RNA Adenosine Methylase and Interacts with a Homolog of a Sex-Specific Splicing Factor. *The Plant Cell*, *20*(5), 1278–1288. <https://doi.org/10.1105/tpc.108.058883>
- Zhou, J., Wan, J., Gao, X., Zhang, X., Jaffrey, S. R., & Qian, S.-B. (2015a). Dynamic m6A mRNA methylation directs translational control of heat shock response. *Nature*, *526*(7574), 591–594. <https://doi.org/10.1038/nature15377>
- Zhou, J., Wan, J., Gao, X., Zhang, X., Jaffrey, S. R., & Qian, S.-B. (2015b). Dynamic m6A mRNA methylation directs translational control of heat shock response. *Nature*, *526*(7574), 591–594. <https://doi.org/10.1038/nature15377>
- Zhu, T., Roundtree, I. A., Wang, P., Wang, X., Wang, L., Sun, C., Tian, Y., Li, J., He, C., & Xu, Y. (2014). Crystal structure of the YTH domain of YTHDF2 reveals mechanism for recognition of N6-methyladenosine. *Cell Research*, *24*(12), 1493–1496. <https://doi.org/10.1038/cr.2014.152>
- Zou, S., Toh, J. D. W., Wong, K. H. Q., Gao, Y.-G., Hong, W., & Woon, E. C. Y. (2016). N6-Methyladenosine: a conformational marker that regulates the substrate specificity of human demethylases FTO and ALKBH5. *Scientific Reports*, *6*.
- Zou, Z., Wei, J., Chen, Y., Kang, Y., Shi, H., Yang, F., Chen, S., Zhou, Y., Sepich-Poore, C., Zhuang, X., Zhou, X., Jiang, H., Wen, Z., Jin, P., Luo, C., & He, C. (2022). FMRP phosphorylation modulates neuronal translation through YTHDF1. *BioRxiv*, 2022.11.29.518448. <https://doi.org/10.1101/2022.11.29.518448>
- Zuo, W., Huang, F., Chiang, Y. J., Li, M., Du, J., Ding, Y., Zhang, T., Lee, H. W., Jeong, L. S., Chen, Y., Deng, H., Feng, X. H., Luo, S., Gao, C., & Chen, Y. G. (2013). c-Cbl-Mediated Neddylation Antagonizes Ubiquitination and Degradation of the TGF- β Type II Receptor. *Molecular Cell*, *49*(3), 499–510. <https://doi.org/10.1016/J.MOLCEL.2012.12.002>

9. Curriculum Vitae

Education

- 12.2016 Master of Science, Neurobiology, Sapienza University (Rome, Italy)
10.2014 Bachelor of Science, Biology, Sapienza University (Rome, Italy)
07.2011 High school diploma (Rome, Italy)

Research experience

10.2017 – 06.2023 **PhD**

CIG, Center for Integrative Genomics, UNIL (Lausanne, Switzerland)

IMB, Institute for Molecular Biology (Mainz, Germany)

- Thesis title: Molecular mechanisms of m⁶A mRNA modification in *Drosophila* neurogenesis
- Supervisor: Prof Jean-Yves Roignant

02.2017 – 08.2017 **Unipharma Erasmus+ Internship**

IRB, Institute for Research in Biomedicine (Barcelona, Spain)

- Project title: Investigating the role of Kif2a and Cep170 in microtubule organization
- Supervisor: Dr Jens Lüders

10.2015 – 12.2016 **Master Thesis**

EBRI, European Brain Research Institute (Rome, Italy)

- Thesis title: BDNF modulates dendritic *Arc* mRNA translation in dependence of splicing
- Supervisor: Dr Corinna Giorgi

03.2014 – 10.2014 **Bachelor Thesis**

Biology Department, Sapienza University (Rome, Italy)

- Thesis title: Regulation of Neurexin 1 expression during neuronal differentiation
- Supervisor: Prof Antonella De Jaco

Scholarships and awards

- 05.2020 Poster award (RNA 2020, The 25th Annual Meeting of the RNA society)
08.2018 – 11.2020 Boehringer Ingelheim Fonds (BIF) PhD fellowship
02.2017 – 08.2017 Erasmus scholarship

Relevant publications

Worpenberg L, **Paolantoni** C, Roignant JY (2022), Functional interplay within the epitranscriptome: Reality or fiction?, *Bioessays*, 44:e2100174

Bawankar* P, Lence* T, **Paolantoni*** C, [...] Beli P, Helm M, Jinek M, Soller M, Roignant JY (2021), Hakai is required for stabilization of core components of the m⁶A mRNA methylation machinery, *Nat Commun*, 12:3778

Soldano* A, Worpenberg* L, **Paolantoni** C, [...] Dieterich C, Quattrone A and Roignant JY (2021), The m⁶A reader Ythdf restricts axonal growth in *Drosophila* through target selection modulation of the Fragile X mental retardation protein, *EMBO Journal*, 40:e104975

Lence* T, **Paolantoni*** C, Worpenberg* L and Roignant JY (2019), Mechanistic insights into m⁶A RNA enzymes, *Biochim Biophys Acta Gene Regul Mech*, 1862: 222-229

*Equal contribution

Conference contributions

6th NCCR RNA&Disease Retreat (03.2022, Engelberg)

Poster title: Hakai is required for stabilization of core components of the m⁶A mRNA methylation machinery

RNA 2020, The 25th Annual Meeting of the RNA society (05.2020, online)

Poster title: m⁶A restricts axonal growth in *Drosophila* through modulation of Fragile X mental retardation protein target selection

5th NCCR RNA&Disease Retreat (01.2020, Kandersteg)

Poster title: m⁶A restricts axonal growth in *Drosophila* through modulation of Fragile X mental retardation protein target selection

26th European Drosophila Research Conference (09.2019, Lausanne)

Poster title: Characterization of the m⁶A methyltransferase complex in *Drosophila melanogaster*

Student supervision and teaching

2020 – 2022 Practicum teacher (Genetics of eukaryotic model: *Drosophila melanogaster*, UNIL)

2019 – 2021 Practicum teacher (Cellular and Molecular Biology, UNIL)

02.2019 – 09.2019 Master student supervisor (IMB, Mainz)

07.2018 – 08.2018 Visiting student supervisor (IMB, Mainz)